UNIVERSITE DE MONTREAL

MULTIPARAMETER GEOPHYSICAL LOGGING FOR THE YAVA LEAD DEPOSIT

par

Anne CINQ-MARS
DEPARTEMENT DE GENIE MINERAL
ECOLE POLYTECHNIQUE

MEMOIRE PRESENTE EN VUE DE L'OBTENTION
DU GRADE DE MAITRE ES SCIENCES APPLIQUEES (M.Sc.A.)
MAI 1990

c Anne Cinq-Mars 1990

cA2PQ
uP 8
1990
C575

National Library
of Canada

Bibliothèque nationale
du Canada

Canadian Theses Service

Service des thèses canadiennes

Ottawa, Canada
K1A 0N4

The author has granted an irrevocable non-exclusive licence allowing the National Library of Canada to reproduce, loan, distribute or sell copies of his/her thesis by any means and in any form or format, making this thesis available to interested persons.

The author retains ownership of the copyright in his/her thesis. Neither the thesis nor substantial extracts from it may be printed or otherwise reproduced without his/her permission.

L'auteur a accordé une licence irrévocable et non exclusive permettant à la Bibliothèque nationale du Canada de reproduire, prêter, distribuer ou vendre des copies de sa thèse de quelque manière et sous quelque forme que ce soit pour mettre des exemplaires de cette thèse à la disposition des personnes intéressées.

L'auteur conserve la propriété du droit d'auteur qui protège sa thèse. Ni la thèse ni des extraits substantiels de celle-ci ne doivent être imprimés ou autrement reproduits sans son autorisation.

ISBN 0-315-58945-0

Canada

UNIVERSITE DE MONTREAL

ECOLE POLYTECHNIQUE

Ce mémoire intitulé:

MULTIPARAMETER GEOPHYSICAL LOGGING FOR THE YAVA LEAD DEPOSIT

présenté par: Anne Cinq-Mars

en vue de l'obtention du grade de : M.Sc.A.

a été dûment accepté par le jury d'examen constitué de:

Mme Marianne Mareschal, Ph.D., présidente

M. Michel Chouteau, Ph.D.

M. Jonathan Mwenifumbo, Ph.D.

M. Patrick Killeen, Ph.D.

To the memory of my friend Sonia Pelletier.

ABSTRACT

Multiparameter geophysical logging was undertaken in the west zone of the Yava sandstone lead deposit, Cape Breton, Nova Scotia in order to characterize the mineralization and its environment. Downhole measurements were made as an unbiased way of getting information from boreholes, and a statistical analysis of these data was applied as an unbiased way to interpret their responses.

The spectral gamma-gamma ray method is a useful technique to delineate both lead mineralization and geology. Linear regression analysis shows a good correlation between lead and the spectral ratio (high energy gamma ray intensities to low energy gamma ray intensities) with a correlation coefficient of 0.82. The high energy window of backscattered gamma rays characterizes both geology and mineralization. Optimal windows should be found to improve the delineation of lithologies, and the correlation between lead and the spectral ratio. This may lead to calibration for in situ assaying in the borehole.

The factor analysis confirmed the qualitative correlations which relate lithologic variations to

Key words: Geophysical logging, applied geophysics, Yava lead deposit, statistics, borehole logging.

resistivity and natural radioactivity variations.

Induced polarization did not accurately delineate the disseminated sulfides, because of the presence of some clay minerals. This was evident in the factor analysis. The geophysical logs did not characterize the zinc enrichment found in the northeast. Sphalerite seems to be a localized feature which may not be detectable.

Since downhole measurements successfully delineated the Yava lead mineralization and its surrounding, it should be extended to other ore body types.

SOMMAIRE

Le gisement monominéralique de plomb de Yava se situe dans le sud-est de l'île du Cap Breton, N.-E. La minéralisation est composée de galène disséminée et stratiforme et est localisée dans un grès fluviatile du Carbonifère. Elle est associée aux paléodépressions du socle rhyolitique.

Une campagne de forage fut entreprise au sud-ouest de la zone ouest de Yava afin de documenter le potentiel de cette partie du gisement. Un enrichissement en zinc y fut observé.

Dans le cadre d'un accord fédéral-provincial, la Commission Géologique du Canada réalisa des sondages diagraphiques dans treize forages. Les méthodes géophysiques telles que la résistivité, la polarisation provoquée et spontanée, la spectrométrie de rayonnement gamma naturel et gamma-gamma, la susceptibilité magnétique et la température furent utilisées.

Deux approches furent suivies dans le but de caractériser la minéralisation de Yava et son environnement. La première est qualitative. L'auteur tente de trouver des corrélations par l'observation des différents profils diagraphiques, géologiques et géochimiques (plomb et zinc).

La seconde approche fait intervenir des techniques statistiques (régressions linéaires simple et multiple, analyse des composantes principales et analyse discriminante) afin de vérifier les corrélations existantes. Les données de deux forages furent utilisées pour compléter cette partie de l'étude.

La minéralisation en plomb fut très bien délimitée par le ratio spectral (rapport des intensités des rayons gamma diffusés de hautes énergies avec celles de basses énergies). La régression linéaire illustre cette relation avec un coefficient de corrélation de 0.82 et une erreur-type d'estimation raisonnable. Le perfectionnement des procédures de calibration améliorait cette corrélation et pourrait amener à un dosage géochimique.

La fenêtre de haute énergie des rayons gamma diffusés délimite la minéralisation et la géologie. La calibration d'une fenêtre optimale permettrait de caractériser la densité des différentes lithologies, et permettrait d'améliorer la délimitation des éléments denses en maximisant le ratio spectral. La spectrométrie gamma-gamma serait donc la technique diagraphique qui permettrait de caractériser la minéralisation en plomb de Yava et son environnement.

L'analyse des composantes principales confirme la corrélation qualitative reliant les variations lithologiques avec les variations de résistivité et de radioactivité.

La polarisation provoquée ne caractérise pas avec succès les sulfures disséminés (pyrite, galène) puisque des minéraux argileux présents, semblent également participer à la réponse géophysique. Ceci fut confirmé par l'analyse en composantes principales.

La caractérisation de l'enrichissement en zinc n'a pu être réalisée avec succès. La sphalérite semble être un événement local ne pouvant être détecté (limitation du rayon d'investigation). Une étude détaillée de la distribution de la sphalérite est recommandée afin de poursuivre les travaux de délimitation des réserves en zinc.

En conclusion, la diagraphie géophysique a permis de caractériser la minéralisation en plomb de Yava et son environnement avec succès, et semble très prometteuse dans l'application de la définition de d'autres gisements, car elle permet d'obtenir l'information des forages avec moins de biais que la méthode visuelle conventionnelle.

Mots-clés: Diagraphie, gisement de plomb Yava, géophysique des sondages, géologie statistique.

ACKNOWLEDGEMENTS

The author wishes to thank the following establishments and people who made this study possible:

The Geological Survey of Canada for use of logging data, computing facilities and financial support, and the Nova Scotia Department of Mines and Energy for allowing the project to be part of this thesis;

From the Geological Survey of Canada, Dr. C.J. Mwenifumbo for his supervision, enthusiasm, guidance and criticism throughout the project , Dr. P.G. Killeen for his interest and support, Bill Hyatt for the logging field work, John Grant for his computing assistance over late nights, Barbara Elliott and Laurel Schock for their welcome assistance, Dr. Alexandre Debarats for his statistical advice, and all others who participated in the project;

Dr. Michel Chouteau from Ecole Polytechnique de Montréal for his supervision, guidance and helpful discussions;

Also from Polytechnique, Dr. Denis Marcotte and Jacques Ouillet for their advice on statistics, Lucette de Gagné for her helpful and welcome assistance and my colleagues for their help and encouragement;

My family and friends for their support and encouragement throughout these years and lastly, my companion Sylvain for his wonderful patience and support.

TABLE OF CONTENTS

ABSTRACT v

SOMMAIRE vii

ACKNOWLEDGEMENTS x

TABLE LIST xv

FIGURE LIST xviii

INTRODUCTION 1

CHAPTER 1. GENERAL INFORMATION 4

1.1 Site location and general information 4

1.2 Yava mine history 6

CHAPTER 2. GEOLOGY 12

2.1 Regional geology (Salmon River District) 12

2.2 Local geology 14

2.2.1 Yava deposit geology (West Zone) 14

2.2.2 Yava west zone mineralization 18

CHAPTER 3. GEOPHYSICAL TECHNIQUES 25

3.1 Nuclear logging methods 25

3.1.1 Natural gamma ray spectral logging method ... 31

3.1.2 Gamma gamma spectral logging method (Density method) 37

3.2 Electrical methods 41
3.2.1 Electrical resistivity logging method 42
3.2.2 Induced polarization logging method (IP) ... 46
3.2.3 Self potential logging method (SP) 50
3.3 Temperature logging methods 54
3.4 Magnetic susceptibility logging method (MS) 58

CHAPTER 4 EQUIPMENT AND CALIBRATION 75
4.1 Geological Survey of Canada logging equipment ... 75
4.2 Calibration facilities 77
4.3 Gamma ray spectral logging equipment 78
4.3.1 Natural gamma ray spectral logging equipment 79
4.3.2 Gamma-gamma ray spectral logging equipment .. 80
4.4 Electrical logging equipment 82
4.5 Temperature logging equipment 84
4.6 Magnetic susceptibility logging equipment 86
4.7 Software 89

CHAPTER 5. STATISTICAL TECHNIQUES 97
5.1 Statistical approach 97
5.2 Classical statistics 97
5.3 Univariate data analysis 98
5.4 Multivariate data analysis 105
5.4.1 Multiple linear regression analysis 107
5.4.2 Principal component analysis (PCA) 110
5.4.3 Discriminant analysis 116

CHAPTER 6. RESULTS 122
6.1 Qualitative geophysical results 123
6.1.1 Mineralization characterization 124
6.1.2 Geological characterization 126
6.1.3 Sections 130
6.2 Statistical results 144
6.2.1 Distributions 145
6.2.2 Univariate data analysis 161
1) Scatterplot diagrams 161
2) Simple linear regression analysis 164
6.2.3 Multivariate data analysis 167
1) Multiple linear regression analysis 167
2) Principal component analysis (PCA) 172
3) Discriminant analysis 179

CHAPTER 7. DISCUSSION 185

CONCLUSION 195

REFERENCES 198

APPENDICES 205

A) Data files 206

B) Multiparameter geophysical profiles 213

C) Sections 227

D) Histograms 241

E) Scatterplot diagrams 252

F) Data (on diskette) 273

1) Geologic core logs 274

2) Geochemical assays 276

3) Multiple linear regression, PCA and discriminant analyses data 278

TABLE LIST

		page
1.1	Borehole information.	11
3.1	Spectral window range.	31
4.1	Window energies for gamma-gamma spectral logging survey. a) all holes except 418, 420 and 421 b) holes 418, 420 and 421	95
4.2	Energy shift correction for the gamma-gamma spectral logging data.	96
5.1	Analysis of Variance.	102
6.1	Primary statistics done with resistivity, hole 404a. Statistics were calculated with resistivity values and natural logarithmic values from all lithologies, and from the Canso Group (sandstone), the Windsor shale and the rhyolite.	155
6.2	Primary statistics done with induced polarization (IP), hole 404a. Statistics were calculated with IP values from all lithologies, and with natural logarithmic values from all lithologies, and from the Canso Group (sandstone), the Windsor shale and the rhyolite.	156
6.3	Primary statistics done with the gamma-gamma density parameter of hole 404a, from all lithologies and from the Canso Group (sandstone), the Windsor shale and the rhyolite.	157
6.4	Primary statistics done with spectral ratio values of hole 404a from all lithologies, and from the Canso Group (sandstone), the Windsor shale and the rhyolite.	157
6.5	Primary statistics done with the natural gamma ray parameter of hole 404a from the Canso Group (sandstone). The natural logarithmic values were analysed within all lithologies, and within the Canso Group, the Windsor shale and the rhyolite.	158

6.6	Primary statistics done for hole 410a within the Canso Group (sandstone) with the natural logarithmic values of resistivity, induced polarization, gamma-gamma density and spectral ratio. The natural logarithmic values of total count were analysed within all lithologies, within the Canso Group, the Windsor shale and the rhyolite.	159
6.7	Primary statistics on chemical assays of lead, zinc and total iron in hole 404a. The concentration values and their natural logarithmic values were analysed.	160
6.8	Primary statistics on chemical assays of lead, zinc and total iron in hole 410a. The concentration values and their natural logarithmic values were analysed.	160
6.9	Description of the scatterplot diagrams for hole 404a (figures E.1 to E.10, appendix E).	161
6.10	Correlation matrix calculated in the multiple regression analysis - Hole 404a. Variables used: lead, zinc, total iron, resistivity, induced polarization (IP), gamma-gamma density, spectral ratio and total count (TC).	168
6.11	Correlation matrix calculated in the multiple regression analysis - Hole 410a. Variables used: lead, zinc, total iron, resistivity, induced polarization (IP), gamma-gamma density, spectral ratio and total count (TC).	168
6.12	Discriminant analysis: Classification results for hole 404a.	180
6.13	Discriminant analysis: Classification results for hole 410a.	182
6.14	Discriminant analysis: Classification results for hole 406a (0.1 metre samples).	183
7.1	Major petrographic and lithologic features that characterize the grey and green sandstone, Canso Group, Yava mine area (after Vaillancourt, 1985).	194
F.1	404a data set used in the multiple regression and factor analysis (PCA).	on disk
F.2	410a data set used in the multiple regression and factor analysis (PCA).	on disk

F.3 404a data set used in the discriminant analysis. on disk

F.4 410a data set used in the discriminant analysis. on disk

FIGURE LIST

		page
1.1	Location map (after Bonham, 1983).	8
1.2	The Yava deposit is characterized by three ore zones known as the west, central and east zone (after Bonham, 1983).	9
1.3	Location of geophysically logged holes at the Yava lead deposit, west zone extension.	10
2.1	General geological setting of the Glengarry Half Graben, southeastern Cape Breton Island (after Prime and Boehner, 1984).	22
2.2	Geology of the Salmon River Basin and the Loch Lomond Basin (after Vaillancourt and Sangster, 1984).	23
2.3	Map and longitudinal section of the Yava deposit (after Vaillancourt, 1985).	24
3.1	Volume of investigation encountered during recording (after Conaway and Killeen, 1980).	62
3.2	Gamma ray spectrum recorded in: a) a thorium zone of a model borehole b) an uranium zone of a model borehole c) a potassium zone of a model borehole The detector used was a 32x125mm sodium iodide detector. The dotted lines illustrate the interference (after Killeen, 1982).	63
3.3	Interplay between the three radioelement windows; α, β, γ, a, b, g being the stripping factors (after Killeen,1982).	63

3.4 Determination of the system constant, α (after Killeen, 1982) 64
a) A family of geological impulse responses curves computed from equation $\phi(z) = \alpha e^{-\alpha z}/2$ for values of α from 0.08 to 0.18 in step of 0.002.
b) The type curves of (a) modified to take detector length into account. In this particular example the detector length was 9cm. These curves were obtained by convolving the curves in (a) with the rectangular pulse of length, L (see Conaway and Killeen, 1978).
c) The measured gamma ray log with a 9cm detector when passing from the barren zone into the ore zone.
d) The impulse response is derived from the measured response in (c) by numerical differentiation:
$(\phi(z_i) = (Cz_{i+1} - Cz_i)/(\Delta z(C_{max} - C_{min}))$
-"full line"). The best fitting curve from (b) is overlain on the derived impulse response and the value of α is then considered to be the best for that detector.

3.5 Types of gamma ray interaction with matter (after Halleux, 1986). 65
a) Photoelectric effect: the photon is absorbed and an electron is ejected.
b) Compton scattering : the photon imparts some of its energy and is scattered at an angle to its original direction, an electron is expelled.
c) Pair production: the photon is destroyed; an electron and a positron are created.

3.6 Gamma ray interactions with matter in relation with gamma ray energies and equivalent atomic number of the material (after Dodds and Eschilman, 1972). 66

3.7 Spectrum of backscattered gamma rays related to Z changes (in low energy range) and to the formation density. 67

3.8 Equipotential lines and flow lines (after Dobrin and Savit, 1988). 68
a) In the vertical plane, below the surface
b) On plane of the earth's surface
(A, B are the current electrodes)

3.9 Electrodes arrays for the electrical borehole logging. 69
a) Normal array (inverted) AM=40cm, MN=2.6m
b) Micronormal array AM=A'M=10cm, A'N=2.6m
A and B are the current electrodes
M and N are the potential electrodes

3.10 Radius of investigation for the normal array with AM = L = 1 (after Roy and Dhar, 1971). 69
R : Radius distance from borehole axis
RIC: Contribution of the cylindrical shell of homogeneous ground to the total measured signal.

3.11 Apparent resistivity profile for the normal array as a function of resistivity and thickness layers (after Serra, 1979) 70
a) Resistive layer thicker than the AM spacing
b) Resistive layer with thickness smaller than the AM spacing
c) Conductive layer thicker than the AM spacing
d) Conductive layer with thickness smaller than the AM spacing
e) Very resistive and thick layer

3.12 Mechanisms that cause the IP phenomena; electrode and membrane polarization (after Telford et al., 1976) 71
a) Electrode polarization
Upper: Before current injection
Lower: When the current is switched on
b) Membrane polarization
Upper: Before current injection
Lower: When the current is switched on

3.13 Voltage decay curve over an 8 second cycle. 72
a) Current injection as a function of time
b) Voltage decay curve as a function of time
V: voltage
V_P : primary voltage
V_t : decaying voltage
I: current injected
t: time

3.14 Electromechanical mechanism for spontaneous potential. 73
a) Typical SP recorded response
b) Sketch of the mechanism

3.15 Spontaneous potential profiles from borehole logging (after Becker and Telford, 1965). 74
a) Barren hole log alongside the sulphide zone less than 30m away
b) Hole intersecting sulphides

4.1 GSC logging system (after Bristow, 1979a). 91

4.2 The computer sums the content of the channels encompassed by the appropriate peaks (selected window energies for K, U and Th) at a selected interval, and generates K, U and Th profiles which can be related to potassium, uranium and thorium concentration (after Bristow, 1979a). 92

4.3 Principle of voltage-to-frequency conversion for the temperature log (after Bristow and Conaway, 1984). 93

4.4 Maxwell bridge circuitry of the Geoinstruments TH-3C magnetic susceptibility probe. 94

6.1 Multiparameter logs for hole 410a. 133

6.2 Detailed geophysical logs and mineralization for hole 410a. 134

6.3 Multiparameter logs for hole 404a. 135

6.4 Detailed geophysical logs and mineralization for hole 404a. 136

6.5 Multiparameter logs for hole 421. 137

6.6 Multiparameter logs for hole 408a. 138

6.7 Multiparameter logs for hole 402a. 139

6.8 Sections location map, Yava lead deposit, west zone extension. 140

6.9 Bedrock topography plan view, Yava lead deposit, west zone extension. 141

6.10 Canso Group thickness plan view, Yava lead deposit, west zone extension. 142

6.11 a) Composite plan and longitudinal geological section through the west zone (after Bonham, 1982). 143
b) Cross section through the west zone along 33W ($D-D_1-D_2$).

6.12 Plot of initial variables (lead, resistivity, total count, gamma-gamma density, spectral ratio) on first two principal factors for hole 404a data set (after rotation). Horizontal axis is factor 1, vertical axis is factor 2. (1- represents lead content, 2- resistivity, 3-induced polarization, 4- gamma-gamma density, 5- spectral ratio and 6- total count natural gamma ray(TC)). 175

6.13 Plot of the regression factor score coefficients for the 404a data set on the first 2 principal factors (after rotation). Horizontal axis is the regression factor score for factor 1 and the vertical axis is the regression factor scores for factor 2. The lithologic variations are represented by:
*: sandstone between depth 7.05-11.25m
.: black shale at 12.05m
+: sandstone from 12.65-14.75m
x: cross-bedded sandstone from 14.85-15.25m. 176

6.14 Plot of initial variables (lead, resistivity, total count, gamma-gamma density, spectral ratio) on first two principal factors for hole 410a data set (after rotation). Horizontal axis is factor 1, vertical axis is factor 2. (1- represents lead content, 2- resistivity, 3-induced polarization, 4- gamma-gamma density, 5- spectral ratio and 6- total count natural gamma ray(TC)). 177

6.15 Plot of the regression factor score coefficients for hole 410a data set on the first 2 principal factors (after rotation). Horizontal axis is the regression factor score for factor 1 and the vertical axis is the regression factor scores for factor 2. The lithologic variations are represented by:
*: sandstone between depth 9.65-10.65m
#: limestone pebble conglomerate from 10.95-15.45m
o: sandstone with coal from 15.55-17.65m 178

B.1 Multiparameter logs for hole 402a. 214

B.2 Multiparameter logs for hole 403. 215

B.3 Multiparameter logs for hole 404a. 216

B.4 Multiparameter logs for hole 405. 217

B.5 Multiparameter logs for hole 406a. 218

B.6 Multiparameter logs for hole 408a. 219

B.7 Multiparameter logs for hole 409a. 220

B.8 Multiparameter logs for hole 410a. 221

B.9 Multiparameter logs for hole 411. 222

B.10 Multiparameter logs for hole 412. 223

B.11 Multiparameter logs for hole 418. 224

B.12 Multiparameter logs for hole 420. 225

B.13 Multiparameter logs for hole 421. 226

C.1 Sections location map, Yava lead deposit, west zone extension. 228

C.2 Longitudinal geological section A. 229
Horizontal scale: 1cm = 13.72m (45ft)
Vertical scale: 1 cm = 5m

C.3 Longitudinal section A - Lead content. 230
Horizontal scale: 1cm = 13.72m (45ft)
Vertical scale: 1 cm = 5m

C.4 Longitudinal section A - Zinc content. 231
Horizontal scale: 1cm = 13.72m (45ft)
Vertical scale: 1 cm = 5m

C.5 Longitudinal section A - Spectral ratio. 232
Horizontal scale: 1cm = 13.72m (45ft)
Vertical scale: 1 cm = 5m

C.6 Geological cross section B. 233
Horizontal scale: 1cm = 13.72m (45ft)
Vertical scale: 1 cm = 5m

C.7 Cross section B - Lead content. 234
Horizontal scale: 1cm = 13.72m (45ft)
Vertical scale: 1 cm = 5m

C.8 Cross section B - Zinc content. 235
Horizontal scale: 1cm = 13.72m (45ft)
Vertical scale: 1 cm = 5m

C.9 Cross section B - Spectral ratio. 236
Horizontal scale: 1cm = 13.72m (45ft)
Vertical scale: 1 cm = 5m

C.10 Geological section C. 237
Horizontal scale: 1cm = 13.72m (45pi)
Vertical scale: 1 cm = 5m

C.11 Section C - Lead content. 238
Horizontal scale: 1cm = 13.72m (45ft)
Vertical scale: 1 cm = 5m

C.12 Section C - Zinc content. 239
Horizontal scale: 1cm = 13.72m (45ft)
Vertical scale: 1 cm = 5m

C.13 Section C - Spectral ratio. 240
Horizontal scale: 1cm = 13.72m (45ft)
Vertical scale: 1 cm = 5m

D.1 Resistivity natural logarithm distribution, hole 404a. 242
a) Values from all lithologies
b) Values from the Canso Group (sandstone)
c) Values from the Windsor shale
d) Values from the rhyolite

D.2 Induced polarization natural logarithm (Ln(IP)) distribution, hole 404a. 243
a) Values from all lithologies
b) Values from the Canso Group (sandstone)
c) Values from the Windsor shale
d) Values from the rhyolite

D.3 Gamma-gamma density distribution, hole 404a. 244
a) Values from all lithologies
b) Values from the Canso Group (sandstone)
c) Values from the Windsor shale
d) Values from the rhyolite

D.4 Spectral ratio distribution, hole 404a. 245
a) Values from all lithologies
b) Values from the Canso Group (sandstone)
c) Values from the Windsor shale
d) Values from the rhyolite

D.5 Total count natural logarithm (Ln(TC)) distribution, hole 404a. 246
a) Values from all lithologies
b) Values from the Canso Group (sandstone)
c) Values from the Windsor shale
d) Values from the rhyolite

D.6 a) Resistivity natural logarithmic distribution. 247
Values from the Canso Group (sandstone).
Top: Hole 404a Bottom: Hole 410a
b) Induced polarization natural logarithm (Ln(IP)) distribution.
Values from the Canso Group (sandstone).
Top: Hole 404a Bottom: Hole 410a

D.7 a) Gamma-gamma density distribution. 248
Values from the Canso Group (sandstone).
Top: Hole 404a Bottom: Hole 410a
b) Spectral ratio distribution.
Values from the Canso Group (sandstone).
Top: Hole 404a Bottom: Hole 410a

D.8 Total count natural logarithm (Ln(TC)) distribution, hole 410a. 249
a) Values from all lithologies
b) Values from the Canso Group (sandstone)
c) Values from the Windsor shale
d) Values from the rhyolite

D.9 Lead natural logarithm (Ln(Pb)) distribution. 250
Values from the Canso Group (sandstone).
Top: Hole 404a Bottom: Hole 410a

D.10 Zinc natural logarithm (Ln(Zn)) distribution. 250
Values from the Canso Group (sandstone).
Top: Hole 404a Bottom: Hole 410a

D.11 Total iron natural logarithm (Ln(Fe)) distribution. Values from the Canso Group (sandstone). Top: Hole 404a Bottom: Hole 410a 251

E.1 Scatterplot diagram of the natural logarithmic values of total count (Ln(TC)) against the natural logarithmic values of resistivity for hole 404a (symbols: (*): Canso Group, (+): Windsor shale and, (x): rhyolite). 253

E.2 Scatterplot diagram of the natural logarithmic values of induced polarization (Ln(IP)) against the natural logarithmic values of resistivity for hole 404a (symbols: (*): Canso Group, (+): Windsor shale and, (x): rhyolite). 254

E.3 Scatterplot diagram of the gamma-gamma density values against the natural logarithmic values of resistivity for hole 404a (symbols: (*): Canso Group, (+): Windsor shale and, (x): rhyolite). 255

E.4 Scatterplot diagram of the spectral ratio values against the natural logarithmic values of resistivity for hole 404a (symbols: (*): Canso Group, (+): Windsor shale and, (x): rhyolite). 256

E.5 Scatterplot diagram of natural logarithmic values of total count (Ln(TC)) against logarithmic values of induced polarization (Ln(IP)) for hole 404a (symbols: (*): Canso Group, (+): Windsor shale and, (x): rhyolite). 257

E.6 Scatterplot diagram for hole 404a. Gamma-gamma density values against natural logarithmic values of induced polarization (Ln(IP)). Symbols: (*): Canso Group, (+): Windsor shale and, (x): rhyolite). 258

E.7 Scatterplot diagram for hole 404a. Spectral ratio values against natural logarithmic values of induced polarization (Ln(IP)). (Symbols: (*): Canso Group, (+): Windsor shale and, (x): rhyolite). 259

E.8 Scatterplot diagram for hole 404a. Natural logarithmic values of total count (Ln(TC)) against gamma-gamma density values. (Symbols: (*): Canso Group, (+): Windsor shale and, (x): rhyolite). 260

E.9 Scatterplot diagram for hole 404a. Spectral ratio values against gamma-gamma density values (Symbols: (*): Canso Group, (+): Windsor shale and, (x): rhyolite). 261

E.10 Scatterplot diagram for hole 404a. Natural logarithmic values of total count (Ln(TC)) against spectral ratio values. (Symbols: (*): Canso Group, (+): Windsor shale and, (x): rhyolite). 262

E.11 Scatterplot diagram for hole 410a. Natural logarithmic values of total count (Ln(TC)) against the natural logarithmic values of resistivity (Symbols: (*): Canso Group, (+): Windsor shale, (o): rhyolite in the Windsor shale and, (x): rhyolite). 263

E.12 Scatterplot diagram for hole 410a. Natural logarithmic values of induced polarization (Ln(IP)) against the natural logarithmic values of resistivity (Symbols: (*): Canso Group, (+): Windsor shale, (o): rhyolite in the Windsor shale and, (x): rhyolite). 264

E.13 Scatterplot diagram for hole 410a. Natural logarithmic values of total count (Ln(TC)) against the natural logarithmic values of induced polarization (Ln(IP)). Symbols: (*): Canso Group, (+): Windsor shale, (o): rhyolite in the Windsor shale and, (x): rhyolite. 265

E.14 Scatterplot diagram for hole 404a. Concentration lead in percent against the spectral ratio parameter. 266

E.15 Scatterplot diagram for hole 404a. Concentration lead in percent against the gamma-gamma density parameter (counts/sec). 267

E.16 Scatterplot diagram for hole 404a. Concentration lead in percent against the induced polarization parameter (IP) in mvolts/volts. 268

E.17 Scatterplot diagram for hole 410a. Concentration lead in percent against the spectral ratio parameter. 269

E.18 Scatterplot diagram for hole 410a. Concentration lead in percent against the gamma-gamma density parameter (counts/sec). 270

E.19 Scatterplot diagram for hole 410a. Concentration lead in percent against the induced polarization parameter (IP) in mvolts/volts. 271

E.20 Scatterplot diagram for hole 410a. Total iron concentration against zinc concentration (both in logarithmic values: the values have been multiplied by 10000 (from % to ppm) before applying the natural logarithm). 272

INTRODUCTION

Since assuming the ownership of the Yava deposit, the Nova Scotia Government has been documenting the potential of the deposit as a low grade open-pit lead mine. The Borehole Geophysics Section of the Geological Survey of Canada (GSC) carried out multiparameter geophysical logging to the Yava mineralization and its environment. This was done under the Federal-Provincial Mineral Development Agreement in order to provide new information on the deposit and its definition.

A drilling program was undertaken in 1986-1987, in the western margin of the Yava west zone. It indicated a relative enrichment in zinc content which lends some support to the possibility of a zinc deposit down-dip (by analogy with the Laisvall Mine in Sweden; Bonham, 1983, Patterson, 1986, Rickard et al., 1979).

Many questions were raised and arose the objectives of this study;

- Is multiparameter borehole logging a useful tool to delineate the Yava lead deposit type?
- If so, which techniques can best characterize and delineate the ore body?
- Can ore reserves be estimated with such techniques?
- Is zinc mineralization differentiable from lead

mineralization?

- If so, is there an enrichment through the southwest?
- What should be the strategic methodology of exploration for this type of deposit?

Similar questions in gold exploration have been raised (Urbancic, 1985) with the fact that the geophysical techniques could not be used as direct gold characterization techniques (they are rather used to delineate the gold environment). In this case, a combination of characteristic physical rock properties is best to delineate the orebody. However, lead mineralization (galena) occurs in a different environment and has strong characteristics (high density, conductive, polarizable) which may be directly distinguished.

To answer the objectives of the project, the present study considers the correlations of the multigeophysical parameters with the mineralization and geology. Two major approaches were taken. In the first, the different logs (geophysical, geological and few lead and zinc assays) for thirteen holes were visually examinated for qualitative correlations. This approach is quite simple and frequently used.

The second approach uses statistical techniques which

allow the quantification of the existing correlations. This approach demands more time than the first one but gives objective results independent of the geophysicist's experience and judgement. Data sets from holes 404a and 410a were used to achieve this part of the study because of the availability of chemical assays (lead, zinc and total iron) sampled every 10 centimetres along the region of interest.

The organization of the thesis is as follows. After the introduction of the project, general information (site location, mine history...) is presented. The regional and local geology of the Yava deposit is described in chapter 2. This is followed in chapters 3 and 4 by the theoretical description of the geophysical techniques and instrumentation used in the project. Chapter 5 informs the reader about the statistical techniques adopted by the author. The results of the qualitative and statistical analyses are summarized in chapter 6, followed by a discussion. Concluding remarks close the thesis in order to improve the quality of subsequent analyses and to pursue the goals of the project that were not attained.

CHAPTER 1

GENERAL INFORMATION

1.1 Site location and general information

The Yava lead deposit is located in the district of Salmon River, on Cape Breton Island, Nova Scotia at latitude 45°51'30"N and longitude 60°51'30"W. It is situated not more than 50km south-west of the town of Sydney (figure 1.1).

The area is topographically hilly and the drainage is generally good: the Salmon river flows eastward across the west and the central zones of the deposit.

The mill located at Lake Enon is joined to the mine by a 12 km road.

The Yava lead deposit is characterized by three ore zones known as the west, central and east zone (figure 1.2). The west zone was mined by Yava Mines Ltd for 2.5 years (1979-1981) and produced 388000 metric tonnes at 4.69% Pb. Proven remaining reserves are as follows (Bonham, 1982):

West zone:	630000 tonnes at 4.95%Pb
Central zone (undeveloped):	340000 tonnes at 4.3%Pb
East zone (undeveloped):	804000 tonnes at 4.1%Pb.

Since assuming ownership, the Nova Scotia Department of Mines and Energy has been documenting the potential of the deposit as a low grade open-pit lead mine. A shallow diamond drilling program was undertaken during the years 1986 and 1987 in the western margin of the west ore zone in order to provide information on the limits of this zone to the west (J.M. Patterson, 1986). Under a Federal Provincial Mineral Development Agreement, the Geological Survey of Canada (GSC) geophysically logged thirteen holes. Figure 1.3 shows the location of the boreholes and table 1.1 summarizes the borehole information.

The drill core from these holes was geologically logged under the supervision of J.M. Patterson (Nova Scotia Department Mines and Energy, Mineral Resources Division). Where visual mineralization occurred, the cores were sampled for chemical analysis of lead, zinc and silver (appendix F). Detailed samples were also taken from the mineralized sandstone of holes 404a and 410a and analysed for lead, zinc and total iron content.

Multiparameter geophysical logging was done for the thirteen holes and appendix A is a compilation of the information for each geophysical technique in the different boreholes. Appendix B groups the multiparameter logs (geology, geophysics and geochemical assays) for each hole.

1.2 Yava mine history

The exploration interests in the Salmon River region date from around 1929 when Aconda Mines Ltd had drilled seven holes in order to test showings of argentiferous galena known in the region since 1880. Following that drilling programme, a few mineralized veins with low grades had been localized in the Windsor Shale.

In 1957, further drilling works was conducted by Minda Scotia Mines Ltd. and more mineralized veins were intersected. In 1959, the discovery of barite and base metal deposit within the Windsor sediments at Walton in Hants County, Nova-Scotia, stimulated further interest in the Salmon River region.

In 1961, Talisman Mines Ltd. took control of 1166 claims in the Salmon River region. In 1962, aeromagnetic and soil geochemistry surveys showed interesting anomalies; a drilling campaign was immediately executed resulting in intersections of disseminated galena in the sandstone. By the end of 1962, Phelps Dodge Corporation of Canada owned the major shares of the property.

Between 1962 and 1969, additional work (drilling

campaign: 219 holes for 81000 feet on a 300 X 250 square feet grid, geological mapping, geophysical and geochemical surveys) was carried out in the region in order to understand the genetic model of mineralization, and to complete information for a mining feasability study.

By 1977, Barymin Explorations became the sole owner of Yava and started a drilling campaign in the west zone to confirm ore reserves (69 holes representing 14000 feet).

In 1978, after the mill acquisition from Kaiser Ltd. at Enon (12 km west of the property), Barymin Explorations prepared the site for production in August 1979. In September 1981, because of financial difficulties, the mine operations were stopped and everything abandoned. Nearly 388000 tonnes at 4.69% lead had been extracted (Bonham, 1982).

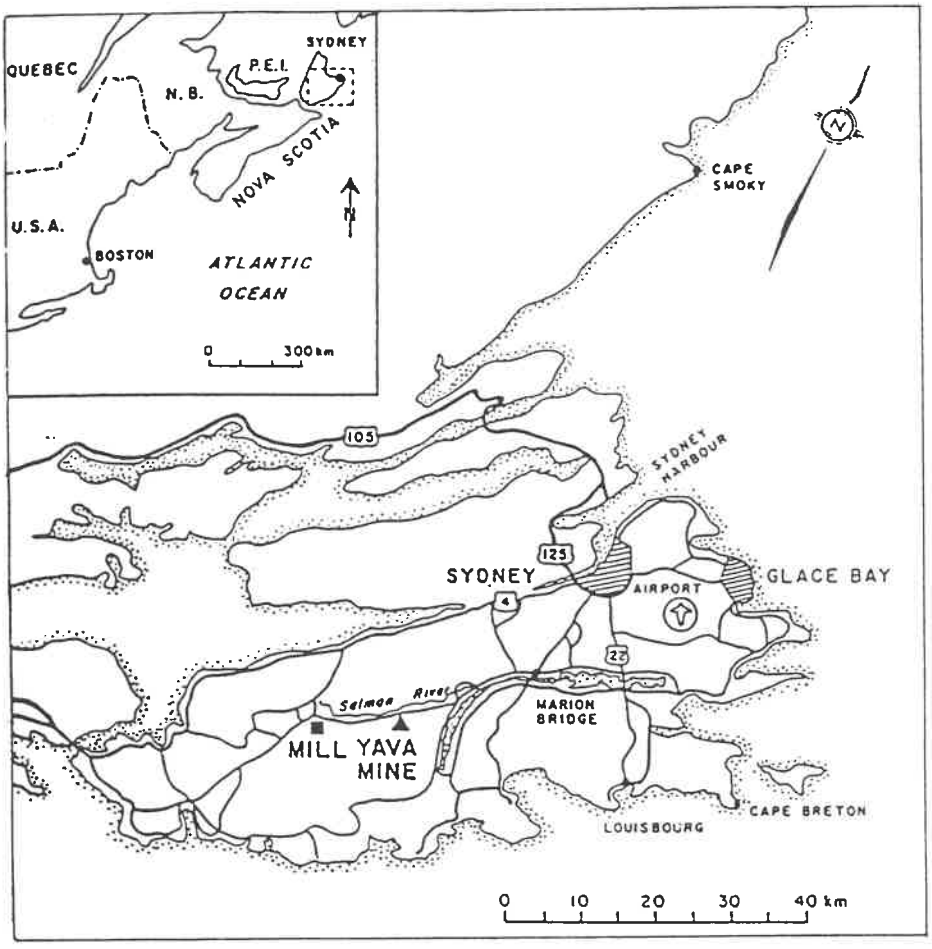


FIGURE 1.1 Location map (after Bonham, 1983).

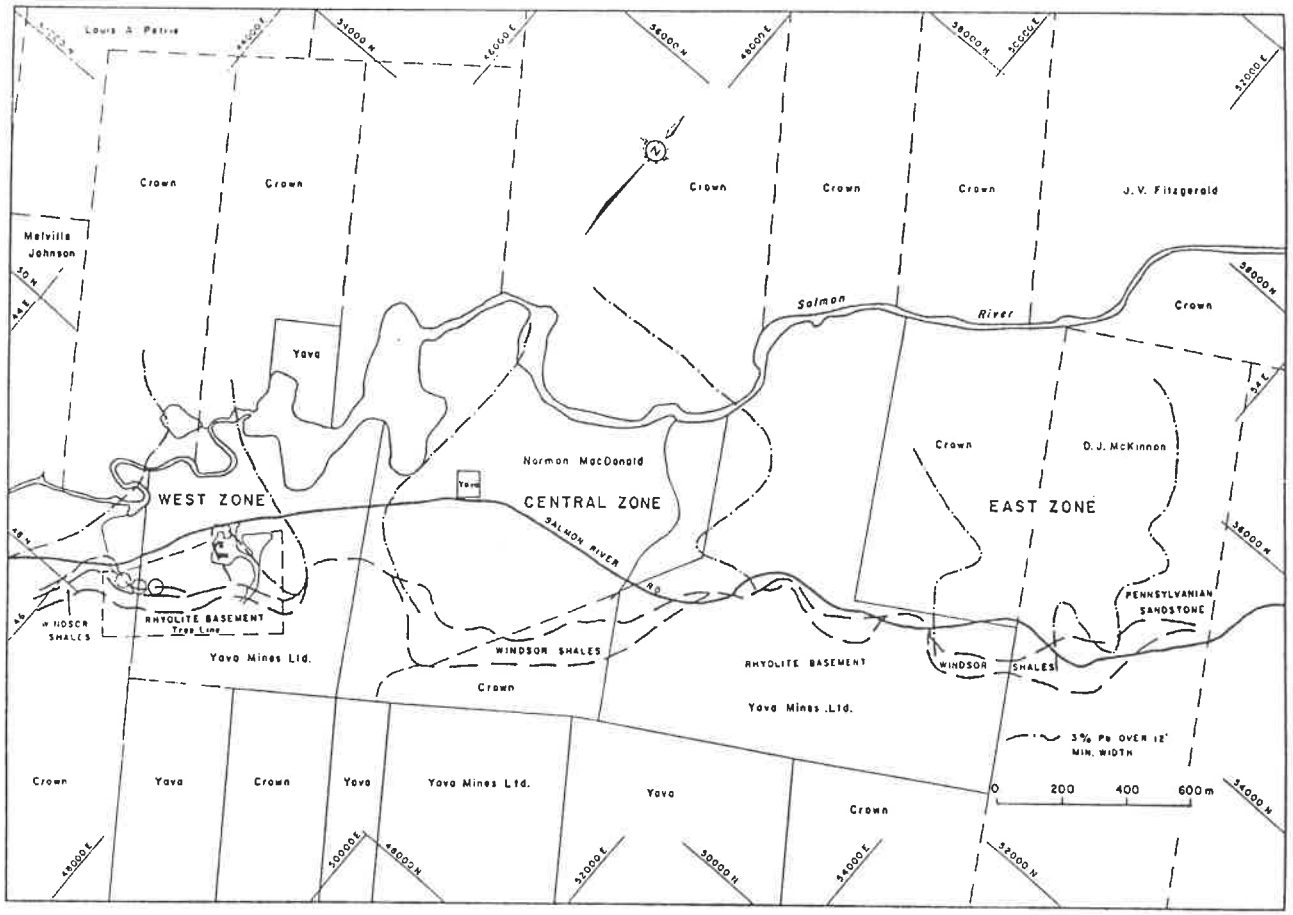


FIGURE 1.2 The Yava deposit is characterized by three ore zones known as the west, central and east zone (after Bonham, 1983).

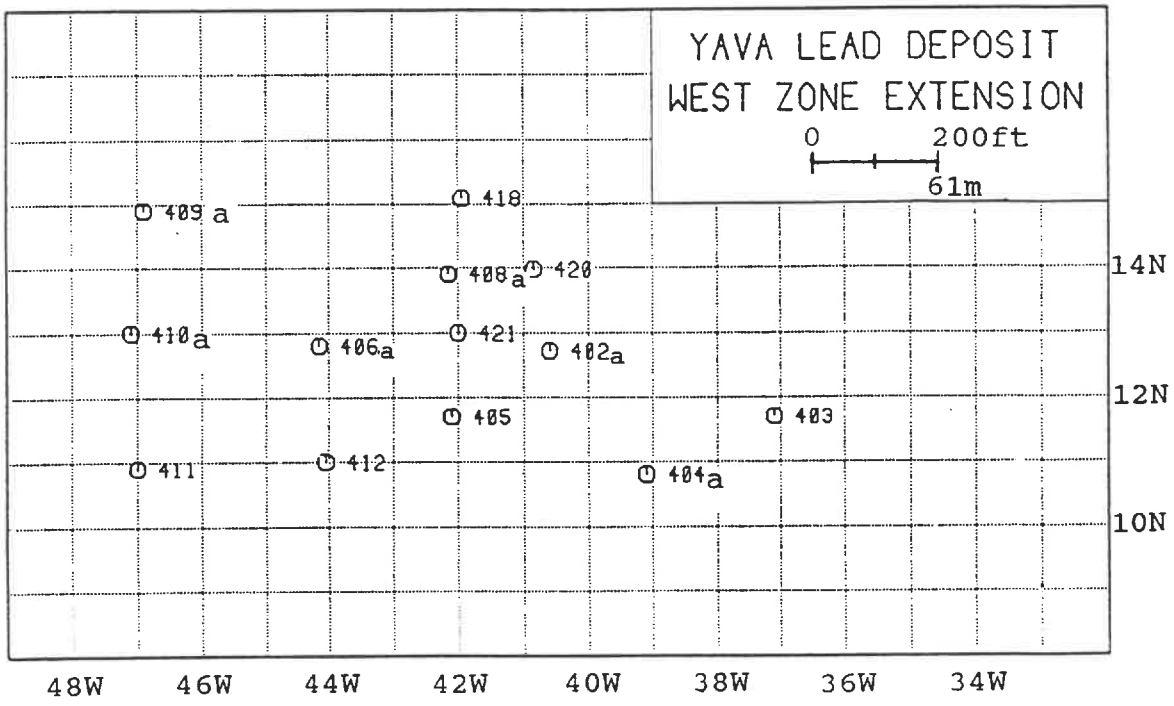


FIGURE 1.3 Location of geophysically logged holes at the Yava lead deposit, west zone extension.

Hole #	Hole size	Coordinates	Elevation (m)	Casing length (m)	Casing height (cm)	Total depth (m)
402a	NQ	40+60W/12+72N	1512.11	7.32	16.6	57.00
403	BQ	37+10W/11+70N	1511.27	3.66	0.0	63.10
404a	NQ	39+10W/10+80N	1517.69	7.32	28.0	60.05
405	BQ	42+10W/11+70N	1515.27	5.89	19.3	47.85
406a	NQ	44+15W/12+80N	1513.81	6.10	65.7	44.81
408a	NQ	42+15W/13+90N	1509.83	7.92	10.7	49.99
409a	NQ	46+90W/14+90N	1509.58	12.19	17.5	38.10
410a	NQ	47+10W/13+00N	1516.32	9.45	7.6	41.76
411	BQ	47+00W/10+90N	1519.99	8.23	29.4	30.78
412	BQ	44+05W/11+00N	1516.66	7.32	28.0	52.73
418	NQ	41+94W/15+09N	1509.97	12.20	60.0	52.44
420	NQ	40+85W/13+97N	1508.61	9.15	20.0	57.00
421	NQ	42+00W/13+00N	1511.86	6.10	70.0	43.29

TABLE 1.1 Borehole information

CHAPTER 2

GEOLOGY

2.1 Regional geology (Salmon River District)

The Yava sandstone-lead deposit is located on the southeast flank of the Glengarry Half-Graben (also called the Salmon River Basin), a portion of the Fundy Basin system (Appalachian Orogen).

The Glengarry Half-Graben (figure 2.1) is a small elongate structural basin which consists of clastic deposits of Upper Carboniferous age (Namurian and Westphalian). This synclinal feature plunges southwesterly and is approximately 30 km long and 10 km wide at its centre. It is bounded to the northwest by the Lennox Passage Fault (a northeasterly trending, high angle normal fault) that separates it from the East Bay Block Hadrynian-Devonian igneous basement.

To the southwest, a northwesterly trending, high angle transverse fault separates it from the Loch Lomond Basin which is structurally similar. The southeast part of the basin where the Yava deposit is located is delimited by an angular unconformity with the Fourchu Block (Hadrinian-Devonian igneous basement). There, the sediments dip 14-15 degrees to the northwest.

In the area, the basement (Upper Proteozoic and Lower Cambrian age) consists of metasediments and metavolcanics (Fourchu and Bourinot Groups) cut by acid and basic intrusions whose ages are uncertain (Upper Precambrian-Lower Cambrian). The basement to the northwest part of the Salmon River Basin is cut by the Huntington Mountain Pluton of dioritic composition, and to the southeast part it is cut by the Loch Lomond Pluton of granitic composition (figure 2.2).

Carboniferous rocks are exposed on the southeastern flank of the Basin. They have been divided into two main sequences. The Windsor Group defines the first main sequence. Its basal unit (Early Visean) consists of a talus breccia overlain by a conglomerate and is interpreted as a dry sub aerial fan type deposit (Bonham, 1983).

During Late Visean, the area was submerged by a marine transgression and resulted in deposition of limestone (absent on the Yava site), black, red and green shales. A period of emergence at the end of the Visean and Early Pennsylvanian is characterized by the Windsor unconformity, a weathered zone that delimits the Windsor Group.

The overall thickness of that unit varies from 0 (where it has been eroded away) to a maximum of 160 m on the west part of the Yava site.

The Canso Group of Namurian age (Upper Carboniferous) consists mainly of continental clastic sediments which lie unconformably on the Windsor Group when present. This second main sequence is subdivided into three sub-units:

1) Lower grey sandstone subdivided into 3 sub-units:
   - .Arenaceous grey sandstone,
   - .Interbedded sandstone, shale and mudstone,
   - .Variable sandstone: interbedded sandstone and conglomerate (poorly exposed in the area).
2) Conglomerate,
3) Upper green sandstone with coal fragments: similar to the lower grey sandstone.

This entire sequence can reach up to 1550m thickness.

2.2 Local geology

2.2.1 Yava deposit geology (West Zone)

The basement rock which underlies the Windsor and Canso Group consists of a brick-red feldspar quartz porphyry, a portion of the Loch Lomond Pluton. It is frequently described as a rhyolite. However, the name rhyolite is not justified, because there is no field or texture evidence to indicate that it formed as the result of an extrusive process (Bonham, 1983).

A whole rock determination of fresh material studied by Bonham (1983) indicates a composition of 75% SiO_2, 13.8% Al_2O_3, 5% K_2O and 4.3% NA_2O; that of potassic granite.

The term rhyolite will, however, be used in the present thesis, in order to conform with the various studies and reports written on this area.

The age of the rhyolite is uncertain. Age information on that intrusive complex is best summarized by Scott (1980). The rhyolite beneath, and immediately south of the mine is part of the Loch Lomond pluton. This has been dated at 563q24 Ma by Rb-Sr whole rock isochron (Cormier, 1972) and recalculated at 548q18 Ma (Keppie and Smith, 1978).

In the Yava area, the basement is characterized by three paleotopographic depressions that delimit three mineralized zones (see chapter 2.2.2) separated by basement highs (figure 2.3).

The Windsor sediments overlie the rhyolite basement rock. The basal unit consists of a talus breccia which is a rhyolitic breccia consisting of angular to sub-angular fragments within a green clayey matrix.

The lithostratigraphic units of limestone and black

shale are absent at Yava. An interbedded black shale with limestone and gypsum overlies the breccia. Beds of shales and brown and green siltstones similar to the previous unit (no limestone and gypsum intercalations) lie near the weathered zone (Bonham, 1983 (p.57)).

A calcareous horizon, up to 2 m thick overlies the top unit of the Windsor Group, over most of the mine area (overlain by a weathered zone). The weathered zone is characterized by a regolith that shows the transition from marine to continental deposition. The regolith analysis indicates a composition that is predominantly aluminum silicate with minor associated iron, potassium and magnesium (Bonham, 1983).

The Canso Group which hosts the lead mineralization, has two major units. The basal unit consists of a green grey arenaceous siltstone assemblage which consists of a sequence of interbedded silty sandstone, mudstone and shale flake conglomerate. It can reach a maximum thickness of 5m where present and includes weak galena mineralization.

A sandstone assemblage which is the principal host of lead mineralization is the next unit and is characterized by:

.Conglomerate with sandy matrix,

.Grey to green sandstone whose grain size decreases upwards toward the surface. Few hand samples show 80% Qz, 15% rock fragments and 1-3% of potassic feldspar (Bonham, 1982). X-ray diffraction studies on selected samples that showed the clay fraction is composed of 75-90% kaolinite with minor amounts of illite, chlorite and occasional montmorillonite (Scott, 1979).

Vaillancourt & Sangster (1984) and Vaillancourt (1985) have studied the sandstone lithology and its relation to galena occurrence. A clay mineralogy analyses showed an increase in the kaolinite/chlorite ratio corresponding to an increase in lead content.

The mineralized grey sandstone has kaolinite as the dominant clay. It is a mature sandstone with medium-to-coarse-grained, well rounded grains. The upper green sandstone is an immature fine-to-medium-grained sandstone. By contrast to the grey sandstone, it is not characterized by pervasive growth of secondary silica around the grain. They contain a greater amount of clay material and as a result, porosity decreases. Coal fragments within the green waste sandstone do not occur as frequently as in the grey sandstone.

2.2.2 Yava west zone mineralization

A number of studies have been done (Bonham, 1983, Vaillancourt and Sangster, 1984) on the Yava mine area in order to understand the control to mineral distribution and localization. Two fundamental aspects must be taken into consideration:

1) Local geological environment,
2) The nature and character of the mineralization itself.

1) Local geological environment

Basement

The underlying basement rocks are of sialic composition (often granitic) containing abundant k-feldspar, considered to be a source rock for lead (Bjorlykke and Sangster, 1981). The lead is not radiogenic: the lead isotope values in ore galena suggest derivation of lead from feldspars in the adjacent feldpar quartz porphyry (Vaillancourt and Sangster, 1986).

The three mineralized zones (west, central and east) exposed at Yava are located in the Canso sediments that overlie paleotopographic depressions within the basement

rock. Mineralization within the sandstone that overlies basement highs is rather unusual. The basement topography is therefore considered as the primary control to mineral distribution.

Host rock

Within the Canso, mineralization is confined to coarse-grained sandstone and the sandy matrix of the conglomerates. Reducing conditions of the host rock (white-grey-green colour) and the presence of organic material are important features. The coal horizons which occur interbedded with the sandstone, generally carry lead grades which are up to twice that of the surrounding sediments (Bonham, 1982). It is felt that the high organic content of these areas lead to highly reducing conditions and this encouraged sulphide precipitation.

The host rock is deposited above an unconformable contact with weathered rock (evidence of emergence during that time of weathering, perhaps pedogenic enrichment).

Spacial local controls

The footwall to ore is considered to be the interface between an impervious floor overlying a porous host rock.

Over most of the deposit, it is marked by the Windsor unconformity. The footwall at few places is, within the sandstone above the Windsor unconformity. Early diagenetic cementation by carbonate sealed the lowermost beds. Effectively, the mineralization is concentrated near the basal unit of the sandstone sequence (Canso Group) within the west zone. For the central and east zones, the mineralization is situated at the Windsor unconformity or near it.

There is no geological hanging wall to the Yava mineralization. It drops off as we move upwards toward the surface.

The flanking margins to the mineralization represent a lateral decrease in grade and ore thickness in a host rock of the same character throughout. In other words, the flanking margins represent the influence of footwall relief (i.e. topographic variations) on grade distribution (Bonham, 1983).

2) Nature and character of mineralization

The mineralization generally occurs as disseminated galena (anhedral crystals) and seems to play the role of cement infilling intergranular areas in the coarse-grained sandstones and sandy matrix of conglomerates in the forms of

bands and patches concordant and discordant to internal sedimentary structures. It does not occur in shale or as replacement of any of the conglomerate clasts. A classification of different mineral styles has been drawn up by Bonham (1983).

Other sulphides such as pyrite and sphalerite are sparsely observed within the Yava deposit. They are generally present in limited calcarous sections in the sandstone where galena is always absent. This can be explained by the following diagenetic events (Bonham, 1983):

- After the deposition of gravel, sand and mudstone, early carbonate cementation sealed the porosity in some areas under low compaction.
- Then, clay silicate cement reduced porosity in areas not already sealed by carbonate.
- Precipitation of first interstitial sulphides (framboidal pyrite and sphalerite) associated with biogenic activity.
- Compaction and pressure solution is responsible for quartz overgrowth (silica cementation).

These diagenic events predate the main galena mineralization; they effectively sealed the porosity and prevented the "deposition" of lead confining it to more porous lithologies.

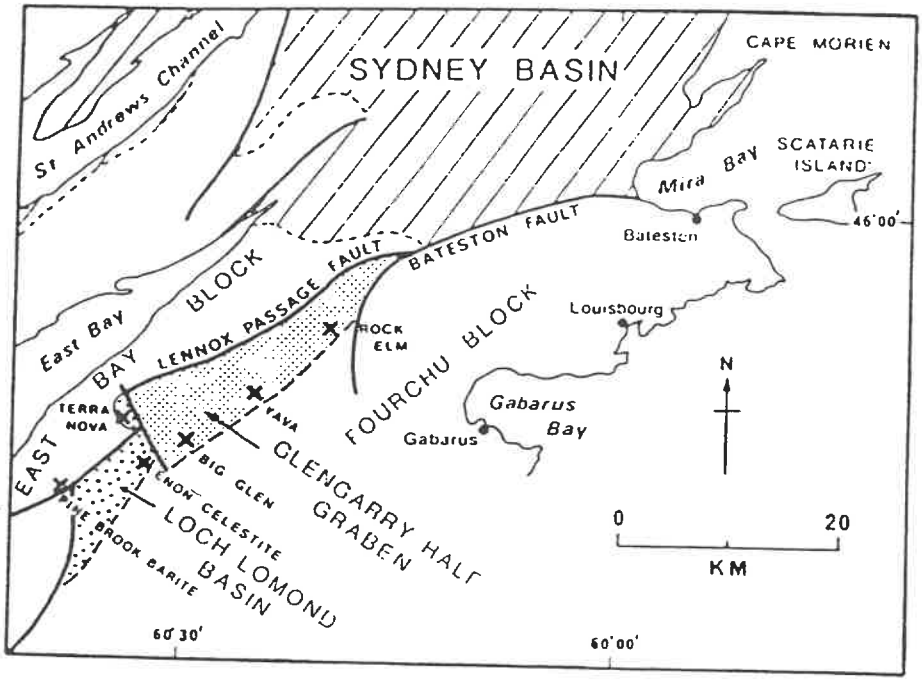


FIGURE 2.1 General geological setting of the Glengarry Half Graben southeastern Cape Breton Island (after Prime and Boehner, 1984).

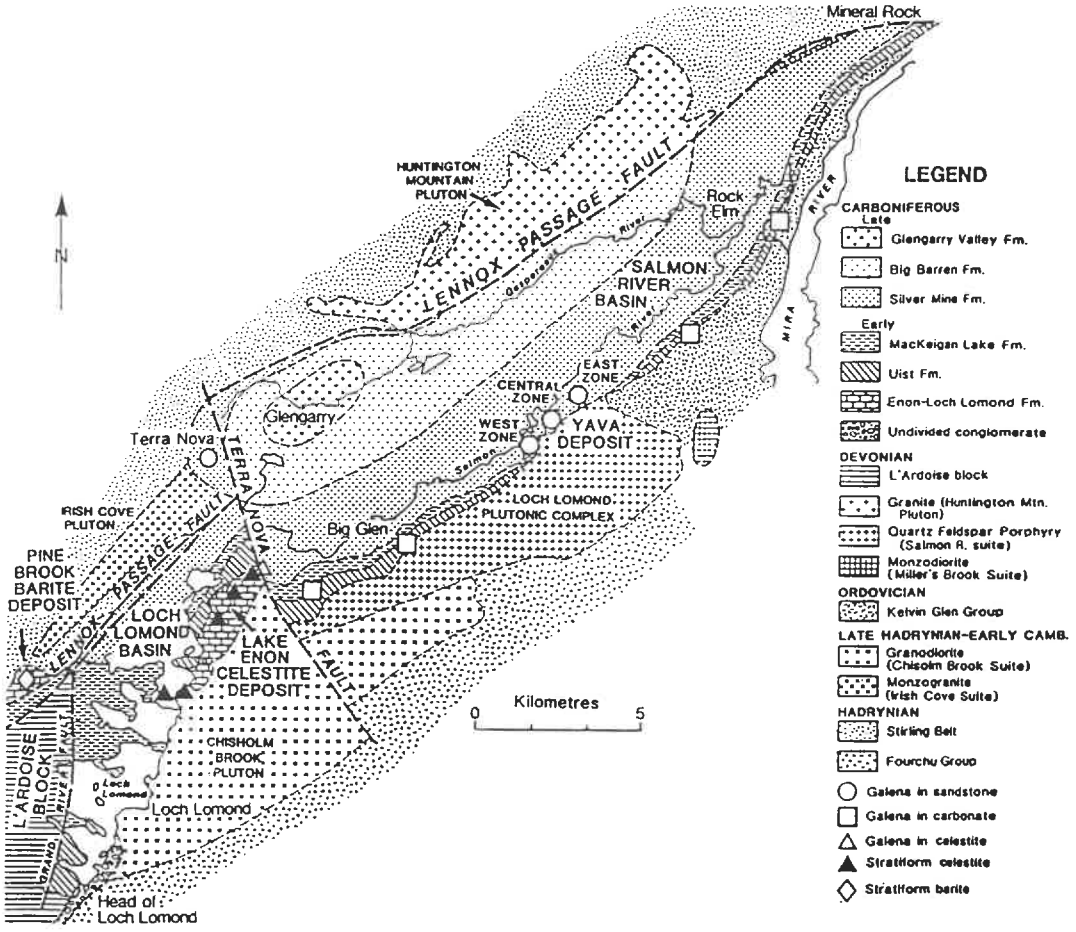


FIGURE 2.2 Geology of the Salmon River Basin and the Loch Lomond Basin (after Vaillancourt and Sangster, 1984).

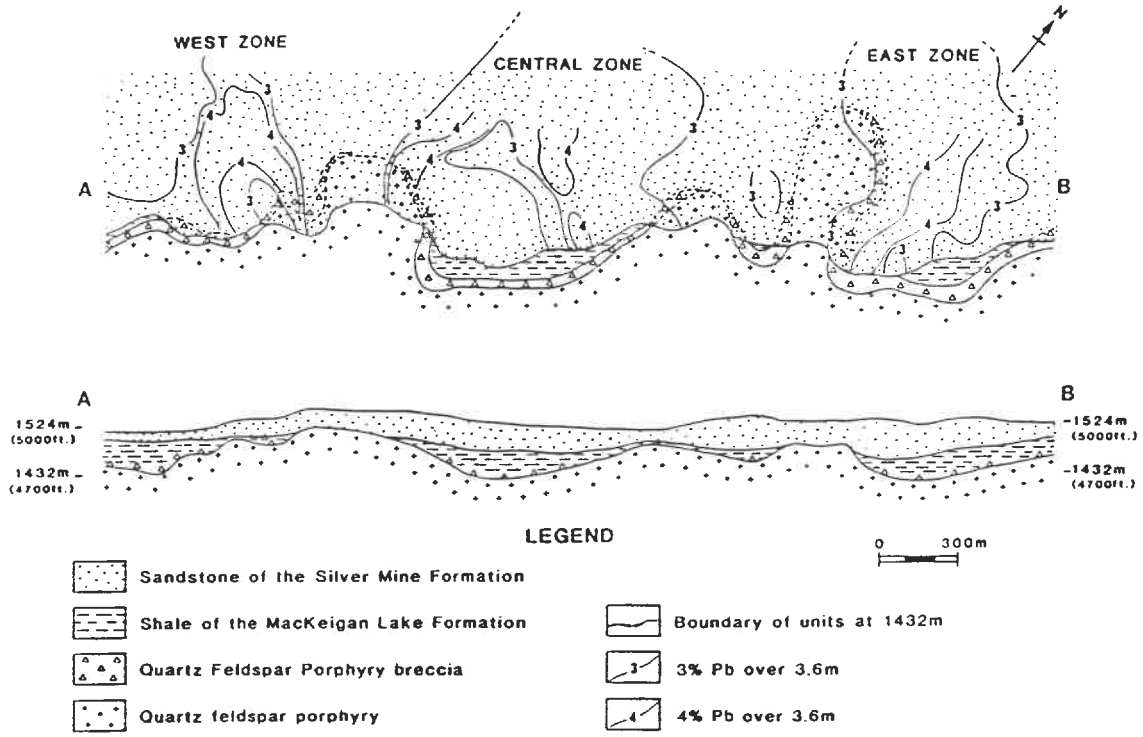


FIGURE 2.3 Map and longitudinal section of the Yava deposit (after Vaillancourt, 1985).

CHAPTER 3

GEOPHYSICAL TECHNIQUES

In this chapter, the logging techniques involved in the survey are described. The nuclear logging techniques including the natural gamma ray and gamma-gamma spectral logging methods are first described, followed by the electrical methods including resistivity, induced polarization (IP) and self potential (SP). Temperature and magnetic susceptibility methods complete the overview of the geophysical techniques.

3.1 Nuclear logging methods

Nuclear borehole logging methods are grouped as either passive or active techniques. In the former, natural gamma radiation from around the borehole is measured by a detector. In the latter, a detector measures the backscattered gamma rays from a radioactive source.

Both techniques were used in the present project and are described in the following sections. For further details on gamma ray nuclear methods, the reader is referred to Killeen (1979) and Halleux (1986).

3.1.1 Natural gamma ray spectral logging method

Basic Theory

Under radioactive equilibrium conditions, the decay rate of a radioactive element is proportional to the quantity of radioelement present. It is then possible to determine the amount of a decay series parent by measuring the radioactivity of any daughter element.

The size of the sample being analyzed in the field is generally defined as the region of rock surrounding the detector from which nearly all detected rays (99%) originate. Figure 3.1 illustrates the volume of investigation that is encountered during measurement (Conaway and Killeen, 1980). The probability of a gamma ray from any disintegrating atom being counted by the detector, decreases rapidly as the distance between that particular atom and the detector increases. It is then easy to understand from this illustration that a zone of radioactive material would be seen by the detector before it reaches it; explaining why response curve rise before the detector reaches the radioactive zone.

The sample volume depends on the gamma ray energy being measured and on the density and absorption coefficient of

the host rock.

Dead time of a gamma ray spectrometer is defined as the time taken by the equipment to analyze a single ray which has been detected. During this period of time, the equipment is busy and cannot analyze any other gamma ray. This time is only a few microseconds but it becomes appreciable at high counting rates.

The true count N can be computed by the following approximation (Killeen, 1979):

$$N = n / (1 - nT) \qquad (3.1)$$

where n: is the measured count
T: dead time

Any survey also requires good counting statistics which means that the number of gamma rays counted in a given measurement must be large enough to be considered as a statistically reliable measurement.

According to Poisson counting statistics, one standard deviation in a counting measurement equals the square root of the count obtained, n:

$$\sigma = \pm\sqrt{n} \qquad (3.2)$$

In the counting rate, (n/t), the standard deviation is:

$$\sigma_{RATE} = \pm\sqrt{n}\ /t = \sqrt{RATE/t} \qquad (3.3)$$

where the counting rate is defined as RATE = n/t (number of

counts per counting time t.

The possible error in the final result is increased when corrections such as background subtraction or spectral stripping are applied. To reduce statistical error, the count rate must be increased. This can be done by increasing the detector size, by moving the detector closer to the source or by counting for a longer time.

For a fixed sampling depth interval, a reduction of the logging speed will improve the counting statistics but as the speed is reduced, geological signal due to inhomogeneities in the rock gain importance. By using a larger sampling interval, the high frequency fluxtuations in each measurement can be reduced. A rule of thumb for the GSC logging system is used: the sampling interval equals one half the detector length.

Gamma rays in nature

Gamma rays originate from radionuclides found in nature, primarily potassium-40 and the uranium-238 and thorium-232 decay series.

Although, potassium has three natural isotopes, only K-40 is radioactive ,emitting a gamma ray with an energy of

1.46 MeV and half life $\tau=1.3*10^9$ years. The ratio (K-40)/(K total) is stable on earth. Measurements of the amount of K-40 are then a direct indication of potassium content.

The major source of potassium is found in igneous rocks such as granite, granodiorite, syenite and rhyolite where potassium feldspars are abundant (microcline 16%K, orthoclase 14%K). Sedimentary rocks also are a source of potassium. Sandstones have an average of 12% feldspar with over 1% of potassium. Potassium in calcareous rocks varies between 0% and 7% with an average of 0.3% (Serra, 1979). Argillaceous minerals have an average potassic content of 2.7% (muscovite 9.8%K, biotite 8.7%K, illite 5.2%K, montmorillonite 0.22%K, kaolinite 0.63%K).

Uranium exists naturally as 3 radioactive isotopes; U-238, U-235, U-234 (daughter isotope of U-238). The final products of the U-238 and U-235 two decay series are stable Pb-206 and Pb-207, respectively. The U-235/U-238 ratio of abundance is about 1/137.8. Therefore, the U-235 decay serie does not emit significant gamma rays for the present purpose. The parent element U-238 does not emit gamma rays but its daughters (Bi-214, Pb-214, Ra-226) when decaying emit most of the gamma ray detected from rocks.

The daughter Bi-214 has a major peak at 1.764 MeV and

is the energy level measured for uranium determination.

Acid igneous rocks are the principal source of uranium. It is also found to a lesser extent in sedimentary rocks; uranium can be easily oxidized by bacteria action and becomes very soluble and mobile until it reaches a reducting environment (Halleux, 1986, Serra, 1979).

Thorium has an unique isotope which has a long half life (Th-232, $\tau = 1.4*10^{10}$ years). The Th-232 decay series ends up with the formation of stable Pb-208. The gamma rays are principally emitted by Tl-208 with its particular energy peak of 2.614 MeV.

Thorium is principally found in acid and intermediate rocks such as granite, pegmatite and syenite. It is a minor constituent of minerals such as apatite, epidote, monazite, sphene and zircon (Halleux, 1986, Serra, 1979).

Natural gamma ray spectral logging method

The natural gamma ray logging method consists of recording gamma rays between 0 and 3 MeV emitted by nuclides in the uranium and thorium decay series and by the radioactive isotope of potassium, K-40.

The gamma ray spectral logging method measures the natural gamma radiation with the added capability of energy discrimination which enables quantificative determinations of radioelements when radioactive equilibrium occurs. Specific window energy range for both U-238 and Th-232 decay series and for K-40 are monitored. Table 3.1 summarizes the different spectral windows used during the survey.

Radioelement	Energy Window range (Mev)	Radioelement energy peak (MeV)	Decay Series
Total Count Window (TC)	0.1 - 3.0		
Potassium-40	1.36-1.56	1.46	
Bismuth -214	1.61- 2.3	1.764	Uranium
Thallium-208	2.4 - 3.0	2.614	Thorium

Table 3.1 Spectral window range

Calibration procedures for gamma ray spectral logging equipment are required in order to make it possible to determine radioelement concentrations from the recorded count rates. The calibration procedure consists of three parts:

1) Determination of stripping factors,

2) Determination of sensitivity factors,

3) Determination of the instrument response characteris-

tics.

1) Determination of stripping factors

Figure 3.2 shows that the uranium window contains gamma rays primarily originating from the U decay series but also from the Th decay series and potassium. Likewise, the thorium window contains gamma rays originating from its own decay series plus those from the U decay series. The potassium window records K gamma rays but also gamma rays originating from the decay series of U and Th.

Figure 3.3 illustrates the interplay between the three radioelement windows and, the stripping factors which are used to correct the recorded count rates are identified.

The stripping factors are applied to the window count rates as follows (Grasty, 1977):

$$Th_s = \frac{Th(1-g\gamma) + U(b\gamma-a) + K(ag-b)}{D} \quad (3.4)$$

$$U_s = \frac{Th(g\beta-\alpha) + U(1-b\beta) + K(b\alpha-g)}{D} \quad (3.5)$$

$$K_s = \frac{Th(\alpha\gamma-\beta) + U(a\beta-\gamma) + K(1-a\alpha)}{D} \quad (3.6)$$

where Th, U, K are the gamma ray intensities recorded in Th, U and K windows, respectively.

Th_s, U_s, K_s are the corrected or stripped gamma ray intensities in the Th, U and K windows.

$$D = 1 - g\gamma - a(\alpha - g\beta) - b(\beta - \alpha\gamma)$$

The factors b and g are often negligible and set to zero simplifying the above equations (Killeen, 1982). The different stripping factors are obtained from calibration model boreholes of different K, U and Th concentrations (see chapter 4).

2) Determination of sensitivities (C factors)

To relate count rates to radioelement content or ore grade, calibration measurements are made in model boreholes in order to determine the sensitivity factors for the K, U and Th windows for a particular probe.

The area beneath a gamma ray log anomaly is proportional to the quantity of radioactive material causing the anomaly (Killeen 1982, Scott et al., 1961). The amplitude of the anomaly is not necessarily proportional to the ore grade unless the ore zone is infinitely thick. However, the area is proportional to the product of the grade and thickness of the radioactive layer;

$$GT = KA \qquad (3.7)$$

where G: average ore grade (ppm or U_r)
T: thickness of layer which is generally considered to be the full-width-half-maximum
A: area under the curve
K: sensitivity factor - constant of proportionality in units of grade / count rate

Ur (Unit of grade): 1%K=2.6 Ur, 1ppm U=1.0 Ur,
1ppm Th=0.477 Ur

Ur being defined as 1 unit of radioelement concentration equivalent to 1 part per million of uranium in equilibrium (valid only for measurements of gamma rays above 0.4 MeV).

The concentrations of potassium, uranium and thorium are then computed using an inverse filtering technique (Killeen, 1982).

3) Determination of the instrument response characteristics

Up to this point, we have applied corrections for the spectral stripping but the anomaly shape of a gamma ray profile does not give the real distribution of the radioactive material along the borehole. In fact, many factors contribute to the response characteristics:

-probe size (length, diameter...),

-logging speed,

-borehole dimensions, fluid content,

-inclination of borehole relative to geology,

-density of the formation fluid...

These factors result in a gamma ray log that appears smoothed. Convolving the input response with an ideal impulse response would give an output that should be closer to the real ore grade profile (Killeen, 1982, Conaway and

Killeen, 1978, and Conaway, 1980).

The shape constant, α, of the geologic response for a given instrument can be determined experimentally in a model borehole containing an infinitely thick monoelemental ore zone (at least 1.0m) adjacent to infinitely thick barren zone (1.2m).

The model borehole is logged slowly from the barren zone into the ore zone with a small sampling interval (Δz=1 or 2cm) so the counting statistics within these intervals are acceptable. The impulse response of the instrument seen in figure 3.4d is obtained by the derivative of the step response log:

$$\Phi(z_i) = \frac{C(z_i) - C(z_i)}{\Delta z \ (C_{max} - C_{min})} \qquad (3.8)$$

where C(z) is the step response and, C_{max} and C_{min} are the asymptotic maximum and minimum of the step response curve (figure 3.4c).

Computed theoretical geologic impulse response for a point detector using different values of α (figure 3.4a) were modified to incorporate the detector length, L (figure 3.4b). The best fit of one of these type curves with the experimental data gives the best value of α for that

detector (figure 3.4d).

In the convolution procedure, a digital inverse filter is used (Conaway and Killeen, 1978) and since it is a high pass filter, any noise that exists will be amplified by a factor which increases with increasing frequency (Bristow et al., 1984). Accordingly, it is often useful to use a smoothing filter (low pass filter). To allow a single pass operation on the data, this smoothing filter is first convolved with the inverse filter.

3.1.2 Gamma-gamma spectral logging method (density method)

The gamma-gamma spectral logging method involves gamma rays emitted from an artificial source in the borehole probe interacting with matter in the borehole walls and scattered back to the detector.

The gamma rays will penetrate a layer of rock, dx with an intensity, I_o, and will be scattered and/or absorbed in the rock. The attenuation, dI may be defined as follows:

$$dI = \nu I dx \qquad (3.9)$$

which can be rewritten as:

$$I = I_o \, e^{-\nu x}$$

where ν is defined as an attenuation coefficient that depends on the type of material (number and type of

atoms/unit volume) and on the photon energies.

Gamma radiation interacts with matter according to Compton scattering, photoelectric effect and pair production. For the purpose of this project, we will consider interactions in common rocks (Z between 12 and 18). Compton scattering occurs when a photon (gamma ray) strikes an electron and imparts some of its energy to it. The photon is scattered at an angle to its original direction and the electron is expelled (figure 3.5a). This type of interaction predominates at moderate energies (figure 3.6).

The photoelectric effect occurs if the photon energy is higher than the energy of the bound electron. The photon gives up all its energy in ejecting the bound electron from the atom (figure 3.5b). This interaction predominates at low energy (< 0.2Mev) with atoms of high atomic number, Z (figure 3.6).

The proportion in which these two main interactions occur depends on gamma ray energy and the equivalent atomic number of the medium, Zeq. Zeq is defined as the atomic number of the element having the same ratio of Compton attenuation to photoelectric attenuation as the complex media such as rocks for a given photon energy.

A third type of interaction which is rare in common rock is pair production. It requires large values of Zeq and gamma rays having energies higher than 1.022 MeV (figures 3.5 and 3.6).

Therefore, the attenuation coefficient is defined as follows:

$$\nu = \nu_{ph} + \nu_c + \nu_p \qquad (3.10)$$

where ν_{ph}: photoelectric attenuation coefficient
ν_c : Compton attenuation coefficient
ν_p : pair production attenuation coefficient

Pair production which occurs at high energies does not play an important role in the interaction of gamma rays in common rocks so that the attenuation coefficient ν_p is not notable.

Below 0.2 MeV the influence of photoelectric absorption becomes important. Tittman and Wahl (1965) have found that the absorption coefficient, ν_{ph}, is related to the material atomic number and the photon energy:

$$\nu_{ph} \simeq Z^{3.6}/E^3 \qquad (3.11)$$

If the mode of interaction is confined to compton scattering alone (energy between 0.2-2 MeV) the atomic number, Z of different mediums does not affect the attenuation coefficients, ν_c. Then, the only property of

the medium required to characterize it is its bulk density.

The tool response is related to formation electron density, ρ_e, (the method measures counts from the attenuation of gamma rays traversing the formation) which is related to bulk density, ρ_b, as follows:

$$\rho_e = \rho_b (Z/A) N \qquad (3.12)$$

where Z/A is the ratio of the number of electrons per atom (atomic number to the atomic weight)
N is Avogadro's number ($6.02*10^{23} mole^{-1}$)

Z/A is approximately equal to 0.5 for most of the elements and common rocks (Perrin, 1981). Hydrogen is an exception with Z/A=1. However, in H_2O, the hydrogen contributes relatively little to the Z/A value of the molecule (Z/A=0.555).

The electron density is then proportional to the bulk density of the formation and so the intensity of backscattered gamma rays is also related to the formation density. As the density of the formation increases, the number of scattered gamma rays decreases.

The spectrum of backscattered gamma rays in figure 3.7 illustrates the discussed relations between the gamma ray energy levels and the atomic number and density of the scattering medium. Below 0.2 MeV where photoelectric

interaction takes place the spectrum is modified. As the atomic number of mediums with the same density decreases, the spectrum intensity increases. Above 0.2 MeV, where compton scattering alone occurs, the spectrum is not affected by Z changes.

Finally, figure 3.7 shows that the spectrum is affected by the density of the medium. The intensity of a spectrum is increased as the density decreases.

The ratio of count rates in the high energy range (affected by density changes, but not Z changes) to the count rate in a low energy range gives a parameter which is sensitive to photoelectric absorption effect alone. Such a ratio would distinguish heavy element concentrations. An increase in the ratio reflects an increase in the photoelectric effect associated with an increase in the atomic number, Z which is associated with an increase of the heavy element concentration.

This spectral ratio may be used for in situ assaying of heavy elements such as barite and lead.

Similarly to the natural gamma ray method, the gamma-gamma spectral method is affected by many factors such as dead time and logging speed. These were considered to

improve the precision of the technique.

The gamma-gamma density data is commonly used to determine the porosity and the compaction of the rocks. The density data may also be used for lithological determination.

At the Geological Survey of Canada, the method is principally used for determining lithological variations. And as just mentioned, the gamma-gamma spectral ratio parameter opens doors to heavy element assaying.

3.2 Electrical methods

Electrical prospecting includes several techniques which could be separated into two major categories; natural and artificial electrical methods. The electrical techniques that use natural electrical and electromagnetic fields include magnetotellurics, telluric current and self potential. Those that require electric currents or fields which are introduced into the earth artificially include electromagnetic (EM), electrical resistivity and induced polarization.

Electrical resistivity, induced polarization and self potential are the electrical techniques used in the present

logging. They will be described separately in the following sections.

3.2.1 Electrical resistivity logging method

The direct current resistivity method is one of the oldest geophysical techniques. It has been applied to a wide variety of exploration problems being most successful and beneficial in mining, groundwater and engineering applications.

If two electrodes are inserted into the ground and an external voltage is applied to them, a current flow will pass through the ground from one to the other creating equipotential lines (perpendicular to current flow lines, figure 3.8).

If a current, I, is injected from a surface electrode into an homogeneous half-space of resistivity, ρ, the potential at a point on the surface, a distance r from the source would be:

$$V_p = \frac{I\rho}{2\pi} \frac{1}{r} \qquad (3.13)$$

where ρ is the resistivity, a measure of a substance's ability to resist the flow of electrical current (The resistance of a block of material increases with the

distance that the current must flow and decreases with greater cross-sectional area. The block's resistivity is defined as ρ=AV/LI according to Ohm's law that states that V=RI, A:area, L:length the current flows).

The measurements of V_p will indicate the nature and the distribution of electrical resistivities underground. Conductive bodies tend to concentrate electric currents while resistive bodies cause the current to flow around them which would disturb the "ideal" equipotential lines.

Because the resistivity measured varies with the electrode configuration, it is convenient to define the apparent resistivity ρ_a:

$$\rho_a = \frac{k\ V_p}{I} \qquad (3.14)$$

where k is the geometric factor that depends on the electrode configuration.

In a non homogeneous subsurface (stratified subsurface for example), the apparent resistivity measured is the resistivity of an equivalent homogeneous subsurface. The apparent resistivity is measured in ohm-metre (Ω-m).

Two electrode arrays were used during the logging: inverted normal and micronormal. Figure 3.9 shows the

configuration of these arrays. The geometric factor k for these two arrays is given by:

$$k = 4\pi R_1 R_2 / (R_2 - R_1) \qquad (3.15)$$

where R_1 = AM spacing
R_2 = AN spacing
and A,B current electrodes B being placed at infinity at surface
M,N potential electrodes.

Roy and Dhar (1971) have studied the volume of rock investigated by resistivity logging for different electrode arrays. Considering a thin cylindrical shell of homogeneous ground having its axis coincident with the probe axis, they have stated that the contribution of the shell usually begins with a small value for small values of shell radii and goes through a few extremes before falling to zero at large radii (figure 3.10). The radius of investigation of the probe was defined as the radius at which the contribution of the cylindrical shell is a maximum (with the same sign as the total measured signal).

For the normal array, the radius of investigation is at r=0.6AM. The response is to a fair extent independent of the material between r=0 and 0.22AM. Thus, for a long electrode spacing, the influence of the borehole should be small.

Roy and Dhar (1971) have compared the radius of investigation for different arrays and have found that the normal array has the largest radius of investigation for a constant value of the AM spacing. The radius of investigation of the micronormal array would be very similar to that of the normal array.

The typical log obtained for a normal or micronormal array is symmetrical about the median plane of layers. When the thickness of a resistive layer is greater than the AM spacing (figure 3.11a) the profile is symmetrical but the apparent thickness t_a is smaller than the real thickness t_r ($t_r = t_a + AM$).

When the thickness of a resistive layer is smaller than the AM spacing, the profile is characterized by a minimum in the middle of the layer and symmetrical maxima (see figure 3.11b, maxima 1 and 2). The real thickness is obtained by $t_r = t_{1,2} - AM$. The apparent resistivity of the layer is reversed. It seems more conductive than its neighbours and this is accentuated as the resistivity of the layer is increased.

For very resistive layers, the profile has a symmetrical bell shape (figure 3.11e).

In conductive layers (figure 3.11c-d), the apparent thickness is greater than the real thickness ($t_r = t_a - AM$) and as the thickness decreases, the less it is possible to discriminate it from its resistive neighbours.

The bed resolution of these arrays is a function of the electrode spacing. The normal and the micronormal logs cannot detect resistive layers of thickness which is less than the potential electrodes spacing (Urbancic,1985).

3.2.2 Induced polarization logging method (IP)

Although the Induced Polarization (IP) phenomena was described by Schlumberger in the early 1920, it is still not completely understood. The mechanisms which would explain induced polarization are complex but most authors agree that they include interactions at the contact of solid particles and electrolytic solutions present in the ground.

When a current is injected into the ground, the surface charges of the solid particles induce in the solution an ion concentration of opposite sign close to the particles's interface and forms a double electric layer (the ions are practically immobilized, creating a barrier to the passage of ions which carry the current). When the current is turned off, the initial equilibrium is reestablished, the

double layer is discharged, the ions start to return to their equilibrium positions. This relaxation constitutes a charge flow that can be measured as a decaying polarization potential (Sumner, 1976).

The principal mechanisms that cause the IP phenomena are electrode polarization (overvoltage) and membrane polarization (electrolytic IP). The former is generally larger than the latter and depends on the presence of metallic minerals in the rock (figure 3.12a). Minerals which exhibit electrode polarization include almost all sulphides (except sphalerite and possibly cinnabar and stibnite, Telford et al., 1976) graphite, and some oxides such as magnetite, ilmenite, pyrolusite, cassiterite.

The magnitude of the electrode polarization response depends on many factors such as the relative amount and nature of the mineral, the grain size, and the nature of the electrolyte present. Since IP is a surface phenomenon, the response is larger when the mineral is disseminated than when it is massive.

Membrane polarization constitutes the background or so-called normal IP effect and may occur in rocks which do not contain metallic minerals (figure 3.12b). The nature of the solid-electrolyte interface (clay minerals...) and the

ion concentrations of the electrolyte are important factors that influence the magnitude of the response.

The electrode and membrane polarization are indistinguishable by IP measurements and they appear to be independent of the atomic or molecular structure in rocks and minerals. Only the contact between solid particles and electrolytes is important.

The IP method can be operated in both time domain (transient pulse) or frequency domain. In time domain technique which was used here, a direct current is injected with alternating polarity into the ground between electrodes A and B, and measuring the potential between electrodes M and N. The IP parameter is analysed during the current off period.

The IP phenomena is characterized by a potential discharge when the current is cut off and is represented by a potential discharge curve in figure 3.13. The integration of potential values for a certain time on this discharge curve, normalized to the primary potential, V_p, measured when the current was on, defines the chargeability parameter m.

$$m = \frac{1}{V_p} \int_{T_1}^{T_2} Vt\,(t)dt \qquad (3.16)$$

where V_p: measured steady voltage during the current flow interval
V_t: potential variation measured at a time, t, after the current is cut off (potential measured during the discharge)
T_1, T_2: time after the cut off between which we want to integrate (define an integration interval)

The chargeability, m, is expressed in milliVolts/Volts.

To improve the signal-to-noise ratio, a number of waveforms may be stacked and the chargeability parameter is determined from the stacked waveform.

In the frequency domain, a steady state a.c. of variable frequency is used rather than the interrupted d.c. IP is determined from resistivity measurements at different frequencies.

The IP parameter is called the frequency effect, f_e which is defined as:

$$f_e = (\rho_{dc} - \rho_{ac}) / \rho_{ac} \qquad (3.17)$$

where ρ_{ac} apparent resistivity measured at very high frequency
ρ_{dc} apparent resistivity measured at dc.

In practice, measurements are made for few frequencies in the range of 0.1 to 10Hz and ρ_{dc} is taken as the value obtained at the lowest frequency.

Generally, the arrays, the electrodes spacing and the

radius of investigation are the same as for the resistivity logging. The shape of the anomaly associated with a polarizable body with a known dip and depth, will also depend on the electrode configuration used (Mwenifumbo, 1986).

Similarly to resistivity, IP logs are useful for stratigraphic correlation. They have often been used in base metal exploration to locate disseminated sulfides. In coal exploration, IP logs have been used to estimate coal quality and/or sulphur content (J. Roy, 1984).

3.2.3 Self potential logging method (SP)

Self potentials (SP) are natural potentials that occur in the earth. They reflect an imbalance of ions principally caused by electrochemical effect. This mechanism is briefly described below. For further information about SP generating mechanisms, the reader is referred to Poldini (1938), Sato and Mooney (1960) and Roy (1984).

The most detailed study of the electrochemical mechanism so far is that proposed by Sato and Mooney (1960). In the presence of an electronic conductor (electrolytes in the country rock) there must exist an exchange of electrons and ions at their boundary.

Sato and Mooney (1960) have stated that the electrochemical mechanism can be explained by two electrochemical half-cell reactions, one cathodic above the water table and the other anodic at depth (figure 3.14). In the cathodic half-cell, the substance in solution is reduced (oxidizing environment which gains electrons) while in the anode cell, the reducing environment, loses electrons. The ore body being a good conductor, transports electrons from the anode to the cathode.

The flow pattern created is characterized by a negative potential over the ore body (figure 3.14a). Figure 3.15 presents typical potential curves for SP borehole logging.

The magnitude of the SP anomaly is determined by the difference in the oxidation potential [Eh] between the two half-cell solutions. Generally, amplitudes range from a few millivolts to one volt. Sato and Mooney (1960) give maximum possible potentials for various sources, such as graphite (0.78V), pyrite (0.73V) and galena (0.33V). Potentials as large as 1.5V has been reported over a graphite body (Telford et al., 1976).

Most of the sulphides with the exception of sphalerite, cinnabar and stibnite are good conductors and give SP anomalies. SP anomalies have, however, been observed over

sphalerite which may behave as a semi-conductor (Telford et al., 1976).

The measurement of SP is quite simple. A potential difference is measured between a pair of electrodes connected by a wire to a millivoltmeter that has a sufficiently high input impedance (greater than 10^8 ohms). Nonpolarizing electrodes are essential for accurate readings; the use of metal stakes in the ground may create potentials of the same size as those being measured (electrochemical action at the ground contacts).

In borehole logging, the SP equipment is still very simple. A recording potentiometer is connected across two electrodes, one at the surface being the reference electrode while the other is moved in the borehole.

Sometimes, the SP gradient between two downhole electrodes is measured. It shows sharp deflections at the edge of the mineral zones. The electrode spacing determines the minimum ore body width which can be detected.

Possible discrepancies in potential measurements may be caused by difference in temperature between both electrodes producing a baseline shift along the borehole. This tempe-rature difference may arise during summer surveys when

the difference between the surface and downhole can reach 20°C.

A baseline drift due to a change in the background potential either suddenly or gradually may occur along the hole. It may be due to a change in rock type.

Erratic readings were also observed near surface if the borehole casing was still in place or if the electrode came out of water (Becker and Telford, 1965) and should be disregarded.

SP logging is used in numerous applications:

.localization of porous formations,

.lithologic correlations,

.determination of water gas contact and oil gas saturation in shaly sands,

.and sulphide exploration,

but today the SP generating mechanisms are still considered more complex than what was explained here and are not totally understood. The interpretation of SP anomalies should then be made with caution.

3.3 Temperature logging methods

The temperature and temperature gradient (first derivative of temperature measurements) methods are used to provide information on heat flow pattern from the earth, radioactive and geochemical heat sources and sinks for waste management studies, groundwater flow and, in some cases, as an aid in stratigraphic correlation (Bristow and Conaway, 1984, Urbancic, 1985).

Continuous temperature logs are now commonly used. As the probe is lowered down the hole, the measured temperature log is degraded by the effect of the probe time constant and has to be compensated.

The thermal sensor (chapter 4.4) has an exponential time response to a step change in temperature. If the time constant T is defined as the time required for the system to reach (1-1/e) of the final temperature, then the sensor's impulse response w(t) is defined as (Bristow and Conaway, 1984):

$$w(t) = \frac{1}{T} e^{(-t/T)} \qquad (3.18)$$

where T is the time constant of the system.

For high resolution, Conaway (1977) derived from

Costain (1970) an approximate inverse filter which is designed to remove the smearing effect of the thermal time constant. It has been expressed in discrete form by the 3-term derived deconvolution operator,

$$(T/2\Delta t , 1 , -T/2\Delta t) \qquad (3.19)$$

This operator can be combined by convolution with a suitable smoothing filter (e.g. Savitzky-Golay least squares polynomial filter) to give a suitable temperature log (Savitzky and Golay, 1964).

A Savitzky-Golay derivative operator (Savitzky and Golay, 1964) may be combined by convolution with the deconvolved and smoothed operators to produce a single operator which, when convolved with the measured temperature log, gives a smoothed deconvolved gradient temperature log. In most cases, the temperature gradient log is a "better" indicator of lithologic variations, contact and fracture location.

Beck (1976) and Conaway (1977) found that temperature gradient logs are a good approximation of thermal resistivity logs. The heat flow along a thermally stable borehole rarely deviates more than 20 percent from a mean equilibrium in the absence of disturbing factors such as

heat sources and sinks. Under these conditions, the thermal gradient is inversely proportional to thermal conductivity, k, of the formation ($q = -k\ gradT^{o}$ where q is the heat flow measured in Watts/m^2 (SI unit)).

The resolution of the method is limited by the noise level and may not be improved with the use of deconvolution and smoothing filters. Noise may be divided into three categories (Conaway and Beck, 1977):

.Instrumental noise which includes electrical and mechanical equipment effects (cable-stretch, depth monitoring, inductive or capacitive pick up in logging cable...),

.Transient thermal disturbances (convection, nonequilibrium thermal regime and ground water flows,

.Geological noise encompasses all steady state sources of geothermal noise (variations in heat flow along the borehole due to radioactive or geochemical heat sources and sinks.

Few studies have investigated the application of temperature and temperature gradient to stratigraphic mapping. Beck (1976) investigated the application for temperature gradient logs to stratigraphic correlation in comparison with electrical resistivity logs. He found an inverse correlation between temperature gradient logs and

electrical resistivity logs except within coal seams where strong positive correlations were pointed out. He also used temperature logs to correct a lithologic horizon that was presumedly mispicked by nearly 100m on the electrical logs.

Conaway and Beck (1977) found good correlations between temperature gradient logs and geological logs. In cases where the thermal resistivity contrast is 50-100%, an isolated strata as thin as 0.5m shows up on the temperature log. In a few cases, a gradient contrast on the order of 1°C/Km over several metres were resolved.

Reiter et al (1980) carried out qualitative correlation of temperature logs with other types of logs including inductive conductivity, gamma ray, seismic, bulk density and lithologic logs. Correlations were done in a variety of sedimentary rocks and generally, they found that shaly and clayey zones (identified as increases in gamma ray, and decreases in density and resistivity) have higher temperature gradients (lower thermal conductivity) compared to more sandy layers with lower temperature gradients. The temperature gradient logs seem to qualitatively correlate best with inductive conductivity logs.

3.4 Magnetic susceptibility method (MS)

Magnetic susceptibity (MS) well logging was first investigated by Broding et al (1952) in the early 1950's, but little research was reported except in the U.S.S.R. until the late 1960's and early 1970's (George and Scott, 1982). During 1970's and 1980's an effort was made to improve the instrumentation. The availability of an accurate magnetic susceptibility logging tool reduces the measurement time and provides a more representative bulk sample than drill core.

Magnetic susceptibility is based on the principle of electromagnetic induction.

The magnetic induction $\vec{B}$ is given as:

$$\vec{B} = \vec{H} + 4\pi\vec{I} \qquad (3.20)$$

where $\vec{H}$: external magnetic field (gauss)
$\vec{I}$: Magnetic polarization: magnetic moment per unit volume (gauss)
$\vec{B}$: (in gauss)
1 gauss = 1 oersted

The magnetic permeability of a substance, μ, is defined as the ratio of the magnetic induction to the magnetic field intensity:

$$\mu = \vec{B}/\vec{H} = (1 + 4\pi\vec{I}/\vec{H}) \qquad (3.21)$$

The magnetic susceptibility which describes the

magnetizing ability of a substance is defined as:

$$k = \vec{I}/\vec{H} \qquad (3.22)$$

and can be expressed as a component of the permeability:

$$\mu = (1 + 4\pi k) \qquad (3.23)$$

k is dimensionless and there is an equivalence for the SI and c.g.s. systems:

$$k[SI] = 4\pi k[c.g.s.]$$

As the magnetic susceptibility value of a material increases, the easier it becomes magnetized.

The principle of operation of the equipment is based on electromagnetic induction. The probe contains a single copper coil wound around a ferrite core. When the system is in operation, a magnetic flux emanates from the ends of the ferrite core and couples with the rock formations surrounding the borehole. The flux density is then affected by the amount of magnetic material contained within the rock changing the apparent inductance of the coil that is related to magnetic susceptibility. The apparent resistance of the coil is also affected and is related to the electrical conductivity of the rock.

In low to medium concentration of magnetic materials, the change in inductance of the coil is proportional to the

ferrimagnetic content but at higher concentration the relationship is more complex. MS increases non-linearly as the volume of ferrimagnetic material increases.

Few sources of errors that reduce the accuracy of MS measurements have been observed (George and Scott, 1982). They are discussed in the following, and correction procedures are given.

The tool is sensitive to the hole size and to the radial position of the probe within the hole (George and Scott, 1982). But when the coil diameter is bigger than half size the borehole diameter, and the boreholes are vertical (the probe is centred in the borehole), the effect is negligeable and corrections are not needed. The Yava data in this project were acquired in such holes and did not require corrections.

Baseline drift can be seen as the deviation of a measurement from the true value. Electronically, baseline drift is a reflection of an imbalance within the Maxwell bridge circuitry. This imbalance occurs because of the inductive characteristics of the coil. It is prominent within high sensitivity ranges.

The main cause of drift is due to temperature

variations within the borehole and surrounding the surface equipment. Small temperature variations within the borehole affect the probe electronics and may change the inductance of the coil that will unbalance the bridge circuitry. Surface processing units are subject to considerable temperature changes and have been known to cause baseline drift. Changes in pressure on the coil in the probe can also cause baseline drift in the signal level.

Baseline drift can be corrected by computer processing. With the Least Squares Method, the best baseline drift fit is found and subtracted from the MS log.

The electrical conductivity of rocks influence magnetic susceptibilities. It creates losses in the detector coil causing an imbalance in the bridge. If the imbalance is too large to be compensated an overload will occur. If the eddy currents induced in the formation are strong and broad, the induced out of phase component becomes noticeable and is inseparable from the susceptibility signal.

The conductivity limit depends on the coil design. Short coils tolerate higher conductivity but are not as sensitive as long coils.

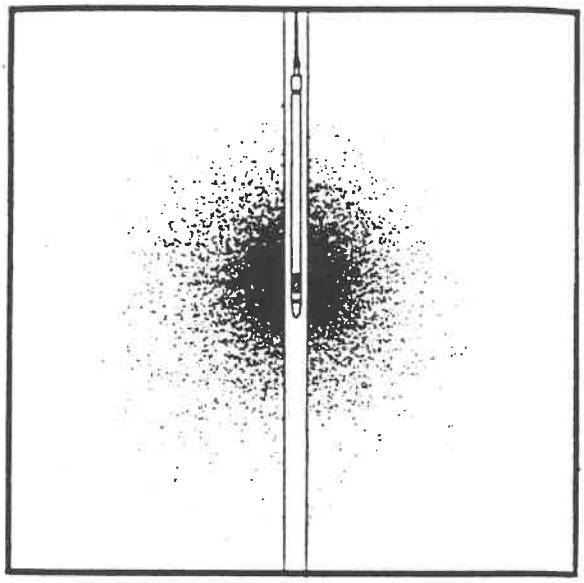


FIGURE 3.1 Volume of investigation encountered during recording (after Conaway and Killeen, 1980).

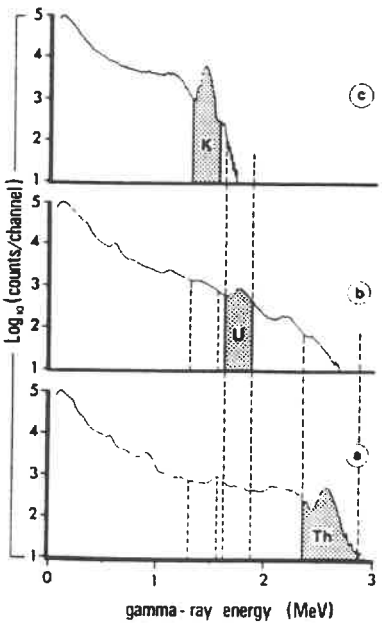


FIGURE 3.2 Gamma ray spectrum recorded in:
a) a thorium zone of a model borehole
b) an uranium zone of a model borehole
c) a potassium zone of a model borehole
The detector used was a 32x125mm sodium iodide detector. The dotted lines illustrate the interference (after Killeen, 1982).

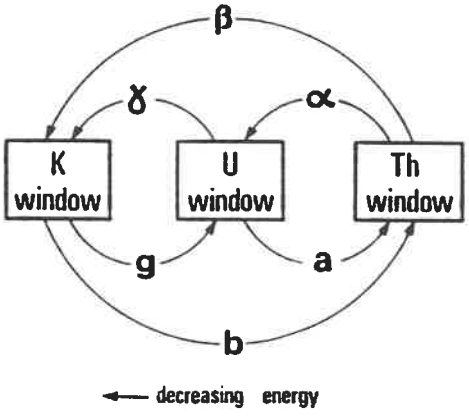


FIGURE 3.3 Interplay between the three radioelement windows; α, β, γ, a, b, g being the stripping factors (after Killeen, 1982).

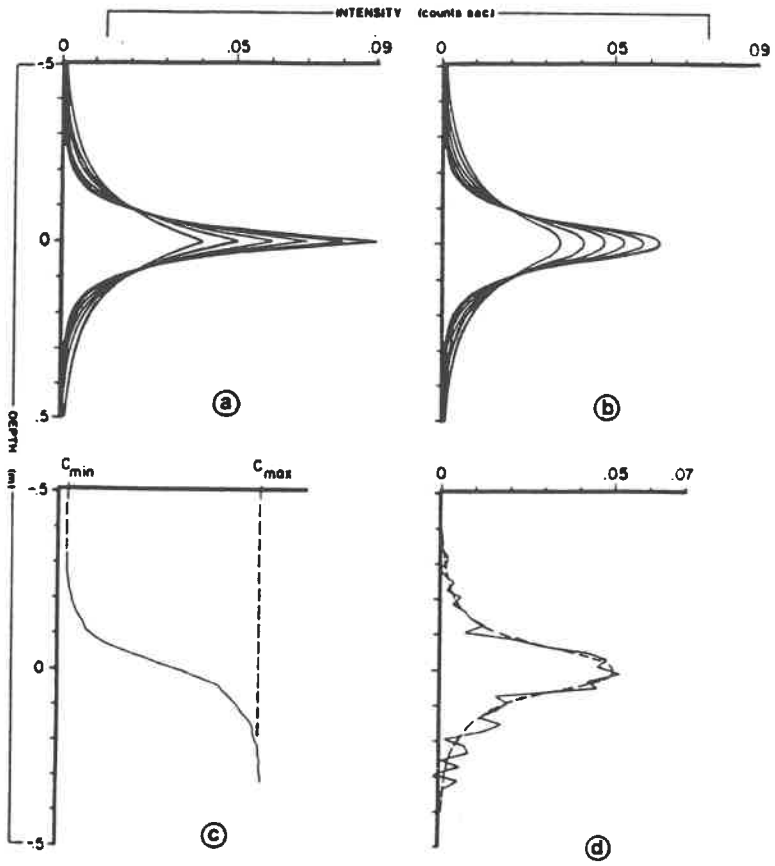


FIGURE 3.4 Determination of the system constant α (after Killeen, 1982)

a) A family of geological impulse responses curves computed from equation $\bar{g}(z) = \alpha e^{-\alpha z}/2$ for values of α from 0.08 to 0.18 in step of 0.002.

b) The type curves of (a) modified to take detector length into account. In this particular example the detector length was 9cm. These curves were obtained by convolving the curves in (a) with the rectangular pulse of length L (see Conaway and Killeen, 1978).

c) The measured gamma ray log with a 9cm detector when passing from the barren zone into the ore zone.

d) The impulse response is derived from the measured response in (c) by numerical differentiation:
$(\bar{g}(z_i) = (Cz_{i+1} - Cz_i)/(\Delta z(C_{max} - C_{min}))$
-"full line"). The best fitting curve from (b) is overlain on the derived impulse response and the value of α is then considered to be the best for that detector.

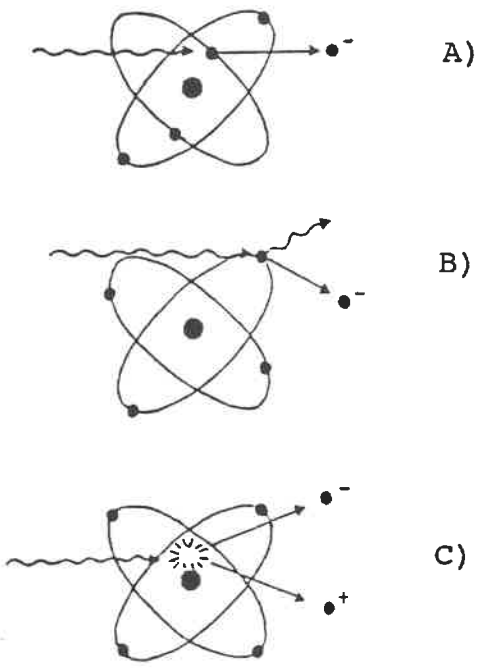


FIGURE 3.5 Types of gamma ray interaction with matter (after Halleux, 1986).

a) Photoelectric effect: the photon is absorbed and an electron is ejected.
b) Compton scattering : the photon imparts some of its energy and is scattered at an angle to its original direction, an electron is expelled.
c) Pair production: the photon is destroyed; an electron and a positron are created.

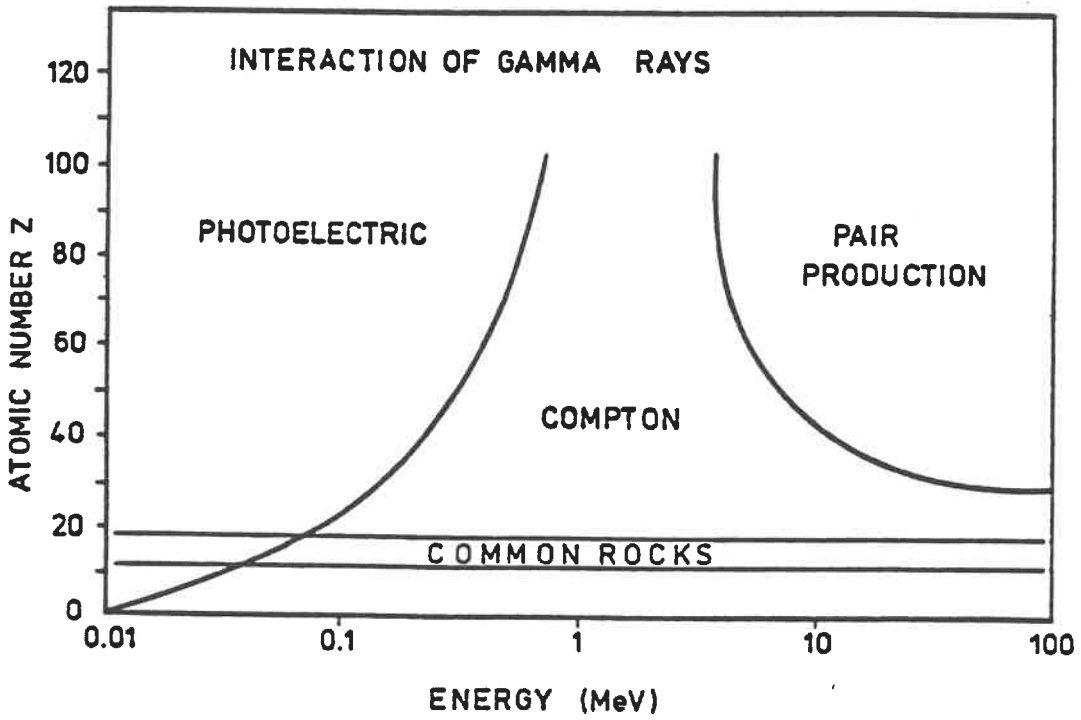


FIGURE 3.6 Gamma ray interactions with matter in relation with gamma ray energies and equivalent atomic number of the material (after Dodds and Eschilman, 1972).

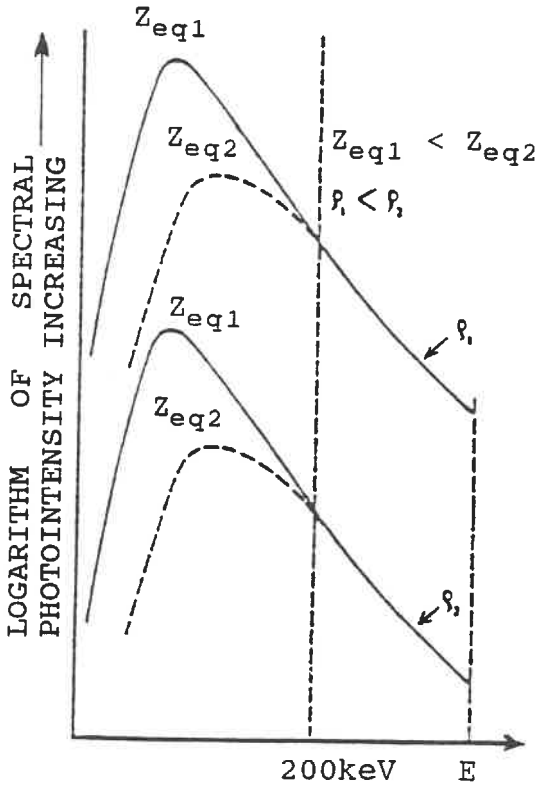
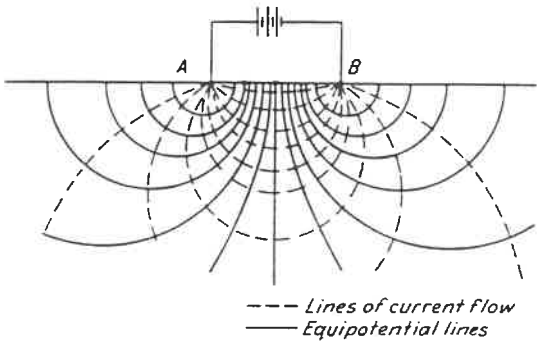
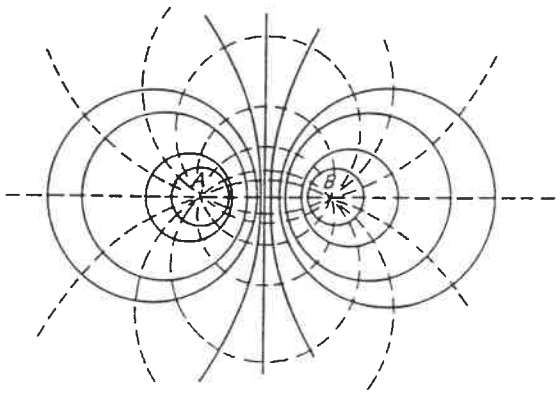


FIGURE 3.7 Spectrum of backscattered gamma rays related to Z changes (in low energy range) and to the formation density.



A)



B)

FIGURE 3.8 Equipotential lines and flow lines (after Dobrin and Savit, 1988).
a) In the vertical plane, below the surface
b) On plane of the earth's surface
(A, B are the current electrodes)

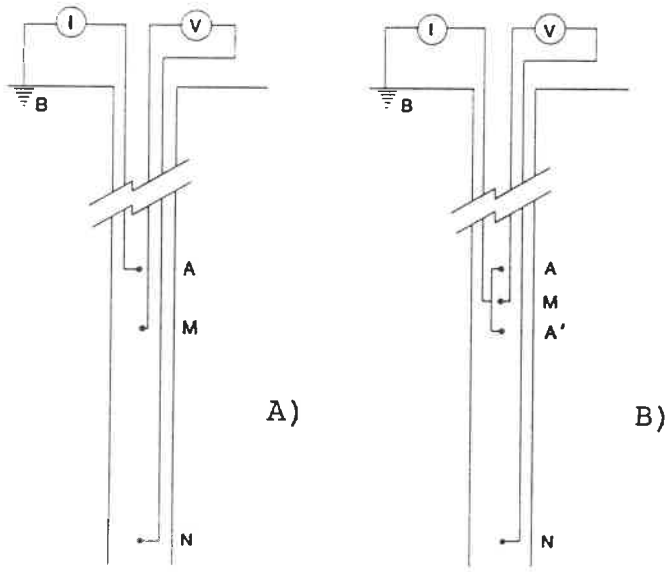


FIGURE 3.9 Electrodes arrays for the electrical borehole logging.
a) Normal array (inverted) AM=40cm, MN=2.6m
b) Micronormal array AM=A'M=10cm, A'N=2.6m
A and B are the current electrodes
M and N are the potential electrodes

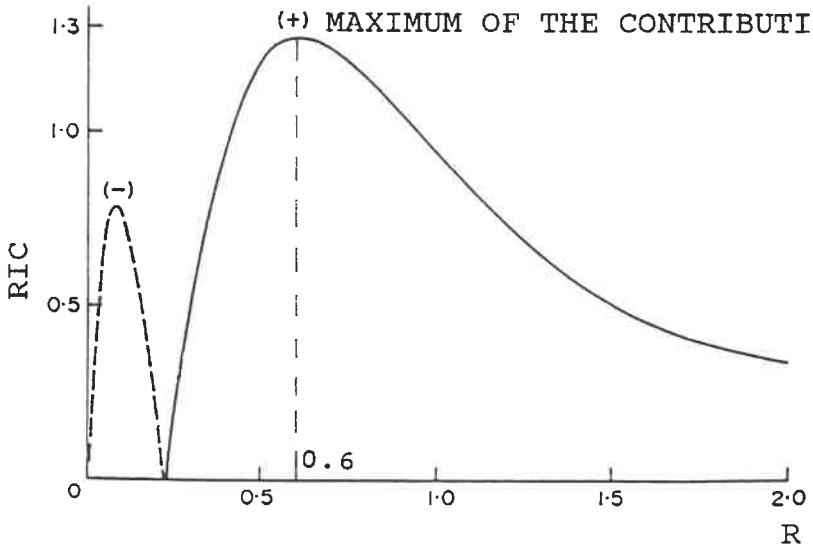


FIGURE 3.10 Radius of investigation for the normal array with AM = L = 1 (after Roy and Dhar, 1971).
R : Radius distance from borehole axis
RIC: Contribution of the cylindrical shell of homogeneous ground to the total measured signal.

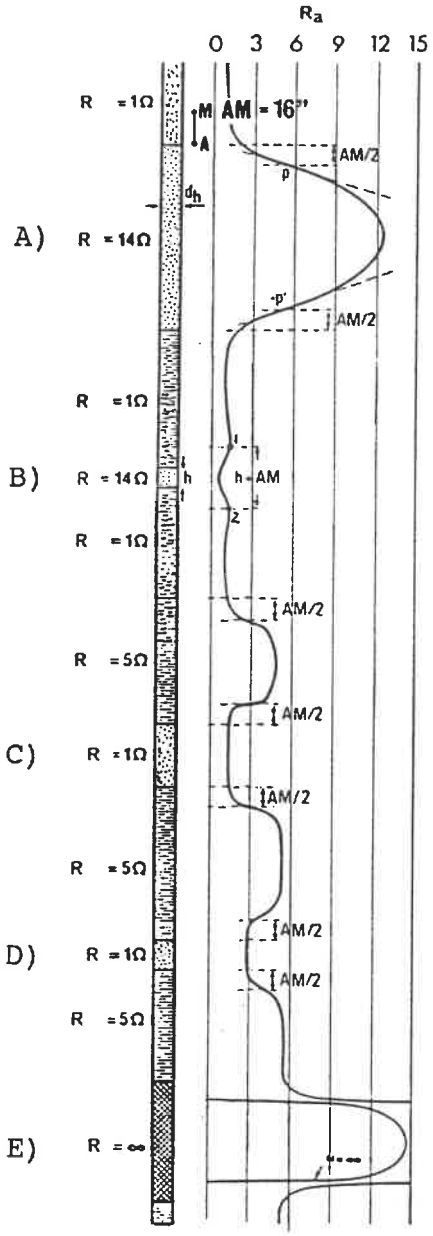


FIGURE 3.11 Apparent resistivity profile for the normal array as a function of resistivity and thickness layers (after Serra, 1979)

a) Resistive layer thicker than the AM spacing
b) Resistive layer with thickness smaller than the AM spacing
c) Conductive layer thicker than the AM spacing
d) Conductive layer with thickness smaller than the AM spacing
e) Very resistive and thick layer

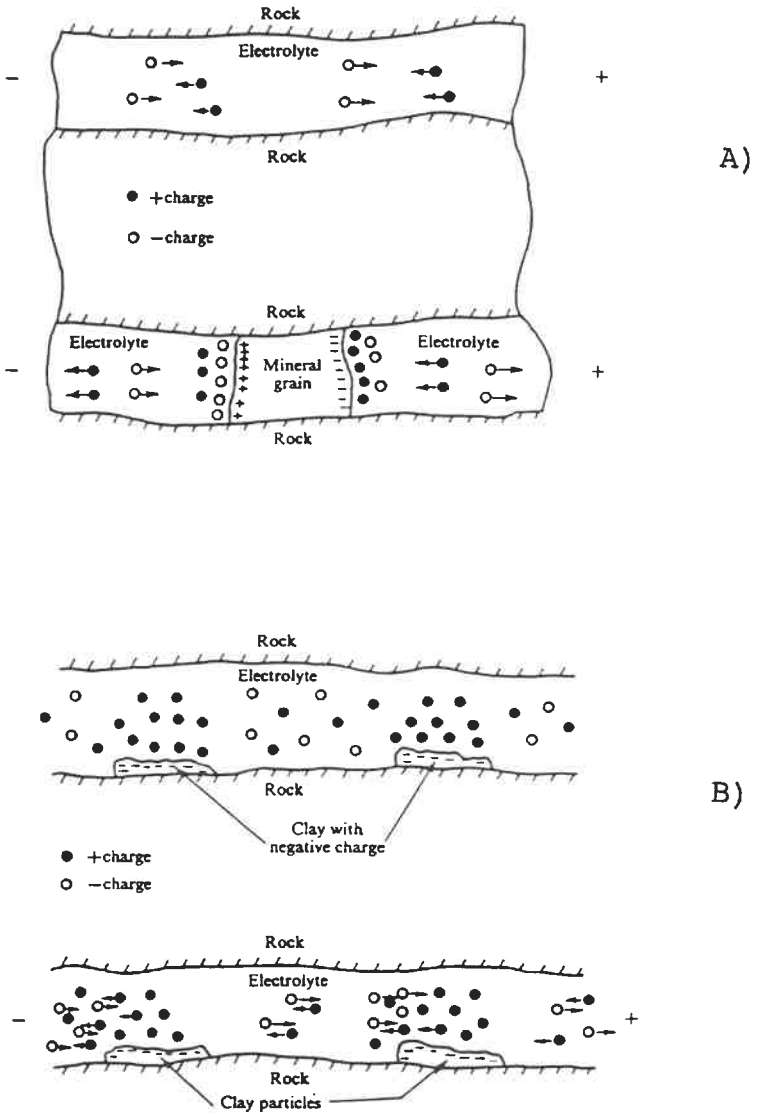


FIGURE 3.12 Mechanisms that cause the IP phenomena; electrode and membrane polarization (after Telford et al., 1976)
a) Electrode polarization
Upper: Before current injection
Lower: When the current is switched on
b) Membrane polarization
Upper: Before current injection
Lower: When the current is switched on

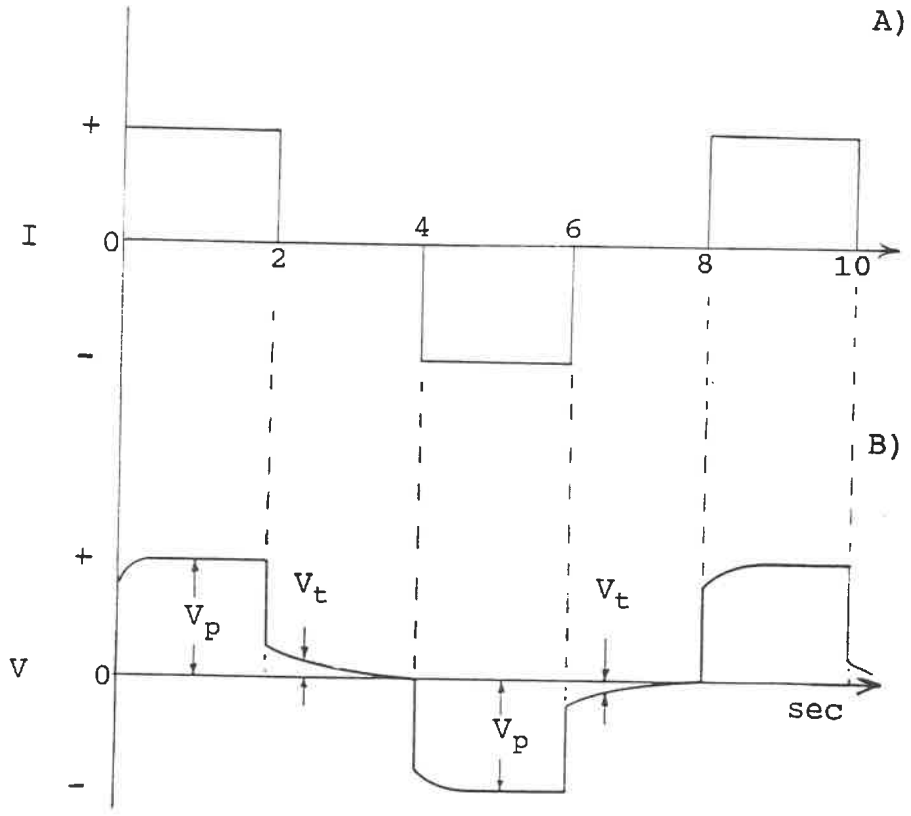


FIGURE 3.13 Voltage decay curve over an 8 second cycle.
a) Current injection as a function of time
b) Voltage decay curve as a function of time
V: voltage
V_p: primary voltage
V_t: decaying voltage
I: current injected
t: time

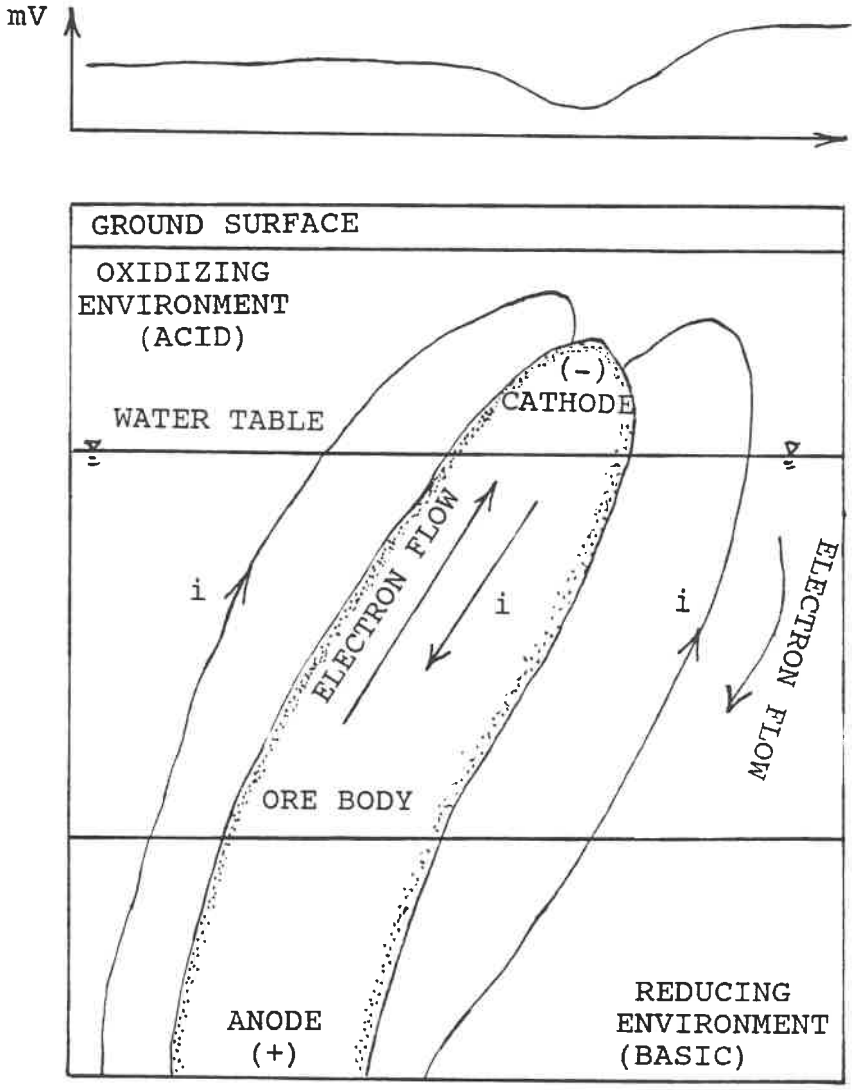
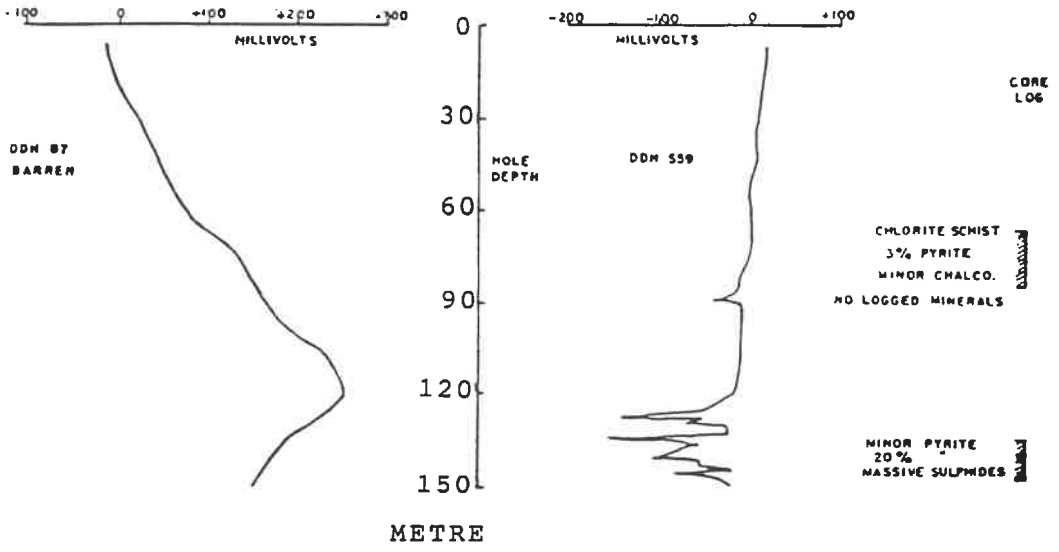


FIGURE 3.14 Electromechanical mechanism for spontaneous potential.
a) Typical SP recorded response
b) Sketch of the mechanism



A) B)

FIGURE 3.15 Spontaneous potential profiles from borehole logging (after Becker and Telford, 1965).
a) Barren hole log alongside the sulphide zone less than 30m away
b) Hole intersecting sulphides

CHAPTER 4

EQUIPMENT AND CALIBRATION

4.1 Geological Survey of Canada logging equipment

The borehole logging system used in the field by the Borehole Geophysics Section of the Geological Survey of Canada (GSC) is briefly described here. For further detailed information the reader is referred to Bristow (1979a, b, c), Killeen (1986), Killeen and Mwenifumbo (1986) and Urbancic (1985).

The GSC borehole logging system is mounted in a 1-ton, four wheel drive truck. The logging system is presented in figure 4.1. It comprises:

1) a probe consisting of a sensor and an electronic section. Each logging technique has its appropriate probe.

2) a 1000m logging cable made of a urethane jacketed 3 conductor shielded cable. It weighs approximately 45 Kg with a breaking strength of 260 Kg,

3) a wellhead pulley including a depth encoder,

4) an electric winch holds the cable. A motor maintains the winch at a constant logging speed regardless of the changing

drum diameter.

5) a 5 kilowatt generator is used for the system's power supply,

6) surface amplifiers and analog to digital converters for some of the logging techniques with probes that transmit analogue signals to the surface.

7) data acquisition system that consists of:

- a 16 bit Data General Nova minicomputer,
- magnetic tape recorder (Digidata 9-track magnetic tape drive: max. speed 10000 characters/sec at a bit density of 800 b.p.i.),
- a Texas Instruments silent 700 terminal used to interact with the computer,
- a Tektronix 604a X-Y monitor (CRT screen),
- a strip chart recorder used to display the data,
- and data acquisition software, written in assembler to maximize the data acquisition capabilities. The computer with peripherals and other electronics are mounted in a 19" rack secured to the truck.

The data recording is similar for each of the different logging techniques. Once the signal is detected by the sensor it is amplified and converted from an analog to

digital signal in the probe and then sent to the surface along a cable. At the surface, the cable passes over a wellhead pulley where the depth is measured electronically by an encoder and transmitted to the data acquisition system. The system acquires data under a foreground/background mode. While the value N is stored in memory, N+1 is being acquired in another block of memory and at the same time, N-1 is being dumped to tape and/or plotted on the chart recorder.

4.2 Calibration facilities

The GSC has established a system of model boreholes and drilled test holes for calibration and testing borehole geophysical equipment. These facilities are situated near Ottawa at Bells Corners, and on Lebreton and formerly Aberdeen streets in Ottawa (Killeen, 1978, Bernius, 1981). The different geophysical techniques used in the present project including temperature, natural gamma ray, gamma-gamma ray, IP, resistivity, MS and SP were calibrated and tested at these facilities. Killeen (1986) has described these model holes and given examples of the different types of borehole geophysical measurements made in some of the test holes.

4.3 Gamma ray spectral logging equipment

In both gamma ray techniques (natural gamma ray spectrometry and gamma-gamma ray spectrometry), gamma rays interact with a crystal detector (NaI(Tl) or CsI(Na)) and are sensed by a photo-multiplier tube.

The pulses are transmitted to the surface and amplified. The signal is then sent to an analog to digital converter which generates in a few microseconds a binary number corresponding to the height of an incoming pulse and to the energy of the gamma ray which was detected. The pulses are then sorted by the Nova computer into a complete energy spectrum.

The accumulation time for each spectrum is normally one second. The Nova computer accumulates a new spectrum as the spectrum just acquired is being processed.

The computer sums the content of the different channels at a selected interval which generates selected energy window logs (figure 4.2). Bristow (1979a) is referred for further information.

4.3.1 Natural gamma ray spectral logging equipment

The acquisition system collects the gamma ray spectra from 0 to 3 MeV in 256 channels at 12KeV/channel. The energy windows can be selected in order to discriminate counts originating from the different radioactive isotopes of K, and from U-238 and Th-232 decay series (Table 3.1).

The size of the probe that was used in all holes except hole 404a was 38 mm (O.D.) with a thallium activated cesium iodide crystal (CsI(Tl)) (25mm diameter x 76mm length). Hole 404a was logged with a 32mm x 127mm cesium iodide crystal detector with an outside housing diameter of 51 mm. These two detectors were calibrated at the Bells Corners calibration facilities.

A few precautions have to be taken during calibration and field surveys in order to get the best results. To reduce drift in the signal, the probe is lowered in the borehole to equilibrate its temperature with the borehole fluid temperature. The stabilization time is a function of detector size and surface temperature. The GSC uses a stabilization time of approximately 30 minutes.

After stabilization, the probe is raised to the surface and first calibrated with a Cs source which has an energy

peak at 661 KeV. The Cs source is placed next to the detector. A spectrum is accumulated while the energy peak is adjusted for a 12 KeV/channel recording. A second calibration is repeated with an Yttrium source (energy peaks at 0.89 MeV and 1.83 MeV). This procedure is needed to verify the linearity of the response in energy.

The probe is then lowered into the borehole and restabilized for 10 to 15 minutes. The holes were logged in the upward direction at a speed of 1 or 3m/min and with a sample time of 1 or 2 seconds (appendix A).

After the run is completed, another calibration spectrum is accumulated with the Cs and Yttrium sources. The spectrum is compared with the preceding one to check for drift.

4.3.2 Gamma-gamma ray spectral logging equipment

The acquisition system records the entire backscattered gamma ray spectra from an energy range of 0 to 3 MeV over 1000 channels of 3 KeV/channel. Ten energy windows are preselected in the field (table 4.1).

The probe used for the gamma-gamma spectral logging is in fact the natural gamma ray probe; the detector (CsI(Tl))

and the electronics are the same (tool D). However, a radioactive source (cobalt-60) is fixed at the extremity of the gamma ray probe. This part of the probe is shielded with tungsten and the gamma rays emitted are collimated to the formation at an angle of 90°.

The Cobalt-60 source emits gamma photons with energy peaks at 1.17 and 1.33 MeV. These photons will predominantly interact with matter by the Compton scattering effect.

The source-detector spacing is 17.5cm (15cm for the spacer and 2.5cm for an adapter) and the measuring point is taken at the mid distance.

The field calibration procedures follow the same steps as for the natural gamma ray probe with the difference that the radioactive source is attached to the probe and detached from it, before and after the run.

The data acquired were recorded in the upward direction at a logging speed of either 1 or 3m/minute and are summarized in appendix A.

The gamma-gamma spectral tool has not been calibrated to determine the formation density. Presently, count rates

which are inversely proportional to bulk density are recorded and displayed. The determination of calibration parameters for the conversion of count rate into density is currently underway.

The data for each hole have to be standardized during the data processing. Amplitude and spectrum shifts produced by field calibration errors has been corrected.

The spectra for different lithologies recorded in each hole are plotted. The maxima of the energy spectrum of the "background lithology" is observed for each hole and the window range noted (Table 4.2). A reference hole is chosen. Rewindowing is made for each hole according to the reference hole.

4.4 Electrical logging equipment

The gamma ray spectrometry software was adapted to record induced polarization measurements in boreholes with accompanying resistivity and spontaneous potential (SP) data (Bristow, 1986).

The system operates in the time domain. A constant current transmitter generates a conventional "positive-on-off-negative-on-off" waveform with currents ranging from 1

to 254 milliamps. The input current is controlled by the computer and varies according to the received signal amplitude.

The complete received signal waveforms are digitized at 4msec intervals and the number of samples recorded per complete waveform are 256, 512, 1024 or 2048 corresponding to 1, 2, 4 or 8 second periods, respectively.

The probe has a diameter of 40 mm and is made of 2 main sections. The top section consists of a stainless steel tube containing the probe electronics. This section consists of 2 parts. The lower part contains the battery pack, a pre-amplifier and a gain switches (x1, 2, 10 and 100). The upper part houses the circuit board electronics which contains a 60Hz low pass filter, and a V/F converter which sends the potential signal as a modulated frequency up to the surface.

The bottom section of the probe contains the current and potential electrodes which are constructed in several configurations using gold-plated brass cylinders to minimize unwanted contact potential variations.

The surface transmitter/receiver module contains a programmable current supply. The current waveform is fed

to the current electrode via one shielded conductor of the cable and a second conductor is used to transmit the frequency signal response to the surface (Bristow, 1986).

A separate system is used for SP measurements. The system employes a surface potential electrode and a downhole potential electrode. The surface electrode consists of a copper wire in a porous pot filled with a solution of copper sulfate, $CuSO_4$, and is located at infinity. The downhole potential electrode consists of a 2 cm long lead cylinder. Measurements are recorded from a multimeter on surface.

The data acquisition system is the same as for the other logging method and was previously described. The data acquired in this study were generally recorded in the upward direction at a logging speed of 3 m/minute or 6m/minute with an 1 second period (appendix A).

4.5 Temperature logging equipment

The GSC developed a temperature probe with a measurement resolution of 10^{-4} K giving a temperature gradient resolution of 1mK/m (milliKelvin per meter) for a depth sampling interval of 0.1m. The probe consists of two parts. The temperature sensor consists of a thin-walled metal tube of 4mm diameter by 15cm long containing thermistor beads

wired in a series combination to give a nominal resistance of 10000 ohms at 20°C. The thermistor element is mounted in a nose piece attached at the end of the probe.

The middle part of the probe contains the circuit board. An integrated circuit voltage-to-frequency converter is used to accomplish an analog-to-digital conversion with a sensitivity of 2 kHz/K (K: kelvin degrees). The frequency is transmitted to the surface module where frequency changes are converted to temperature changes (figure 4.6).

Power is supplied to the probe electronics from the surface through one of the conductors of the cable.

The sonde pressure and water seal consists of a stainless steel tube, 32mm in diameter.

The holes were logged in the downward direction at a speed of either 3 or 6 m/minute with a sampling depth interval of 1.5 or 3 cm (appendix A). No stabilization is required to equilibrate the probe with its surrounding. As mentioned before, a time constant correction is used to correct the delayed probe response (chapter 3.3).

4.6 Magnetic susceptibility logging equipment

The MS logging system used by the Borehole Geophysics Section of the GSC has two major components: the probe and the surface module.

The MS probe (model TH-3C) was designed by GeoInstruments Company and a brief description of its different components follows. The probe contains two main components: an inductive coil and the Maxwell bridge circuitry which is energized at a resonance frequency of 1450 Hz (figure 4.4).

When the probe moves into a magnetically susceptible material an apparent change of the coil inductance is reflected by an imbalance in the Maxwell bridge. A crystal-controlled oscillator in the upper part of the probe is used to balance the Maxwell bridge with a required energizing frequency. This required frequency creates a change in the inductance, and is thus a measure of magnetic susceptibility (out of phase bridge output). A change in conductivity is manifested by a change in the resistance of the coil and generates a voltage at the output of the bridge which is in phase with the oscillator frequency. However, resistivity measurements, governed by the Maxwell bridge, are limited to a range of 10^{-1} Ω-m to 10^{3}Ω-m.

The susceptibility signal is sent to the surface module in the form of a frequency signal. The circuitry in the probe has a voltage to frequency converter. A frequency signal is more desirable for transmission up the borehole since a voltage is susceptible to electrical interference by the surrounding borehole rock and would distort the MS information. The resistivity signal is transmitted to the surface as a DC voltage.

The TH-3C probe and surface module were originally powered by 4 internal Ni-Cd cells. The probe is now powered from the surface and thus, gives better results.

The housing of the coil is made of a non-magnetic fibreglass material, that can withstand pressures of up to 150 bars. The copper coil which is wound around a ferrite core (high magnetic permeability) is 42mm in diameter and 50cm in length. The coil axis length is parallel to the borehole for the best coupling into the rock formation.

The reader is referred to Bristow and Bernius (1984) and GeoInstruments, for the technical specifications of the TH-3C magnetic susceptibility logging tool.

The surface module contains a frequency to voltage converter (f/v converter) to convert frequency modulated

susceptibility information to an analog voltage and an amplifier for the resistivity signal. These voltages are then recorded on tape as a function of depth.

The GSC Borehole Geophysics Section routinely calibrates the probe in the air and then with a calibration sample of 550 $*10^{-5}$ SI before and after the logging runs. During the calibration, the probe must be removed from magnetic materials to a distant of at least 3 m.

A few precautions have to be taken in the field to reduce drift. The probe has to stabilize to the borehole fluid temperatures. George and Scott (1982) suggest a stabilization of 30 to 90 minutes for good results. The GSC Borehole Geophysics Section recommends a stabilization time of 75 minutes for accurate results. During the stabilisation the probe must be powered. Whenever the probe is moved to new borehole locations, it should be restabilized. The GSC has produced accurate MS logs with 30 minute restabilization. It is also important that the surface module be at a constant temperature.

The GSC modified the GeoInstruments surface module to combat the baseline drifts. New features were introduced; a power supply that has been discussed previously and a digital signal processing unit.

The digital signal processing unit was designed to improve the accuracy and stability of the measurement with the help of a crystal-controlled clock (Bristow, 1985). Any observed drift will be due to the sensor alone.

The different holes were logged in the upward direction (except hole 420) at a speed of either 3 or 6m/minute and the recording information sheet for each hole is available in appendix A.

4.7 Software

The field data were extracted and processed with the software package developed by the Borehole Geophysics Section of the GSC. The programs are written in Data General AOS Fortran 5 for a 16-bit Data General NOVA minicomputer.

The data reduction have followed two main stages before the statistical analysis took place. These stages are summarized as follows (Urbancic, 1985):

1) Extraction of the raw data from field tapes and standard processing (interpolation, averaging...),
2) Depth correlation between the multiparameter logs,

Urbancic (1985) has described the software used during

the extraction and processing of data, and the reader is referred to his work for further details.

The statistical analysis followed two steps. The first step which consisted of an univariate data analysis used the Lotus 123 (Lotus Development Corp., 1985) software package. A program in basic for an IBM compatible written by Jacques Ouillet, Ph.D. student in Mining engineering, Ecole Polytechnique, was utilized for the distribution analysis.

The multivariate data analysis was done with the SPSS package (Norusis, 1986a, b).

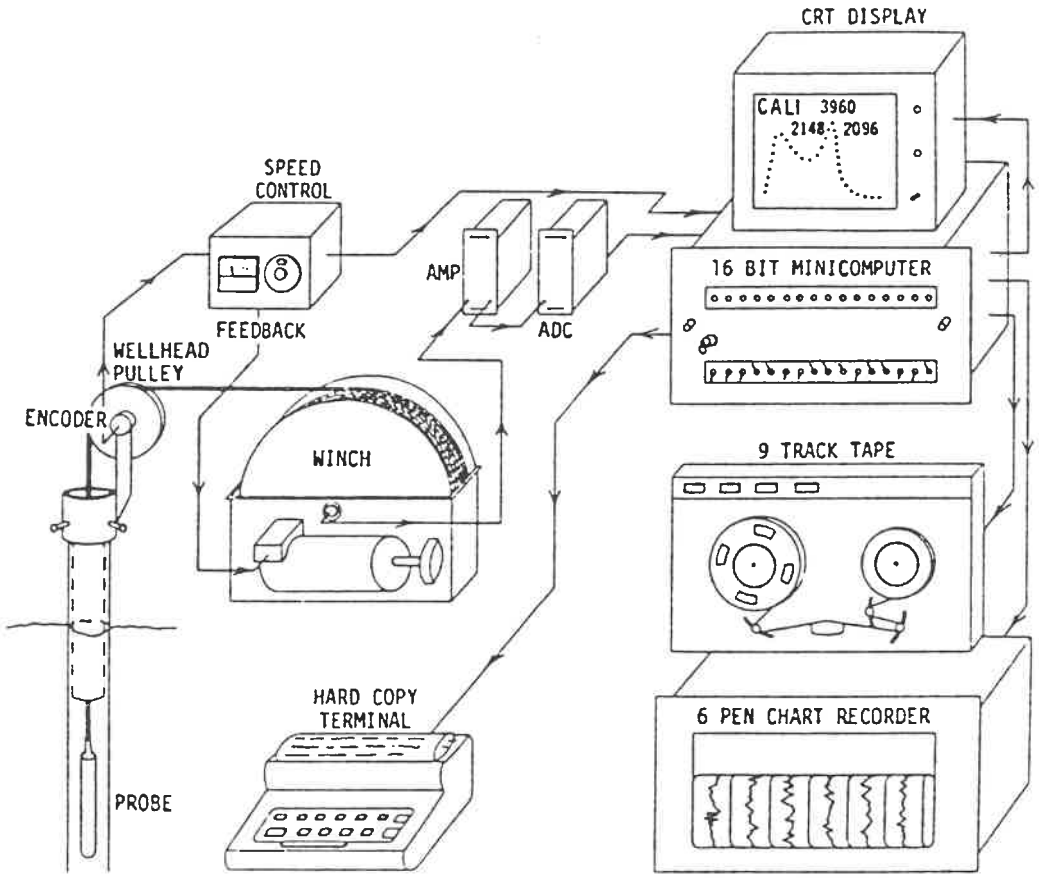


FIGURE 4.1 GSC logging system (after Bristow, 1979a).

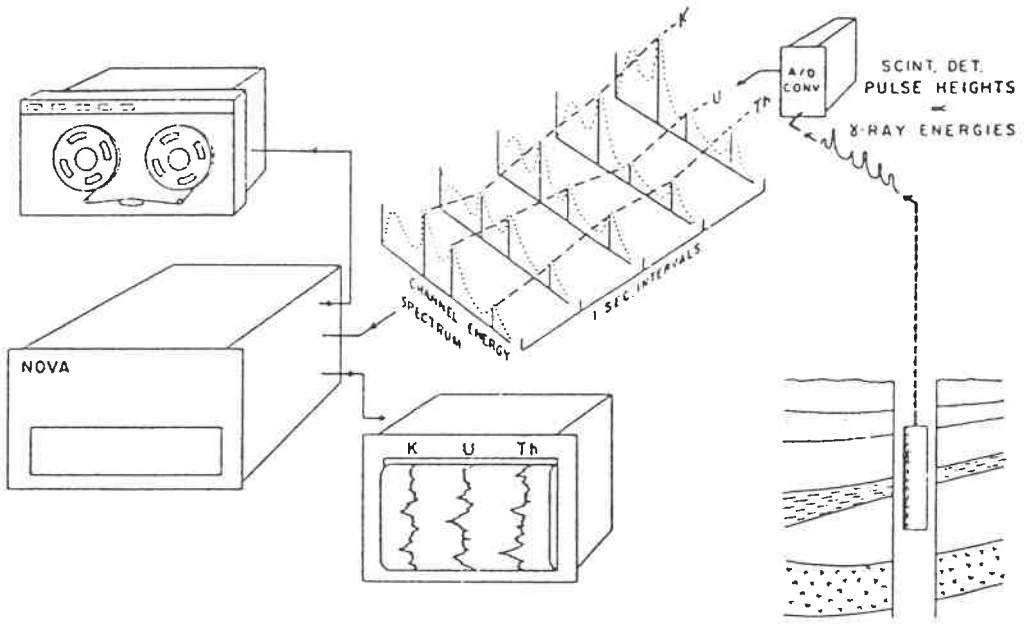


FIGURE 4.2 The computer sums the content of the channels encompassed by the appropriate peaks (selected window energies for K, U and Th) at a selected interval, and generates K, U and Th profiles which can be related to potassium, uranium and thorium concentration (after Bristow, 1979a).

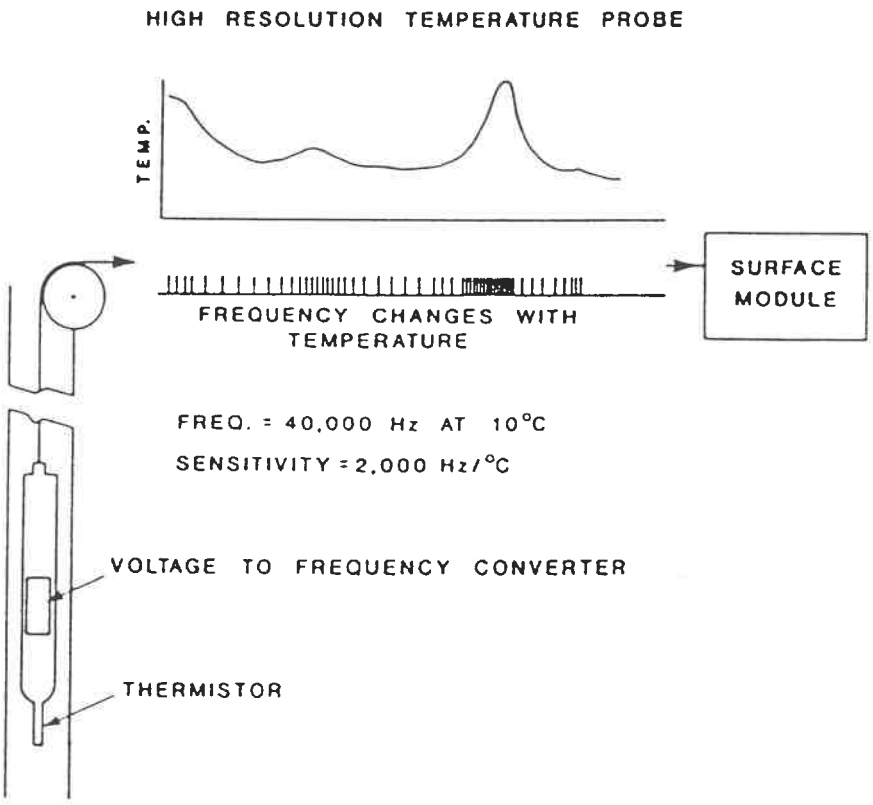


FIGURE 4.3 Principle of voltage-to-frequency conversion for the temperature log (after Bristow and Conaway, 1984).

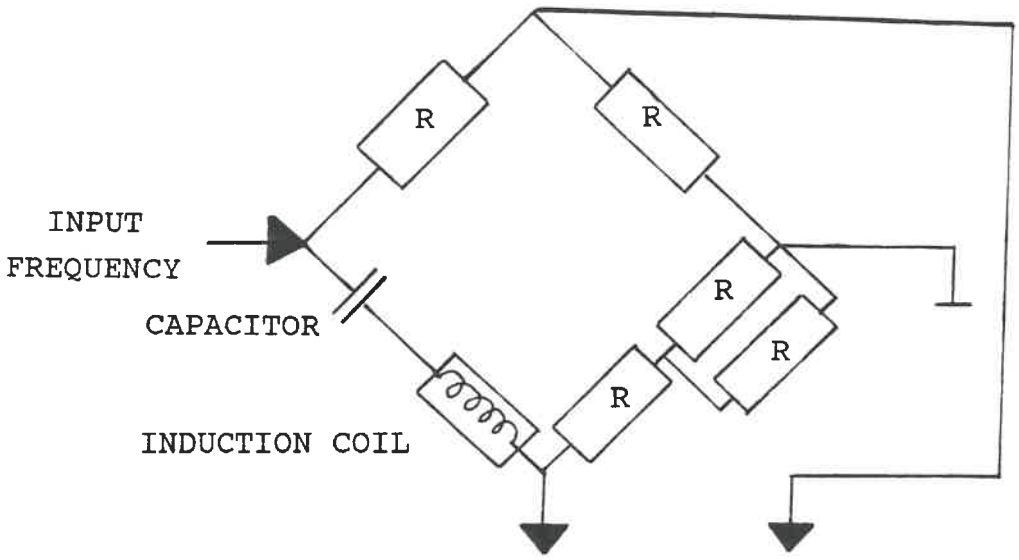


FIGURE 4.4 Maxwell bridge circuitry of the Geoinstruments TH-3C magnetic susceptibility probe.

Original window limits(keV)
100- 120
120- 180
180- 240
240- 300
180- 300
180- 600
400-3000
1360-1560
1610-2300
2400-3000

a)

Original window limits(keV)
70- 140
140- 160
160- 300
300- 400
400-1000
1000-1500
400-3000
1360-1560
1610-2300
2400-3000

b)

Table 4.1 Window energies for gamma-gamma spectral logging survey.
a) all holes except 418, 420 and 420
b) holes 418, 420 and 421

Hole	Size	Run no.	Tape no.	Peak max-keV	Rewindow (keV) w01	w03	w07
402a	NQ	2	FNDYA635	40	20-60	120-260	260-460
403	BQ	2	FNDYA623	115	95-135	195-335	335-535
404a	NQ	2	FNDYA636	80	60-100	160-300	300-500
405	BQ	2	FNDYA619	80	60-100	160-300	300-500
406a	NQ	5	FNDYA632	90	70-110	170-310	310-510
408a	NQ	2	FNDYA634	90	70-110	170-310	310-510
409a	NQ	2	FNDYA633	95	75-115	175-315	315-515
410a	NQ	2	FNDYA632	95	75-115	175-315	315-515
411	BQ	3	FNDYA621	80	60-100	160-300	300-500
412	BQ	2	FNDYA620	80	60-100	160-300	300-500
418	NQ	2	FNDYA711	45	25-65	125-265	265-465
420	NQ	2	FNDYA716	55	35-75	135-275	275-475
421	NQ	3	FNDYA709	100	80-120	180-320	320-520

Table 4.2 Energy shift correction for the gamma-gamma spectral logging data.

CHAPTER 5

STATISTICAL TECHNIQUES

5.1 Statistical approach

The main goal of the project was to decide which geophysical techniques are best to determine different lead concentrations and, if possible for discriminating between zinc and lead concentrations.

The second goal of the project was to geophysically delineate the mineralized environment in case of unsatisfactory successes with the direct lead characterization.

In order to quantify and confirm relationships between mineralization or its lithological environment and the geophysical parameters, statistical techniques were utilized.

Distribution studies, scatterplot diagrams, regression, discriminant and principal component analyses are the main techniques that the author used to reach these goals.

5.2 Classical statistics

Classical statistics are used as a first step in order

to get initial and general information about the different geophysical and geochemical parameters in relation to lithologies or mineralization.

Before any rigorous statistical analyses on the data were undertaken, basic statistical calculations (sample mean, median, mode, variance, standard deviation, coefficient of variation, coefficient of asymmetry) are performed to get information about its distribution. Histograms are used to quantitatively examine the distribution of the sample.

Hines and Montgomery (1980), Krumbein and Graybill (1965) and Davis (1973) are few good references for further detailed readings on basic statistics.

5.3 Univariate data analysis

To consider any relationship between pairs of variables, scatterplot diagrams (cross plots) should be one of the first steps in a statistical analysis. It is the simplest way of expressing relationships between two variables.

The visual relationships found from these diagrams are useful in choosing further statistical techniques.

To examine the nature of the relationships, regression analysis is used to model and investigate the relationship between two (simple regression) or more variables (multiple regression, see section 5.4.1).

In many situations, a straight line relationship can be valuable in summarizing the observed dependence of one variable on another (Draper and Smith, 1966).

Let us assume that the regression line of Y on variable X has the form $\beta_o + \beta_1 X$. For a simple linear first order model:

$$Y = \beta_o + \beta_1 X + \epsilon \qquad (5.1)$$

where β_o, β_1 are parameters of the model,

ϵ is the error

For a given X, a corresponding observation Y is equal to $\beta_o + \beta_1 X$ plus an amount ϵ which represent the deviation of Y from the regression line.

Since β_o, β_1 and ϵ are unknown (ϵ changes for each observation Y), we will get estimates b_o and b_1 of β_o and β_1. Thus, we can write:

$$\hat{Y} = b_o + b_1 X \qquad (5.2)$$

where $\hat{Y}$ denotes the predicted value of Y for a given X. The estimation procedure will be that of least squares.

Similarly to the sample mean, the regression line has the characteristics that:

$$\sum_{i=1}^{n}(Y_i - \hat{Y}_i) = 0$$

and $\sum_{i=1}^{n}(Y_i - a)^2$ is a minimum when $a = \hat{Y}_i$

where i=1,n and n corresponds to the number of observations.

From these characteristics, the normal equations are determined as follows:

$$b_o + b_1 \sum_{i=1}^{n} X_i = \sum_{i=1}^{n} Y_i \qquad (5.3)$$

$$b_o + b_1 \sum_{i=1}^{n} X_i^2 = \sum_{i=1}^{n} X_i Y_i \qquad (5.4)$$

which define b_o and b_1 (Draper and Smith, 1966).

With few substitutions, we finally find the estimated regression equation to be:

$$\hat{Y}_i = \bar{Y} + b_1 (X_i - \bar{X}) \qquad (5.5)$$

where $b_o = \bar{Y} - b_1 \bar{X}$

The centred model is then given by:

$$Y_i - \bar{Y} = \beta (X_i - \bar{X}) + \epsilon \qquad (5.6)$$

We want to know the significance and the measure of precision associated with the estimate of the regression

line. From the identity:

$$Y_i - \hat{Y}_i = Y_i - \bar{Y} - (\hat{Y}_i - \bar{Y}) \qquad (5.7)$$

We square both sides to obtain:

$$\sum_{i=1}^{n}(Y_i - \bar{Y})^2 = \sum_{i=1}^{n}(Y_i - \hat{Y}_i)^2 + \sum_{i=1}^{n}(\hat{Y}_i - \bar{Y})^2 \qquad (5.8)$$

where $(Y_i - \bar{Y})$ is the deviation of the ith observation from the overall mean,

$(Y_i - \hat{Y}_i)$ is the deviation of the ith observation from its predicted value,

$(\hat{Y}_i - \bar{Y})$ is the deviation of the predicted value of the ith observation from the mean.

The previous equation can be expressed in words as follows:

$$SS_T = SS_E + SS_R \qquad (5.9)$$

where SS_T is the sum of squares about the mean,

SS_E is the sum of squares about regression (error sum of square),

SS_R is the sum of squares due to regression (amount of variability in the Y_i).

From this process, we would use the analysis of variance to test the significance of the regression. The analysis of variance is summarized in the following table.

Source of variation	Sum of squares	Degree of freedom[1]	Mean square	Fo
Regression	$SS_R = b_1 S_{xy}$	k	$MS_R = SS_R / k$	MS_R / MS_E
Residual or error	$SS_E = S_{yy} - b_1 S_{xy}$	(n-k-1)	$MS_E = SS_E / (n-k-1)$	
Total	$SS_R + SS_E = SS_T$	(n-1)		

[1] The degree of freedom indicates how many independent pieces of information involving the n independent numbers Y1, Y2,...,Yn are needed to compile the sum of squares (Draper and Smith, 1966).

Table 5.1 Analysis of variance

where $b_1 = S_{xy} / S_{xx}$
k: number of independent variables
n: number of observations
$S_{xx} = \Sigma (X_i - X)^2$
$S_{xy} = \Sigma Y_i (X_i - X)$
$S_{yy} = SS_T = \Sigma (Y_i - Y)^2$

In the specific case where we want to relate the significance of the regression, the appropriate hypotheses are:

$H_o : \beta_1 = 0$

$H_1 : \beta_1 \neq 0$

We would reject H_o if F_o (MS_R / MS_E) exceeds the percentage point of the distribution F, $F_{\alpha, \upsilon, \nu}$ (where α is

the significance level, $\upsilon = k$ and $\nu = n-k-1$), and conclude that there is a linear relationship between X and Y.

Fitting the regression model requires several assumptions (errors are normally distributed, the order of the model is correct...) and the analyst should always consider the validity of these assumptions to be doubtful and conduct analyses to examine the adequacy of the model.

In model building, residuals are what is left after the model is fitted. It is the difference between an observed value and the value predicted by the model:

$$\epsilon_i = Y_i - \hat{Y}_i \qquad (5.10)$$

where $i=1,n$

Y_i : observation i

$\hat{Y}_i$: corresponding fitted value obtained by use of the fitted regression equation.

That is, the error is the amount that the regression equation has not been able to explain.

To perform the regression analysis we have made assumptions about the errors: the errors are independent, have a zero mean, a constant variance and follow a normal distribution.

A scatterplot of residuals would help to judge if the assumptions are violated or not. The scatterplot diagrams present the residuals against the fitted values Y_i or the independent variables. There should be no relationship between the residuals and the fitted values or independent variables. Systematic patterns between them suggest possible violations of the linearity assumptions.

The coefficient of determination is often used to judge the adequacy of a regression model:

$$R^2 = \frac{SS_R}{SS_T} = \frac{\text{Variation explained by regression}}{\text{Total variation}} \qquad (5.11)$$

Clearly, $0 \leq R^2 \leq 1$. R^2 is often referred as the amount of variability in the data explained by the regression model and could be expressed in percentage.

The correlation coefficient is the root square of the determination coefficient expressed as follows:

$$R = \sqrt{R^2} = \sqrt{SS_R / SS_T} \qquad (5.12)$$
$$= S_{xy} / (S_{xx} S_{yy})^{1/2}$$

R is a measure of the linear association between Y and X. It varies between $-1 \leq R \leq 1$.

It is often useful to know the standard error of the

estimate s. The residual mean square (MS_E) is an estimate of the variance about the regression. The standard error of the estimate is defined as:

$$s = \sqrt{\text{Residual mean square}} = \sqrt{MS_E} \qquad (5.13)$$

Examination of this statistic indicates that the smaller it is the better, that is, the more precise will be the prediction (Draper and Smith, 1966).

The standard error of estimate is often calculated when the stepwise method (see description in multiple regression section) is used. It is checked before and after adding a new variable to the model, to verify if that variable improves the precision of the estimate.

In the present work, simple linear regression was used to quantify the relationships observed on the scatterplot diagrams. The Lotus 123 program (Lotus Development Corp., 1986) was used for the simple regression analysis of the data.

5.4 Multivariate data analysis

Multivariate methods are extremely useful because they allow observation of changes in several properties simultaneously. They may be complicated both in their theoretical

structure and operational methodology but because most of the problems involved in geology suggest complex and interacting forces which are impossible to isolate and study independently, multivariate analysis is an essential tool.

In this study, the best procedure would be to use different multivariate techniques that will examine many facets of the problem and sort out the major factors.

Multiple linear regression, principal component and discriminant analyses are the three multivariate methods that one would use for data analysis.

In the present work, multiple regression is used to establish quantitative correlation between variables. The relationships between the mineralization and number of geophysical parameters are examined.

In general, principal component analysis tries to calculate a relatively small number of factors that can be used to represent relationships among a set of many interrelated variables. In this study, the calculated factors are inspected to see if they correlate with mineralization and lithology.

Discriminant analysis determines a combination of

variables that best define the groups to differentiate. In the present case, it will try to best describe the two main geological units of interest: either the Canso Group where the mineralization occurs or the Windsor Shale that lies underneath the former.

The regression, factor and discriminant functions of the SPSS/PC program (Norusis, 1986, 1a-1b) have been utilized for the purpose of these respective statistical analyses. Default criteria were used in these analysis and are described in Norusis, 1986 1a-1b.

5.4.1 Multiple linear regression analysis

A regression model that involve more than one independent variable is defined as a multiple regression. This technique quantitatively determines correlations that exist in the multiparameter data set.

The assumptions that the independent variables X_i are linearly associated to the dependent variable Y describe a multiple linear regression. The regression model would then be of the form:

$$Y = \beta_o + \beta_1 X_1 + \beta_2 X_2 + \ldots + \beta_k X_k + \epsilon \qquad (5.14)$$

where β_j are the regression coefficients $j=1,k$ and k is the number of variables

Multiple linear regression, as in the simple linear regression tries to minimize the errors with the least squares function:

$$L = \sum_{i=1}^{n} \epsilon_i = \Sigma (Y_i - \beta_o - \Sigma \beta_j X_{ij})^2 \qquad (5.15)$$

The different steps required in the analysis of the significance and adequacy of the regression are similar to the simple regression (analysis of variance, residual analysis, coefficients of correlation and determination) except that they involve more than two variables.

Multiple regression considers the variables all together. A few of the variables may not provide much more information (they may be related to other variables) so they do not need to be entered into the equation. The procedure used for selecting variables is the stepwise method and is retained in the present work.

The first variable considered for entry into the equation is the one with the largest positive or negative correlation with the dependent variable. If the variable fails to meet entry requirements (SPSS defaults) the

procedure terminates with no independent variables in the equation. If it passes the criterion, the second variable is selected based on the highest partial correlation coefficient which is interpreted as the correlation between the ith independent variable and the dependent one when the linear effects of the other independent variables have been removed from both X_i and Y. The partial correlation coefficient is expressed by:

$$PR_i = \sqrt{(R^2 - R_i^2)/(1 - R_i^2)} \qquad (5.16)$$

where R^2, besides being the square of the correlation coefficient between variable X and Y, is the square of the correlation coefficient between Y, the observed value of the dependent variable, and $\hat{Y}$ the predicted value of Y from the fitted line (Norusis, 1986 -1a). R_i^2 is the coefficient of determination when all independent variables except the ith variable are in the equation. $(R^2 - R_i^2)$ represents the R^2 changes when a variable is entered into the equation that already contains other independent variables. A large change indicates that the ith variable provides unique information about the dependent variable that is not available from the other independent variables in the equation. $(1 - R_i^2)$ defines the proportion of variability not explained by the other variables called the tolerance of the variable.

After each step, variables in the equation are examined to see if they should be removed according to the removal criterion. The variable with the smallest partial correlation coefficient is examined. If the probability of its F_o is greater than the maximum probability authorized (SPSS default, α=0.1) the variable is removed from the equation. The other variables in the equation are also inspected for removal before the selection of new variables is undertaken. Variables selection terminates when no more variables meet entry or removal criteria.

Details about multiple regression analysis may be found in Hines and Montgomery (1980).

5.4.2 Principal component analysis (PCA)

Principal component analysis (PCA) is a statistical technique that determines a relatively small number of factors that are used to represent the relationships among a set of many interrelated variables. The basic principle of the method is to find linear combinations of orthogonal variables with maximum variance.

The first step in the PCA involves the preparation of a correlation matrix obtained from a set of multivariate observations. These observations are generally converted to

a standardized form. It can be done by subtracting from each observation the mean of the data set and dividing by the standard deviation. The data will then have a mean of 0 and a variance of 1. This procedure is useful if we wish to compare the distribution of one variable to that of another when the two variables are not expressed in the same units of measurements.

The correlation matrix can be set up from the variance-covariance of standardized variables that is nothing more than a correlation matrix.

The second step is to explore the data reduction possibilities by constructing a set of new variables on the basis of interrelations exhibited in the data (Nie et al, 1975). Elements in the variance-covariance matrix (dimension k x k) can be regarded as defining points lying on an k dimensional ellipsoid. From this matrix, eigen-vectors and eigenvalues are determined . The orthogonal eigenvectors define the principal axes of the ellipsoid and the eigenvalues define the lengths of these axes.

We can define the total variance of the data set as the sum of the individual variances. These are located on the diagonal of the variance-covariance matrix so the sum is equivalent to finding the trace of the matrix.

As a simple example, start with the variance-covariance matrix: $\begin{bmatrix} 12 & 5 \\ 5 & 9 \end{bmatrix}$

The total variance is 12 + 9 = 21. Variable X_1 contributes to 57% (12/21) of the total variance and variable X_2 contributes to 43% (9/21) of the total variance. Its first eigenvector is: $\begin{bmatrix} 1 \\ -0.744 \end{bmatrix}$

and its second is: $\begin{bmatrix} 1 \\ 0.744 \end{bmatrix}$

Their respective eigenvalues are 15.72 and 5.28. They respectively represent the length of the two principal axes. Their sum is equal to the trace of the matrix (15.72 + 5.28 = 21) and also represent the total variance of the data set. The first principal axis contains 75% (15.72 / 21) of the total variance and the second contains 25% (5.28 / 21).

Then, we can make transformations of the form:

$$Y_{1i} = \alpha_1 X_{1i} + \alpha_2 X_{2i} \qquad (5.17)$$

$$Y_{2i} = \beta_1 X_{1i} + \beta_2 X_{2i}$$

where α's are elements of the first eigenvector

β's are elements of the second eigenvector.

The α's and β's are called loading factors.

To summarize, PCA consists of a linear transformation of k original variables to k new variables, where each of the new variable is a linear combination of the old.

In a general form, the principal component model for the ith standardized variable is written as:

$$Z_i = A_{i1}F_1 + A_{i2}F_2 + \ldots + A_{ik}F_k \qquad (5.18)$$

where Z_i : standardized variable i

F_k are the uncorrelated factors

A_{ik} are the loading factors of variable i on factor k,

k equals the number of factors.

Another step in the principal component analysis technique is to find scores for each factor for each case. Factor scores are the product of standardized variables and factor scores coefficients. The general expression for the estimate of the jth factor F_j for the observation n is:

$$F_{jn} = \sum_{(i=1)}^{p} W_{ji} Z_{in} = W_{j1}Z_{1n} + W_{j2}Z_{2n} + \ldots + W_{jp}Z_{pn} \qquad (5.19)$$

where the W_i's are known as factor score coefficients.

The factor score coefficients may be estimated by several methods such as regression, Barlett and Anderson-Rubin methods (Norusis, 1986, 1b). The regression method is

retained here. Once we have the correlation coefficients and the loading factor coefficients, the regression coefficients (factor score coefficients) can be calculated from the relation:

$$A_{ji} = \sum_{L=1}^{p} W_{jL} R_{Li} \qquad (5.20)$$

where A_{ij} are the loading factor coefficients of p variables by k factors,

R_{ij} represent the correlation coefficients (p x p variables)

W_{ij} are the regression coefficients -factor score coefficients of p variables by k factors.

It is usual to rotate the extracted factors after they have been calculated. Usually a factor is more interpretable when a few variables load highly on it and the rest do not. Rotation is then used after extraction to maximize the variance of the factor loadings for each factor by making high loadings higher and low loadings, lower.

Few rotational techniques are available (Nie et al, 1975); the varimax technique was kept for the purpose of this work.

The technique is centred on simplifying the columns of the factor matrix A_{pk} which is equivalent to maximizing the variance of the squared loadings in each column (Lindeman

et al, 1980, Nie et al, 1975):

$$\sum_{p=1}^{K} n \sum_{j=1}^{n}\{A_{jp}/H_j\}^4 - \sum_{p=1}^{K}\{\sum_{j=1}^{n} A_{jp}^2/H_j^2\}^2 \;/\; n^2 \text{ is a maximum} \qquad (5.21)$$

where j: variable

p:factor

$$H_j^2 = A_{j1}^2 + A_{j2}^2 + \ldots + A_{jp}^2 = \sum_{p=1}^{K} A_{jp}^2$$

H_j^2 defines the total variance of the jth variable accounted for, by the combination of all common factors. It is usually referred to the communality of the variable. In that sense, the communality represents the extent to which the jth variable is measuring something in common with the other variables in the set. The complement of communality ($1-H_j^2$) indicates the proportion of the unique variance of the jth variable.

As the residual in regression analysis, the residual correlation matrix which is the difference between the observed correlation matrix and the reproduced correlation matrix ($\mathbf{R_r} = \mathbf{AA'}$ where **A** is the factor loading matrix) indicates how well the fitted model reproduces the observed correlations. If the magnitude of residuals is large, the model does not fit the data well and should be reconsidered.

PCA belongs to that category of techniques in which utility is judged by performance and not by theoretical

considerations (Davis, 1973). It is not strictly speaking a statistical procedure but a mathematical manipulation. Nevertheless, statistical tests are available on SPSS/PC (Norusis, 1986,1b) for checking the significance of the model and sampling adequacy.

5.4.3 Discriminant analysis

Discriminant analysis attempts to separate the observations into groups that are relatively homogeneous and distinct from one another. The number of groups in a discriminant function is set prior to the analysis and each original observations is defined as belonging to a specific group. In the present work, the Canso Group where the mineralization occurs and the Windsor Shale Group will be studied (the rhyolite does not have a significant number of observations).

The method will tell us if it is possible to distinguish these two groups with a linear combinations of standardized variables Z:

$$D_{ig} = d_1 Z_{1ig} + d_2 Z_{2ig} + \ldots + d_p Z_{pig} \qquad (5.22)$$

where D_{ig} is the score of the ith member of group g and d's are weighting coefficients chosen to maximize the separation between groups. The Z's are standardized values of the p

discriminating variables used in the analysis ($g=1,2,...G$ and $i=1,2,...ng$).

If so, the function that we have found could then be allocated to new observations of unknown origin to one of the groups.

In many instances, the full set of independent variables contains excess information. Few variables may not be useful to discriminate the different groups. In the present work, the stepwise method which sequentially selects the next best discriminator at each step (introduction of variables in the function one by one instead of considering the full set of variables) will be used.

For the linear discriminant function few assumptions must be made to minimize the probability of misclassification. These are that:

-the observations are random,

-the probability that an observation belongs to one of the group is equal,

-each group must be a sample from a normal multivariate population,

-each group has equal size variance-covariance matrix and,

-none of the observations used in the calculation of

the function are misclassified.

In its general form, the sample is separated into G groups. The separation among groups is expressed in terms of the variability among means on the variable D. Such variability can be represented, as in the univariate analysis of variance, by the sum of squares among group means. That is,

$$SSa = \sum_{g=1}^{G} ng(\bar{D}g - \bar{D})^2 \qquad (5.23)$$

in which $\bar{D}g = d_1\bar{Z}_1g + d_2\bar{Z}_2g + \ldots + d_p\bar{Z}_pg$ is the mean of D for the gth group and $\bar{D} = d_1\bar{Z}_1 + d_2\bar{Z}_2 + \ldots + d_p\bar{Z}_p$ is the total mean for all groups combined (based on n individuals $n = n_1 + n_2 + \ldots n_G$). In these expressions, the set $(\bar{Z}_1g, \bar{Z}_2g, \ldots, \bar{Z}_pg)$ is called the centroid of group g and the set $(\bar{Z}_1, \bar{Z}_2, \ldots \bar{Z}_p)$ is called the centroid of the total sample.

The sum of squares among group can be define as:

$$SSa = \mathbf{d'Bd} \qquad (5.24)$$

where $\mathbf{B} = \sum_{g=1}^{G} ng(\bar{\mathbf{Z}}\mathbf{g} - \bar{\mathbf{Z}})(\bar{\mathbf{Z}}\mathbf{g} - \bar{\mathbf{Z}})'$

d is the matrix of weighting coefficients and

d' is **d** transposed.

The variability among means is partly due to variability among individuals. The within-groups sum of

squares (SS_w) is expressed by:

$$\mathbf{SS_w = d'Vd} \qquad (5.25)$$

where $\mathbf{V}$ is a matrix obtained by adding the sum of squares for G groups, that is $\mathbf{V = S_{jk}^1 + S_{jk}^2 + \ldots + S_{jk}^G}$, $(j,k = 1,p)$.

In the case of G groups, the discriminant criterion y is then defined as the ratio of variability among means SS_a to the one of within groups SS_w:

$$y = \mathbf{SS_a/SS_w = d'Vd/d'Bd} \qquad (5.26)$$

The values of the d's are chosen to maximize y (Lindeman et al, 1980). From the partial derivative of y with respect to d, we set the equation to zero to obtain:

$$\mathbf{(V^{-1}B - yI)d} = 0 \qquad (5.27)$$

In general, if there are G groups, G-1 discriminant functions can be computed. They are all uncorrelated with each other and maximize the ratio of between-groups to within-groups sums of squares.

A few criteria such as the Mahalanobis' distance, Rao's V or the Wilk's lambda are used to select variables within

the stepwise method (Norusis, 1986 -1b). In the present work, the Wilk's lambda criterion is considered. The Wilk's lambda is defined by the ratio of the within-groups sum of squares to the total sum of squares. Large values of lambda (close to 1) indicate that group means do not appear to be different, while small values (close to 0) indicate that group means do appear to be different (most of the total variability is attributable to differences between the means of the groups).

The significance of the change in Wilk's lambda when the variable is entered or removed from the model can be based on an F statistic (Norusis, 1986 -1b).

As in regression analysis, the variable tolerance which is defined as the measure of degree of linear association between the independent variables is checked before the variable is entered into the model. If $(1-R_i^2)$ corresponds to small value it indicates that the ith variable is almost a linear combination of the other independent variables and should not enter the model.

Based on the d's coefficients, it is then possible to calculate the discriminant score for each case.

The percentage of cases classified correctly is an

index of the effectiveness of the discriminant function. This can be achieved by calculating the ratio of cases classified within the original groups with the discriminant functions over the total number of cases.

From the example that is shown below, twenty-nine cases were well classified giving a percentage of cases classified correctly of 96.7%.

	No. of	Predicted group membership		
Actual Group	cases	1	2	3
1	10	10	0	0
2	10	0	10	0
3	10	0	1	9

The observation classification within groups is done with the calculation of observation distance with the centroid of each group. The observation would be classified within the group where the distance is minimum.

CHAPTER 6

RESULTS

The west zone of the Yava deposit has been investigated by a shallow drill hole programme in 1986 and 1987. The Geological Survey of Canada (GSC) carried out geophysical logging in thirteen holes. These holes were logged with several techniques including natural gamma ray spectrometry, spectral gamma-gamma (density, heavy element assaying), induced polarization, resistivity, and self potential, magnetic susceptibility and temperature (temperature and temperature gradient).

All these logs were recorded on magnetic tapes which are kept at the GSC. Details on these recorded data are available in appendix A.

The raw data were processed with the GSC software. Each hole is characterized by its processed logs shown as vertical profiles (geophysical parameter versus depth). The geology and the metal content of each hole are also presented as logs. Multiparameter logs for each of the 13 holes are found in appendix B.

The qualitative correlations between the mineralization, geology and the geophysical parameters are presented

first. Statistical analyses applied to the geophysical data including regressions, principal component analysis and discriminant analysis are exposed in second. A discussion on the qualitative and statistical analyses is presented in the following chapter.

6.1 Qualitative geophysical results

A tremendous amount of data were collected and processed from the thirteen holes logged. Correlation between mineralization, geology and different geophysical parameters were observed and will be discussed in this section.

The geophysical logging techniques that respond to the Yava mineralization are described first. A few of geophysical logging methods that characterize the local geology of Yava are then discussed. Since the statistical analysis utilizes data sets from holes 404a and 410a, the description of results will principally refer to these two holes. Similar results were observed in the other holes and they can be found in appendix D.

Lastly, a few sections were drawn over the Yava grid in order to verify the topographic control on mineralization that was stated by Bonham (1983) and Patterson (1986).

6.1.1 Mineralization characterization

Induced polarization (IP) is a good technique for delineating disseminated mineralization and as expected, in most of these holes, IP anomalies seem to be associated with lead concentration (figures 6.1 and 6.2). On the other hand, the IP profile for hole 404a does not correlate as well (figures 6.3 and 6.4). It is rather similar to the total iron content profile (the total iron content is not significant in the black shale since it was sampled only once at 12m).

The highest IP values are located in the Canso Group. Where IP values reach up to 40 and 50 mV/V, lead mineralization occurs (hole 410a, between 9 and 17.5m, figure 6.2). The black shale is characterized by lower IP values and is flanked by anomalies caused by the presence of pyrite and/or galena (figure 6.4, between 11m and 12.5m).

Few IP peaks are observed in the Windsor shale (hole 404a, around 42m, figure 6.3), or near the contact between the rhyolite breccia and rhyolite (hole 410a, around 37m, figure 6.1), or Windsor shale and rhyolite breccia (hole 404a, 51m, figure 6.3). These peaks suggest the presence of galena and/or pyrite since they are also associated with high spectral ratios. They are interpreted as small

mineralized veins found in fractures or at lithologic contacts (confirmed in hole 410a by the drill core geological log).

The gamma-gamma spectral ratio which is the ratio of high energy gamma ray intensities to low energy intensities of the backscattered gamma rays, is proportional to heavy element content. In the present study, the spectral ratio successfully delineated the lead mineralization in every hole since galena is principally characterized by its high density (7.4 -7.6 g/cm^3) and high atomic number. Barite which also has a high density (4.5 g/cm^3) and high atomic number occurs in the Yava area but it can be easily distinguished from lead. Barite is not polarizable and hence does not produce an IP anomaly (hole 421, at depth 31.5m, figure 6.5).

The density log outlines lithologic changes but at the same time responds to lead concentration. For example, the sandstone has the highest density values (mainly due to the presence of mineralization). The gamma-gamma density data are presented in counts per second, the count rate being inversely proportional to density.

Hole 404a is a typical example where lead mineralization is associated with high spectral ratios (figure 6.4,

from 7 to 15.5m) and to a lesser extent with the density log. Minor occurrences of mineralization appear in the Windsor shale or near the rhyolite breccia (figure 6.3, around 42m and 51m) .

Self potential (SP) anomalies can be related to either mineralization or geology but no significant correlation is found from hole-to-hole. For example, the SP anomaly for hole 404a seen at 42m (figure 6.3), is associated to mineralization while for hole 408a, the SP anomalies seem to be related to geology (figure 6.6).

Qualitative analysis of SP log indicates that there are no significant SP anomalies that are associated with either mineralization or lithology. Furthermore, during data acquisition, the polarity of the electrical wires, the location of the reference electrodes and the grounding conditions were not kept the same for every hole. Only the relative variations in the logs are meaningful. Therefore, these data have not been used in the statistical analysis.

6.1.2 Geological characterization

Lithology variations are principally characterized by the resistivity and the natural gamma ray logs.

The rhyolite is the most resistive rock type at the Yava mine area. The Windsor group which is primarily shales, shows fairly constant resistivities and is the most conductive rock type. The presence of a 'rhyolitic boulder' in hole 410a (figure 6.1, between 28m and 32m) or gypsum in hole 404a (figure 6.3, between 34 and 41.5m), decreases the conductivity of the unit.

Resistivity variations are observed in the Canso group. This unit has more lithologic variations than the others (sandstone, conglomerate, black shale, coal fragments...) and is mineralized. The mineralized sandstone, the puggy shale and the black shale are more conductive than the unmineralized sandstone and limestone pebble conglomerate.

Gamma rays in nature come from radionuclides originating from the radioactive isotope of potassium (K-40), the uranium-238 and thorium-252 decay series. Since the Yava deposit type is not associated with uranium or thorium, the natural gamma ray spectometry logging technique would then indicate the potassic variations in the three major stratigraphic units.

The potassium, uranium and thorium logs are not presented here and will not be used for the statistical analysis. The counting statistics were too poor to

accurately determine the relative concentrations of K, U and Th.

The total count logs (energy window from 0.1 to 3MeV) characterize the three major stratigraphic units in every hole. The Canso group generally has the lowest radioactivity and the rhyolite has the highest one. The black shale in the Canso group is characterized by elevated counts (hole 404a, at 12m, figure 6.3) and the puggy shale behaves similarly (hole 408a, at 14m and 16m, figure 6.6).

The total count logs show the variation in clay content within the Windsor shale unit. They also point out fracture zones filled with accumulated clays (hole 410a, at 18m, figure 6.1, hole 404a, at 18 and 27m, figure 6.3). The resistivity also decreases in these zones. The 'rhyolitic boulder' encountered in the Windsor shale unit (hole 410a, figure 6.1, around 30m) is characterized by an increase in radioactivity and resistivity. The Canso Group and the Windsor shale are often separated by a weathered zone which is typified by high radioactivity and low resistivity (hole 410a, figure 6.1, at 18m).

As mentioned previously, self potential profiles (SP) sometimes correlate with geology. The SP profile of hole 408a (figure 6.6) seems to delineate the Canso group from

the Windsor shale but generally, there is no significant correlation found from hole-to-hole.

The temperature and temperature gradient logs indicate the presence of some fractures or lithologic contacts where there is ground water flow. Abrupt changes in temperature and high temperature gradients were observed along fractures with ground water movement. These observations are consistent in a number of holes. For example, in hole 402a, an unique fracture zone is found at 44.5m with anomalous temperature and temperature gradient (figure 6.7). Few fracture zones without groundwater movement do not show anomalous temperatures (density log, at 19m and 32.5m). No correlation between temperature and gradient temperature with either geology or mineralization was observed. Thus, the temperature data were not used in the statistical analysis.

Small variations are observed along magnetic susceptibility logs (MS) and are usually related to magnetite and/or ilmenite which here are hardly related to the mineralization. There is no easy correlation from hole-to-hole. Each rock type has its own susceptibility characteristic and in some of these holes the MS log reflects the different lithologies (figures 6.1 and 6.5). Generally, the Canso group susceptibility values are lower

than the Windsor shale which is higher than the rhyolite.

Calibration and stabilization problems were encountered in the field during the acquisition of MS data. Therefore, only the relative variation of MS values is meaningful. Thus, the MS logging technique was not selected for statistical purposes.

6.1.3 Sections

Figure 6.8 shows the location of a few sections that were drawn across the grid in order to verify the topographic mineralization control. The geology, lead and zinc content, and the spectral ratio logs are plotted for each section and are presented in appendix E.

The lithologic logs were principally used to determine the bedrock topography. Lead and zinc profiles outline the mineralization occurrences. In most of the holes, geochemical samples were taken in the sandstone where the mineralization was visually identified, except for hole 404a and 410a where samples were taken every 10cm in the Canso Group. Since the spectral ratio seems to be the best technique for delineating mineralization, it was chosen for display.

Figures 6.9 and 6.10 are plan views of the bedrock topography and the Canso Group thickness. The bedrock topography increases in the northerly direction.

Section A

Figure 6.11a is a composite plan and a longitudinal section showing lead enrichments occurring in sediments infilling valleys in the basement topography (Bonham, 1982). Section A is a continuation towards the west of this section.

Figure C.2 (appendix C) shows the longitudinal geological section with holes 404a and 403 located in the lowest parts of the bedrock depression. Assays of lead and zinc are presented in figures C.3 and C.4 (appendix C), respectively. In holes 404a and 403, lead content has increased in grade and in thickness (the sandstone is also thicker). No zinc enrichment is observed along the section except for some narrow increases in hole 403. The spectral ratio data are presented in figure C.5 (appendix C) and delineate quite well the thickness of the lead-zinc mineralization.

Section B

This cross section is very interesting with regard to the enrichment in zinc to the north associated with a decrease in lead grade. Figures C.6, C.7, C.8 and C.9 (appendix C) show sections of the geology, lead and zinc assays, and the spectral logs, respectively. The spectral ratio clearly shows this lead depletion. Sphalerite is not particularly characterized by high spectral ratios because of the relatively low zinc concentrations. Hole 418 shows anomalous IP and SP values between 17m and 24m where sphalerite is encountered, probably caused by associated pyrite (figure D.12, appendix D).

Section C

This section was selected because it shows an increase in depth to bedrock towards the north (figures 6.8 and 6.9). Figures C.13, C.14, C.15 and C.16 (appendix C) show sections of the geology, lead and zinc assays, and the spectral ratio logs, respectively. Zinc enrichment is observed down-dip where the Canso Group thickness is the greatest (figures C.13 and C.15, appendix C). Hole 420 which has zinc enrichment also has lower lead mineralization covering a larger thickness range (see spectral ratio profile, figure C.16, appendix C).

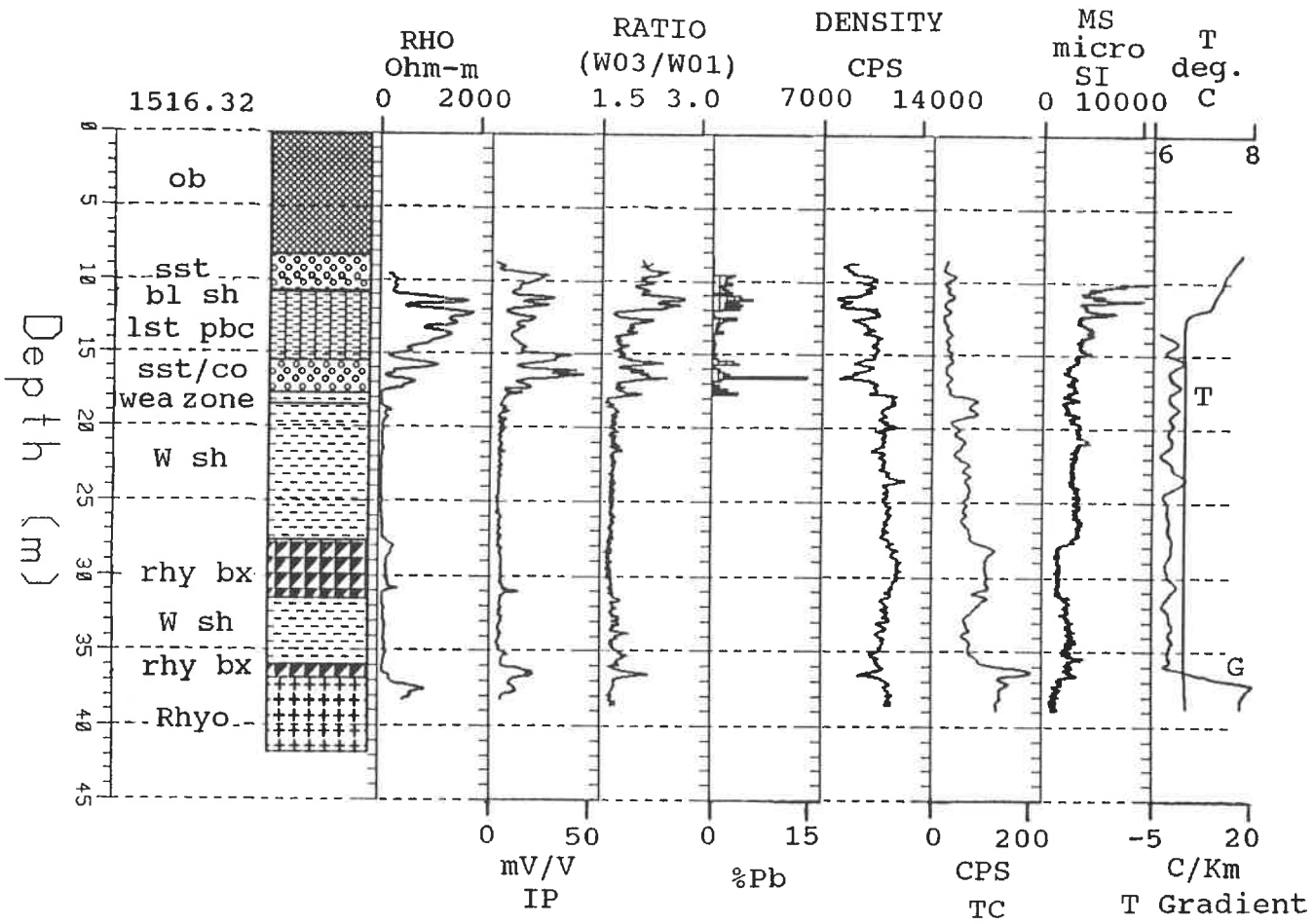


FIGURE 6.1 Multiparameter logs for hole 410a.

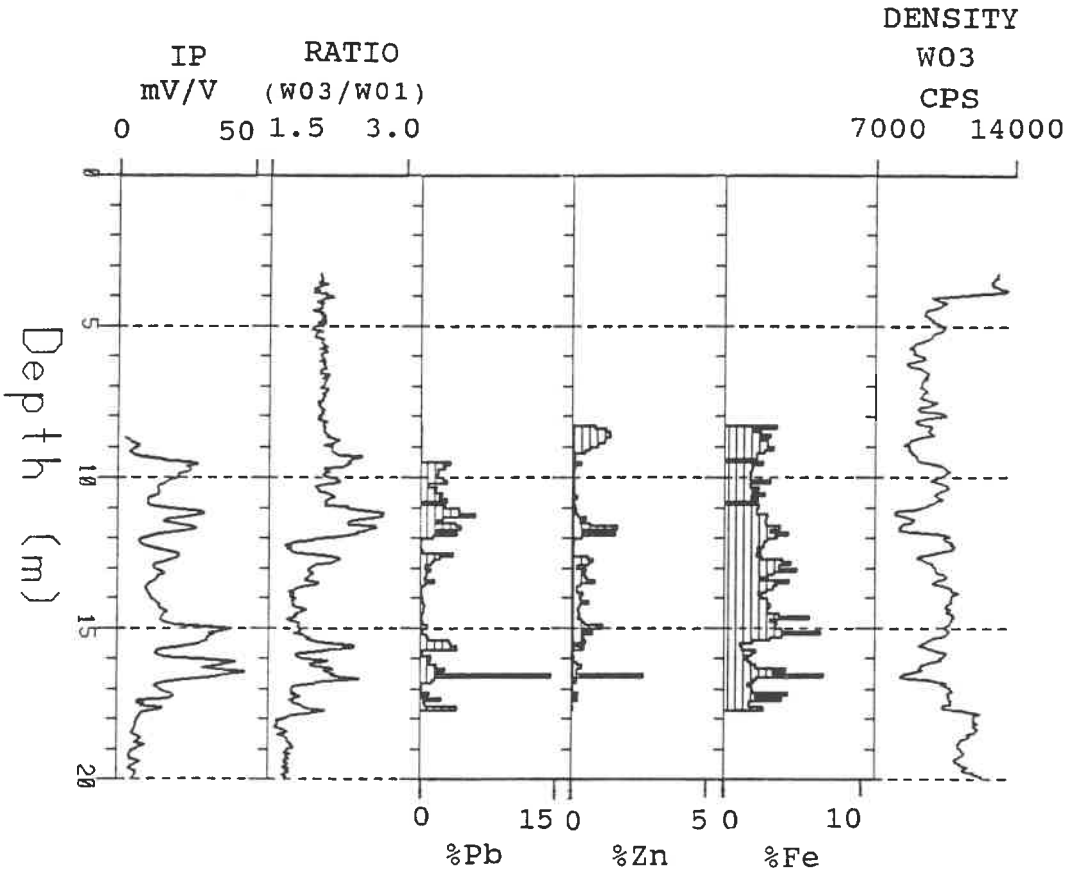


FIGURE 6.2 Detailed geophysical logs and mineralization for hole 410a.

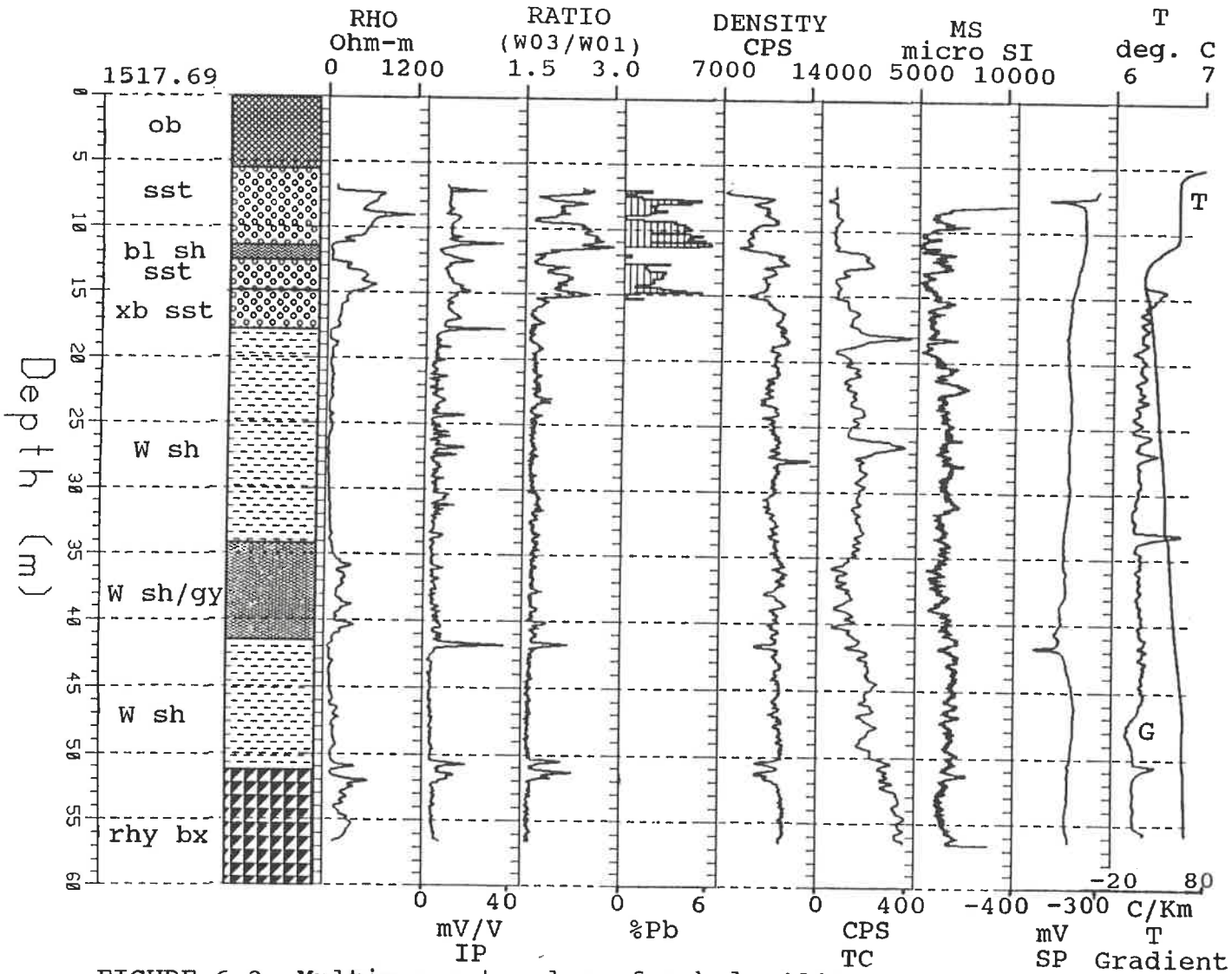


FIGURE 6.3 Multiparameter logs for hole 404a.

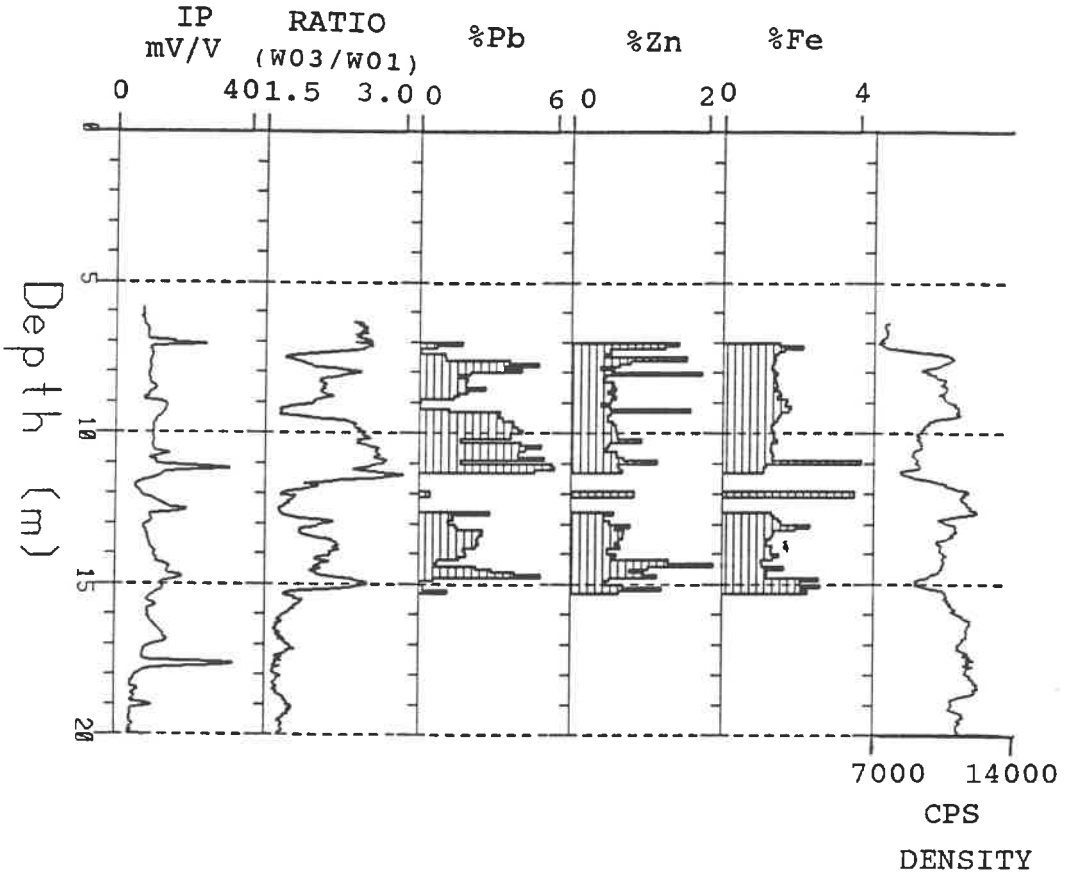


FIGURE 6.4 Detailed geophysical logs and mineralization for hole 404a.

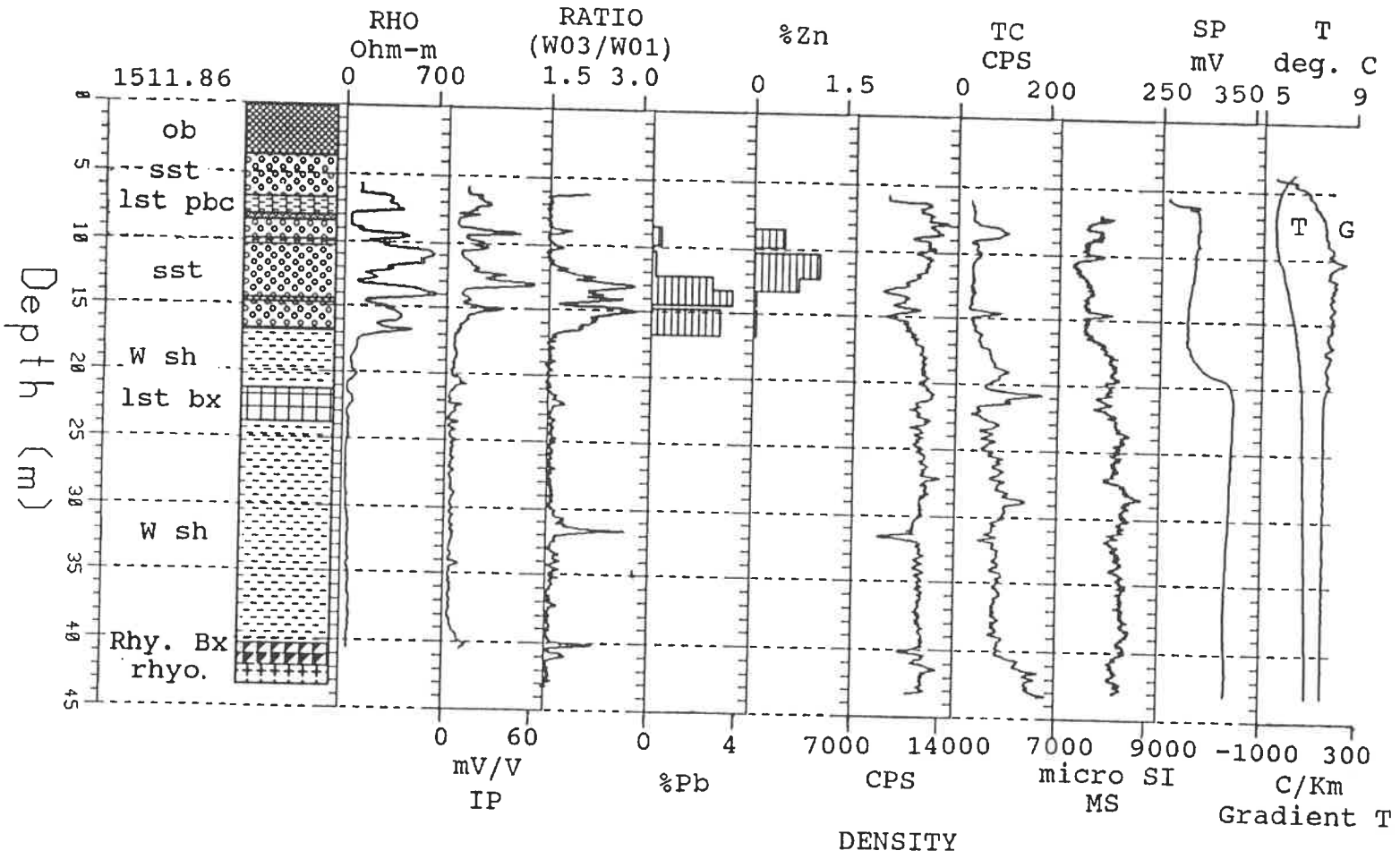


FIGURE 6.5 Multiparameter logs for hole 421.

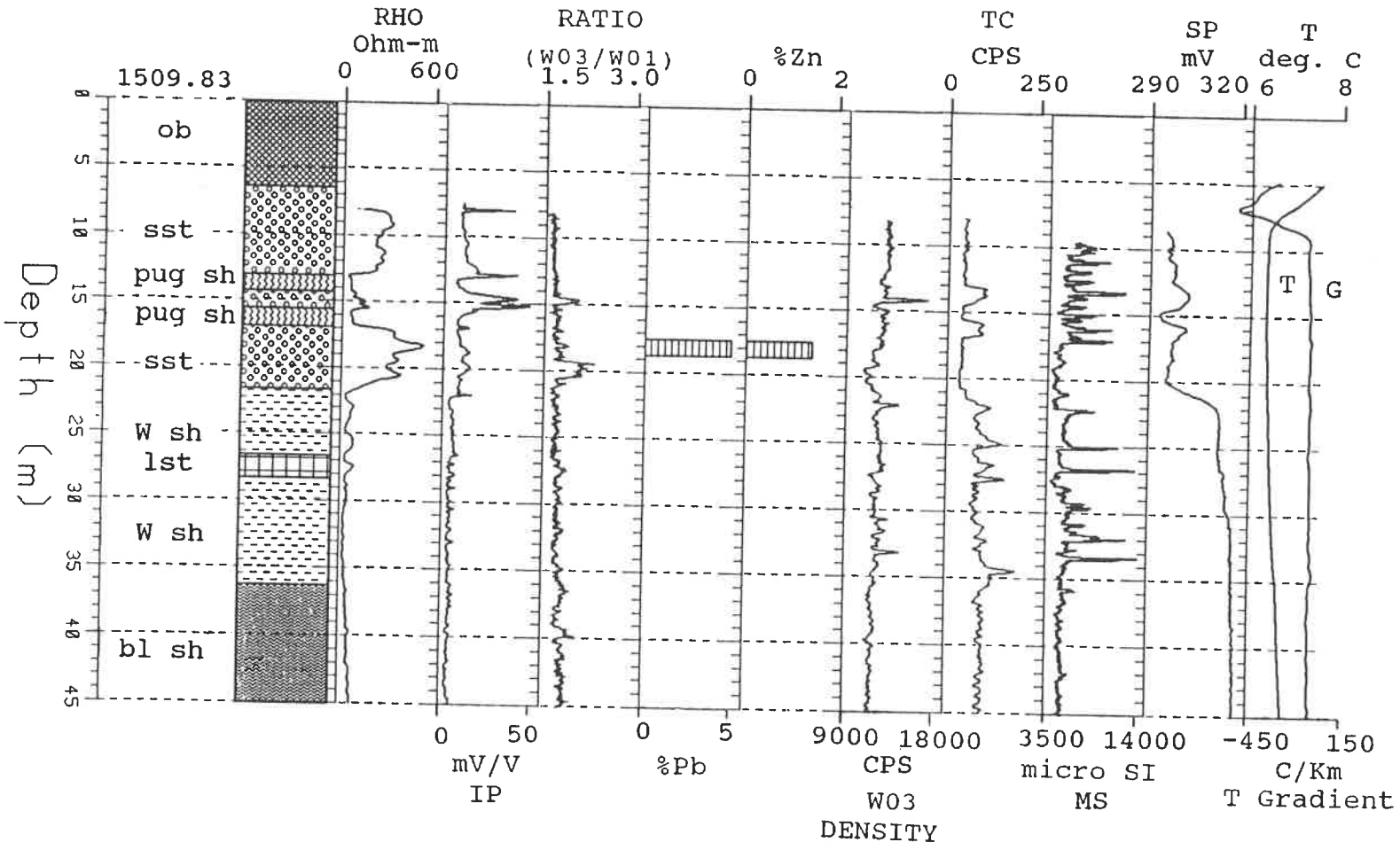


FIGURE 6.6 Multiparameter logs for hole 408a.

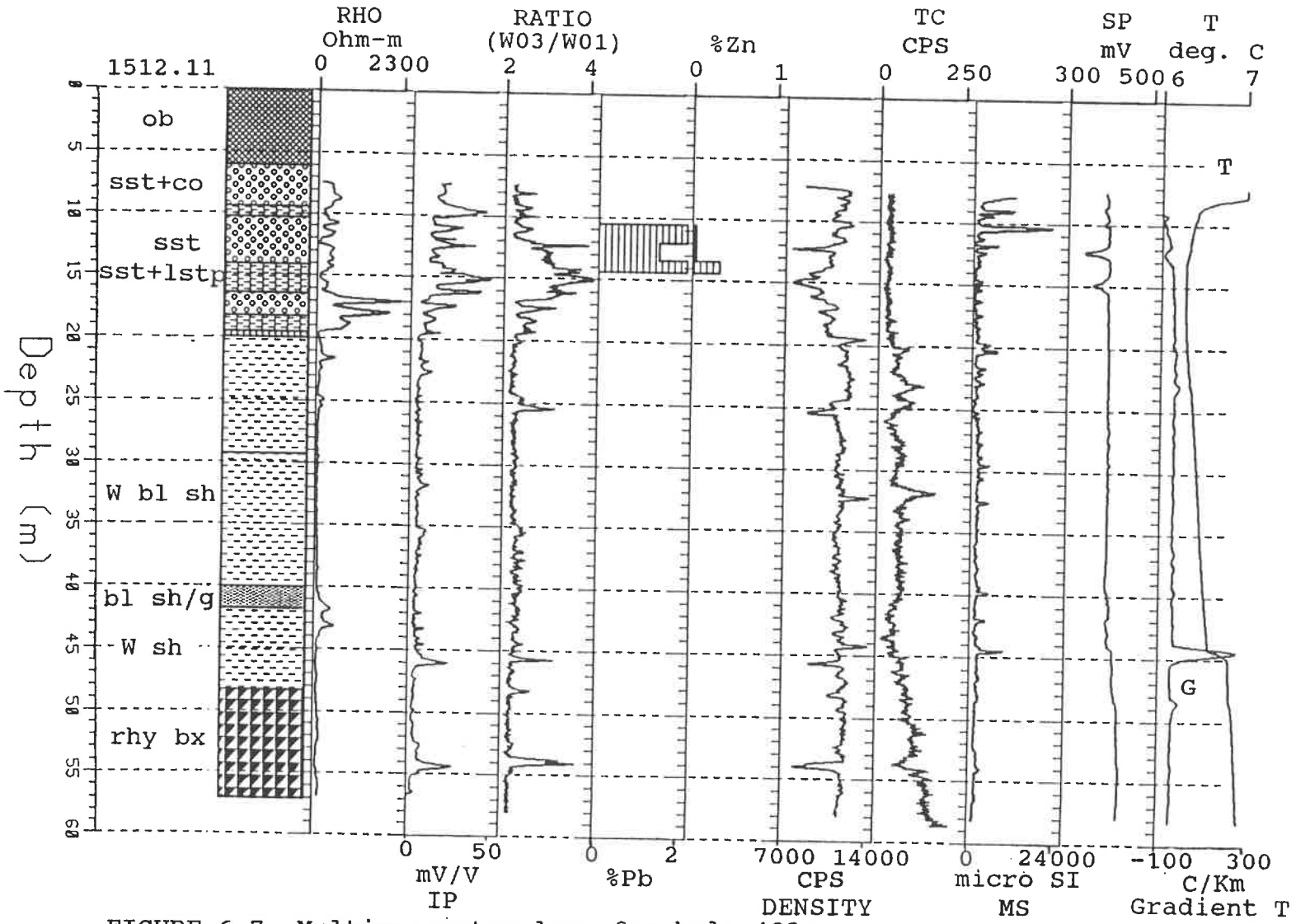


FIGURE 6.7 Multiparameter logs for hole 402a.

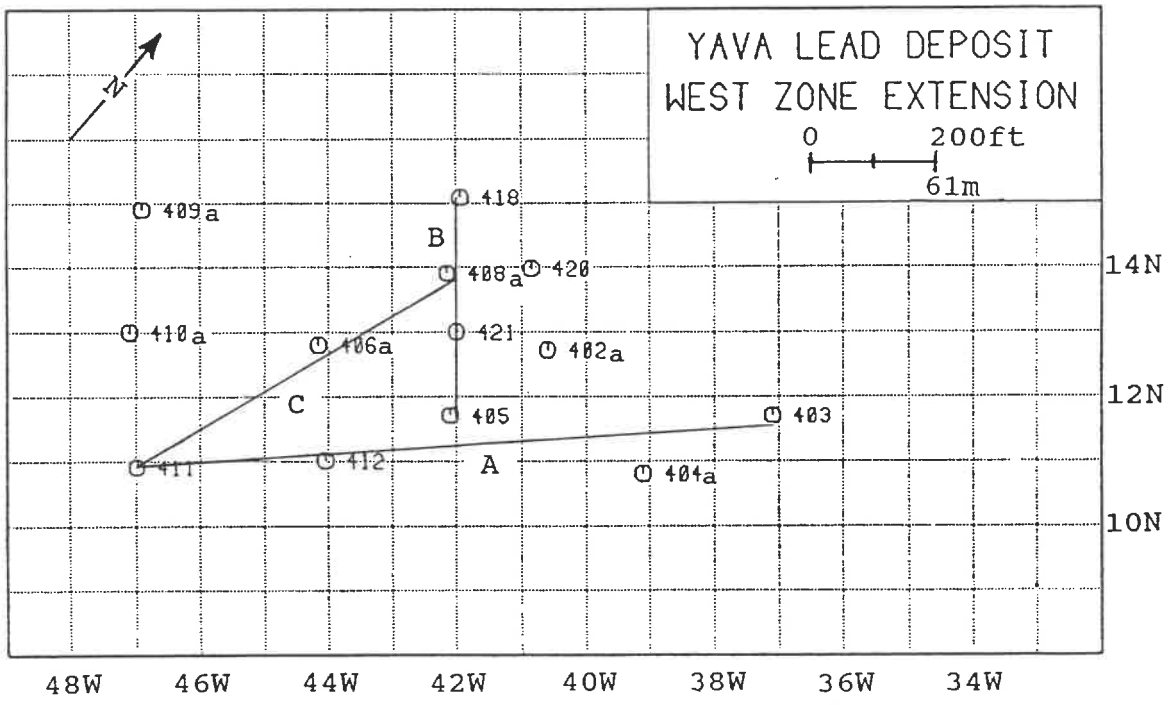


FIGURE 6.8 Sections location map, Yava lead deposit, west zone extension.

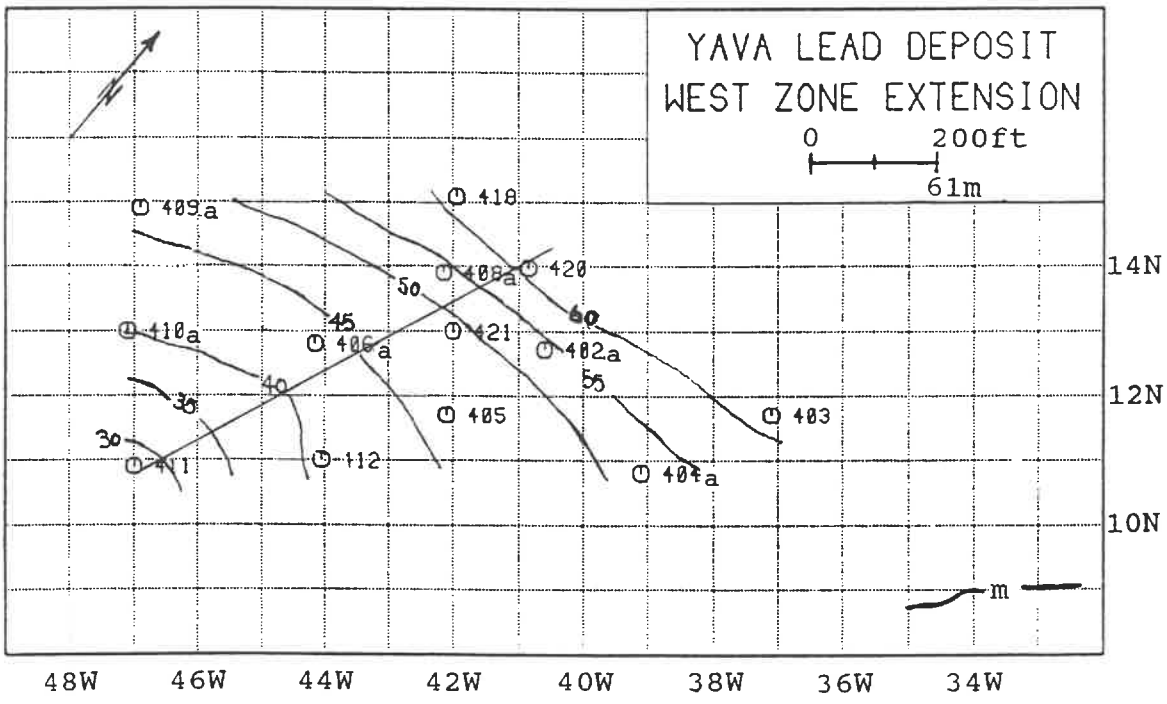


FIGURE 6.9 Bedrock topography plan view, Yava lead deposit, west zone extension.

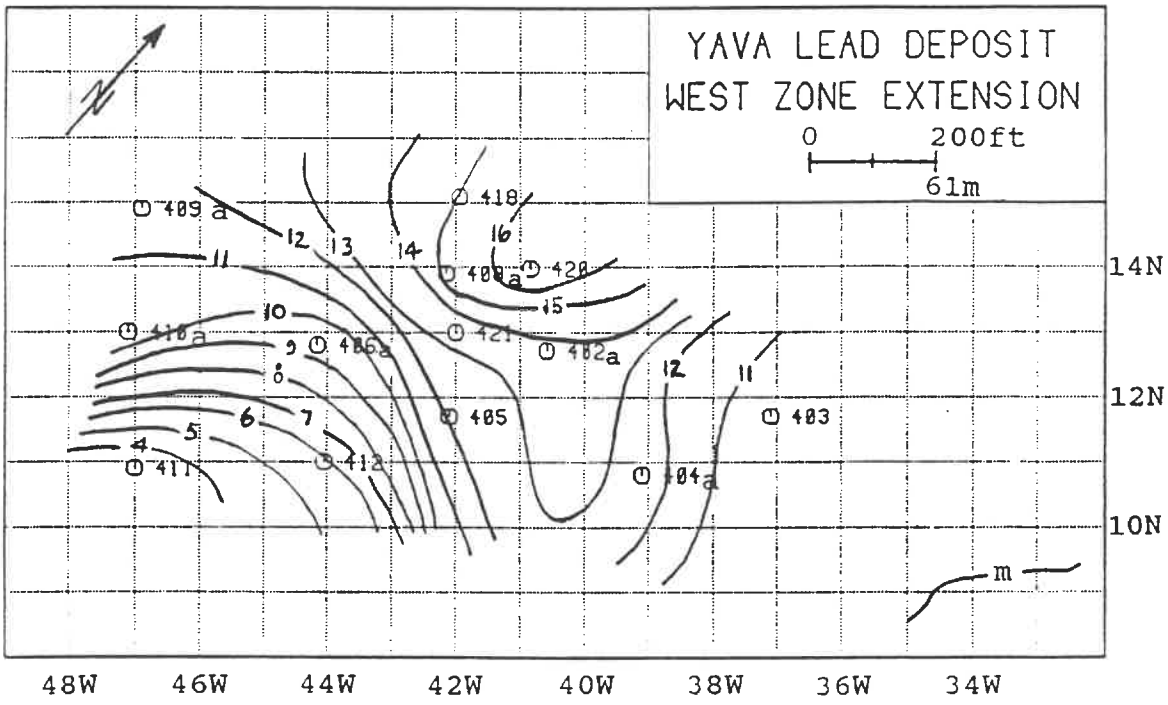


FIGURE 6.10 Canso Group thickness plan view, Yava lead deposit, west zone extension.

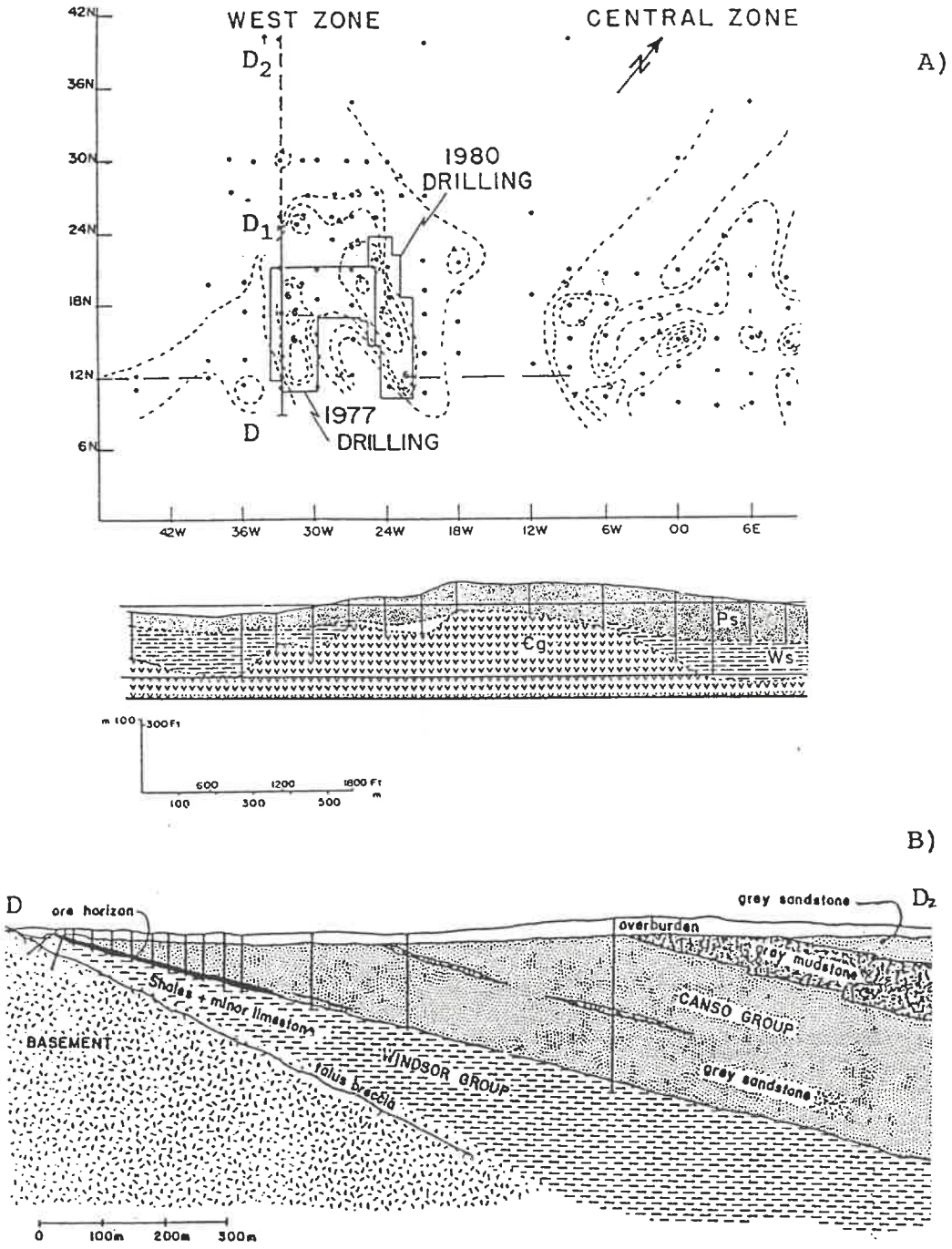


FIGURE 6.11 a) Composite plan and longitudinal geological section through the west zone (after Bonham, 1982).
b) Cross section through the west zone along 33W ($D-D_1-D_2$).

6.2 Statistical results

A number of different statistical analyses were done with samples from two of the thirteen holes logged; hole 404a and 410a. Detailed sampling for lead, zinc and total iron assays was carried out on these two holes in order to verify Bonham's observations (1982) which stated that variations in mineralization concentration occur in less than 1 metre thicknesses. The drill cores of holes 404a and 410a were sampled over ten centimetre intervals between depth, 7m and 15.3m, and 8.3m and 17.7m, respectively.

Unfortunately, the other holes were sampled only where mineralization was visually identified over different sampling intervals. For statistical purposes, the sampling interval of these holes has been regulated to 1m interval. They were analysed for lead and zinc. The chemical assay data are presented in appendix F.

Resistivity, induced polarization (IP), natural gamma ray spectrometry, gamma-gamma density and gamma-gamma spectral ratio were the geophysical parameters selected for the statistical analysis as discussed in the preceding sections.

6.2.1 Distributions

Distribution analyses are first described for samples from hole 404a. In a first step, the distribution analysis of the geophysical parameters was done with samples all along the borehole. In a second step, the distribution analysis was done with samples from each of the individual lithologies (Canso Group, Windsor Shale Group and rhyolite). The chemical samples were obtained only within the Canso Group and their distribution are studied as a whole. The geophysical distributions for hole 410a are then presented (Canso Group populations) and compared with the ones of hole 404a.

The primary statistics on the resistivity parameter are presented in Table 6.1. They show high standard deviation values and high coefficients of variation.

The next step was to verify if the distributions within the three different lithologies agree more with lognormal distributions. Table 6.1 shows that the distributions have better coefficient of variation and standard deviation. These three distributions (3 main lithologies) are better defined by the natural logarithm of resistivity.

Figure D.1 (appendix D) shows the frequency distri-

bution of the natural logarithm of resistivity for the entire hole 404a and for each lithology. Figure D.1a. shows that the distribution for the whole borehole data set is not unimodal. Figures D.1b,D.1c and D.1d help to discriminate the different populations. Figure D.1b which represents the distribution within the Canso Group exhibits different modes (around 5.1, 5.5 and 6.25). Within the Windsor shale (figure D.1c), the distribution of the natural logarithm of resistivity also has a few modes (around 3.40, 4.10, 4.90).

The variations in lithology and ore grade within the Canso Group seems to reflect these different modes. A few modes are observed in the Windsor Group although it is known to have less variations. The contact between the Canso and the Windsor groups is not always clearly marked. There is some gradation. A sandstone may sometimes be close in grain size and porosity to a shale, that would mean that one resistivity mode (values lower than 4.90 within the Canso distribution) may correspond to a shale population and that, the highest mode within the Windsor distribution may correspond to a sandstone population. The rhyolite resistivity distribution shown in figure D.1d is spread through the mean due to the small number of samples.

To summarize, the logarithm of resistivity is a good geophysical parameter to discriminate between the lithologic

groups (Canso and Windsor Groups), and to observe lithologic variations within a group.

The natural logarithm of induced polarization has more desirable values than the linear induced polarization (good coefficient of variation and standard deviation, table 6.2). The distributions for the logarithmic IP values within the shale and the rhyolite are similar. Their average mean value is around 1.65 and their average median is around 1.57, reflecting a general "IP background" of unpolarizable material.

Within the sandstone which hosts mineralization, the highest IP values are observed. The distribution has a mean of 2.45 ±.27 with a median of 2.4 (natural logarithm values).

Figure D.2a which shows the distribution of the logarithm of IP values within all lithologies displays two modes around 1.4 and 2.3. These seem to represent unpolarizable and polarizable samples, respectively. The distributions within the shale and the rhyolite (figures D.2c and D.2d) show principally one mode which represents the lowest IP values. Few high values around 2.5 are observed within these two distributions. The rhyolite is mainly unmineralized but discontinuous galena veins were

observed within the breccia. The galena veins correspond to high IP values.

The Windsor shale is not mineralized. In thin sections, only small, widely dispersed grains of pyrite and galena can be seen. More grains of pyrite were observed within coarser shale horizons (Bonham, 1983). The contact between the Canso and the Windsor Groups is not always clear; a mineralized sandstone (pyrite, sphalerite or galena) may have been misclassified within the Windsor shale which may explain the high IP values.

Figure D.2b which shows the Canso Group distribution is characterized by a unimodal distribution. It has the highest polarizable values which are associated with disseminated lead mineralization.

Table 6.3 summarizes the statistics applied to the gamma-gamma density parameter. It follows a normal distribution with reasonable coefficient of variation and standard deviation. Gamma-gamma density seems to show variations with lithology (figure D.3). The sandstone distribution (figure D.3b) is the one that is the most spread out with a mean of 10601 ±958 (median 10630) and shows a few modes. The Canso Group has mineralized and unmineralized sandstones and it is the unit that has the

most lithologic variations (sandstones, black shales, limestone pebble conglomerate).

The Windsor shale distribution (figure D.3c) has a mean of 11419 ±464 (median 11445). Shales characteristically are unmineralized and their distribution is principally unimodal. Windsor shales have less lithologic variations than the Canso Group. The rhyolite distribution (figure D.3d) has a mean of 11930 ±350 (median 12042). It shows high values corresponding to low density.

Table 6.4 shows that the spectral ratio distribution is similar to a normal distribution (small CV). The sandstone distribution shows more than 2 modes (figure D.4). The high values corresponding to mineralized zones contribute approximately 53% of the distribution and are higher than 2.00. The other 47% represent lower values concentrated around 1.75 (figure D.4b).

The shale distribution shown in figure D.4c is unimodal. Approximately 97% of the distribution reflects unmineralized samples (values around 1.70). The other values reflect higher concentration of heavy elements (values from 1.95 to 2.25). The shale is known to be unmineralized. These high values are probably the result of mineralized veins in fractured zones. They could also be due to the

presence of barite (Vaillancourt and Sangster, 1984 , Vaillancourt, 1985) or a mineralized sandstone zone that was not logged properly.

Figure D.4d shows that the rhyolite distribution displays one mode that reflects the unmineralized rhyolite which has values around 1.65. Few high values (between 1.80 and 2.00) probably represent mineralized veins seen in the breccia.

The natural gamma ray has close correlation with lithology. One expects that the counts within the rhyolite will be higher than within the shale and sandstone. As was mentioned before, the rhyolite has potassic feldspars which are responsible for increases in radioactivity. The sandstone is "clean" of clay minerals and is characterized by fairly low radioactivity.

Table 6.5 summarizes the classical statistics applied to the total count data (TC). It shows that the distributions are close to a lognormal (small coefficients of variation). There are, however, few modes corresponding to different lithologies (figure D.5a). Figures D.5b, D.5c and D.5d display logarithmic natural gamma ray distributions within the sandstone, the shale and the rhyolite, respectively.

Similarly to resistivity distributions , the total count distribution within the sandstone and the shale are not unimodal. The natural gamma ray data show lithologic variations between groups and within group (for example, black shale within the Canso Group corresponds to high count rates).

The classical statistics for the different parameters for hole 410a have been calculated only for the Canso Group population and are summarized in Table 6.6. They will be compared with those of hole 404a.

In hole 410a, the Canso Group is mainly composed of sandstone, and limestone pebble conglomerate (less abundant in hole 404a). Black shale beds are almost absent in hole 410a (see figure B.10, appendix B). These differences can be observed in figure D.6a where black shale has lower resistivity values and limestone pebble conglomerate has the highest resistivity values.

410a and 404a have similar IP distributions: one seems to be "shifted" compared to the other. This could be explained by small differences within the mineralization and geology (figure D.6b).

The density distributions (figure D.7a) within the

sandstone for holes 404a and 410a are similar as their distribution has more than one mode which seems to correspond to differences in geology within the Canso Group. Hole 410a has lower count rates than 404a (mode 11900 is absent).

Figure D.7b shows the ratio distribution of hole 410a and hole 404a within the Canso Group. They follow similar distribution pattern except that the spectral ratio range for 410a is smaller than for 404a.

The count rates (TC values) of hole 410a cannot be compared with the ones of 404a because different probes were used in the field. However, its distributions give similar information to that of hole 404a (figure D.8).

Figure D.8a shows that the distinction between each main lithologic group is more clear in this hole. There is less lithologic variation within the Canso Group and it is reflected in its total count distribution (figure D.8b). The values are less spread out around the mean (mean of 3.41±.22 and CV=6.3%, against a mean of 4.60±.46 and CV=10% for hole 404a).

The natural gamma ray distribution statistics done for the whole borehole and for each geological unit are

summarized in table 6.6.

Geochemical assays

Statistics were applied on 71 samples from borehole 404a and show that Pb ,Zn and Fe distributions are close to lognormal distributions (Table 6.7).

Figure D.9 (top) shows that the distribution of the logarithm of lead is negatively asymmetric (CA -1.91 and the mean is smaller than median). This distribution is spread around the median (9.95 which means a concentration of 2.1% Pb). Low lead concentrations can be seen between 5.3 and 9.00 (between 0.02% and 0.81%), contributing to 18.3% of the distribution.

Figure D.10 (hole 404a, on top) illustrates the distribution of the logarithmic zinc values. It shows two principal modes; one is located around 5.75 (0.03% Zn) and the other at 6.50 (0.67% Zn), corresponding to two zinc concentrations. The second population is not well defined and represent 18.3% of the distribution.

We observe that the logarithmic iron distribution in figure D.11 (top) is unimodal and is concentrated around the mean (9.7 which means 1.6% Fe). It has to be noted that

total iron assay includes all types of iron content (from pyrite, clays,etc).

The distributions of lead and zinc for hole 410a do not appear to be lognormal. They appear to be distributed over a larger range of concentrations compared with the distributions of hole 404a.

In general, compared to 404a values, hole 410a has higher concentrations of zinc and total iron and lower concentration of lead. Figures D.9 to D.11 show these different geochemical distributions and the statistics are presented in table 6.8.

RESISTIVITY					
	Mean	Median	Standard Deviation	Coeff. Variat.	Coeff. of asymmetry
All litho.	176.37	109.72	170.95	97%	1.81
Sandstone	361.44	304.70	234.76	65%	0.44
Shale	100.70	73.31	74.20	74%	1.64
Rhyolite	284.13	299.90	96.73	34%	0.34
Ln(RESISTIVITY)					
	Mean	Median	S	CV	CA
All litho.	4.77	4.69	0.90	18.9%	0.22
Sandstone	5.59	5.72	0.89	16.0%	-0.83
Shale	4.38	4.30	0.67	15.4%	0.21
Rhyolite	5.58	5.70	0.39	6.9%	-0.95

Table 6.1 Primary statistics done with resistivity, hole 404a. Statistics were calculated with resistivity values and natural logarithmic values from all lithologies, and from the Canso Group (sandstone), the Windsor Shale and the rhyolite, respectively.

INDUCED POLARIZATION					
	Mean	Median	Standard Deviat.	Coeff. Variat.	Coeff. asymmetry
All litho.	6.95	5.33	4.24	61%	2.27
Ln(INDUCED POLARIZATION)					
	Mean	Median	S	CV	CA
All litho.	1.80	1.67	0.51	28.1%	0.63
Sandstone	2.45	2.40	0.27	11.2%	0.93
Shale	1.61	1.53	0.40	24.9%	1.19
Rhyolite	1.69	1.61	0.33	19.3%	1.64

Table 6.2 Primary statistics done with induced polarization (IP), hole 404a. Statistics were calculated with IP values from all lithologies, and with natural logarithmic values from all lithologies, and from the Canso Group (sandstone), the Windsor shale and the rhyolite.

DENSITY	Mean	Median	Standard Deviation	Coeff. Variat.	Coeff. of Asymmetry
All litho.	11291	11426	718	6.4%	-1.22
Sandstone	10601	10630	958	9.0%	-0.35
Shale	11419	11445	464	4.0%	0.08
Rhyolite	11930	12042	350	2.9%	-2.29

Table 6.3 Primary statistics done with gamma-gamma density parameter of hole 404a, from all lithologies, and from the Canso Group (sandstone), the Windsor shale and the rhyolite.

SPECTRAL RATIO	Mean	Median	Standard Deviation	Coeff. Variat.	Coeff. of Asymmetry
All litho.	1.76	1.68	0.24	13.7%	2.48
Sandstone	2.06	2.02	0.36	17.3%	0.50
Shale	1.69	1.67	0.09	5.2%	3.02
Rhyolite	1.65	1.62	0.08	4.7%	2.96

Table 6.4 Primary statistics done with spectral ratio values of hole 404a from all lithologies, and from the Canso Group (sandstone), the Windsor shale and the rhyolite.

TOTAL COUNT (TC)					
	Mean	Median	Standard Deviation	Coeff. Variat.	Coeff. of Asymmetry
Sandstone	110.59	84.09	52.55	47.5%	0.89
Ln(TC)					
	Mean	Median	S	CV	CA
All litho.	5.12	5.18	0.49	9.5%	-0.48
Sandstone	4.60	4.43	0.46	10.0%	0.05
Shale	5.18	5.20	0.33	6.3%	-0.42
Rhyolite	5.87	5.89	0.09	1.5%	-0.85

Table 6.5 Primary statistics done with the natural gamma ray parameter of hole 404a within the Canso Group (sandstone) . The natural logarithmic values were analysed within all lithologies, and within the Canso Group, the Windsor shale and the rhyolite.

Ln(RESISTIVITY)					
	Mean	Median	Standard Deviation	Coeff. Variat.	Coeff. of Asymmetry
Sandstone	6.40	6.48	0.81	12.6%	-0.85
Ln(INDUCED POLARIZATION)					
Sandstone	2.86	2.81	0.43	14.9%	0.18
DENSITY					
Sandstone	10144	10454	766	7.6%	-1.15
SPECTRAL RATIO					
Sandstone	2.03	1.97	0.26	12.9%	0.84
Ln(TOTAL COUNT)					
All litho.	4.12	4.22	0.54	13.1%	-0.23
Sandstone	3.41	3.38	0.22	6.3%	-0.21
Shale	4.21	4.23	0.21	4.9%	-0.76
Rhyolite	5.00	4.93	0.14	2.9%	1.34

Table 6.6 Primary statistics done for hole 410a within the Canso Group (sandstone) with the natural logarithmic values of resistivity, induced polarization, gamma-gamma density and spectral ratio. The natural logarithmic values of total count were analysed within all lithologies, and within the Canso Group, the Windsor shale and the rhyolite.

CHEMICAL ASSAYS - Hole 404a					
	Mean	Median	Standard Deviation	Coeff. Variat.	Coeff. of Asymmetry
Pb (%)	2.52	2.08	1.63	64.6%	0.27
Ln(Pb)*	9.68	9.94	1.34	13.9%	-1.91
Zn (%)	0.04	0.03	0.02	46.1%	1.95
Ln(Zn)*	5.89	5.77	0.37	6.3%	1.24
Fe (%)	1.69	1.51	0.53	31.3%	2.70
Ln(Fe)*	9.70	9.62	0.25	2.6%	1.74

*: The values in percent have been multiplied by 10000 before applying the logarithm.

Table 6.7 Primary statistics on chemical assays of lead, zinc and total iron for hole 404a. The concentration values and their natural logarithmic values were analysed.

CHEMICAL ASSAYS - Hole 410a					
	Mean	Median	Standard Deviation	Coeff. Variat.	Coeff. of Asymmetry
Ln(Pb)*	8.82	9.22	1.51	17.1%	-0.91
Ln(Zn)*	7.32	7.50	1.19	16.3%	-0.26
Ln(Fe)*	10.25	10.28	0.35	3.5%	-0.03

*: The values in percent have been multiplied by 10000 before applying the logarithm.

Table 6.8 Primary statistics on chemical assays of lead, zinc and total iron for hole 410a. The concentration values and their natural logarithmic values were analysed.

6.2.2 Univariate data analysis

1)Scatterplot diagrams

Scatterplot diagrams for geophysical parameters of hole 404a are first presented in appendix E. The description of any relationship or grouping for each scatterplot diagram is summarized in table 6.9 which follows. The relationships found from the crossplots of hole 410a are then compared with the ones of 404a.

Correlations between mineralization (chemical assays) and geophysical parameters are discussed in the following section.

	X axis
Y axis	Ln(RESISTIVITY)
Ln(TC) (Fig. E.1)	-It shows 3 distinct lithologies (3 distinct clouds). -Few samples of the Canso Group are within the cloud of the Windsor shale.
Ln(IP) (Fig. E.2)	-It presents three main groups. -Few Canso samples seem to be misclassified.

Table 6.9 Description of the scatterplot diagrams for hole 404a (figures E.1 to E.10, appendix E)

	X axis
Y axis	Ln(RESISTIVITY)
ɣ-ɣ DENSITY (Fig. E.3)	-The three lithologies can be separated into three main clouds. -The Windsor shale and the rhyolite have nearly the same density but the rhyolite has higher resistivity values. -Few Canso samples are classified into the Windsor shale.
RATIO (Fig. E.4)	-Two major groups: -1) Canso Group has the highest resistivity values with spectral ratio values that are spread out from the lowest to the highest values. -2) including the Windsor shale and the rhyolite, has a smaller range of spectral ratio values with low values. -Few Canso sandstone samples seem to be part of the Windsor population.
	Ln(IP)
Ln(TC) (Fig. E.5)	-Shows the three distinct lithologies.
ɣ-ɣ DENSITY (Fig. E.6)	-The Canso group has highest IP values and has the lowest count rates (no direct correlation between these two parameters).
RATIO (Fig. E.7)	-The Canso group varies from low to high spectral ratio values and has higher IP values than the Windsor Group and the rhyolite. -Low spectral ratio values mainly characterized the Windsor shale and the rhyolite but there is no correlation

Table 6.9 (cont'd)

	X axis
Y axis	γ-γ DENSITY
Ln(TC) (Fig. E.8)	-There is no evident correlation between these two parameters within all lithologies but we can easily see the 3 lithologies . -Few Canso samples were classified within the Windsor population.
Ratio (Fig. E.9)	-This shows a linear correlation (R=.87)
	Ratio
Ln(TC) (Fig.E.10)	.Two main groups are observed: one with low ratio values where the rhyolite and the Windsor shale occur, and the other which is spread out from low to high ratio values. The Canso population occurs in this second group.

Table 6.9 (cont'd)

The different scatterplot diagrams for hole 410a show closely the same relationships observed from hole 404a. Figures E.11 to E.13 are a few selected plots that confirm their similarities. However, the natural radioactivity gamma ray count rates measured in each of these two holes cannot be quantitatively compared because two different probes were used. For the same lithology, the count rates within hole 404a are almost double. Notice also that the lithologies within hole 410a were divided into four groups instead of three. A "rhyolitic boulder" which forms the fourth group was observed within the Windsor shale.

2) Simple linear regression analysis

Qualitative relationships between the geophysical parameters for holes 404a and 410a have been discussed in the preceding sections. In this section quantitative relationships between geophysical parameters and mineralization will be determined in order to predict the concentration of mineralization from geophysical variables.

The most significant analyses for both holes are discussed in the following.

Hole 404a

A cross plot of lead concentration versus spectral ratio is shown in figure E.14. They have the best correlation coefficient (r =.82) and the lead concentration can be expressed by:

$$\%Pb = 4.23*RATIO - 6.91 \qquad (6.1)$$

with a standard error of the estimate equal to 0.95.

A cross plot of lead concentration versus gamma-gamma density is shown in figure E.15 and also shows a reasonable correlation (r=.74). The lead concentration can be predicted as follows:

$$\%Pb = -1.54*10^{-3} * \gamma\text{-}\gamma \text{ DENSITY} + 18.12 \qquad (6.2)$$

with a standard error of the estimate equal to 1.1.

It was expected that IP will have a good correlation with lead concentration but this is not what was observed from the scatter diagrams and the simple linear regression analysis. IP is poorly associated with lead mineralization with a correlation coefficient of .23 (figure E.16).

The zinc and total iron concentrations do not show any good correlation with different geophysical parameters.

Hole 410a

A cross plot of lead concentration versus the spectral ratio for hole 410a is given in figure E.17 and shows the best correlation (r=.83). The lead concentration can be predicted as follows:

$$\%Pb = 4.33 * \text{RATIO} - 7.37 \qquad (6.3)$$

with a standard error of estimate equal to 0.76. This equation (eq. 6.1) is almost the same as for hole 404a. Lead concentration versus gamma-gamma density is shown in figure E.18 and also has a reasonable correlation (r=.73). The associated regression equation is:

$$\%Pb = -1.3*10^{-3} * \gamma\text{-}\gamma \text{ DENSITY} + 14.6 \qquad (6.4)$$

with a standard error of the estimate equal to 0.93 which is almost the same equation as for hole 404a (eq. 6.2).

Lead concentration versus IP (figure E.19) has a poor correlation (r=.29) which confirms that IP is not well correlated with lead mineralization.

The zinc and total iron do not show good correlation with geophysical parameters. However, a correlation coefficient of .62 was found between total iron and zinc concentrations (logarithmic values, figure E.20). Many studies (Vaillancourt and Sangster, 1984, Bonham, 1983) have observed that pyrite and sphalerite occur in the same environment which could explain this correlation. However, it must be realized that the chemical analyses were made for whole iron content which probably masks part of the correlation.

The correlation between zinc and total iron was not observed in hole 404a. For logarithmic values, the correlation coefficient, r, was 0.09. The lead concentration is higher in this hole, and zinc and total iron concentrations are lower.

6.2.3 Multivariate data analysis

1) Multiple linear regression analysis

Hole 404a

Table F.1 in appendix F includes the data used in the multiple regression analysis. The correlation matrix with lead, zinc, total iron and the different geophysical parameters was first calculated and is shown in Table 6.10. There is good correlations between Pb and the spectral ratio or gamma-gamma density. Pb and Fe have a coefficient of correlation of -.487 which is poor, but still it is among the best correlation coefficients in the correlation matrix.

We do not observe any good correlation between Zn or FeO and the geophysical parameters. Multiple regression with these two chemical assays as dependent variables will then not be carried out.

From the stepwise method, the lead concentration is characterized by:

$$\%Pb\ pred. = 4.23 * Ratio - 6.91 \qquad (6.5)$$

with a correlation coefficient of .82 and a standard error of estimate equal to 0.95. The residuals appear to have a normal distribution.

	Pb	Fe	Zn	Resis.	IP	Density	Ratio	TC
Pb	1.00							
Fe	-0.49	1.00						
Zn	-0.17	0.11	1.00					
Resist.	-0.12	-0.33	-0.07	1.00				
IP	0.23	-0.11	0.23	-0.22	1.00			
Density	-0.74	0.25	-0.05	0.26	-0.49	1.00		
Ratio	0.82	-0.32	-0.10	-0.24	0.33	-0.92	1.00	
TC	-0.22	0.21	-0.11	-0.37	-0.08	0.40	-0.33	1.00

Table 6.10 Correlation matrix calculated in the multiple regression analysis - Hole 404a. Variables used: lead, zinc, total iron, resistivity, induced polarization (IP), gamma-gamma density, spectral ratio and total count (TC).

	Pb	Fe	Zn	Resis.	IP	Density	Ratio	TC
Pb	1.00							
Fe	-0.13	1.00						
Zn	0.22	0.52	1.00					
Resist.	-0.13	0.10	0.11	1.00				
IP	0.29	0.05	0.15	-0.41	1.00			
Density	-0.73	0.03	-0.27	-0.10	-0.43	1.00		
Ratio	0.83	-0.12	0.25	-0.01	0.31	-0.89	1.00	
TC	-0.03	0.06	-0.06	-0.37	0.11	0.17	-0.07	1.00

Table 6.11 Correlation matrix calculated in the multiple regression analysis - Hole 410a. Variables used: lead, zinc, total iron, resistivity, induced polarization (IP), gamma-gamma density, spectral ratio and total count (TC).

Hole 410a

The data set used for this hole is available in table F.2 (appendix F). The correlations between the chemical assays of Pb, FeO and Zn and the different geophysical parameters are given in the correlation matrix presented in Table 6.11. We observe that total iron and Zn have a correlation coefficient of 0.52.

The lead seems to be associated with the spectral ratio and the density parameters with correlation coefficients of 0.83 and -.73, respectively (spectral ratio and density have a good correlation (R=-.89)).

The other correlations between assays and geophysical parameters are poor and a multiple regression will be applied using lead concentration only as a dependent variable (iron and zinc will be omitted).

From the stepwise method, the spectral ratio was selected and explains by itself 69% of the sample (r=.83). The regression equation is defined by:

$$\%Pb = 4.33 * Ratio - 7.37 \qquad (6.6)$$

with a standard error of the estimate equal to 0.76, giving almost the same equation as for hole 404a (equation 6.5).

The distribution of residuals is close to a normal distribution. From residual scatterplots, the predicted values versus standardized residuals have unequal variance. The spread of the residual increases with the magnitude of the predicted values. The gamma-gamma density values versus the standardized residuals show a spread of the residual increasing with decreasing gamma-gamma density values (the cross plot of gamma-gamma density versus lead concentration already showed this increasing spread).

We also have forced IP, density and ratio to enter into the equation. With a correlation coefficient of .83 the regression equation is:

$$\%Pb = (4.53 * ratio - 7.6*10^{-3} * IP + 1.04*10^{-4} * density - 8.96) \quad (6.7)$$

where the standard error of the estimate equals 0.763. This new equation does not improve the precision of the estimate and is not retained.

If we take the values in hole 410a and sample them every metre, the simple linear regression equation determined with Lotus 123 is then:

$$\%Pb = 4.54 * Ratio - 7.843 \quad (6.8)$$

where r equals .98 and the standard error of the

estimate, equals 0.189. This equation is quite similar to the ones calculated with observations sampled every 10cm, but r and s values are improved.

Lets take a hole where chemical assays were analysed over one metre and evaluate lead content with this last equation (eq. 6.8). For hole 406a, the results are summarized as follows:

depth	%Pb-assay	%Pb pred.
9m	0.03	0.79
10m	2.36	2.60
11m	1.10	1.42

We observe that the low lead concentration value is not well predicted, whereas the two other values are only slighly overestimated.

The regression analysis done previously for holes 404a and 410a showed that the regression was efficient for lead values close to the mean value. Low values are over estimated by the regression model whereas high values are under estimated. It has been found that lead concentration is best predicted by the ratio parameter and that the zinc content is not characterized by any parameter.

Multiple regression confirms the correlation equations obtained with the simple regression analysis. Regression

equations 6.5 and 6.6 calculated for both hole 404a and 410a are exactly the same as the simple linear regression equations 6.1 and 6.2, respectively. This supports the assumptions made for the simple regression analysis and for the multiple regression and they are acceptable.

2) Principal component analysis (PCA)

PCA was carried out on data from holes 404a and 410a, respectively. Geophysical variables that were included in the analysis are resistivity, induced polarization (IP), total count natural gamma ray, gamma-gamma density and the spectral ratio. The lead content was also considered in the analysis. These data sets are the same as those used in the multiple regression analysis.

Two major factors resulting from the analysis of hole 404a data set have eigenvalues of 3.05 and 1.40. They explain over 74.0% of the total variance of the data set.

Figure 6.12 shows the different variables entered into the analysis plotted on the first two principal factors. We observe that the lead content, the spectral ratio and the gamma-gamma count rates (inversely proportional to lead content) typify factor 1. The resistivity and total count represent factor 2. They are located on opposite sides

implying that an increase in resistivity corresponds to a decrease in count rate. IP is mainly related to factor 1. Then, factor 1 seems to characterize the lead mineralization and factor 2, the lithology.

Figure 6.13 shows the regression factor score coefficient for each observation of the data set plotted on the first two principal factors. The data were sampled in the Canso group within the following lithologic sections: sandstone between 7.05-11.25m, black shale at 12.05m, sandstone from 12.65-14.75m and a cross bedded sandstone from 14.85-15.25m. This information was obtained from the study of the drill cores. Comparing the sandstone sequences, the upper sandstone (5.49-11.4m) seems to be more resistive, has less potassic minerals and has variable lead concentrations (from low to high values). The black shale is characterized by high natural gamma count rates and is not mineralized.

As in hole 404a, two major factors result from the PCA of hole 410a data set. Their respective eigenvalues are 2.85 and 1.57 which explain near 74% of the total variance of the data set.

The variables are plotted on the first two factors and are shown in figure 6.14. As in hole 404a, factor 1

typifies variables that have good correlation with lead content and factor 2 denotes variables associated with lithology. The IP variable is characterized by both factors implying that it is associated with mineralization as well as geology.

Figure 6.15 shows the regression factor score coefficients of the data set plotted on the first two factors. The lithology illustrated is a sandstone at 9.65-10.65m, a limestone pebble conglomerate from 10.95-15.45m, and a sandstone with coal from 15.55-17.65m.

Each lithologic variation within the Canso Group appears to have variations in mineralization. Generally, the limestone pebble conglomerate can be easily differentiated from the other sandstone sequences. It is more resistive and has less potassic minerals. It has the highest ore grade. The sandstone with coal has few high values of lead and has higher potassic content than the limestone.

In summary, the following conclusions may be drawn from the PCA analysis:

1) Lead mineralization is mainly correlated with the spectral ratio and the gamma-gamma count rates,

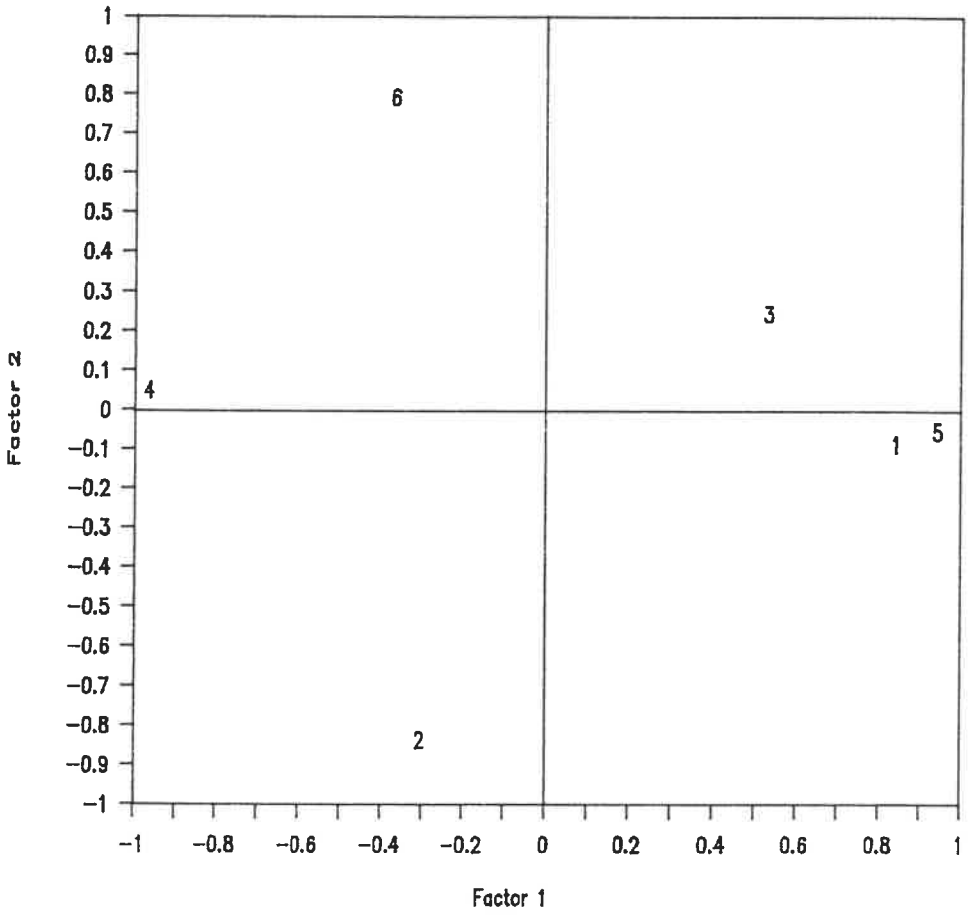


FIGURE 6.12 Plot of initial variables (lead, resistivity, total count, gamma-gamma density, spectral ratio) on first two principal factors for hole 404a data set (after rotation). Horizontal axis is factor 1, vertical axis is factor 2.
(1- represents lead content, 2- resistivity, 3-induced polarization,4- gamma-gamma density, 5- spectral ratio and 6- total count natural gamma ray(TC)).

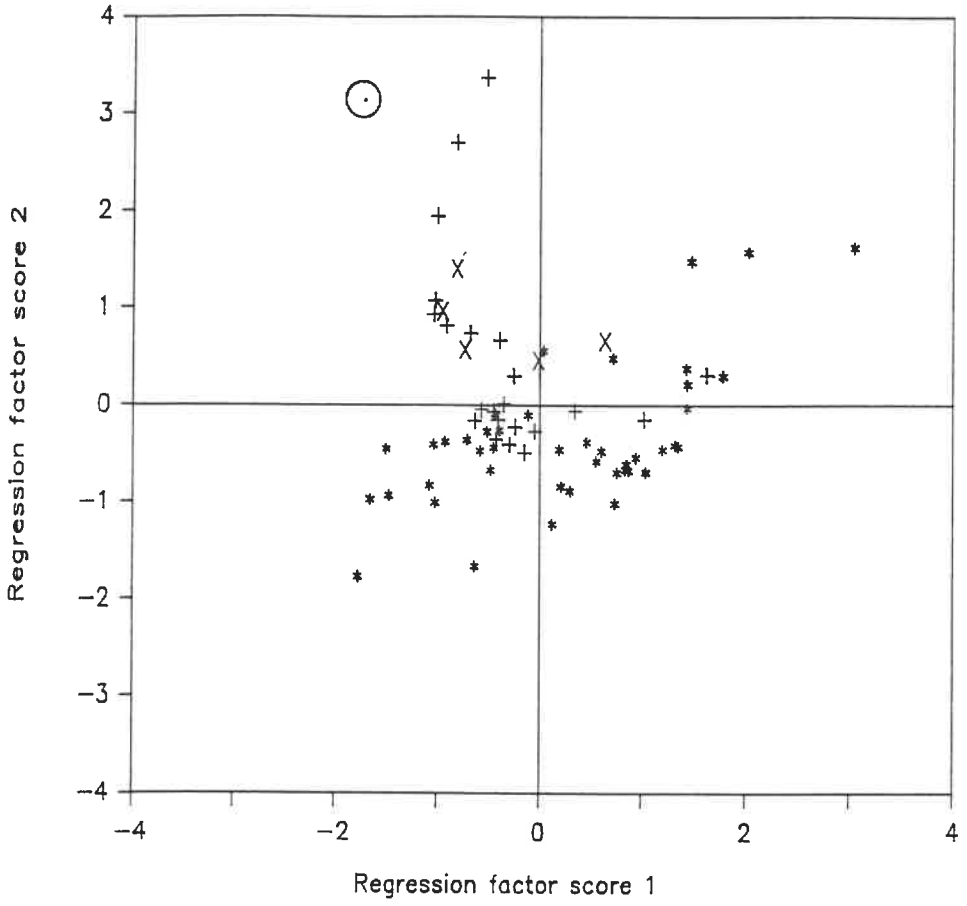


FIGURE 6.13 Plot of the regression factor score coefficients for the 404a data set on the first 2 principal factors (after rotation). Horizontal axis is the regression factor score for factor 1 and the vertical axis is the regression factor score for factor 2. The lithologic variations are represented by:

*: sandstone between depth 7.05-11.25m
⊙: black shale at 12.05m
+: sandstone from 12.65-14.75m
x: cross-bedded sandstone from 14.85-15.25m.

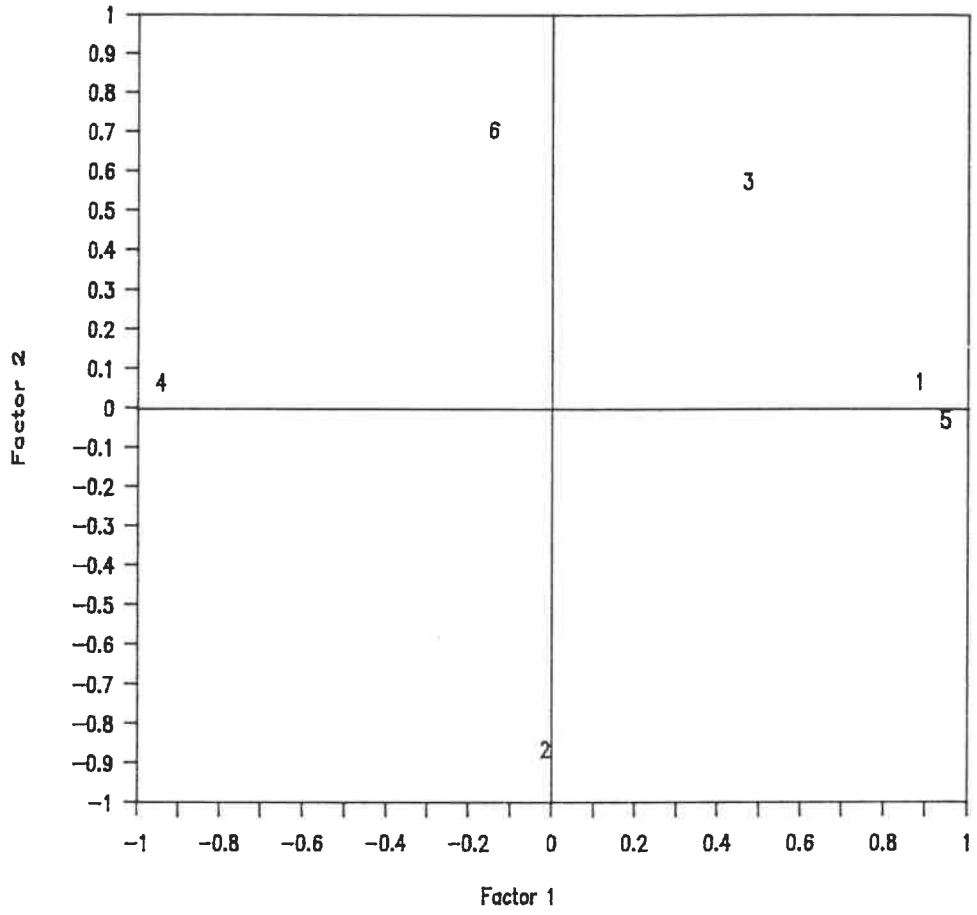


FIGURE 6.14 Plot of initial variables (lead, resistivity, total count, gamma-gamma density, spectral ratio) on first two principal factors for hole 410a data set (after rotation). Horizontal axis is factor 1, vertical axis is factor 2.
(1- represents lead content, 2- resistivity, 3-induced polarization,4- gamma-gamma density, 5- spectral ratio and 6- total count natural gamma ray(TC)).

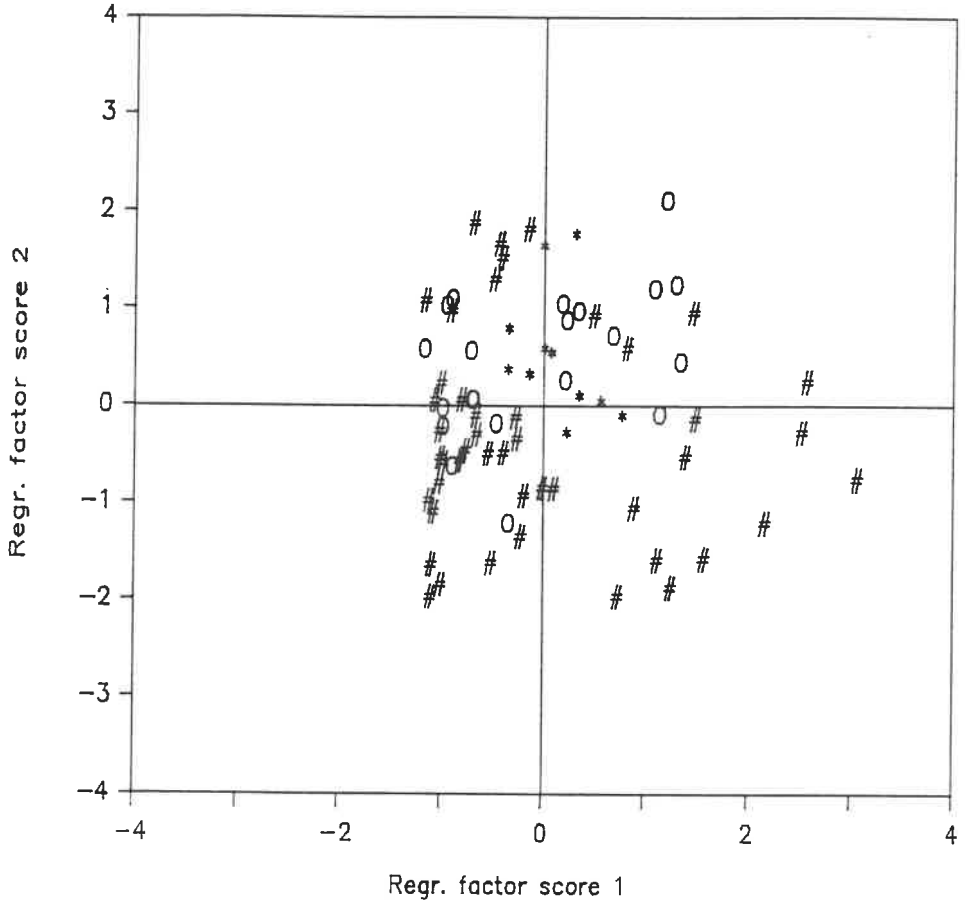


FIGURE 6.15 Plot of the regression factor score coefficients for hole 410a data set on the first 2 principal factors (after rotation). Horizontal axis is the regression factor score for factor 1 and the vertical axis is the regression factor score for factor 2. The lithologic variations are represented by:

*: sandstone between depth 9.65-10.65m
#: limestone pebble conglomerate from 10.95-15.45m
o: sandstone with coal from 15.55-17.65m

2) The lithology is characterized by the resistivity and natural gamma ray parameters,
3) Induced polarization seems to respond to both lithology and mineralization,
4) Generally, high concentrations of lead occur in the Canso sequence that is the most resistive and has less potassic minerals (clays).

3) Discriminant analysis

Discriminant analysis was carried out in order to define the two main geological units, the Canso Group and the Windsor Shale Group, with a combination of geophysical parameters.

Discriminant analysis was first executed with data from hole 404a. The same analysis was repeated for data from hole 410a. The data sets used for both hole are listed in tables F.3 and F.4 (appendix F), respectively .

The last step in the discriminant analysis was to classify the hole 406a observations into groups with the estimated equation from hole 410a data.

Discriminant analysis for 404a

The variables selected in the discriminant analysis were chosen with the stepwise method where the Wilk's lambda criterion was considered (see section 5.5.3). All of the five variables (Ln(resistivity), Ln(IP), gamma-gamma density, spectral ratio and Ln(TC)) were selected with the discriminant score D_{ig} defined as:

$$D_{ig} = 0.49 * \text{Ln(resistivity)} + 1.70 * \ln(\text{IP}) + 5.22e\text{-}4 * \text{density} + 3.56 * \text{Ratio} - 0.43 * \ln(\text{TC}) - 15.38 \quad (6.9)$$

where i: represents the observation number

g: represents the group number

The group centroid of the Canso group and the Windsor shale are 2.475 and -0.76, respectively. The percentage of cases classified correctly is 92.47% and details are summarized in the following table.

Actual Group	Group #	Number of cases	Predicted group membership 1	2
Canso Group	1	103	90	13
Windsor shale	2	335	20	315

Table 6.12 Discriminant analysis: Classification results for hole 404a

The cases that were not well classified are effectively different from the average groups. In the Canso Group, around 11.95m depth, we observe very low resistivity values and high radioactivity which is not particular to that group; it corresponds to the black shale unit.

The cases near the contact between two groups were also misclassified. As it was mentioned earlier, this contact is gradational and a few cases may have been misclassified.

At the base of the Windsor shale we also may have misclassified cases with high count rates and resistivity values as we approach the rhyolitic breccia. Observations around 40m where resistivity values are high, may have been misclassified because of the presence of gypsum (Patterson, 1986).

The five variables were also selected in the 410a data analysis and the discriminant score is expressed as:

$$D_{ig} = 0.47 * \text{Ln(resistivity)} + 2.39 * \text{Ln(IP)} \qquad (6.10)$$
$$+1.11e\text{-}3 * \text{density} + 2.28 * \text{Ratio} - 1.39 * \text{Ln(TC)} - 18.31$$

where i represents the case number

g represents the group number

The group centroids for the Canso group and the Windsor shale are 2.436 and -1.655, respectively. The

percentage of cases classified correctly is summarized in the following table.

Actual Group	Group #	Number of cases	Predicted group membership 1	2
Canso Group	1	89	80	9
Windsor shale	2	131	0	131

Table 6.13 Discriminant analysis: Classification results for hole 410a

The total number of cases is 220 and 211 of these cases (95.91%) were correctly classified.

The misclassified cases occur near the contact of the two major units with low resistivity values and higher TC values. The contact is a "weathered zone" described an unconsolidated argillaceous zone.

Let's take another hole where the geology and the geophysical parameters were also averaged every 0.1m. The classification results for this hole 406a are as follows.

Actual Group	Group #	Number of cases	Predicted group membership 1	2
Canso Group	1	91	69	22
Windsor Shale	2	214	2	212

Table 6.14 Discriminant analysis: Classification results for hole 406a (0.1 metre samples)

Using the estimated equation 6.10, 92.13% of the cases from hole 406a were well classified. 99% of the Windsor shale cases were well classified against 75.8% in the Canso group.

In the Canso group, a group of eleven misclassified cases are located near the casing (depth 5.75 to 6.85). The second group of misclassified cases occurs between 11.85 and 12.35m where sharp geophysical anomalies have been observed. At those depths, an increase in lead and zinc content is associated with high IP and density values and a sharp decrease in resistivity.

Five other misclassified cases are located around the contact between the two groups (around 14.45 and 15.05m). The last two misclassified cases located in the Canso Group (depth 13.15 and 13.45m) cannot be related to any particular

geological events (geological information is not precise).

The Canso group has more geologic variations than the Windsor Shale and should be divided in sub-groups to get a better classification.

In summary, the discriminant function appears to classify observations sampled at 0.1 metre within groups, with over 90% of cases well classified.

CHAPTER 7

DISCUSSION

Multiparameter geophysical logging techniques are very attractive and promising as they can provide:

- information lost by poor core recovery (continuous logging),

- several simultaneous types of information. A combination of characteristic physical rock properties is often useful to delineate the mineralization where direct characterization fails. For example, in gold exploration, it is very useful since gold is not directly recognizable (Urbancic, 1985, Urbancic and Mwenifumbo, 1986).

Furthermore, the multiparameter logging methods have several other advantages:

- the data are immediately available for processing and evaluation compared to the delays in assay sampling,

- it requires a minimal storage space compared to drill core,

- they are statistically more reliable than core samples because the volume of investigation is generally greater. The recorded data are less biased since there is no personal observation.

Thirteen holes were geophysically logged. They were

analysed qualitatively and two selected holes (404a, 410a) were analysed quantitatively and statistically. The qualitative results have shown that the lead mineralization is mainly characterized by high gamma-gamma spectral ratios and to a lesser extent, by high chargeability values (IP).

The geology is well delineated by the resistivity and natural spectral gamma ray logs. The rhyolite is the most resistive rock type of the Yava mine area and also has the highest radioactivity. The Windsor shale is the most conductive rock type and has higher radioactivity than the Canso Group. The latter group has more lithologic variations which are associated with resistivity variations (mineralized sandstone, black shale and "puggy" shale units are more conductive than the nonmineralized sandstone and limestone pebble conglomerate).

The spectral gamma-gamma density log delineates mineralization, fractures and lithologies. An optimal high energy window should be found so that it would mainly characterize lithologies while the spectral ratio would delineate heavy elements. The standardization procedures (section 4.3.2) should be improved so the correlation between the spectral gamma-gamma measurements obtained in different holes could be accurately related. The gamma-gamma spectral logging method would then appear to be

the most useful technique to delineate both lead mineralization and geology.

We expected to differentiate galena from sphalerite with induced polarization (IP) since disseminated galena responds to IP while sphalerite does not. Because sphalerite occurs most of the time with disseminated pyrite (Bonham, 1983), it was not possible to distinguish sphalerite from pyrite and galena.

Pyrite was hardly differentiated from lead mineralization since both disseminated sulphides respond to IP and have high spectral ratios, and seem to occur together most of the time.

Vaillancourt (1985) has mentioned that the mineralized sandstone is mature with detrital muscovite, and kaolinite as dominant clay, while the unmineralized sandstone is greenish, immature and has chlorite as dominant clay (table 7.1). We expected to differentiate these two types of sandstone with natural gamma ray logs which would have been a very good way to delineate the mineralized sandstone. According to the author's observation, the sandstone is often mineralized up to the top of the sequence, and from Bonham's work (figure 6.11), the immature green sandstone is not present in the working area.

In the event of further explorations to the north, natural gamma ray spectrometry should be considered for mapping the potassic sandstone.

Vaillancourt (1985) gives the sandstone porosity of the mature sandstone as varying from 1% to 5% within the galena-rich portion and 15% to 25% in the galena-poor portion. The porosity measurement is then an indirect method for lead delineation. In oil reservoirs studies, the rock porosity determination is very important and is often defined by resistivity or density logging. Since the disseminated mineralization seems to influence the lithology conductivity and density, neither the resistivity nor density were in this case a useful tool for porosity determination.

Bonham (1983) has stated that lead enrichments generally occur in bedrock depressions where the Pennsylvanian sandstone (Canso Group) thickness is greater. He showed the some similarities of the Yava deposit to other deposits which related to the sandstone thickness role. He quoted Christofferson et al. (1979) who stated that the Vassbo and Guttusjo deposits in Sweden were related to underlying diabase, paleodepressions and thicker sandstone. Mineralized solutions flowed through the sedimentary sequence along low pressure conduits provided by the thicker sandstone overlying the diabases.

Since this study is limited to the southwestern part of the west zone, these two major ore relationships (sandstone thickness and paleodepressions) were not corroborated in the section study. However, they should be considered in further studies.

Very few holes (holes 408, 418, 420 and 421) shows zinc enrichments down-dip which are generally associated with lower lead grades. The spectral ratio clearly characterizes and delineates the lead mineralization. Zinc, however, is not characterized by any of the geophysical parameters. The section study does not show further correlations since the assay sampling is inadequate.

The distribution and univariate (scatterplot diagrams) analyses brought essential information at the beginning of the statistical study: resistivity and radioactivity delineates the different lithologies; IP has two response levels; so does the spectral ratio (high values associated with mineralization, and low background values); some Canso samples are not differentiable statistically from the Winsdor samples. These simple and rapid statistics should always be part of an interpretation study as they outline fundamental correlations.

Some expected correlations did not show up (eg. Zn with

FeS_2), and may be attributed to the geochemical assay type and the assay sampling choice . Neither zinc nor total iron content had meaningful correlations with the geochemical or geophysical parameters in contrast with the previous observations made by Bonham (1983) who noticed that sphalerite and pyrite were present together in limited calcareous sections within the sandstone, while galena rather occurs outside these sections.

In the present study, the author tried to find correlations between sulfides (galena, pyrite and sphalerite) and the geophysical parameters. Unfortunately, the total iron assay is not the best assay to delineate the pyrite content since there are some clay minerals with iron particles within the sampled sandstone that are considered.

The assay sampling also has its own limitations. Averaging over a large sample interval can reduce the local inhomogeneities that exist, emphasizing regional features (dilution effect). With very low zinc content (ppm level) averaging over half a metre or so cannot be as accurate as averaging over a smaller interval. On the other hand, the radius of investigation encountered during the logging depends on probe characteristics and is limited to a defined depth interval. A core sample interval smaller than the defined interval will not likely show meaningful

correlations between geochemical assays and geophysical parameters.

Multiple linear regression like the simple linear regression revealed that lead mineralization best correlates with the spectral ratio. Regressions were able to predict lead content with a correlation coefficient of approximately 0.82 with a standard error of estimate varying from 0.76 to 0.95 for hole 404a and 410a respectively (sampled every 10 cm). In general, the predicted linear model overestimates low lead content and underestimates high lead content. A non-linear regression model may predict lead content with better correlation coefficient and standard error of estimate. Once improved, the predicted lead content could be used for ore reserve estimation instead of lead assays of drill core from which selected samples depend on the geologist judgement and experience (in the present case, they were selected where mineralization visually occurred over different intervals).

Two major factors result from the factor analysis and explain 74% of the total variance of the data set in both hole 404a and 410a. The first factor is related to lead content. The spectral ratio is proportional to lead concentration while the gamma-gamma density (presented in count/sec) is inversely proportional (figures 6.12 to 6.15).

The second factor is related to lithologic variations and, as observed in the qualitative interpretation, is mainly characterized by resistivity and natural radioactivity. As the Canso Group resistivity increases, the natural radioactivity decreases.

Both factors are influenced by the chargeability (IP parameter), especially in hole 410a. The total iron content along this hole is higher than along hole 404a (average value of 3% FeO against 1.7% FeO for hole 404a) and predicates the presence of clay minerals which can produce polarization. In this particular hole, IP responds to disseminated sulfides but also to some extent, to lithologic variations.

The discriminant analysis was carried out in order to distinguish the Windsor shale Group from the Canso Group with a combination of geophysical parameters. Since it appeared to classify observations with a percentage of well classified cases over 90% within these two major groups, the discriminant analysis should now be use to classify the lithologic variations that occur in the main group of interest (Canso Group). The mineralized sandstone may be characterized by a combination of geophysical parameters which could be used as a guide during exploration. Detailed assays for a few additional holes are needed for further

studies.

In summary, multiparameter geophysical logging successfully delineated the mineralization and environment of the Yava sandstone lead deposit. The geophysical data may be useful for ore reserve estimation with some assay calibrations. This subject is a good candidate for further research. The present type of study should be extended to other deposit types in order to assist people in ore zone definition.

	Porosity	Quartz Grains	Clay Content
Grey sandstone	- 1-5% in galena-rich portion - 15-22% in galena-poor portion	- medium to coarse grained - mature, well rounded - overgrowths common	- 1-15%
Green sandstone	- 8-10%	- medium grained - immature, angular - overgrowths not common	- 15-25%

	Clay Mineralogy	Sulphide, Sulphate Mineralogy	Coal	Other Minerals
Grey sandstone	- high kaolinite/chlorite ratio	- galena - pyrite - sphalerite - barite	- abundant at base of sequence - silicified - associated with abundant pyrite, sphalerite and galena	- rutile, zircon - potassium feldspar - detrital muscovite } common
Green sandstone	- low kaolinite/chlorite ratio	- pyrite	- present in minor amounts - non-silicified - associated with minor pyrite	- rutile, zircon - potassium feldspar - detrital muscovite } rare

TABLE 7.1 Major petrographic and lithologic features that characterize the grey and green sandstone, Canso Group, Yava mine area (after Vaillancourt, 1985).

CONCLUSION

The main purpose of this project was to provide new information on the Yava lead deposit, Cape Breton, N.S. Thirteen holes were geophysically logged in the southwestern limits of the west zone, and analysed qualitatively. Two selected holes were analysed statistically. A major objective of the study was to geophysically characterize the mineralization and its environment.

The lead mineralization is well delineated by the spectral gamma-gamma ratio. Linear regressions yielded a simple correlation between lead content and the spectral ratio with a correlation coefficient of approximately 0.82 and a standard error of estimate of 0.76 and 0.95 (% Pb) for holes 404a and 410a, respectively. The linear model generally overestimates low lead content and underestimates high lead content. A non-linear model may improve the correlation so the predicted lead values could be utilized for ore reserve estimation.

The high energy window count rate of backscattered gamma rays is related to both mineralization and lithologies. Optimal low and high energy windows should be found so that the high energy window would principally characterize the lithology (density variations) while the

spectral ratio (high energy window/ low energy window) would distinguish heavy elements. Calibration procedures (standardization) should be improved to facilitate hole-to-hole correlations. The gamma-gamma spectral logging method would be the most useful technique to delineate both lead mineralization and geology.

The three main lithologies were geophysically delineated with resistivity and natural gamma spectrometry. In the studied area, the rhyolite is the most resistive rock type with the highest radioactivity. The Windsor shale is the most conductive rock type and has higher radioactivity than the Canso Group. The latter has more lithologic variations associated to resistivity variations.

The results of statistical analysis of the geophysical data support the previous above correlations. The Canso Group data sets from hole 404a and 410a were used for the factor analysis. The two major factors 1 and 2 explained 74% of the total variance. The first factor is related to lead content (spectral ratio proportional to lead content while the count rates in the density window are inversely proportional). The second factor is related to lithology; as the resistivity increases, the natural radioactivity decreases.

The discriminant analysis was carried out in order to distinguish the Windsor Shale Group from the Canso Group with a combination of geophysical parameters. Since the discriminant analysis appeared to classify observations with a percentage of well classified cases over 90%, it is suggested for further studies, to use this statistical technique to discriminate the Canso Group lithologic variations. Chemical assays should be done in order to characterize the different lithologies since discriminant analysis is built upon initial known groups.

Zinc enrichments were observed in very few holes in the northern part of the studied area where lead grade is low. The zinc mineralization was not geophysically delineated. It seems to be a local feature (few centimetres) which may not be detectable by geophysics (radius of investigation limitation). Further detailed studies on zinc relationships should be done since the assay samples were inadequate to discover any correlation.

Multiparameter geophysical logging techniques are very attractive and promising since they successfully characterized the Yava sandstone deposit. The spectral gamma-gamma method may lead to in situ assaying and should be extended to other deposit types in order to assist people in ore zone delineation and estimation.

REFERENCES

BECK, A.E.
1976: The use of thermal resistivity logs in stratigraphic correlation. Geophysics, v.41, no.2, p.300-309.

BECKER, A. and TELFORD, W.M.
1965: Spontaneous polarization studies. Geophys. Prosp. v.13, p.173-188.

BERNIUS, G.R.
1981: Boreholes near Ottawa for the development and testing of borehole logging equipment - a preliminary report: in Current Research, Part C, Geological Survey of Canada, Paper 81-1C, p.51-53.

BJORLYKKE, A. and SANGSTER, D.F.
1981: An Overview of Sandstone Lead Deposits and their Relation to Red-bed Copper and Carbonate-Hosted Lead - Zinc deposits. Economic Geology, 75th Anniversary Volume, p.179-213.

BONHAM, O.J.
1982: The Yava Lead Deposit, Salmon River, Cape Breton, Exploration (1962-1981) and Mining Activities (1979-1981). Prepared for the Nova Scotia Department of Mines and Energy, January 15, 55p.

1983: Geology of the Yava Sandstone-Lead Deposit, Cape Breton, Nova Scotia. Unpublished M.Sc. thesis, Dalhousie University, Halifax, Nova Scotia, 181p.

BRISTOW, Q.
1979a: Airborne and vehicle mounted geophysical data acquisition systems controlled by Nova minicomputers. Proceedings of the Annual Meeting, Data General Users Group, New Orleans, p.615-634.

1979b: A gamma ray spectrometry system for airborne geological research: in Current Research, Part C, GSC, Paper 79-1C, p.55-61.

1979c: Gamma ray spectrometric methods in uranium exploration-Airborne instrumentation: in Geophysics and Geochemistry in the search for metallic ores, Peter J. Hood, editor, GSC, Economic Geology Report 31, p. 135-146.

1985: A digital signal processing unit for the GeoInstruments magnetics susceptibility sensors, with analogue and RS-232C outputs: in Current Research Part B, Geological Survey of Canada, Paper 85-1b p.463-466.

1986: A system for the digital transmission and recording of induced polarization measurements in boreholes: in Borehole Geophysics for Mining and Geotechnical Applications, ed. P.G. Killeen, GSC, Paper 85-27, p.127-143.

BRISTOW, Q. and BERNIUS, G.R.
1984: Field evaluation of a magnetic susceptibility logging tool: in Current Research, Part A, GSC, Paper 84-1A, p.453-462.

BRISTOW, Q. and CONAWAY, J.G.
1984: Temperature gradient measurements in boreholes using low noise high resolution digital techniques: in Current Research, Part B, GSC, Paper 84-1B, p.101-108.

BRISTOW, Q., CONAWAY, J.G. and KILLEEN, P.G.
1984: Short Note: Application of inverse filtering to gamma-ray logs: A case study. Geophysics, v.49, p.1369-1373.

BRODING, R.A., ZIMMERMAN, C.W., SOMERS, E.V., WILHELM E.S. and STRIPLING, A.A.
1952: Magnetic well logging. Geophysics, v.17, p.1-26.

CONAWAY, J.G.
1977: Deconvolution of temperature gradient logs. Geophysics, v. 42, p.823-837.

CONAWAY, J.G. and BECK, A.E.
1977: Fine-scale correlation between temperature gradient logs and lithology. Geophysics, v.42, p.1401-1410.

CONAWAY, J.G. and KILLEEN, P.G.
1978: Quantitative uranium determinations from gamma-ray logs by application of digital time series analysis. Geophysics, v.43, p.1204-1221.

1980: Gamma-ray spectral logging for uranium. CIM bulletin, p.115-123.

CHRISTOFFERSON, H.C., WALLIN, B., SELKMAN, S., and RICKARD, D.T.
1979: Mineralization Controls in the Sandstone Lead-Zinc Deposits at Vassbo, Sweden. Econ. Geol., v.74, p.1239-1249.

CORMIER, R.F.
1972: Radiometric ages of granitic rocks, Cape Breton Island, Nova Scotia. Can. J. Earth Sci., v.9, p.1074-1086.

DAVIS, J.C.
1973: Statistics and Data Analysis in Geology. Wiley & Sons Inc, 550p.

DOBRIN, M.B. and SAVIT C.H.
1988: Introduction to Geophysical Prospecting. McGraw-Hill Book Company, Fourth Edition, 867p.

DODDS, P.H. and ESCHLIMAN, D.H.
1972: Borehole Logging Techniques for Uranium Exploration and Evaluation; in Uranium Prospecting Handbook, Instit. Min. Met., London, p.244-275

DRAPER, N.R. and SMITH, H.
1966: Applied Regression Analysis: in Wiley Series in Probability and Mathematical Statistics. Wiley & Sons Inc., 407p.

GEOINSTRUMENTS
TH-3 and TH-3C Instruction Manual. GeoInstruments, Helsinki, Finland.

GEORGE, D.C. and SCOTT, J.H.
1982: Review of magnetic susceptibility logging and its application to uranium exploration: in Proceedings of Uranium Exploration Methods Symposium, OECD/IAEA, Paris.

GRASTY, R.L.
1977: A general calibration procedure for airborne gamma-ray spectrometers: in Report of Activities, GSC, Part C, Paper 77-1C, p.61-62.

HALLEUX, I.
1986: Traitement de diagraphies en sondages miniers. Thèse présentée pour l'obtention du grade de Docteur en Sciences Appliquées, Université de Liège, 191p.

HINES, W.W. and MONTGOMERY, D.C.,
1980: Probability and Statistics in Engineering and Management Science. Wiley & Sons Inc., Second edition, 634p.

KEPPIE, D. and SMITH, P.K.
1978: Compilation of isotopic age data of Nova Scotia. Nova Scotia Department of Mines and Energy, Rept.78-4.

KILLEEN, P.G.
1978: Gamma-ray spectrometric calibration facilities - A preliminary report: in Current Research, Part A, GSC, Paper 78-1A, p.243-247.

1979: Gamma ray spectrometric methods in uranium exploration - application and interpretation: in Geophysics and Geochemistry in the Search for Metallic Ores, Peter J. Hood editor, GSC, Economic Geology Report 31, p.163-229.

1982: Gamma-ray logging and interpretation: in Developments in Geophysical Exploration Methods -3, Chapter 4, edited by A.A. Fitch, Published by Applied Science Publishers Ltd, p.95-150.

1986: A System of Deep Test Holes and Calibration Facilities for Developing and Testing New Borehole Geophysical Techniques: in Borehole Geophysics for Mining and Geotechnical Applications, ed. P.G. Killeen, GSC, Paper 85-27, p.29-46.

KILLEEN, P.G. and CONAWAY, J.G.
1978: New facilities for calibrating gamma-ray spectrometric logging and surface exploration equipment. CIM Bulletin, p.84-87.

KILLEEN, P.G. and MWENIFUMBO, C.J.
1986: Current Developments in Nuclear Techniques for Coal Logging in Canada. Proceedings of an Advisory Group Meeting on Gamma, X-ray and Neutron Techniques for the Coal Industry organized by the International Atomic Energy Agency and held in Vienna, 4 - 7 december 1984, International Atomic Energy Agency, Vienna, p.67-79.

LINDEMAN, R.H., MERENDA, P.F. and GOLD, R.Z.
1980: Introduction to Bivariate and Multivariate Analysis. Scott, Foresman & Company, 432p.

LOTUS DEVELOPMENT CORP.
1986: Lotus 123 Release 2.01, Copyright 1986, Lotus Development Corporation, 55 Cambridge Parkway, Cambridge.

MWENIFUMBO, C.J.
1986: Drill hole mise-à-la-masse induced polarization and potential measurements in a Zn-Pb-Cu sulphide deposit: in Borehole Geophysics for Mining and Geotechnical Applications, ed. P.G. Killeen, GSC, Paper 85-27, p.145-158.

NIE, N.H., HULL, C.H., JENKINS, J.G., STEINBRENNER, K. and BENT, D.H.
1975: SPSS : Statistical Package for the Social Sciences. Second edition, McGraw-Hill Company.

NORUSIS, M.J.
1986 (1a): SPSS/PC+ for IBM PC/XT/AT. SPSS Inc.

1986 (1b): Advance Statistics: SPSS/PC+ for IBM PC XT/AT SPSS Inc.

PATTERSON, J.M.
1986: Yava Lead Deposit, Cape Breton, N.S. Report on Diamond Drilling Programme-Summer 1986. Mineral Resources Division, Nova Scotia Department Mines and Energy, Halifax.

PERRIN, J.
1986: Application des sondes gamma-gamma à la détection et à la caractérisation des veines minéralisées en sulfures, Mémoire de fin d'étude Ecole Supérieure de Ressources et Matériaux Minéraux, Rapport du BRGM 81 SGN 830 GPN, 69p.

POLDINI, E.
1938: Les phénomènes de polarisation spontannée électrique du sous-sol et leur application à la recherche des gîtes métallifères, Bulletin des Laboratoires de Géol. de l'Université de Lausanne, no. 61, 43p.

PRIME, G.A. and BOEHNER, R.C.
1984: Preliminary Report on the Geology of the Glengarry Half-Graben and Vicinity, Cape Breton Island, N.S.: in Mines and Minerals Branch, Report of Activities, 1983, N.S., Department of Mines and Energy, Report 84-1, p.61-69.

REITER, M., MANSURE, A.J. and PETERSON, B.K.
1980: Precision continuous temperature logging and comparison with other types of logs, Geophysics, v.45, p. 1857-1868.

RICKARD, D.T., WILLDEN, M.Y., MARINDER, N.E. and DONNELLY, T.H.
1979: Studies on the Genesis of the Laisvall Sandstone Lead-Zinc Deposit, Sweden, Econ. Geol., v.74, p.1255-1285.

ROY, A. and DHAR, R.L.
1971: Radius of investigation in dc resistivity well logging, Geophysics, v.36, p.754-760.

1974: Errata in: Geophysics, v.39, p.566.

ROY, J.
1984: Electrical methods in mineral well logging. Ph.D. Thesis, Mc Gill University, Dept. of Mining and Metallurgical Engineering.

SATO, M. and MOONEY, H.M.
1960: Electrochemical mechanism of sulfide self potentials: Geophysics, v.25, p.226-249.

SAVITZKY, A. and GOLAY, M.
1964: Smoothing and differentiation of data by simplified least squares procedures. Anal. Chem. 36, p. 1627-39.

SCOTT, J.H., DODD, P.H., DROULLARD, R.F. and MUDRA, P.J.
1961: Quantitative interpretation of gamma ray logs. Geophysics, v.26, no.2, p.182-191.

SCOTT, P.
1979: Salmon River Lead Deposit. Mineral Resources Division Report of Activities, N.S. Dept. Mines and Energy, Rep. 80-1, 91-93p., Mc Millan K.A. editor.

1980: Geochemistry and petrography of the Salmon River Lead deposit, Cape Breton Island, Nova Scotia. Unpublished M.Sc.thesis, Acadia Univ., Wolfville, Can., 111p.

SERRA, O.
1979: Diagraphies différées. Bases de l'interprétation. Tome 1: Acquisition des données diagraphiques: Bull. Cent. Rech. Explor.-Prod. Elf-Aquitaine, Mem. 1., 328 p.

SUMNER, J.S.
1976: Principles of induced polarization for geophysical exploration. Amsterdam, Elsevier, 277p.

TELFORD, W.M., GELDART, L.P., SHERIFF, R.E. and KEYS, D.A.
1976: Applied Geophysics. Cambridge University Press, 860p.

TITTMAN, J. and WAHL, J.S.
1965: The physical foundations of formation density logging (gamma gamma). Geophysics, v.30, p.284-294.

URBANCIC, T.I.
1985: Multiparameter geophysical logging for gold: A statistical approach. M. Sc.A. Thesis, Toronto University, 274p.

URBANCIC, T.I. and MWENIFUMBO, C.J.
1986: Multiparameter logging techniques applied to gold exploration: in Borehole Geophysics for Mining and Geotechnical Applications, ed. P.G. Killeen, GSC, Paper 85-27, p.13-28.

VAILLANCOURT, P.D.
1985: Sandstone Lithology in the Silver Mine Formation and its Relation to Galena Occurrence in the Yava Deposit, Cape Breton Island, N.Scotia:in Current Research, Part A, Geological Survey of Canada, Paper 85-1A, p. 743-751.

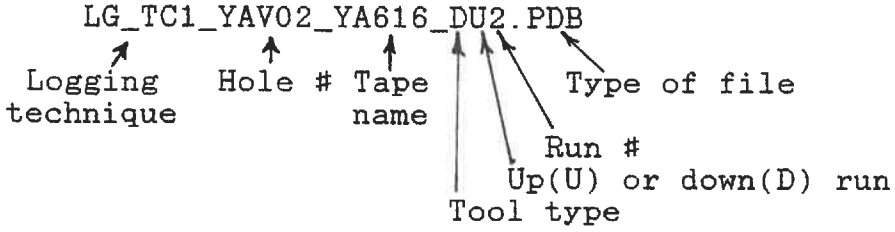
VAILLANCOURT, P.D., SANGSTER, D.F.
1984: Petrography of Mineralisation at the Yava Sandstone-Lead Deposit, N.S.: in Current Research, Part A, Geological Survey of Canada, Paper 84-1A, p.345-352.

1986: Isotope and Hydrocarbon Studies of the Yava Sandstone-Lead Deposit, Cape Breton Island, Nova Scotia;a Progress Report: in Current Research, Part A, Geological Survey of Canada, Paper 86-1A, p.133-140.

APPENDICES

APPENDIX A - DATA FILES

Filename explanation:



Hole	Size	Tool used	Filename	Log. speed m/min	Samp. time (sec)	Samp. depth incr. (cm)
402a	NQ	I	IP_*_YAV02_YA641_IU1.PBD	3	1	5
403	BQ	-	-	-	-	-
404a	NQ	I	IP_*_YAV04_YA646_IU1.PBD	3	1	5
405	BQ	I	IP_*_YAV05_YA605_IU1.PBD	3	1	5
406a	NQ	I	IP_*_YAV06_YA636_DU4.PBD	0.75	8	10
408a	NQ	I	IP_*_YAV08_YA635_IU1.PBD	3	1	5
409a	NQ	I	IP_*_YAV09_YA637_IU1.PBD	3	1	5
410a	NQ	I	IP_*_YAV10_YA636_IU1.PBD	3	1	5
411	BQ	N	IP_*_YAV11_YA610_NU1.PBD	3	1	5
412	BQ	I	IP_*_YAV12_YA643_DU5.PBD	3	1	5
418	NQ	I	IP_*_YA418_YA713_DU2.PBD	3	1	5
420	NQ	I	IP_*_YA420_YA711_DU2.PBD	3	1	5
421	NQ	I	IP_*_YA421_YA712_DU3.PBD	3	1	5

* either RES: Resistivity
NIP: Induced polarization
Tool used: N: 40cm Normal Array
I: 10cm Micronormal Array

Resitivity and induced polarization data file information

Hole	Size	Tool used	Filename	Log. speed m/min	Samp. time (sec)	Samp. depth incr. (cm)
402a	NQ	I	IP_*_YAV02_YA641_IU2.RBD	6	1	10
403	BQ	-	-	-	-	-
404a	NQ	I	IP_*_YAV04_YA646_IU4.RBD	3	1	5
405	BQ	-	-	-	-	-
406a	NQ	-	-	-	-	-
408a	NQ	I	IP_*_YAV08_YA640_IU2.RBD	6	1	10
409a	NQ	I	IP_*_YAV09_YA639_IU1.PBD	3	1	5
410a	NQ	-	-	-	-	-
411	BQ	I	IP_*_YAV11_YA643_IU3.RBD	3	1	5
412	BQ	I	IP_*_YAV12_YA643_IU4.RBD	3	1	5
418	NQ	I	IP_*_YA418_YA713_IU3.PBD	3	1	5
420	NQ	I	IP_*_YA420_YA711_IU4.PBD	3	1	5
421	NQ	I	IP_*_YA421_YA712_IU4.RBD	3	1	5

*: SPP
.RBD: reversed permanent binary files
Tool I: Lead Electrode

Self potential data file information

Hole	Size	Tool used	Filename	Log. speed m/min	Samp. time (sec)	Samp. depth incr. (cm)
402a	NQ	D[1]	LG_*_YAV02_YA616_IU1.PB7	3	1	5.0
403	BQ	D	LG_*_YAV03_YA605_IU2.PB5	1	1	1.7
404a	NQ	6[2]	LG_*_YAV04_YA618_6U2.PB7	1	2	3.3
405	BQ	D	LG_*_YAV05_YA602_DU2.P11	1	1	1.7
406a	NQ	D	LG_*_YAV06_YA614_DU5.PB5	3	2	2.5
408a	NQ	D	LG_*_YAV08_YA613_DU2.PB7	1	2	3.3
409a	NQ	D	LG_*_YAV09_YAG61_DU2.PB5	3	2	2.5
410a	NQ	D	LG_*_YAV10_YA614_DU2.PB7	3	1	5.0
411	BQ	D	LG_*_YAV11_YA617_DU3.P11	1	1	1.7
412	BQ	D	LG_*_YAV12_YA603_DU2.PB7	1	1	1.7
418	NQ	D	LG_*_YA418_YA713_DU2.PB7	1	1	1.7
420	NQ	D	LG_*_YA420_YA712_DU2.P11	1	1	1.7
421	NQ	D	LG_*_YA421_YA711_DU3.P11	1	1	1.7

1: CsI(Tl) (1"x3")
2: CsI(Tl) (1 1/4"x5")
*: TC1: Total count, window .1-3MeV

Natural gamma ray spectrometry data file information

Hole	Size	Tool used	Filename	Log. speed m/min	Samp. time (sec)	Samp. depth incr. (cm)
402a	NQ	D	LG_*_YAV02_YA635_DU2.PBD	3	1	5.0
403	BQ	D	LG_*_YAV03_YA623_DU2.PBD	3	1	5.0
404a	NQ	D	LG_*_YAV04_YA636_DU2.PBD	3	1	5.0
405	BQ	D	LG_*_YAV05_YA619_DU2.PBD	3	1	5.0
406a	NQ	D	LG_*_YAV06_YA632_DU5.PBD	3	1	5.0
408a	NQ	D	LG_*_YAV08_YA634_DU2.PBD	3	1	5.0
409a	NQ	D	LG_*_YAV09_YA633_DU2.PBD	3	1	5.0
410a	NQ	D	LG_*_YAV10_YA632_DU2.PBD	3	1	5.0
411	BQ	D	LG_*_YAV11_YA621_DU3.PBD	3	1	5.0
412	BQ	D	LG_*_YAV12_YA620_DU2.PBD	3	1	5.0
418	NQ	D	LG_*_YA418_YA711_DU2.PBD	1	1	1.7
420	NQ	D	LG_*_YA420_YA716_DU2.PBD	1	1	1.7
421	NQ	D	LG_*_YA421_YA709_DU3.PBD	3	1	5.0

* either : W01, window 1
W03, window 3
RA1, ratio W03/W01
Tool D: CsI(Tl) (1"x3")

Spectral gamma-gamma (density) data file information

Hole	Size	Tool used	Filename	Log. speed m/min	Samp. time (sec)	Samp. depth incr. (cm)
402a	NQ	T	TE_*_YAV02_YA617_TD2.PBD	3	0.3	1.5
403	BQ	T	TE_*_YAV03_YA604_TD1.PBD	6	0.3	3.0
404a	NQ	T	TE_*_YAV04_YA618_TD1.PBD	3	0.3	1.5
405	BQ	T	TE_*_YAV05_YA601_TD1.PBD	6	0.3	3.0
406a	NQ	T	TE_*_YAV06_YA617_TD5.PBD	3	0.3	1.5
408a	NQ	T	TE_*_YAV08_YA617_TD3.PBD	3	0.3	1.5
409a	NQ	T	TE_*_YAV09_YA617_TD6.PBD	3	0.3	1.5
410a	NQ	T	TE_*_YAV10_YA615_TD1.PBD	3	0.3	1.5
411	BQ	T	TE_*_YAV11_YA602_TD2.PBD	6	0.3	3.0
412	BQ	T	TE_*_YAV12_YA602_TD1.PBD	6	0.3	3.0
418	NQ	T	TE_*_YA418_YA706_TD3.PBD	6	0.3	3.0
420	NQ	T	TE_*_YA420_YA706_TD2.PBD	6	0.3	3.0
421	NQ	T	TE_*_YA421_YA706_TD1.PBD	6	0.3	3.0

* either TMP: Temperature
TMG: Temperature gradiant

Temperature data file information

Hole	Size	Tool used	Filename	Log. speed m/min	Samp. time (sec)	Samp. depth incr. (cm)
402a	NQ	M	ML_*_YAV02_YA630_MU1.PBD	3	0.3	1.5
403	BQ	-	-	-	-	-
404a	NQ	M	ML_*_YAV04_YA632_MU1.PBD	3	0.3	1.5
405	BQ	M	MS_*_YAV05_YA610_MU1.PBD	6	0.3	3.0
406a	NQ	M	CH_#_YAV06_YA629_MU3.PBD	3	0.3	1.5
408a	NQ	M	CH_#_YAV08_YA629_MU6.PBD	3	0.3	1.5
409a	NQ	M	CH_#_YAV09_YA629_MU1.PBD	6	0.3	3.0
410a	NQ	M	ML_*_YAV10_YA629_MU5.PBD	3	0.3	1.5
411	BQ	-	-	-	-	-
412	BQ	M	CH_#_YAV12_YA611_MU1.PBD	6	0.3	3.0
418	NQ	M	ML_*_YA418_YA704_MU1.PBD	6	0.3	3.0
420	NQ	M	ML_*_YA420_YA703_MD4.PBD	3	0.3	1.5
421	NQ	M	CH_#_YA421_YA703_MU2.PBD	3	0.3	1.5

*: MSM
#: MAG

Magnetic susceptibility data file information

APPENDIX B - MULTIPARAMETER GEOPHYSICAL PROFILES

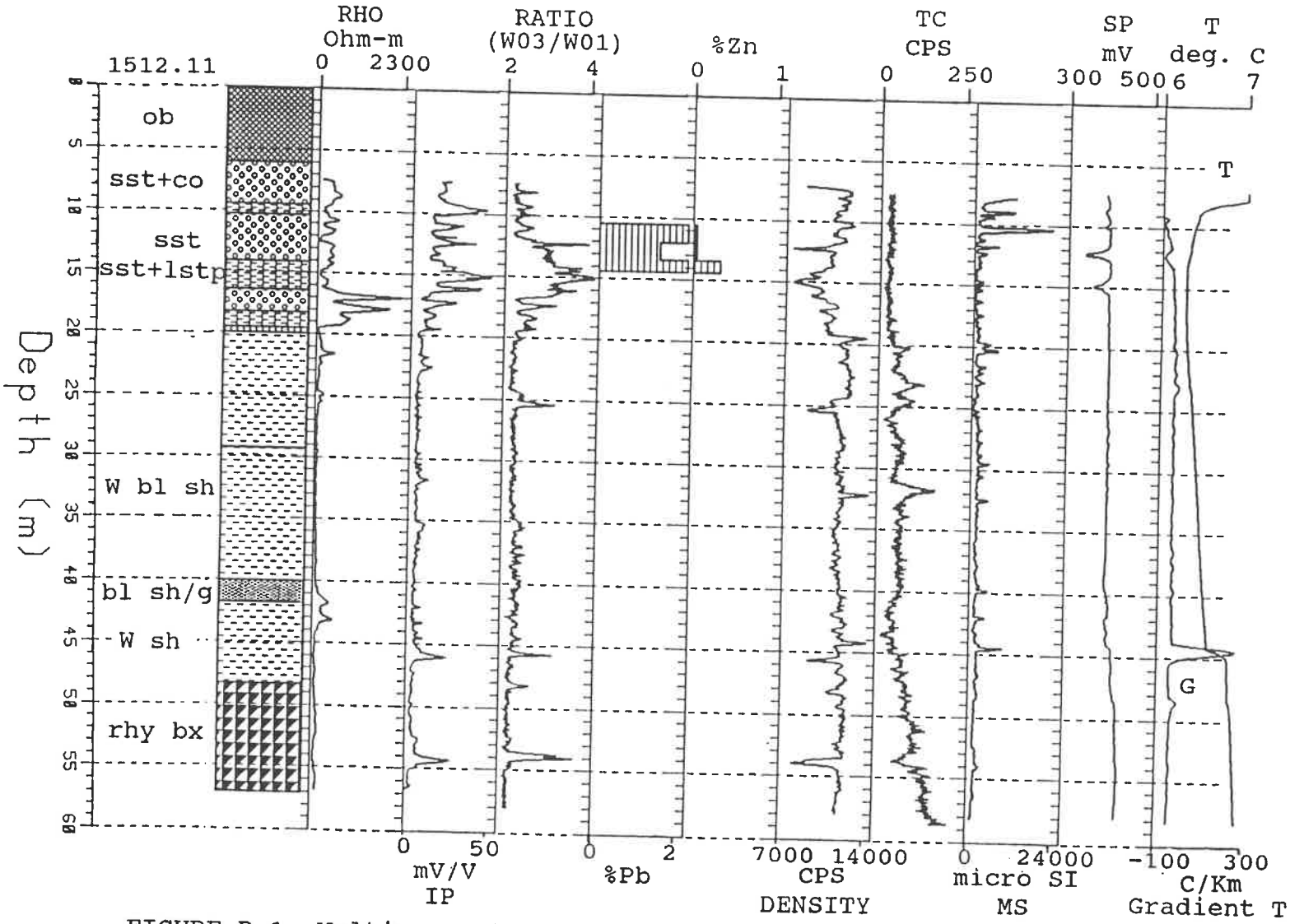


FIGURE B.1. Multiparameter logs for hole 402a.

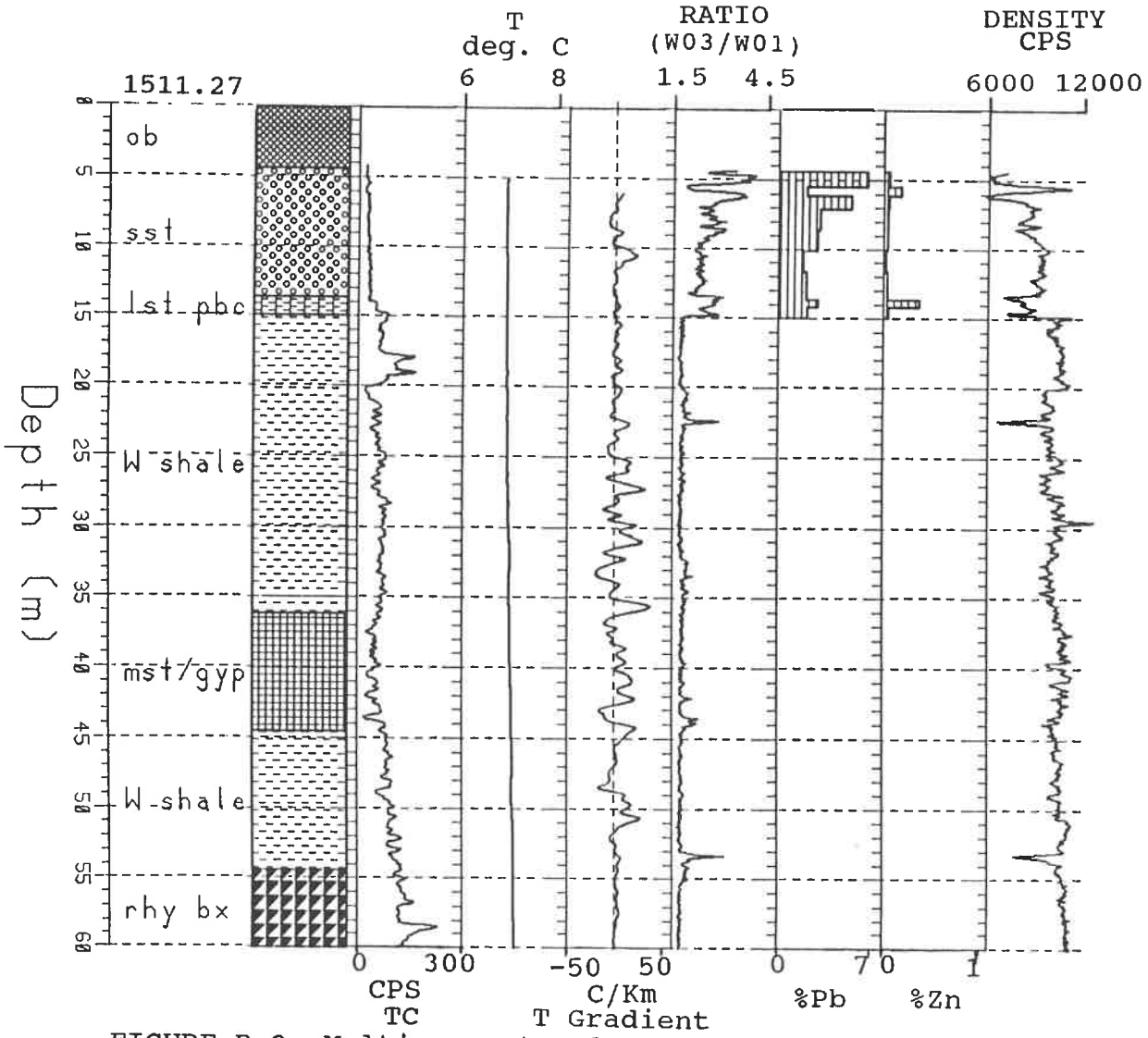


FIGURE B.2 Multiparameter logs for hole 403.

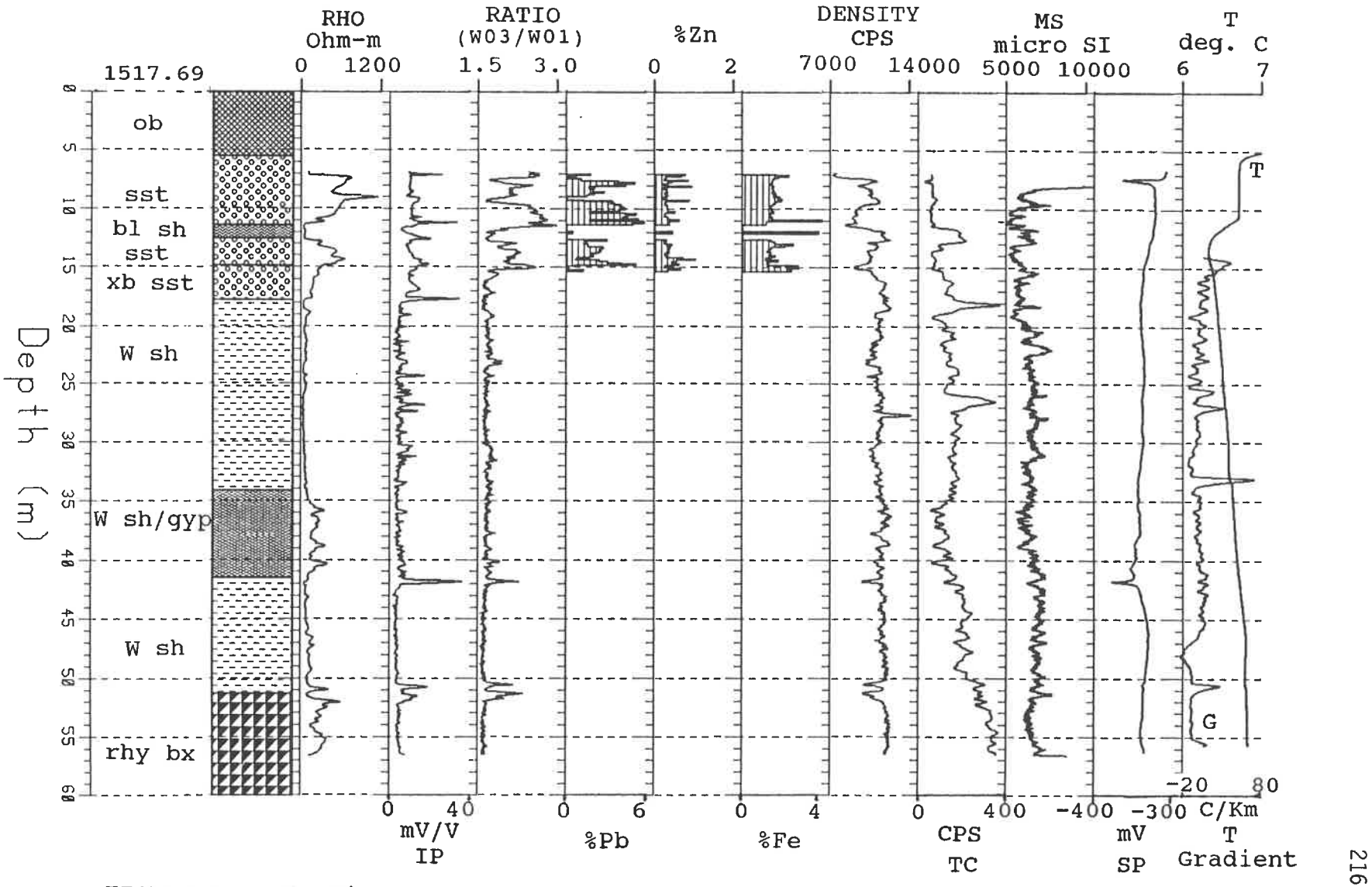


FIGURE B.3 Multiparameter logs for hole 404a.

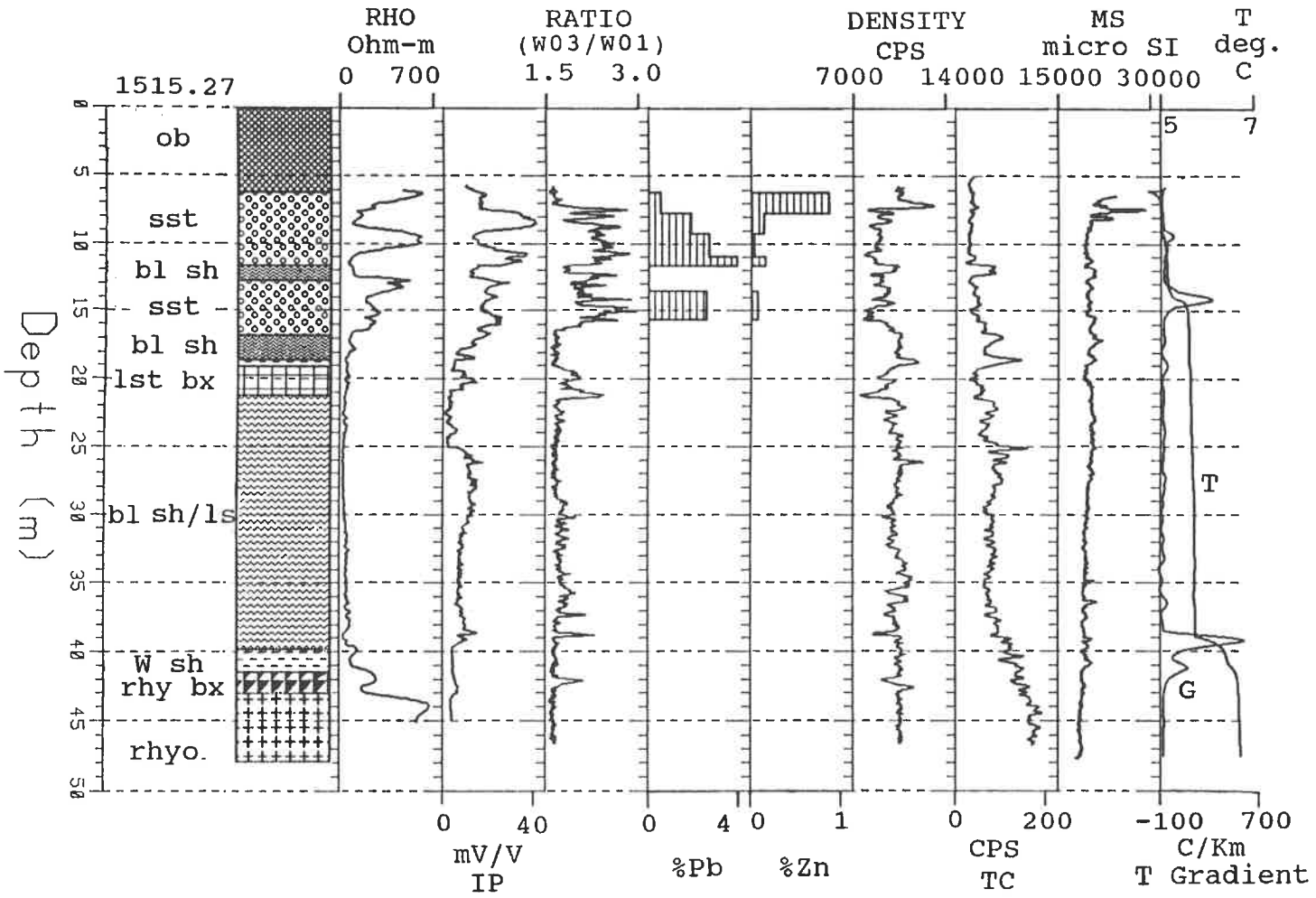


FIGURE B.4 Multiparameter logs for hole 405.

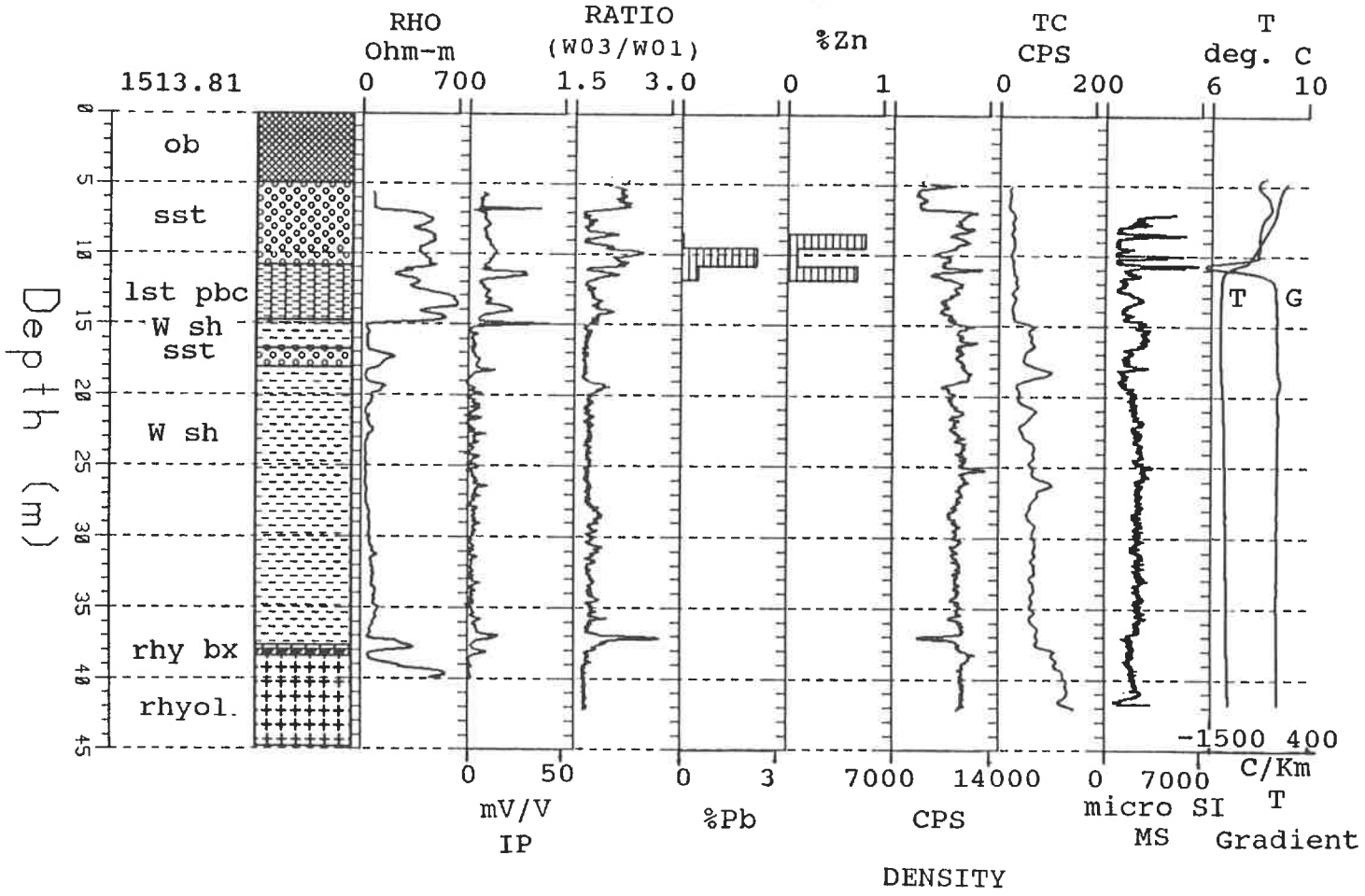


FIGURE B.5 Multiparameter logs for hole 406a.

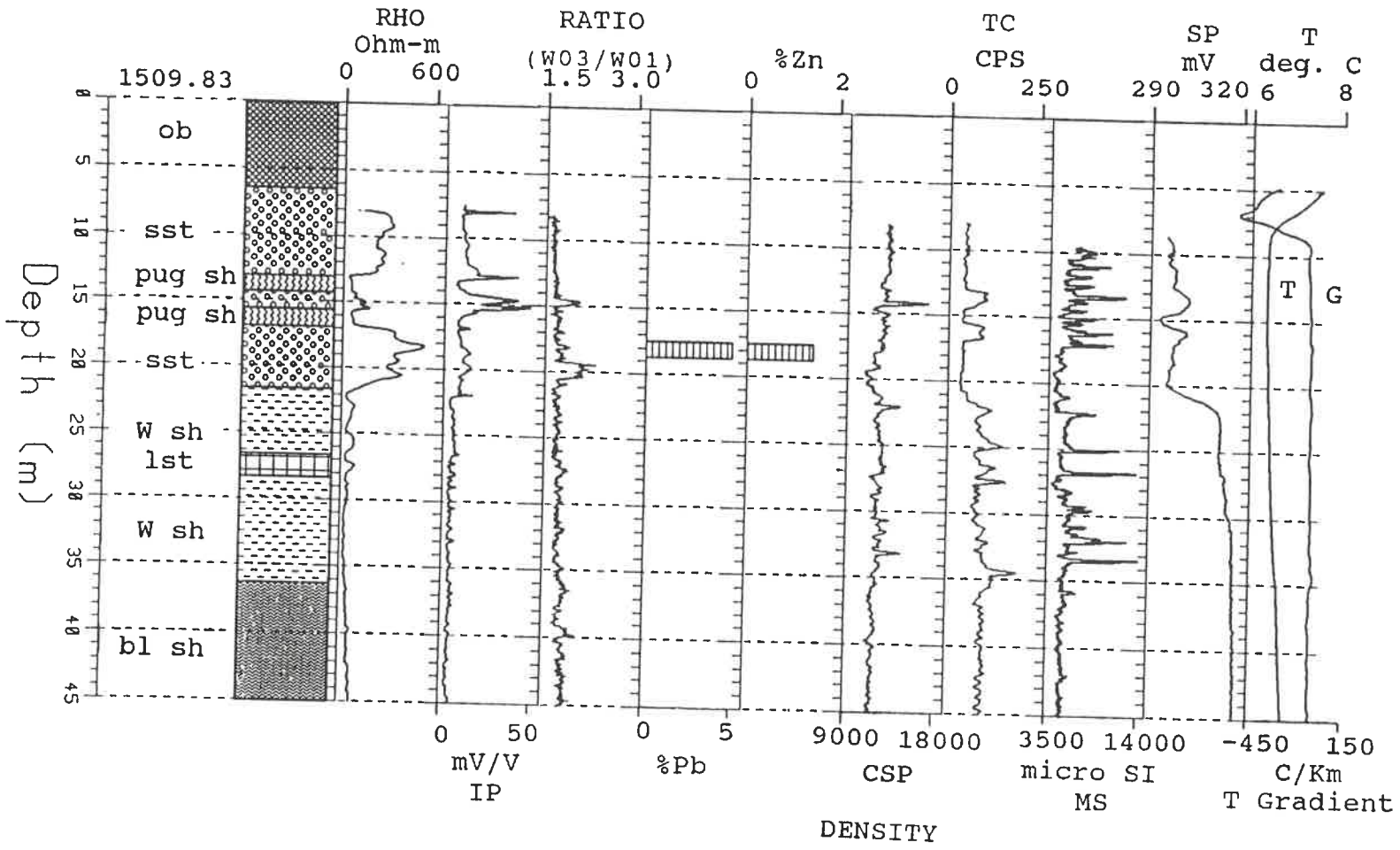


FIGURE B.6 Multiparameter logs for hole 408a.

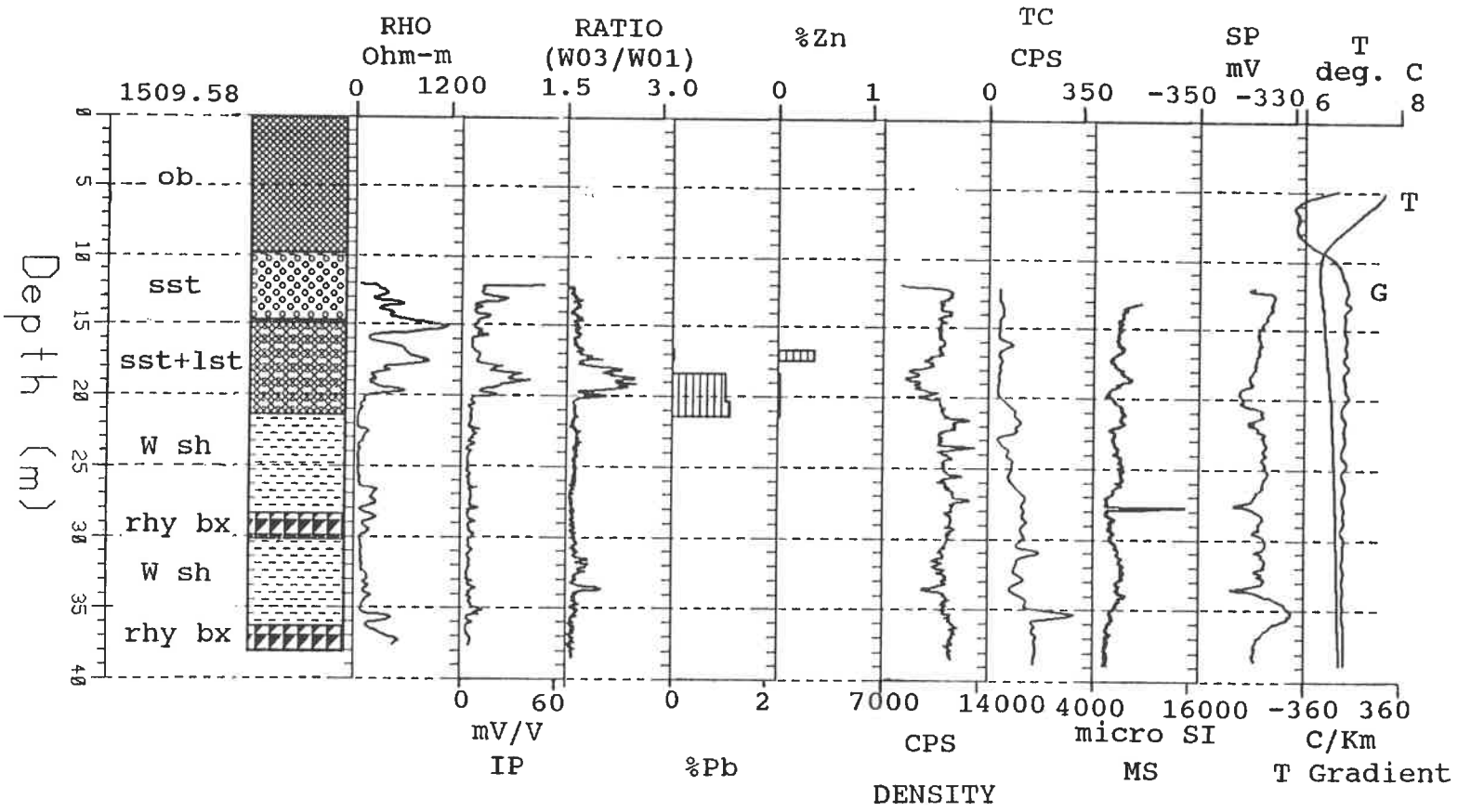


FIGURE B.7 Multiparameter logs for hole 409a.

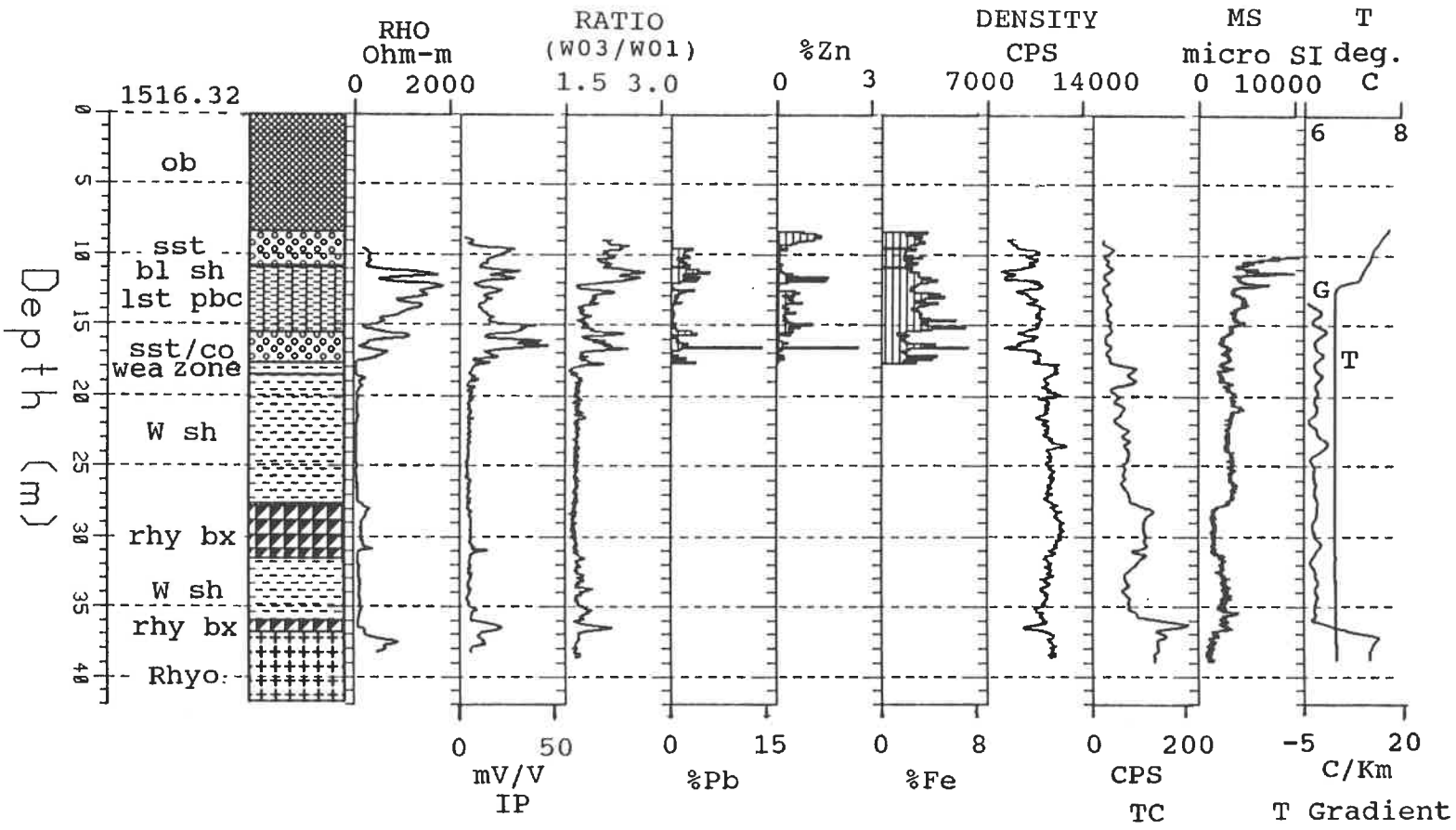


FIGURE B.8 Multiparameter logs for hole 410a.

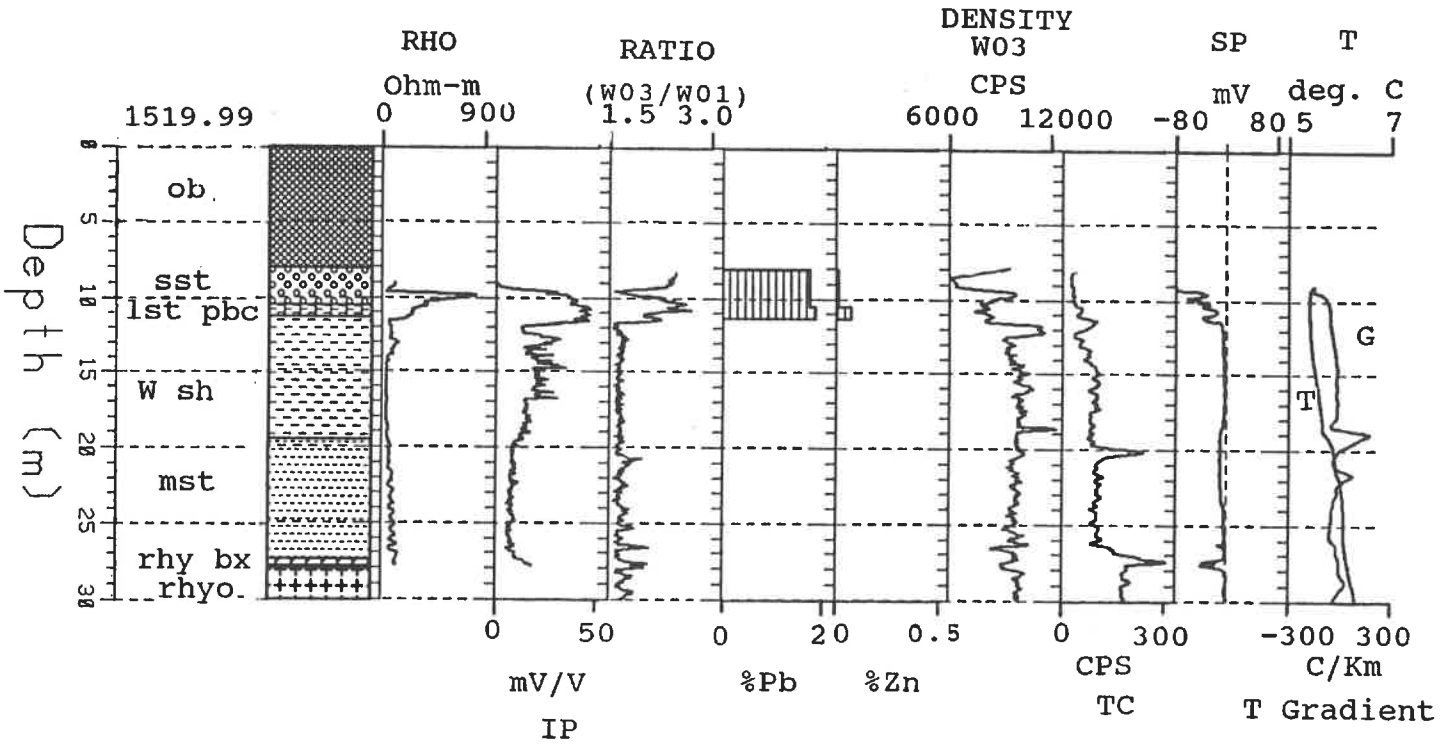


FIGURE B.9 Multiparameter logs for hole 411.

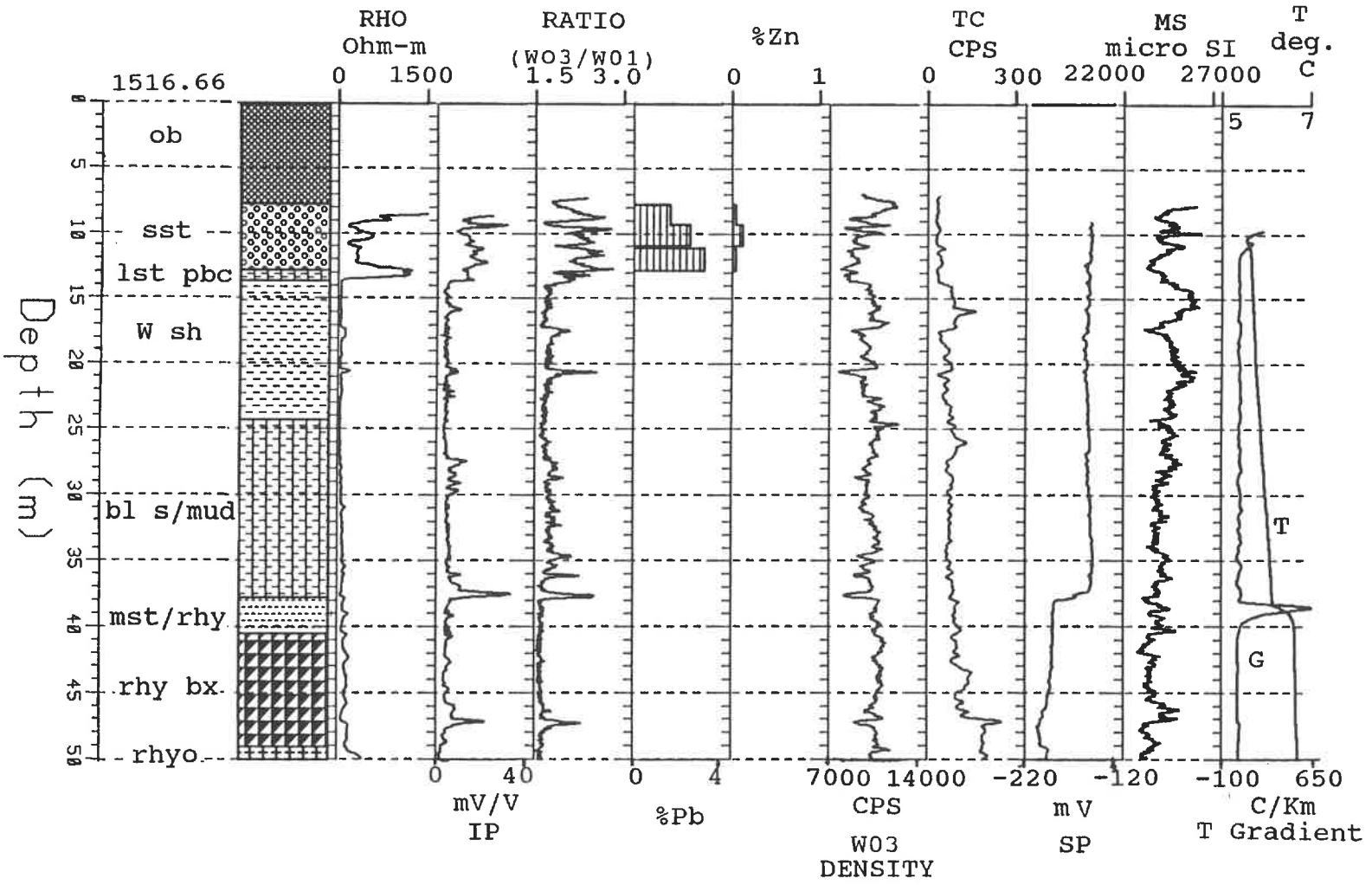


FIGURE B.10 Multiparameter logs for hole 412.

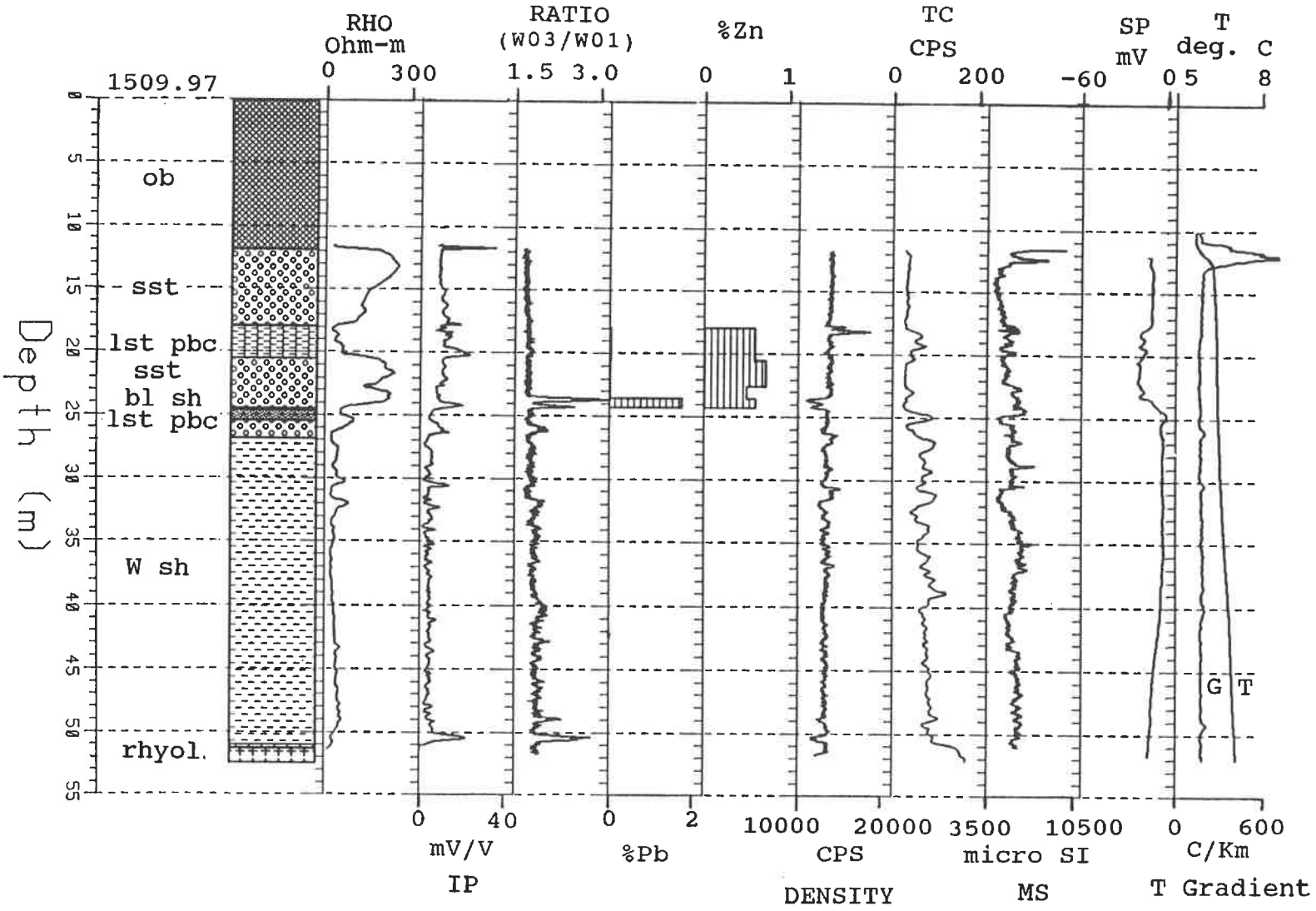


FIGURE B.11 Multiparameter logs for hole 418.

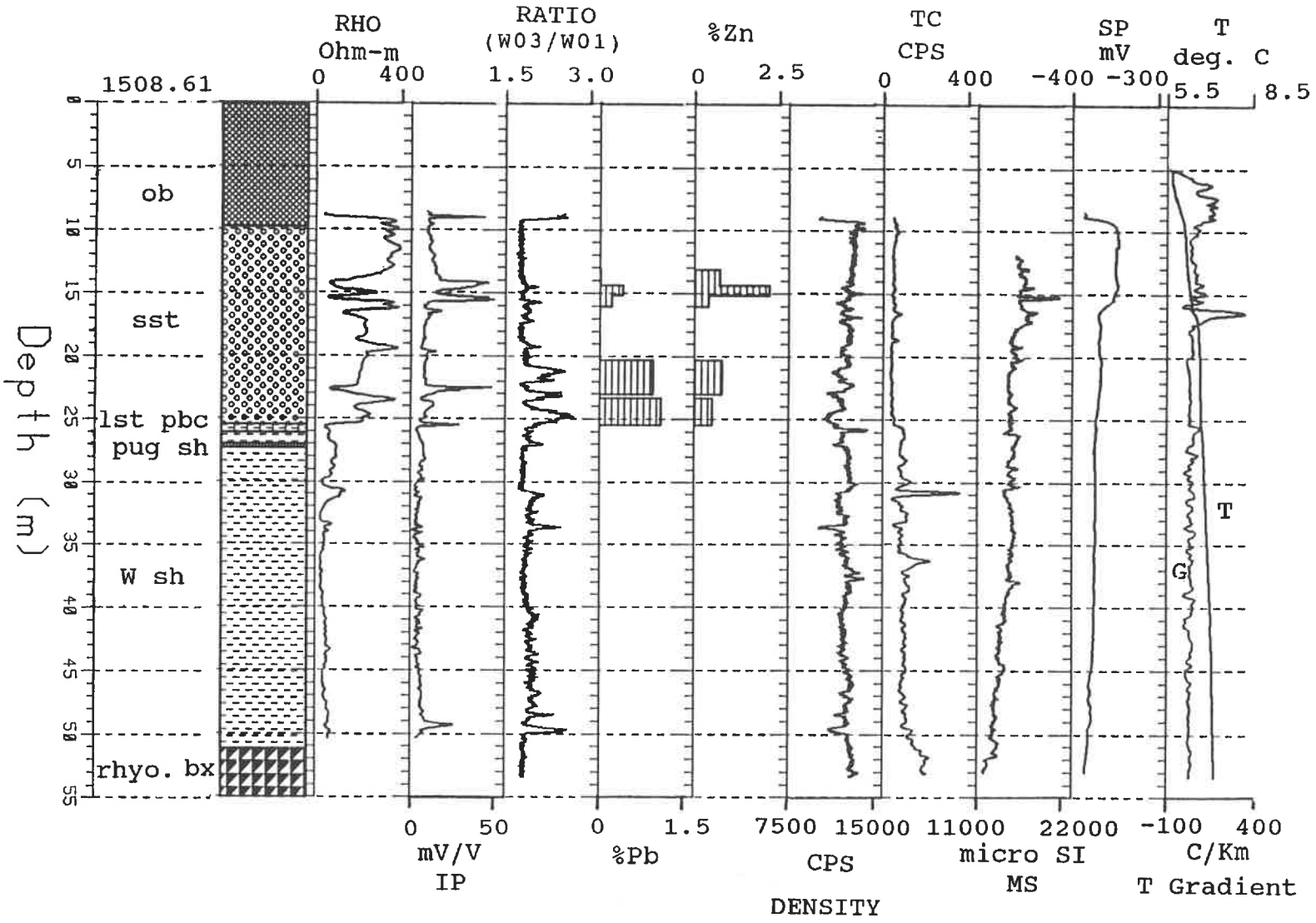


FIGURE B.12 Multiparameter logs for hole 420.

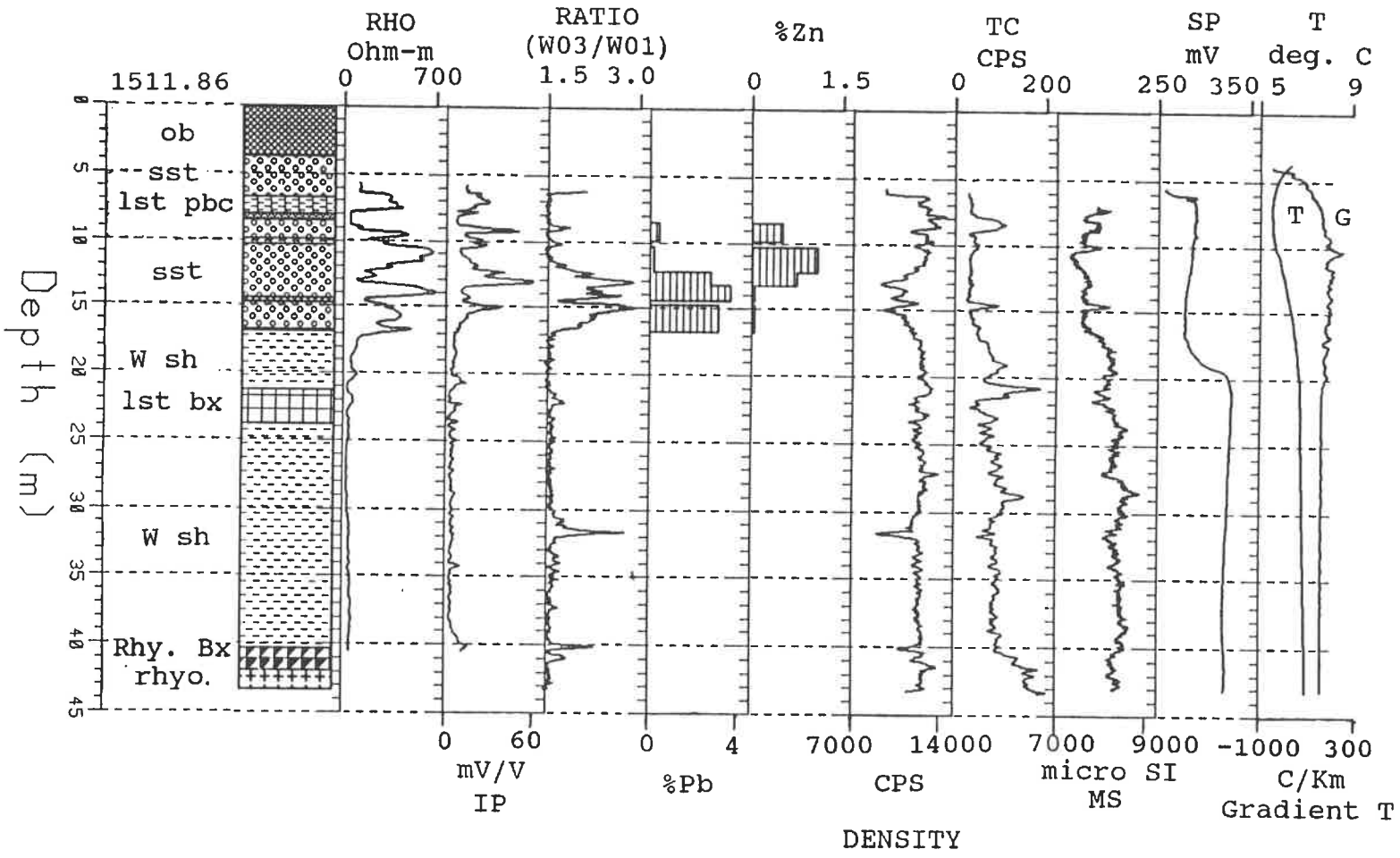


FIGURE B.13 Multiparameter logs for hole 421.

APPENDIX C - SECTIONS

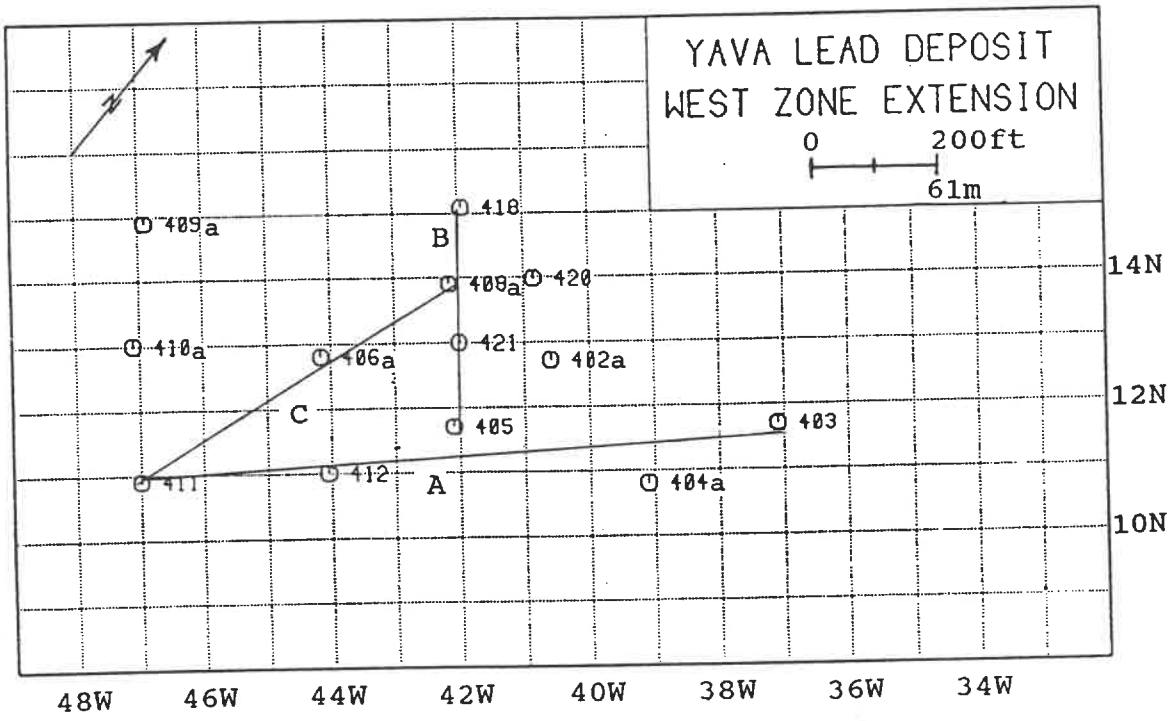


FIGURE C.1 Sections location map, Yava lead deposit, west zone extension.

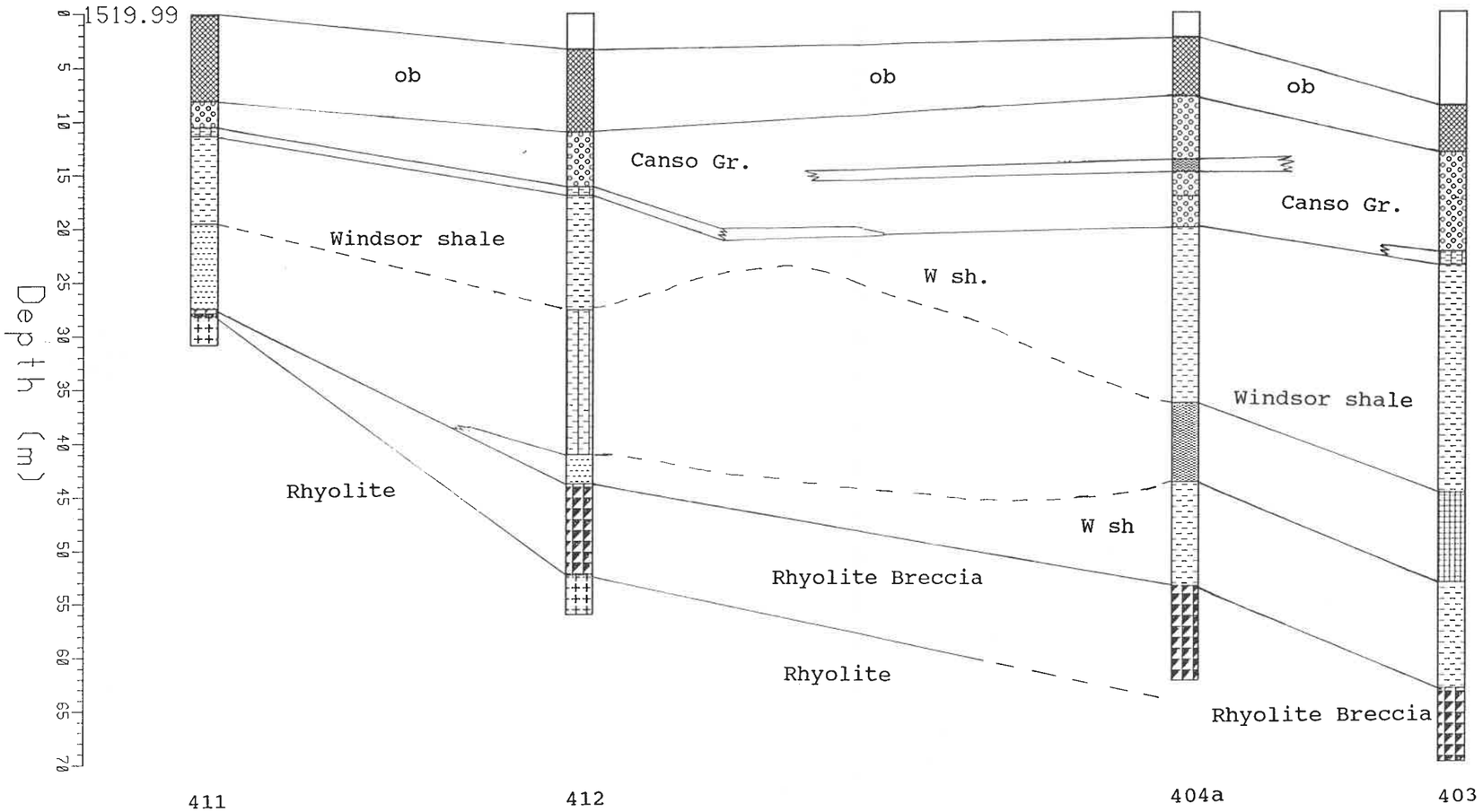


FIGURE C.2 Longitudinal geological section A.
Horizontal scale: 1cm = 13.72m (45ft)
Vertical scale: 1 cm = 5m

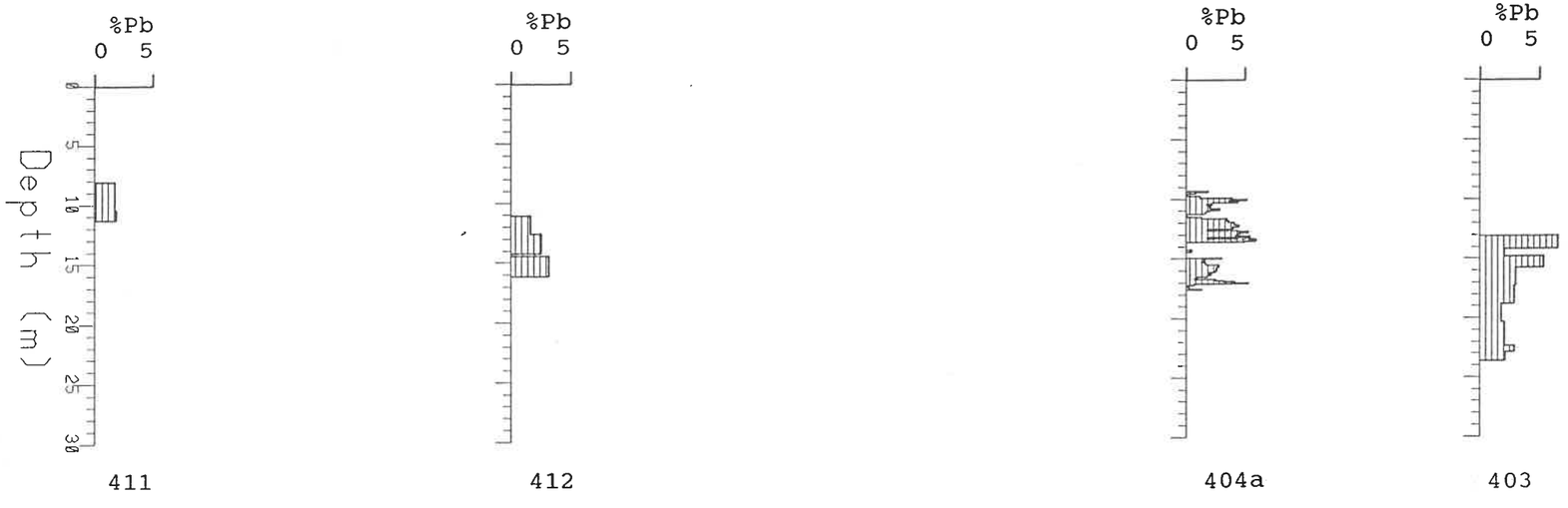


FIGURE C.3 Longitudinal section A - Lead content.
Horizontal scale: 1cm = 13.72m (45ft)
Vertical scale: 1 cm = 5m

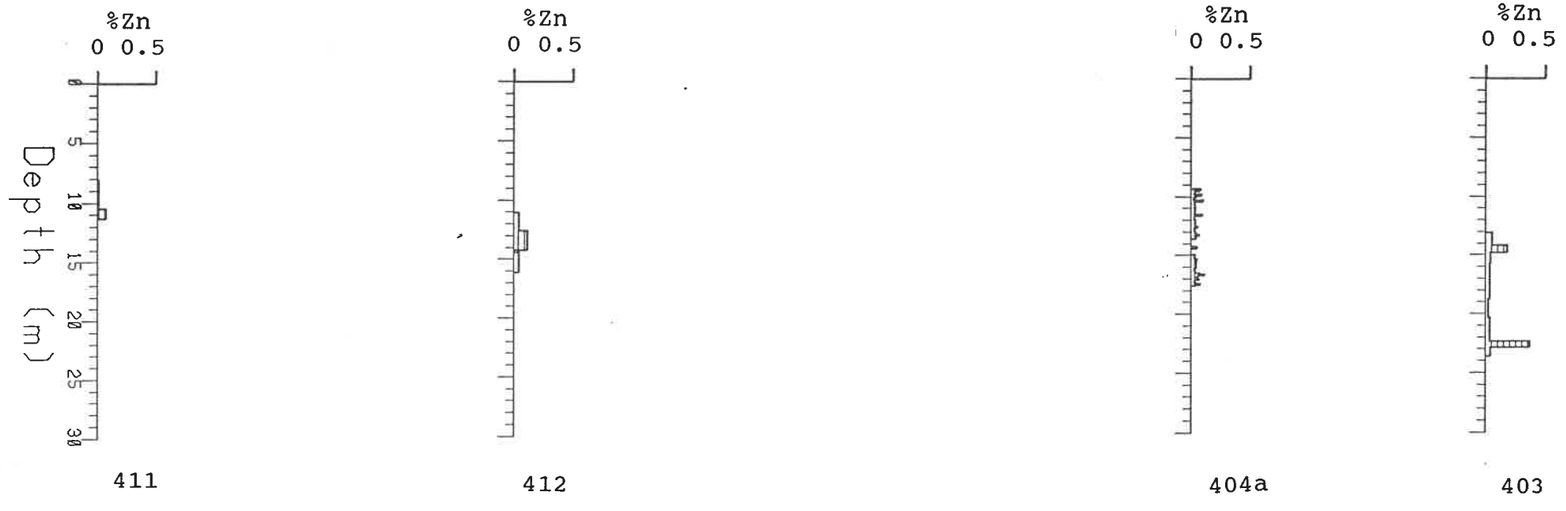


FIGURE C.4 Longitudinal section A - Zinc content.
Horizontal scale: 1cm = 13.72m (45ft)
Vertical scale: 1 cm = 5m

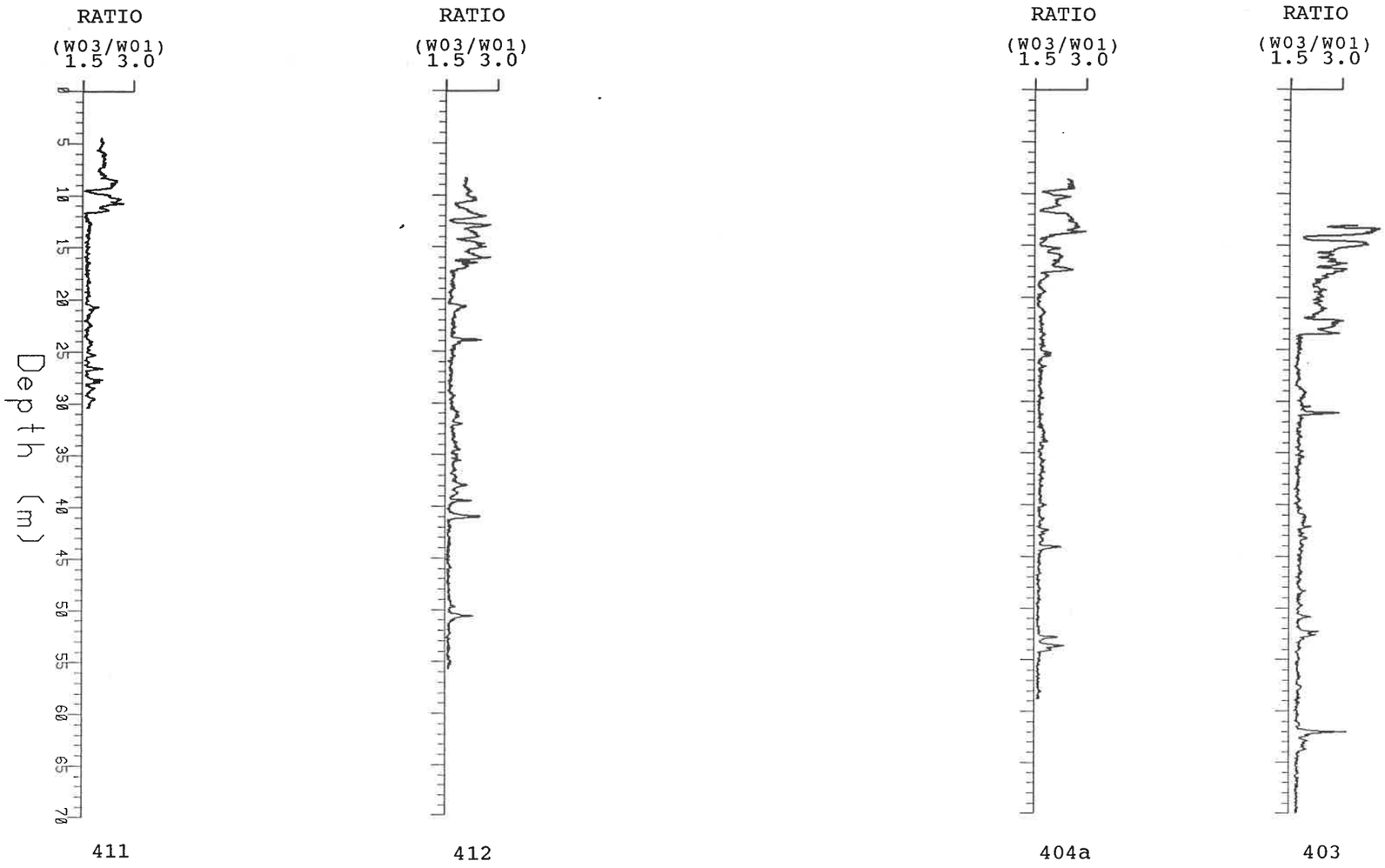


FIGURE C.5 Longitudinal section A - Spectral ratio.
Horizontal scale: 1cm = 13.72m (45ft)
Vertical scale: 1 cm = 5m

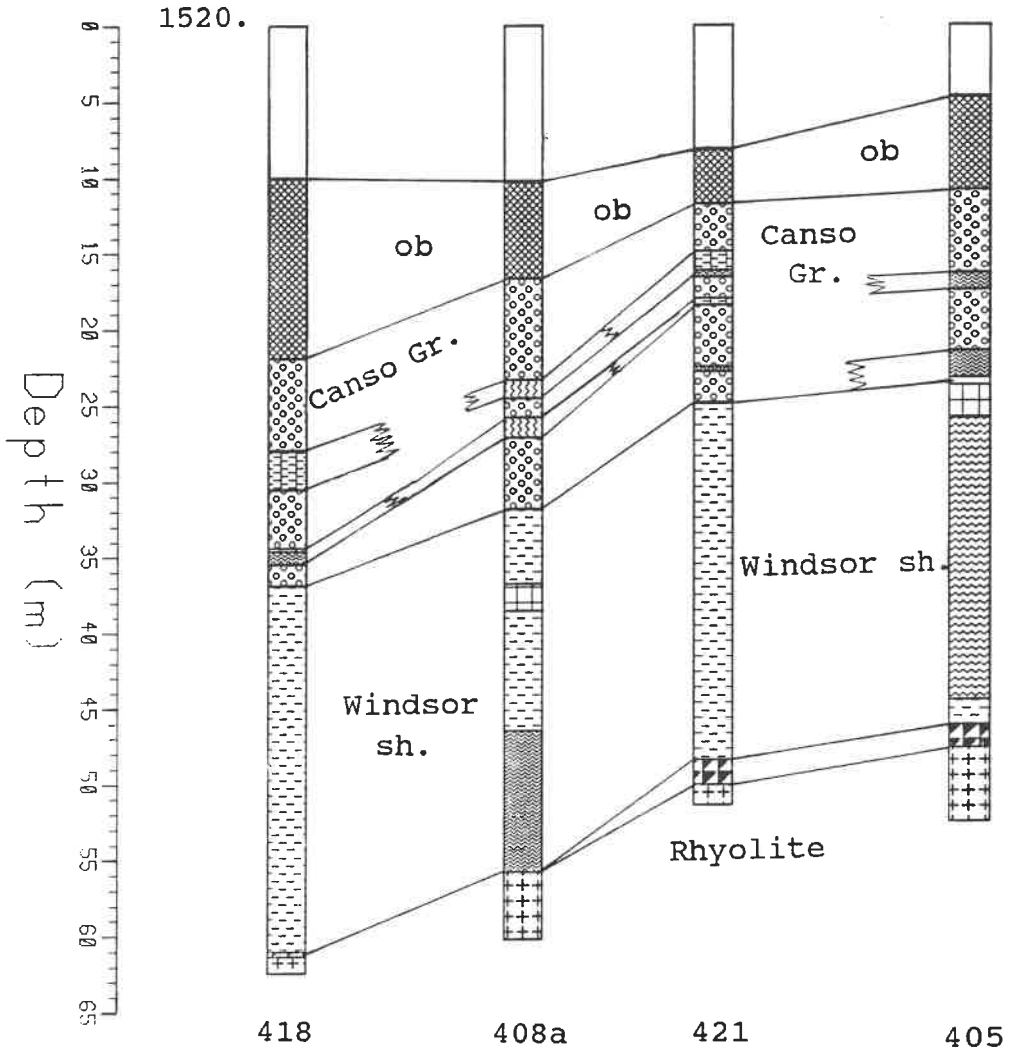


FIGURE C.6 Geological cross section B.
Horizontal scale: 1cm = 13.72m (45ft)
Vertical scale: 1 cm = 5m

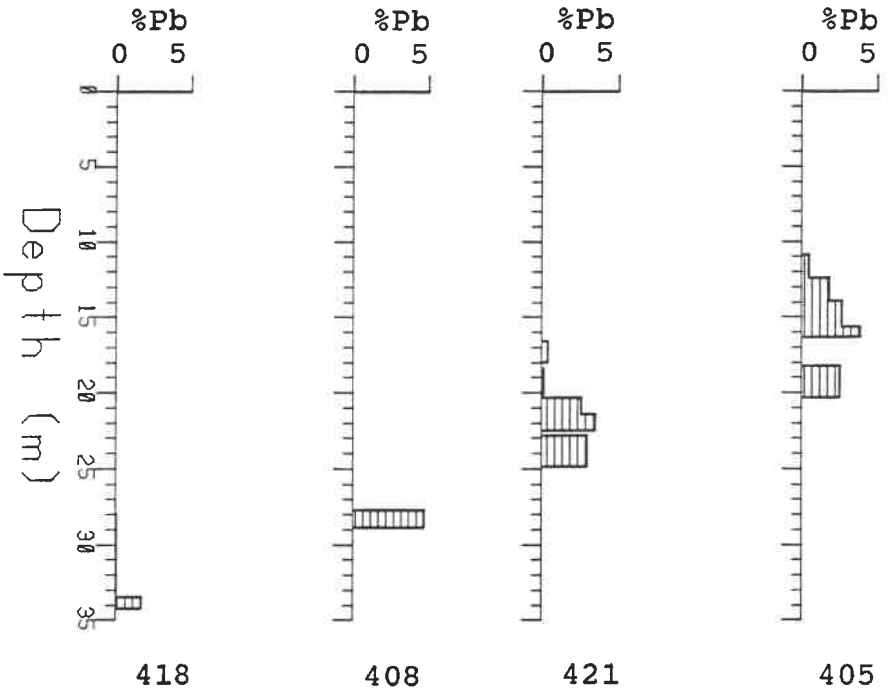


FIGURE C.7 Cross section B - Lead content.
Horizontal scale: 1cm = 13.72m (45ft)
Vertical scale: 1 cm = 5m

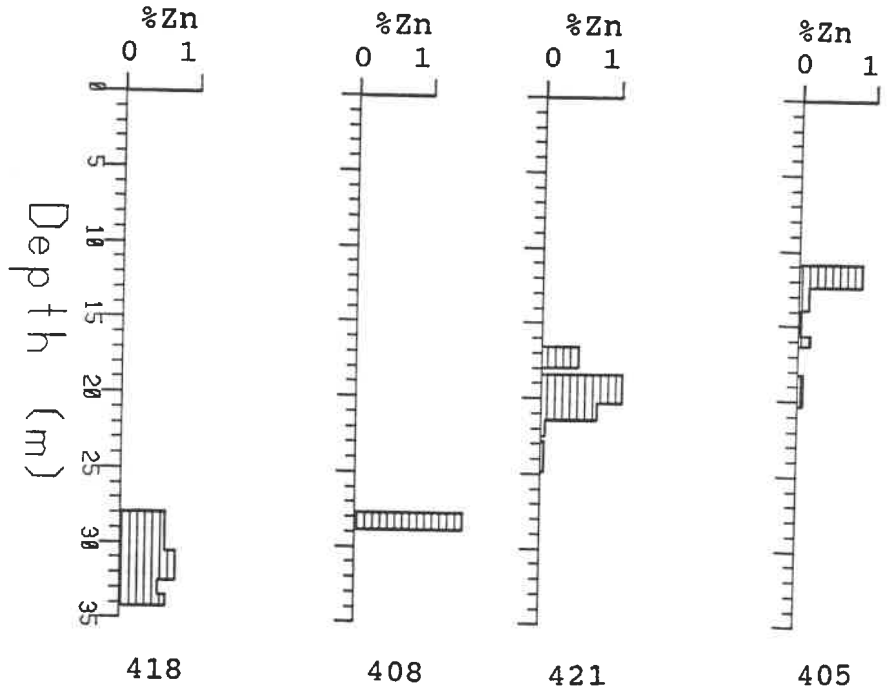


FIGURE C.8 Cross section B - Zinc content.
Horizontal scale: 1cm = 13.72m (45ft)
Vertical scale: 1 cm = 5m

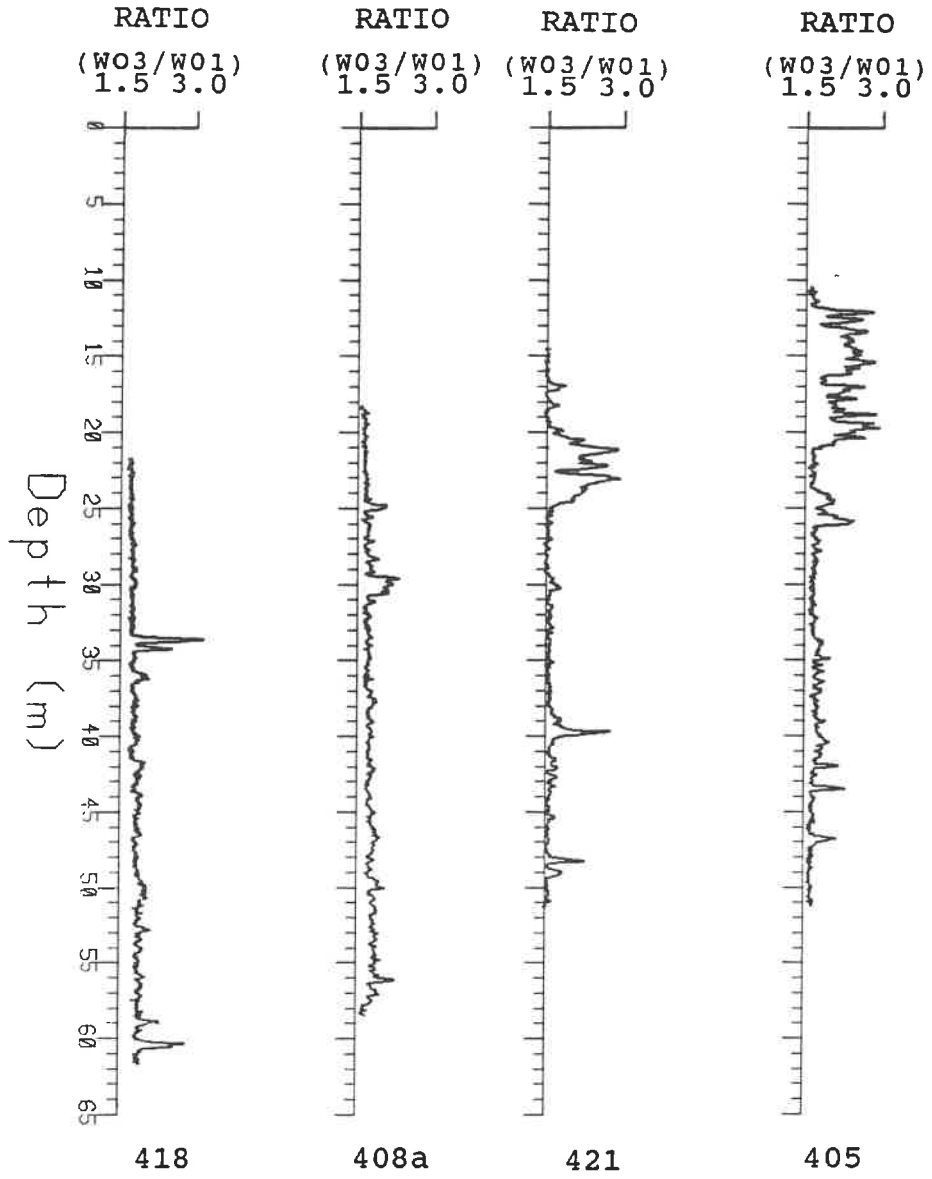


FIGURE C.9 Cross section B - Spectral ratio.
Horizontal scale: 1cm = 13.72m (45ft)
Vertical scale: 1 cm = 5m

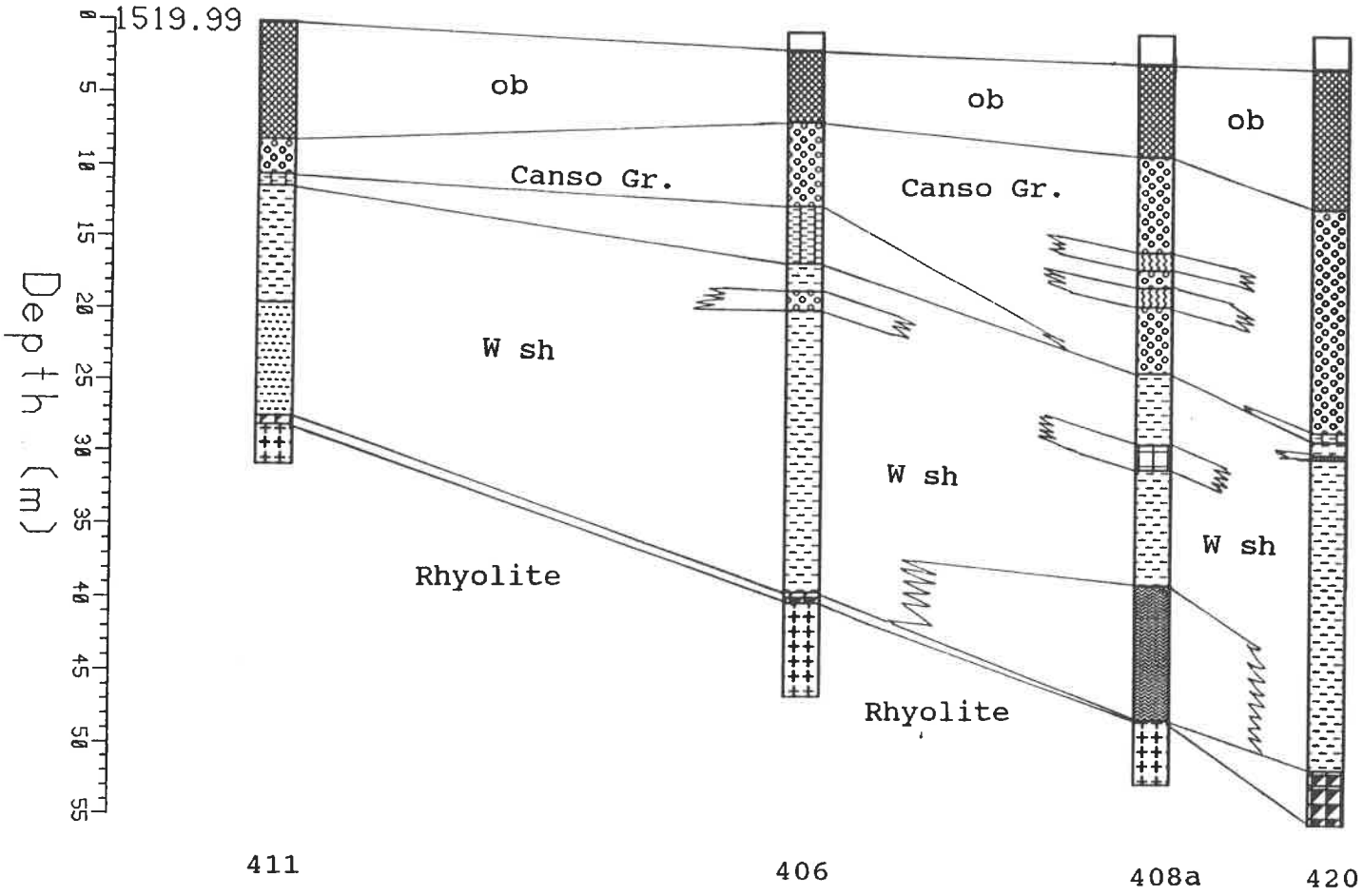


FIGURE C.10 Geological section C.
Horizontal scale: 1cm = 13.72m (45pi)
Vertical scale: 1 cm = 5m

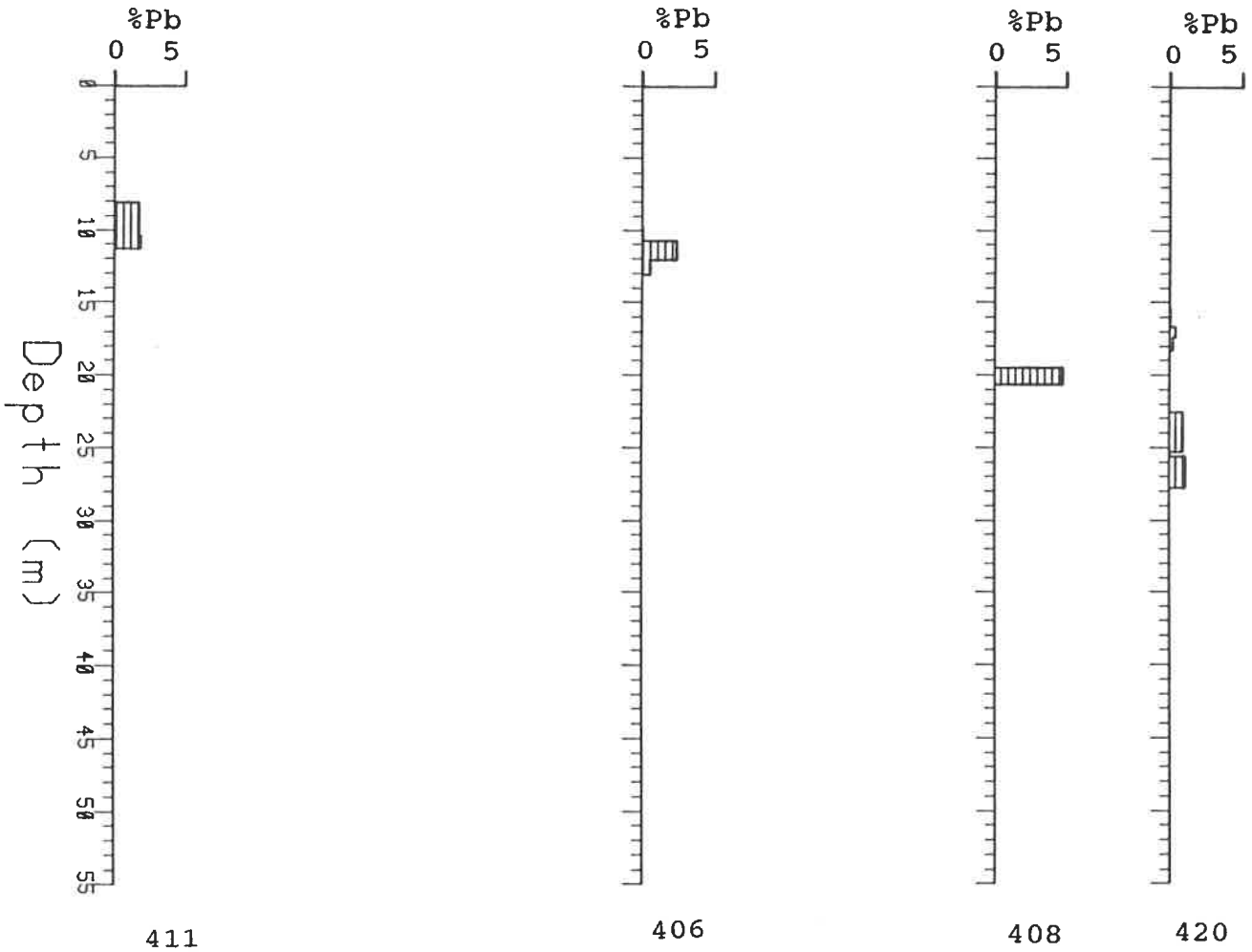


FIGURE C.11 Section C - Lead content.
Horizontal scale: 1cm = 13.72m (45ft)
Vertical scale: 1 cm = 5m

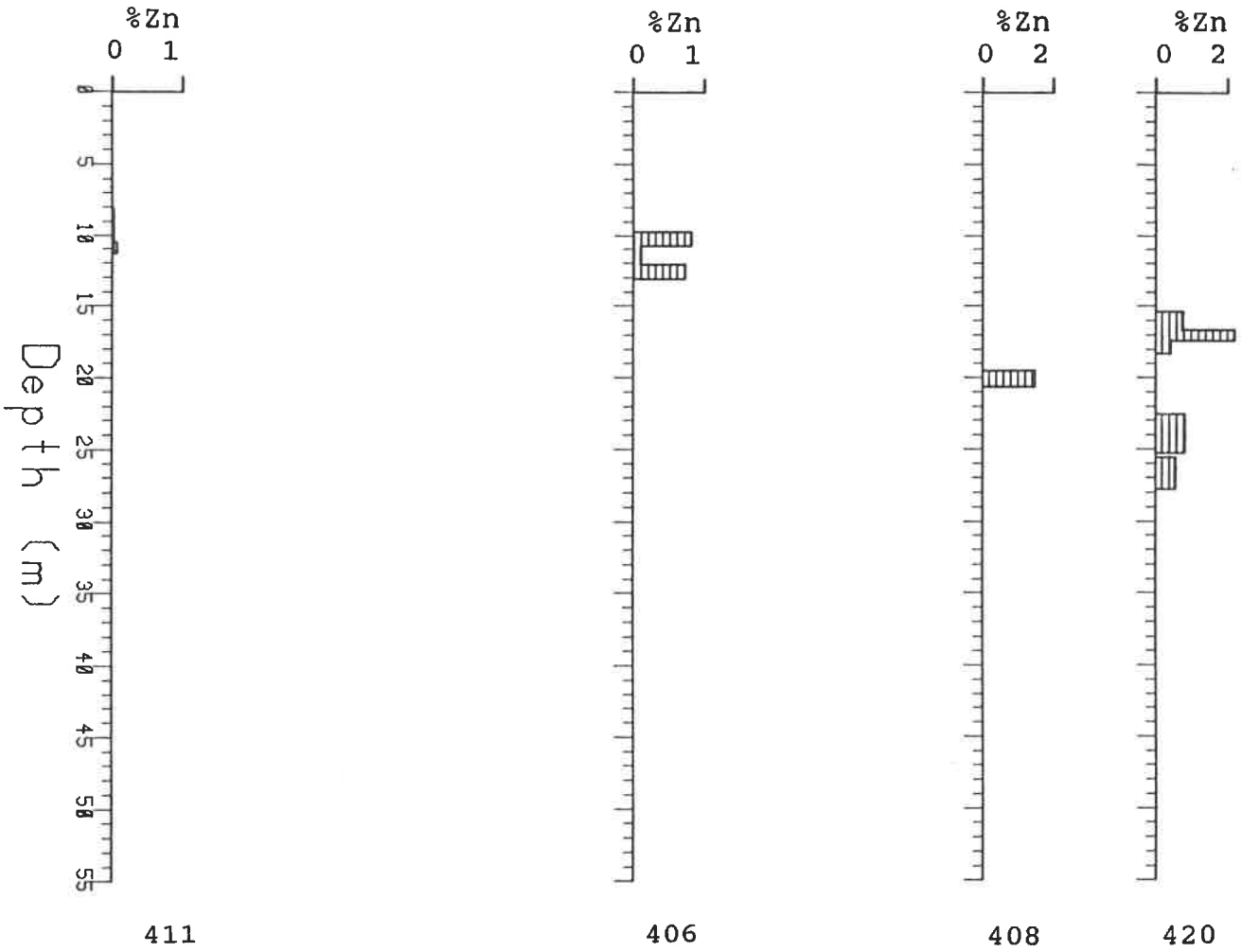


FIGURE C.12 Section C - Zinc content.
Horizontal scale: 1cm = 13.72m (45ft)
Vertical scale: 1 cm = 5m

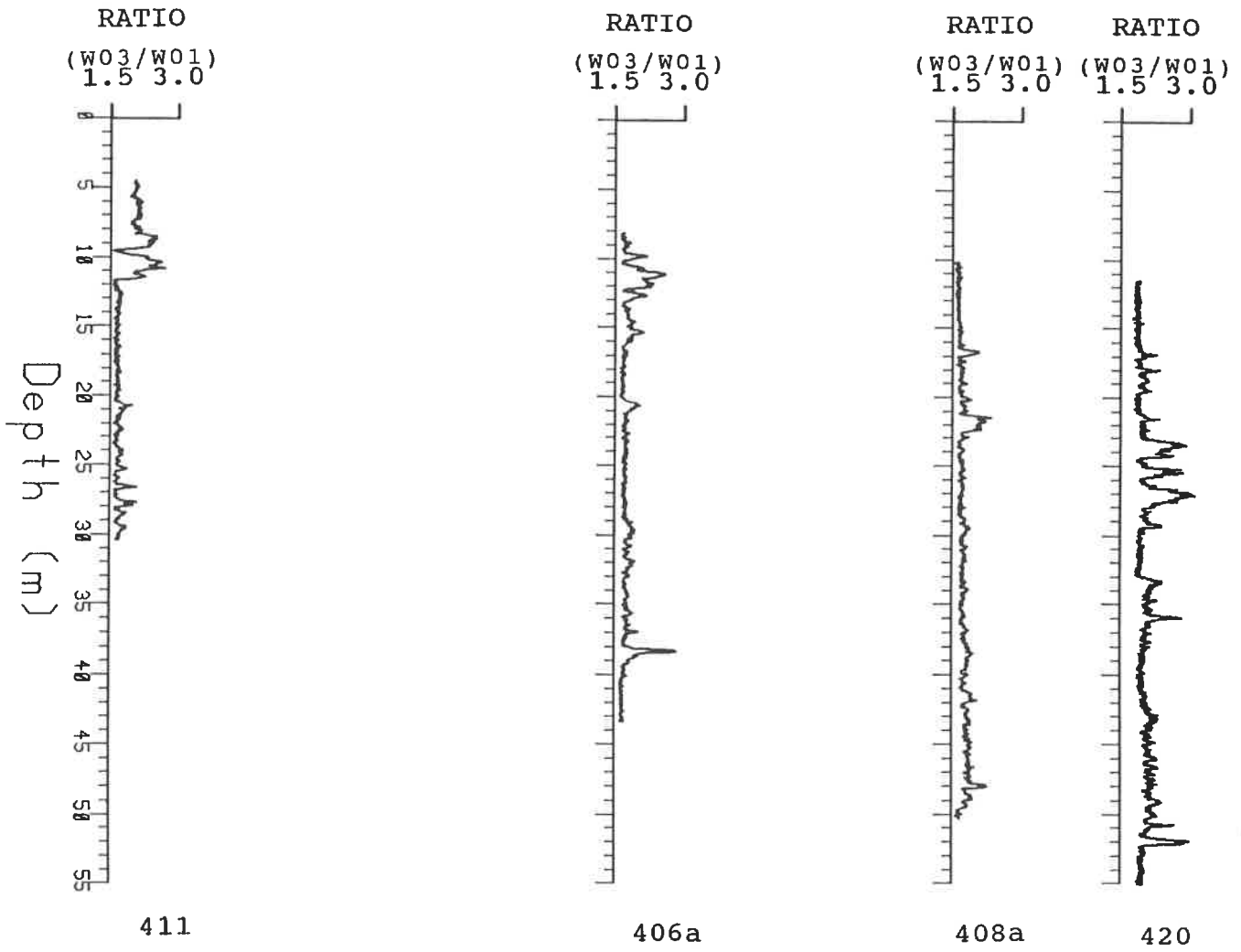


FIGURE C.13 Section C - Spectral ratio.
Horizontal scale: 1cm = 13.72m (45ft)
Vertical scale: 1 cm = 5m

APPENDIX D - HISTOGRAMS

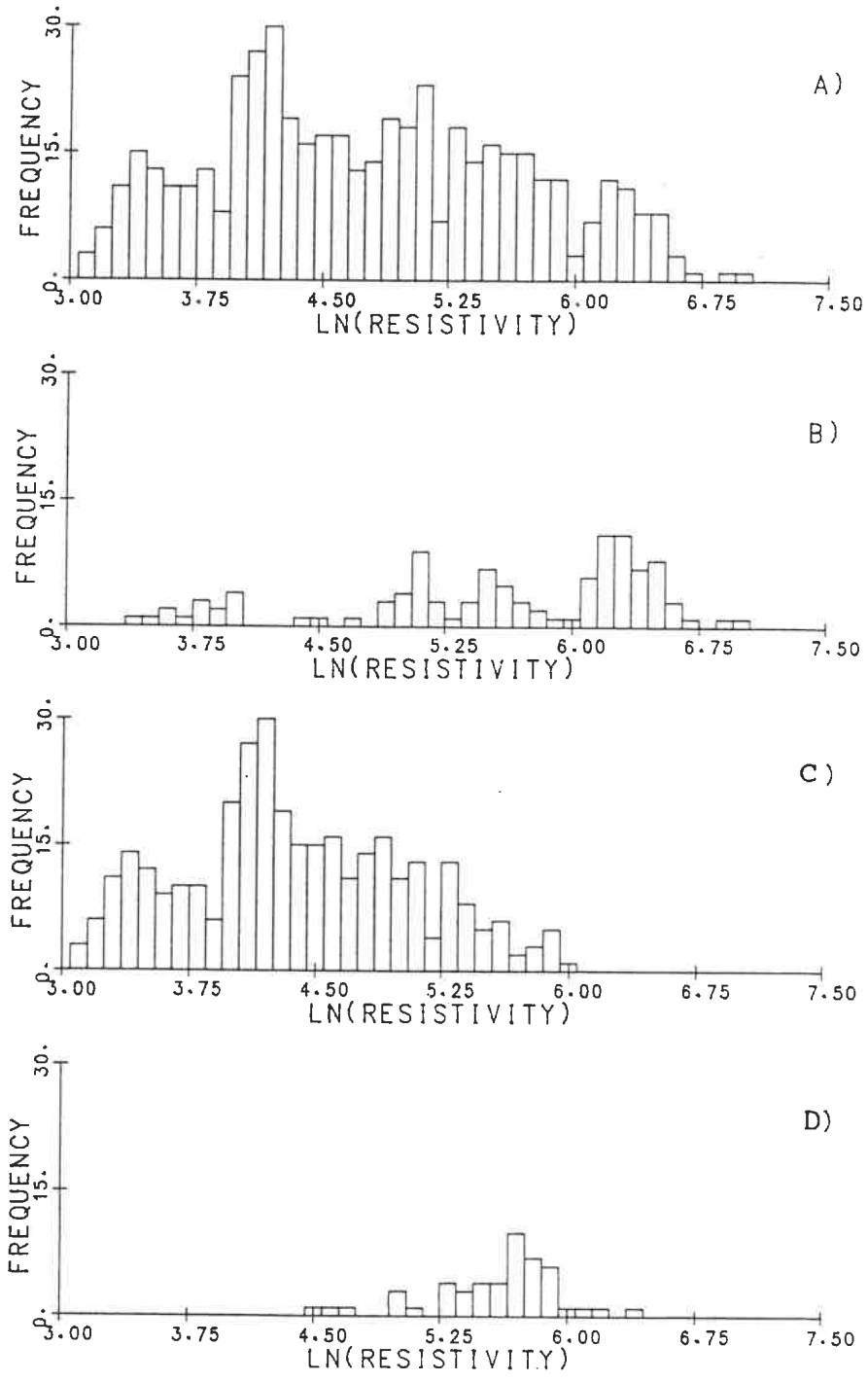


FIGURE D.1 Resistivity natural logarithm distribution, hole 404a.
a) Values from all lithologies
b) Values from the Canso Group (sandstone)
c) Values from the Windsor shale
d) Values from the rhyolite

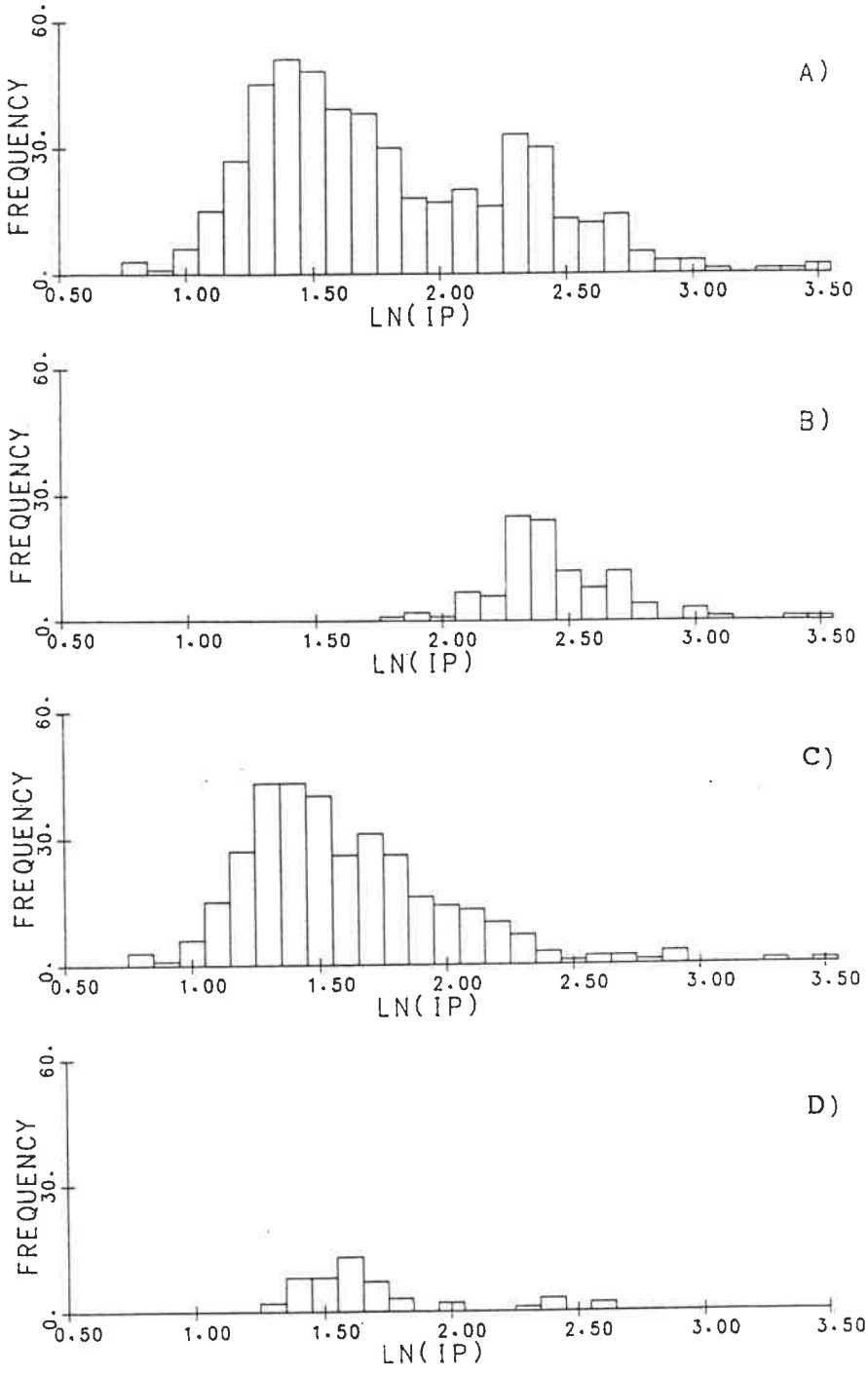


FIGURE D.2 Induced polarization natural logarithm (Ln(IP)) distribution, hole 404a.
a) Values from all lithologies
b) Values from the Canso Group (sandstone)
c) Values from the Windsor shale
d) Values from the rhyolite

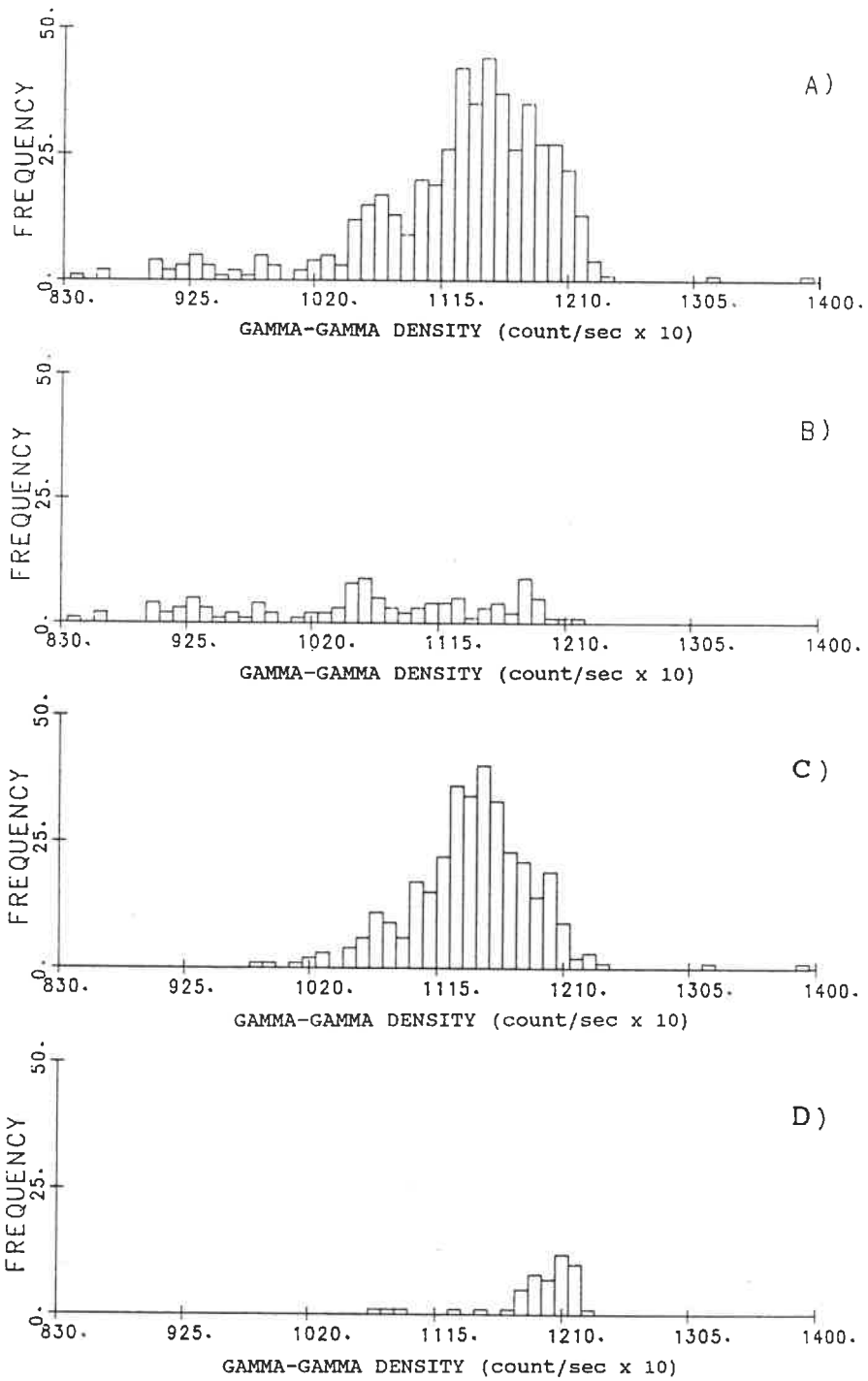


FIGURE D.3 Gamma-gamma density distribution, hole 404a.
a) Values from all lithologies
b) Values from the Canso Group (sandstone)
c) Values from the Windsor shale
d) Values from the rhyolite

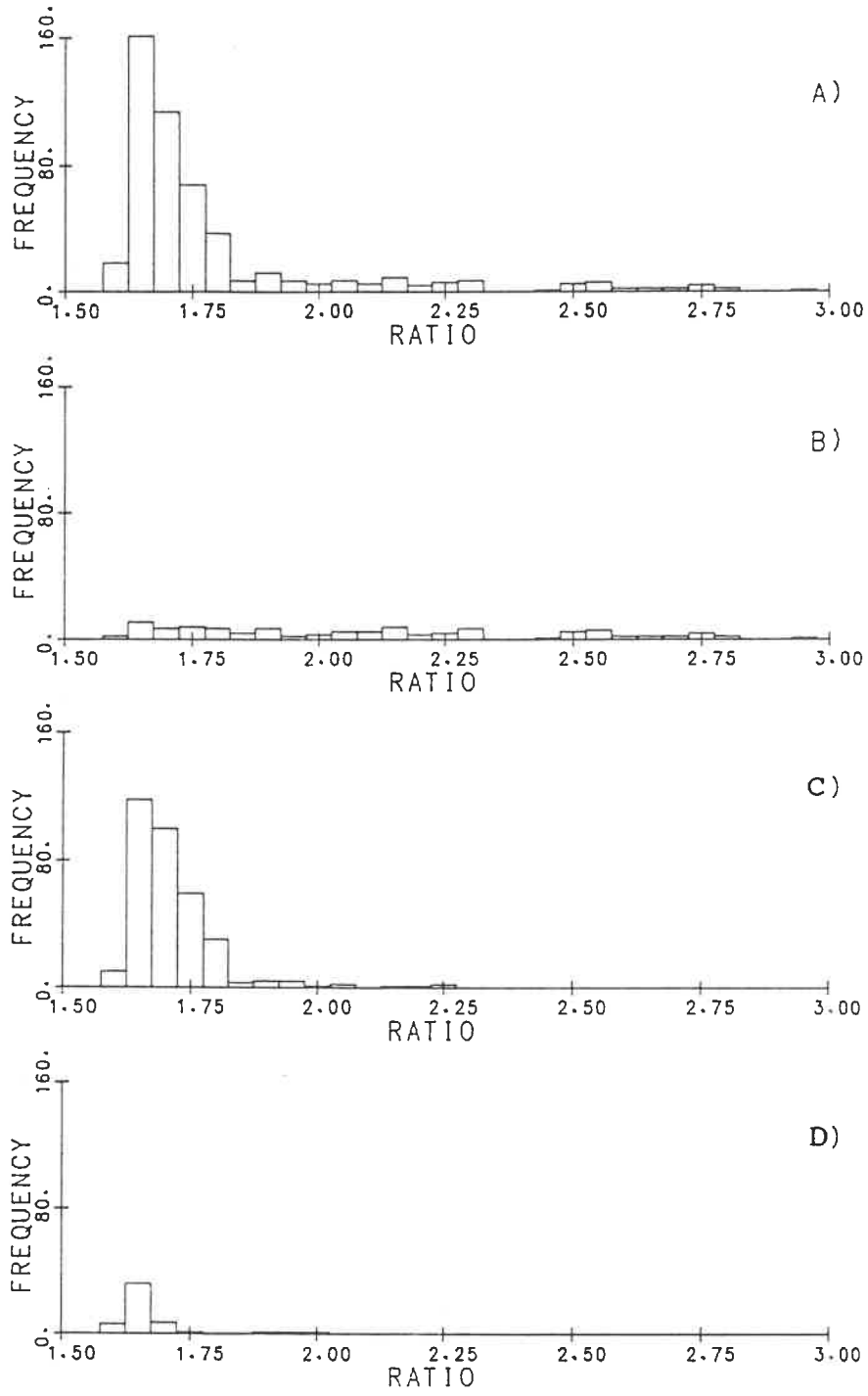


FIGURE D.4 Spectral ratio distribution, hole 404a.
a) Values from all lithologies
b) Values from the Canso Group (sandstone)
c) Values from the Windsor shale
d) Values from the rhyolite

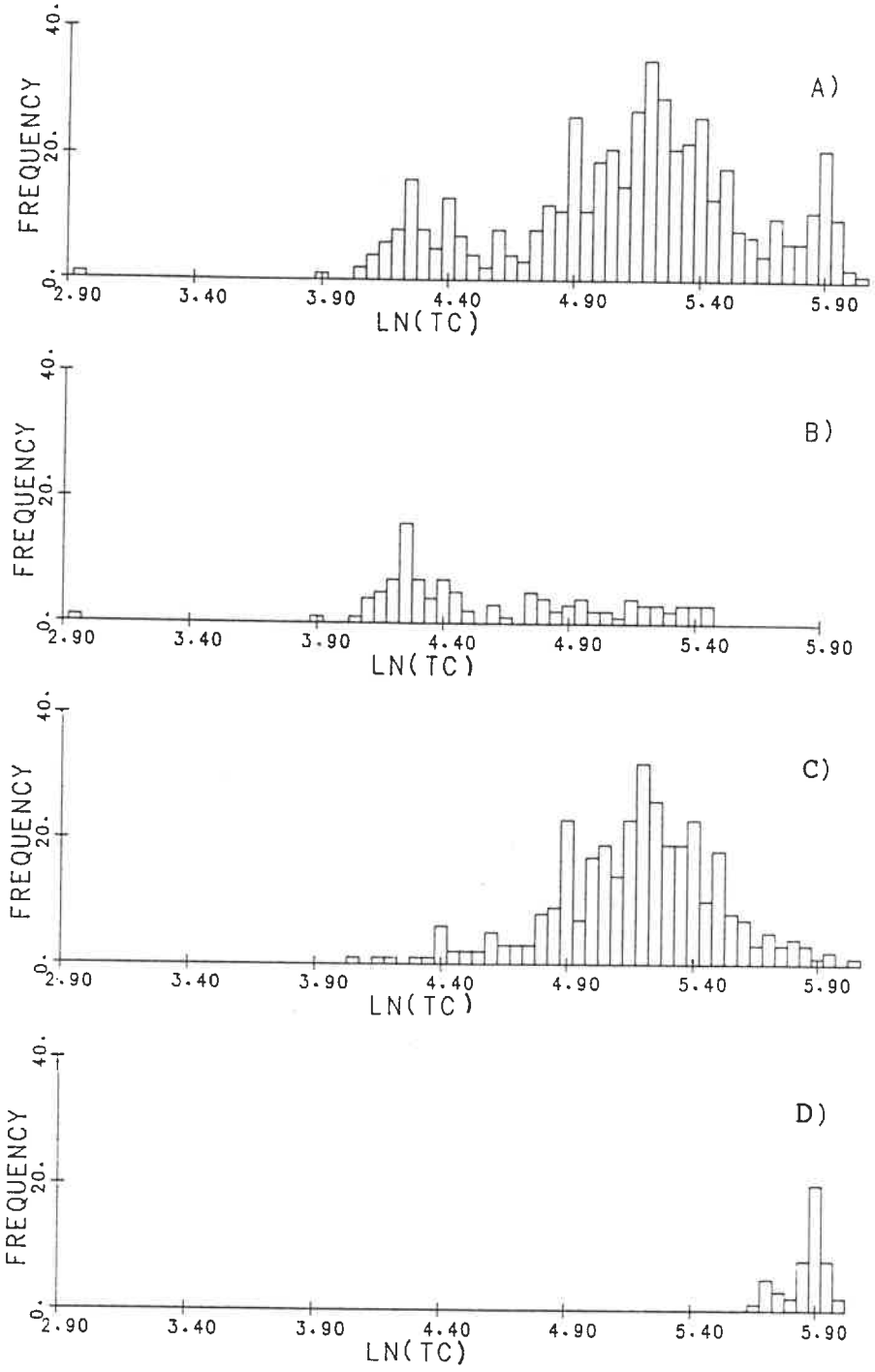


FIGURE D.5 Total count natural logarithm (Ln(TC)) distribution, hole 404a.
a) Values from all lithologies
b) Values from the Canso Group (sandstone)
c) Values from the Windsor shale
d) Values from the rhyolite

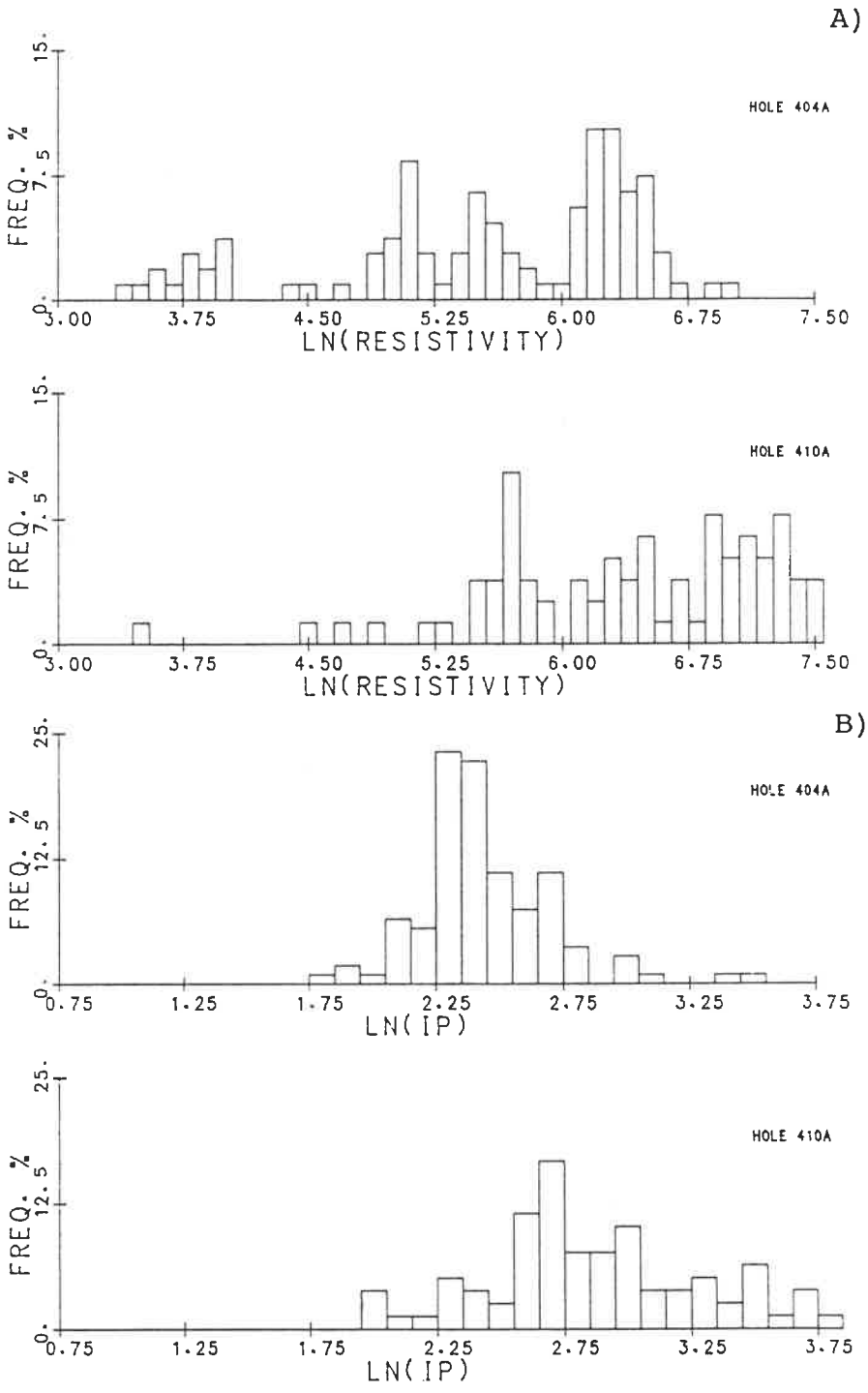


FIGURE D.6 a) Resistivity natural logarithmic distribution.
Values from the Canso Group (sandstone).
Top: Hole 404a Bottom: Hole 410a
b) Induced polarization natural logarithm (Ln(IP)) distribution.
Values from the Canso Group (sandstone).
Top: Hole 404a Bottom: Hole 410a

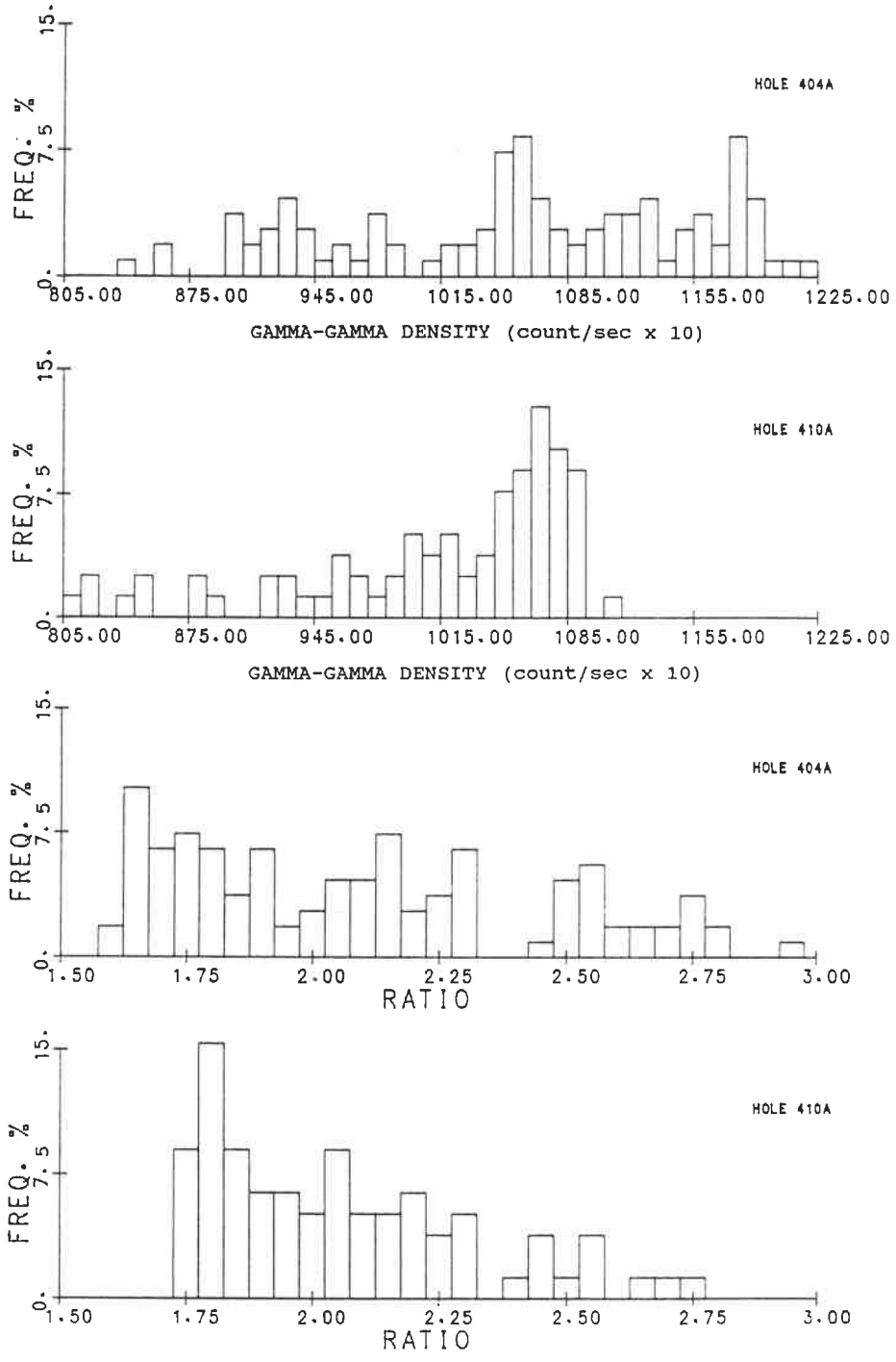


FIGURE D.7 a) Gamma-gamma density distribution.
Values from the Canso Group (sandstone).
Top: Hole 404a Bottom: Hole 410a
b) Spectral ratio distribution.
Values from the Canso Group (sandstone).
Top: Hole 404a Bottom: Hole 410a

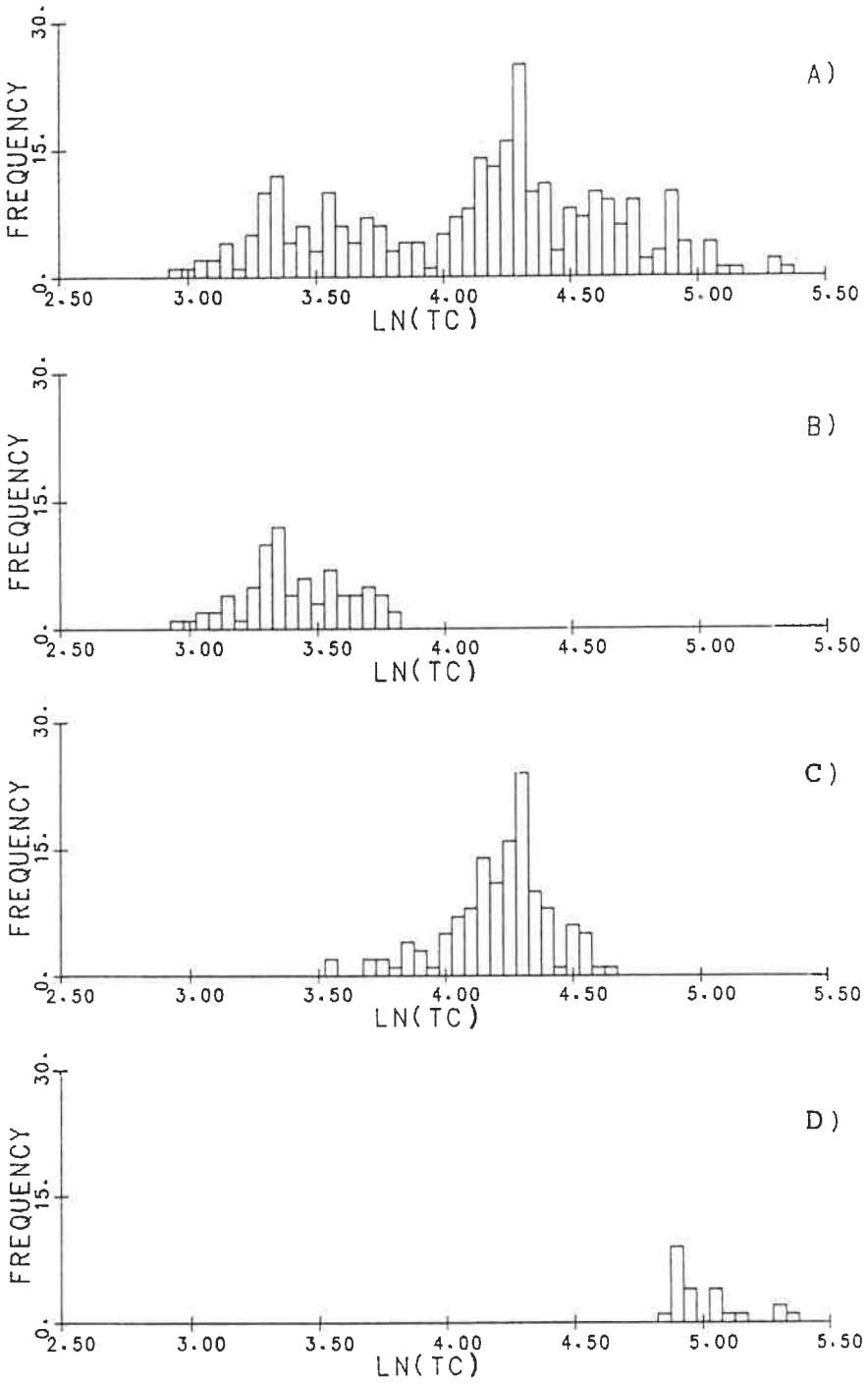


FIGURE D.8 Total count natural logarithm (Ln(TC)) distribution, hole 410a.
a) Values from all lithologies
b) Values from the Canso Group (sandstone)
c) Values from the Windsor shale
d) Values from the rhyolite

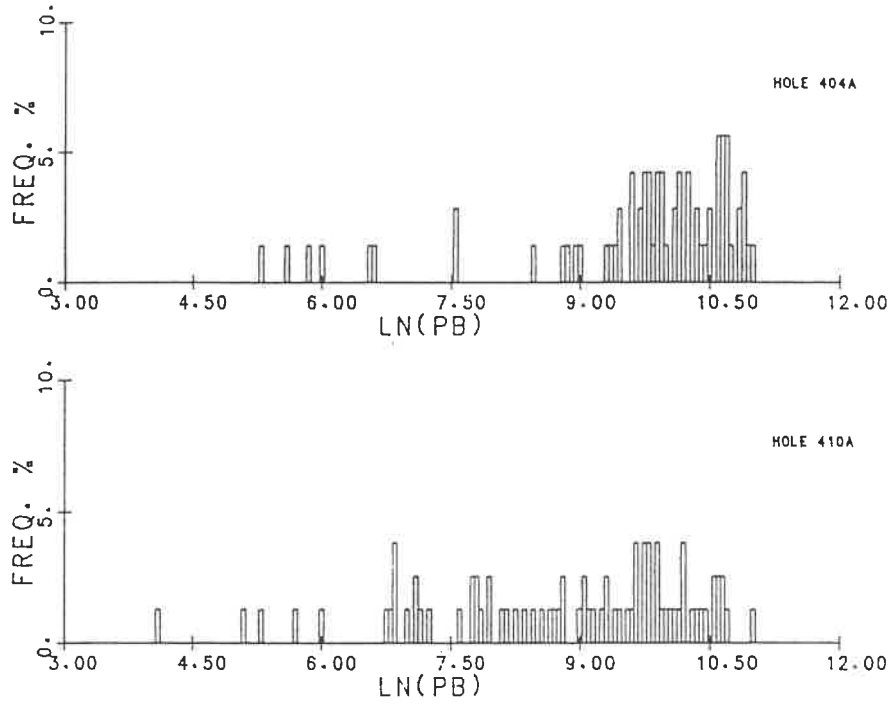


FIGURE D.9 Lead natural logarithm (Ln(Pb)) distribution.
Values from the Canso Group (sandstone).
Top: Hole 404a Bottom: Hole 410a

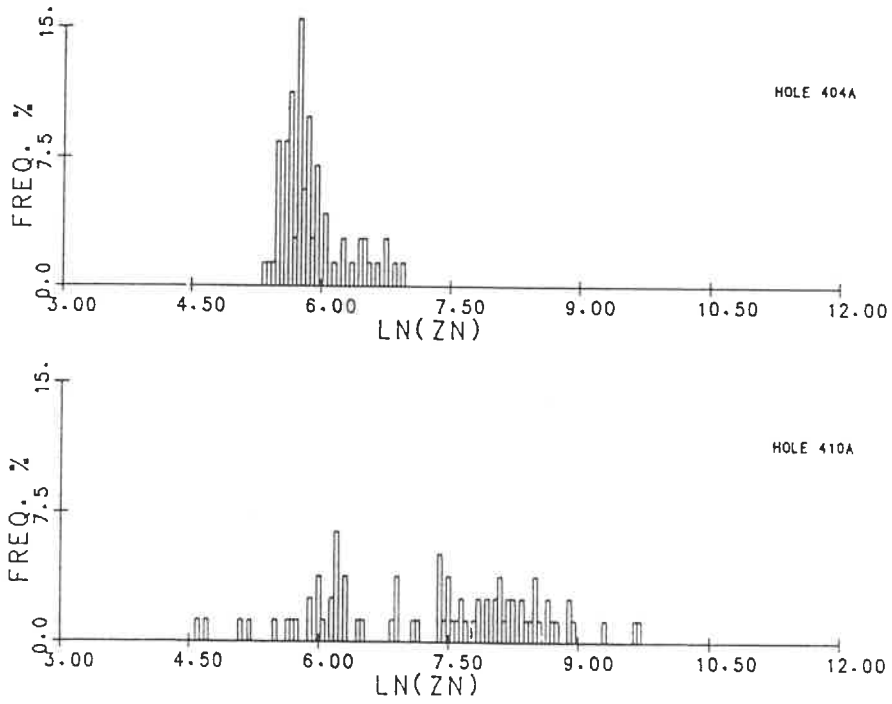


FIGURE D.10 Zinc natural logarithm (Ln(Zn)) distribution.
Values from the Canso Group (sandstone).
Top: Hole 404a Bottom: Hole 410a

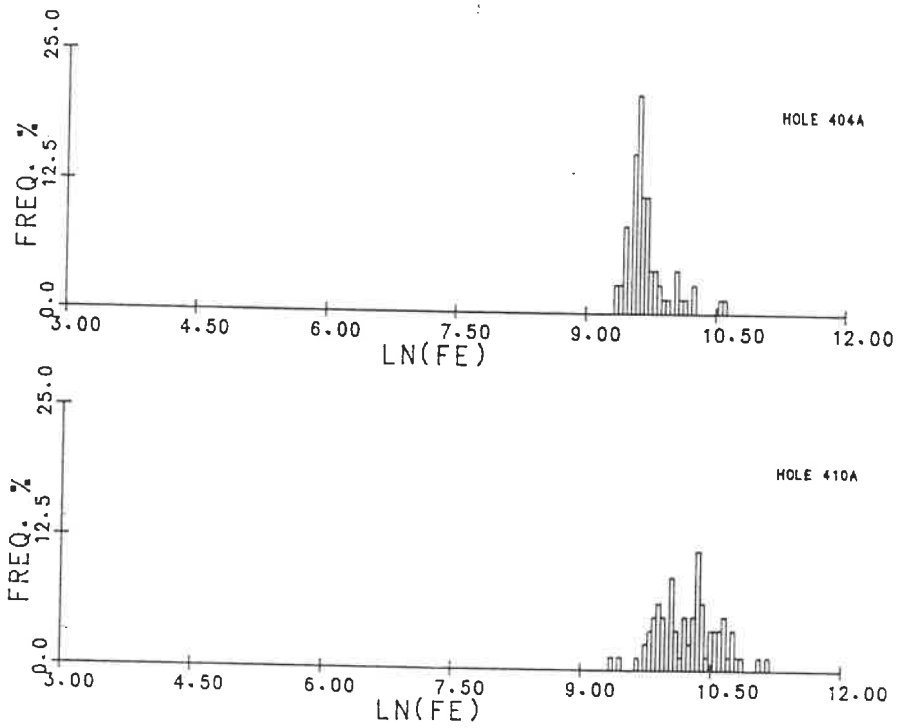


FIGURE D.11 Total iron natural logarithm (Ln(Fe)) distribution. Values from the Canso Group (sandstone). Top: Hole 404a Bottom: Hole 410a

APPENDIX E - SCATTERPLOT DIAGRAMS

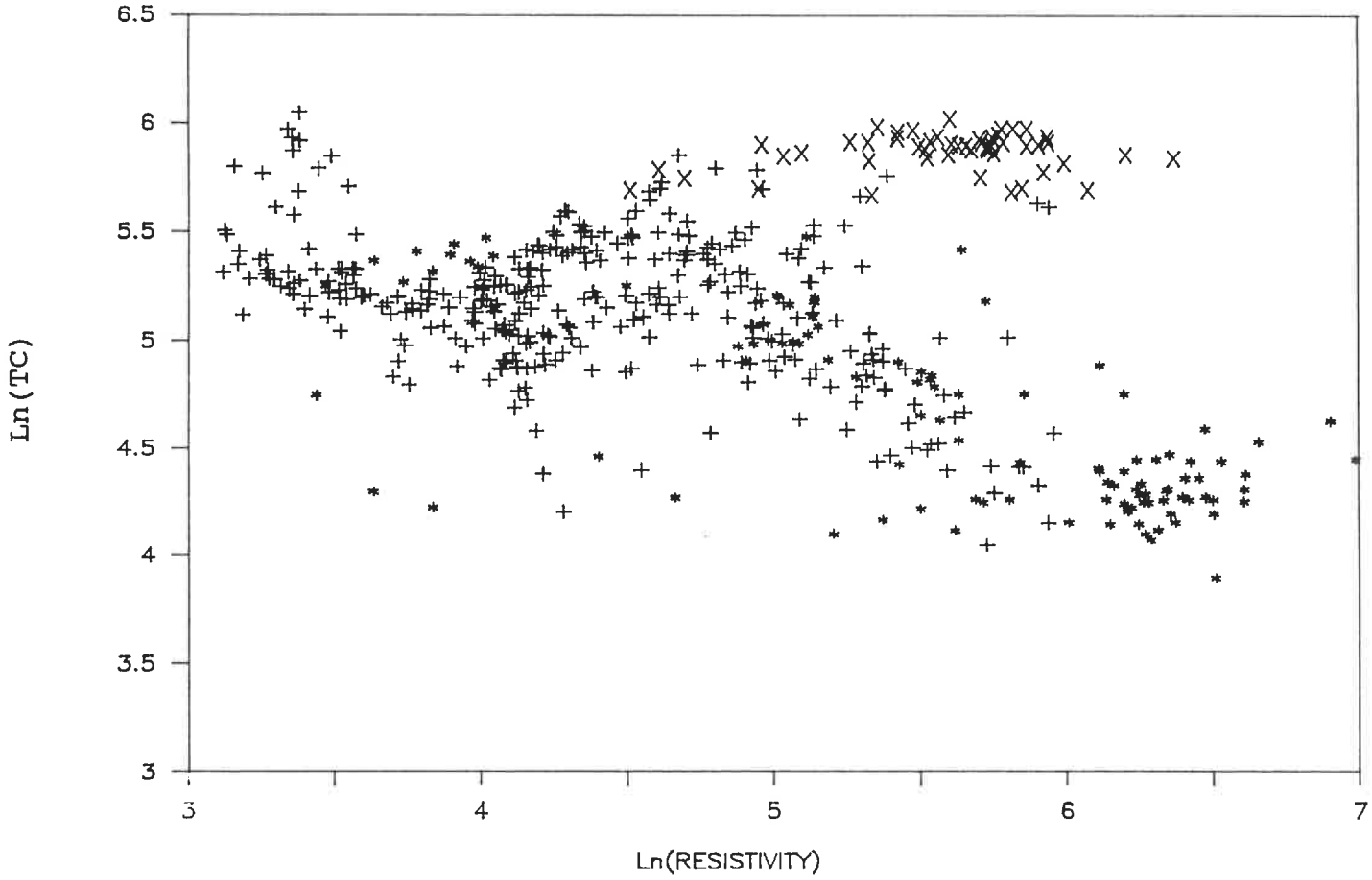


FIGURE E.1 Scatterplot diagram of the natural logarithmic values of total count (Ln(TC)) against the natural logarithmic values of resistivity for hole 404a (symbols: (*): Canso Group, (+): Windsor shale and, (x): rhyolite).

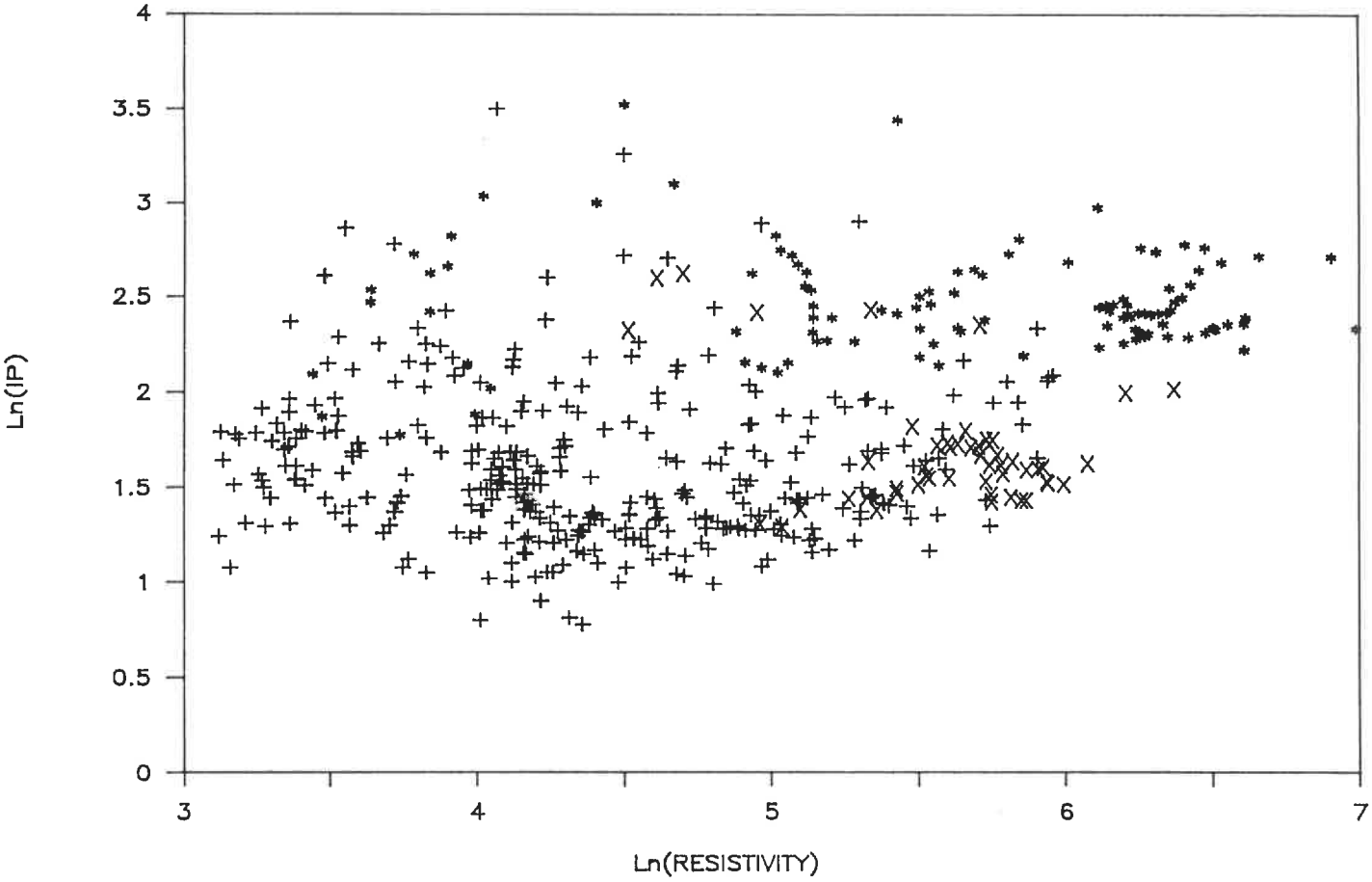


FIGURE E.2 Scatterplot diagram of the natural logarithmic values of induced polarization (Ln(IP)) against the natural logarithmic values of resistivity for hole 404a (symbols: (*): Canso Group, (+): Windsor shale and, (x): rhyolite).

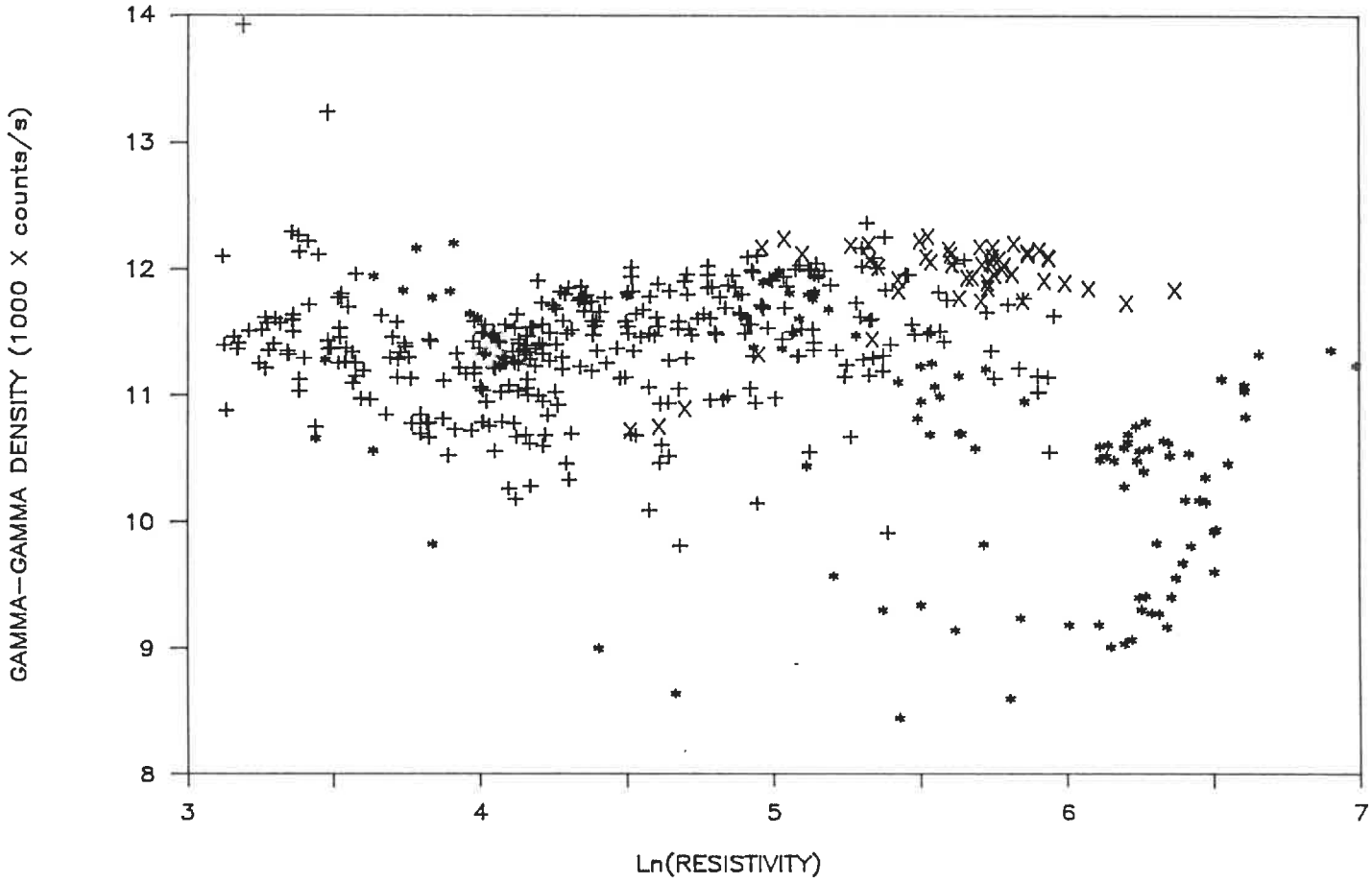


FIGURE E.3 Scatterplot diagram of the gamma-gamma density values against the natural logarithmic values of resistivity for hole 404a (symbols: (*): Canso Group, (+): Windsor shale and, (x): rhyolite).

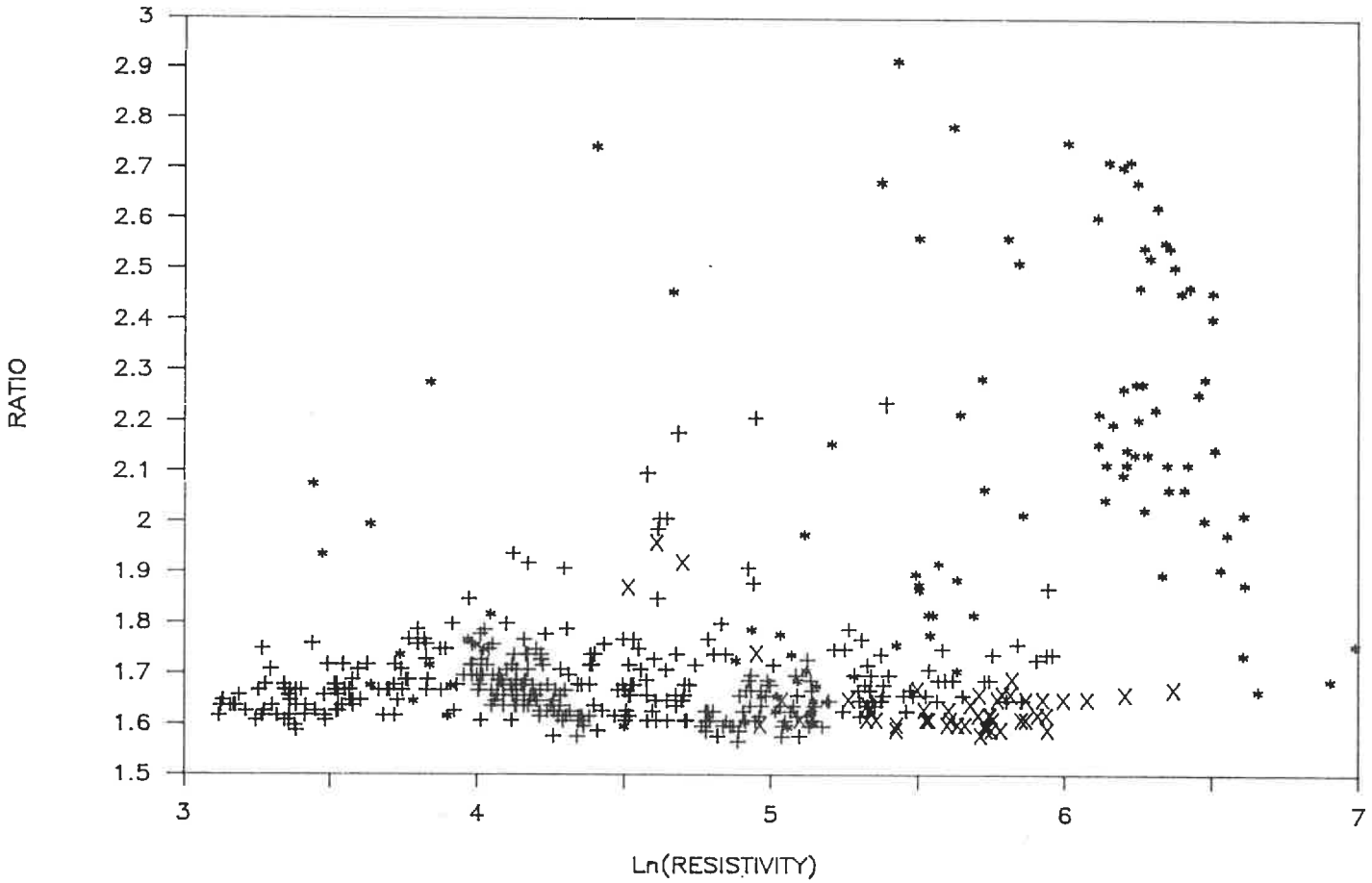


FIGURE E.4 Scatterplot diagram of the spectral ratio values against the natural logarithmic values of resistivity for hole 404a (symbols: (*): Canso Group, (+): Windsor shale and, (x): rhyolite).

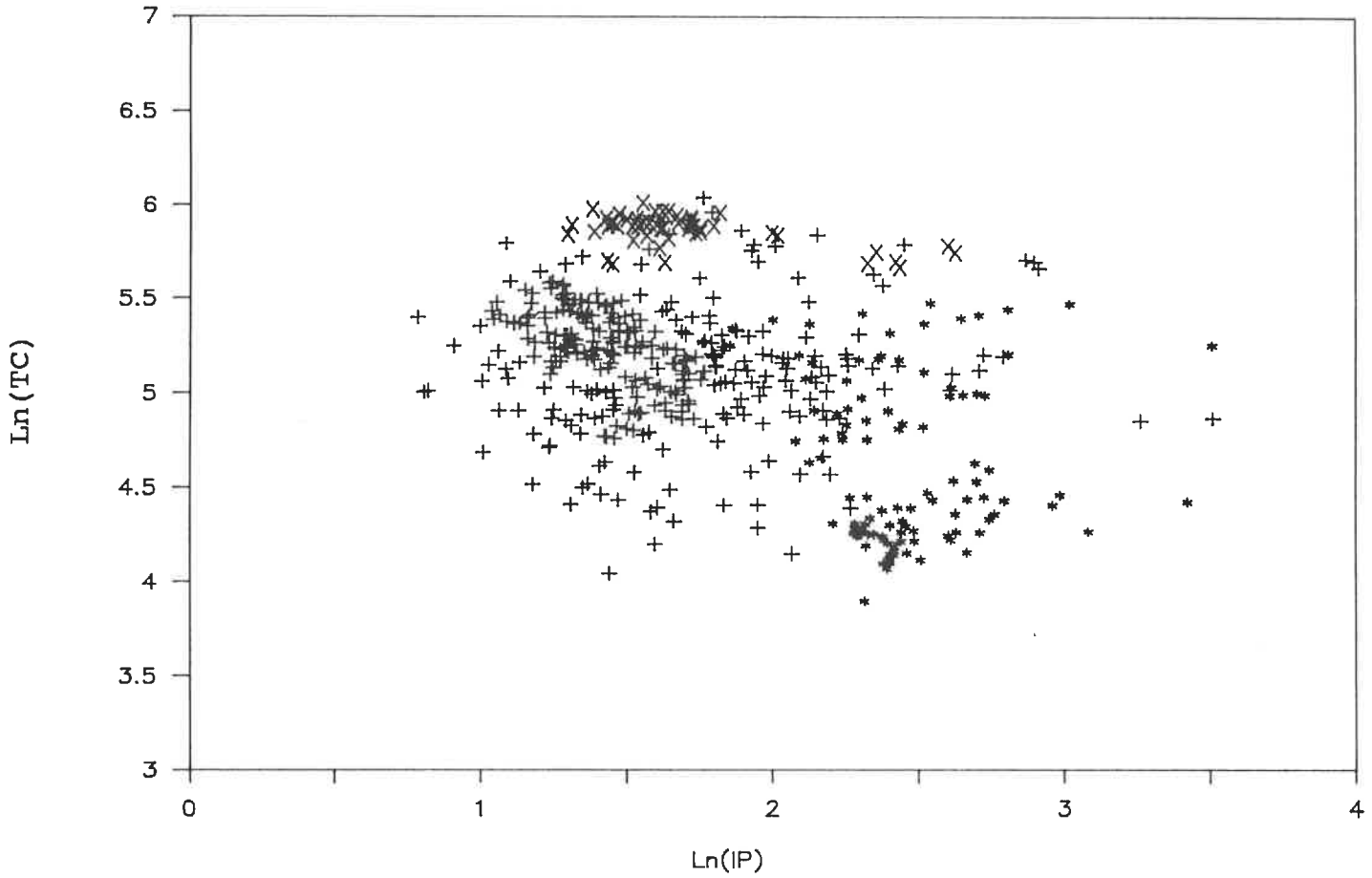


FIGURE E.5 Scatterplot diagram of natural logarithmic values of total count (Ln(TC)) against logarithmic values of induced polarization (Ln(IP)) for hole 404a (symbols: (*): Canso Group, (+): Windsor shale and, (x): rhyolite).

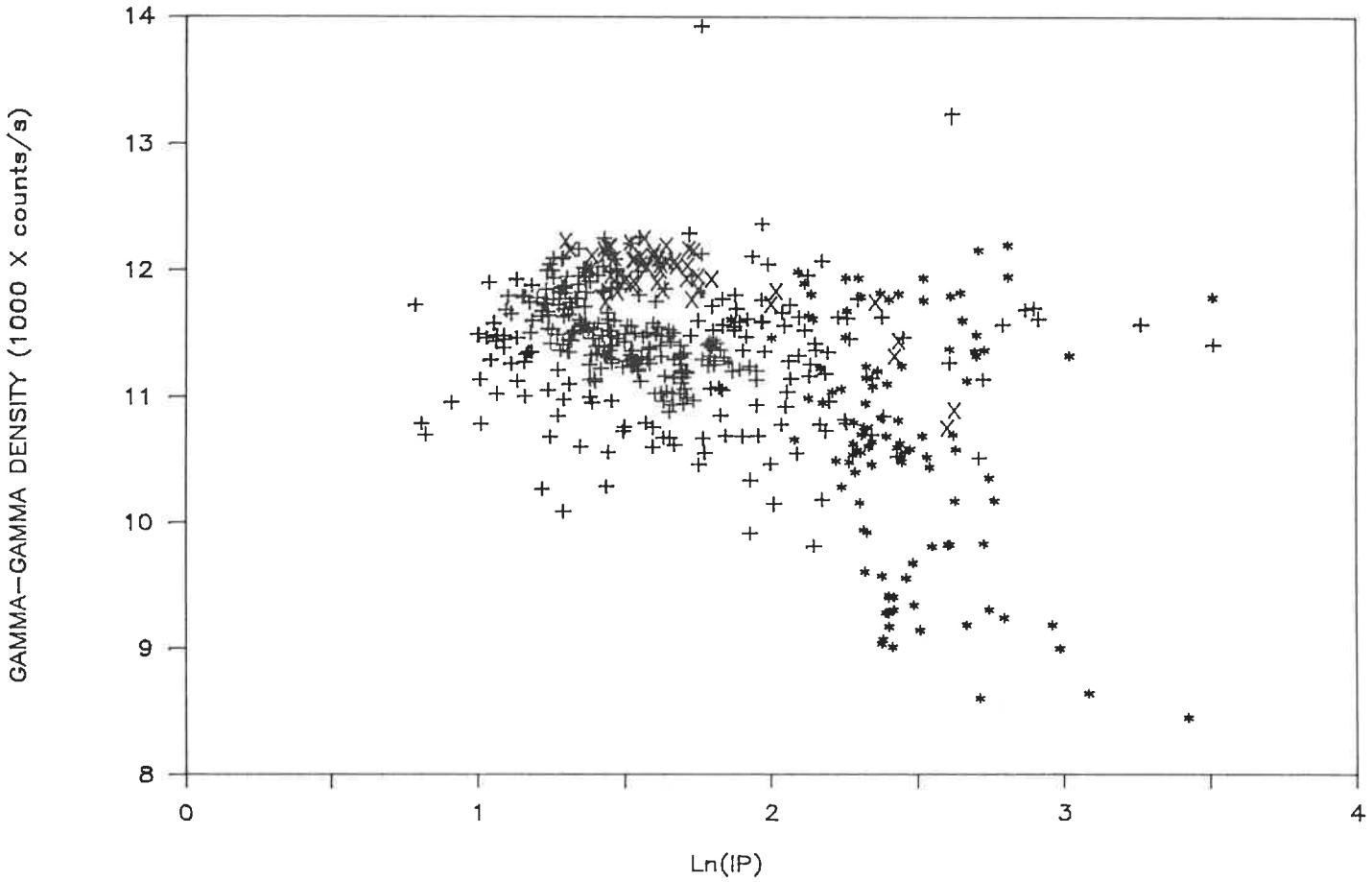


FIGURE E.6 Scatterplot diagram for hole 404a. Gamma-gamma density values against natural logarithmic values of induced polarization (Ln(IP)). Symbols: (*): Canso Group, (+): Windsor shale and, (x): rhyolite).

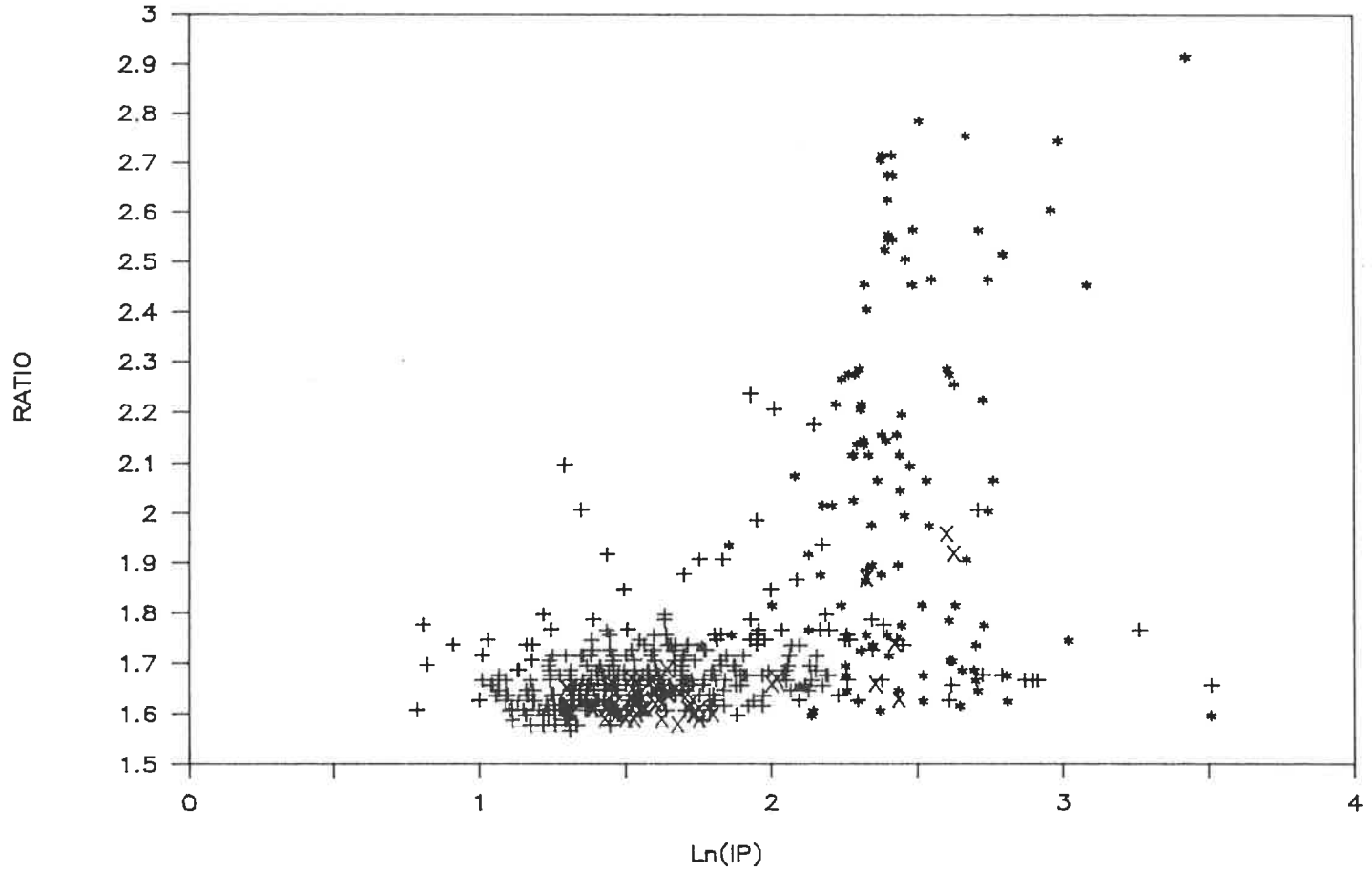


FIGURE E.7 Scatterplot diagram for hole 404a. Spectral ratio values against natural logarithmic values of induced polarization (Ln(IP)).
(Symbols: (*): Canso Group, (+): Windsor shale and, (x): rhyolite).

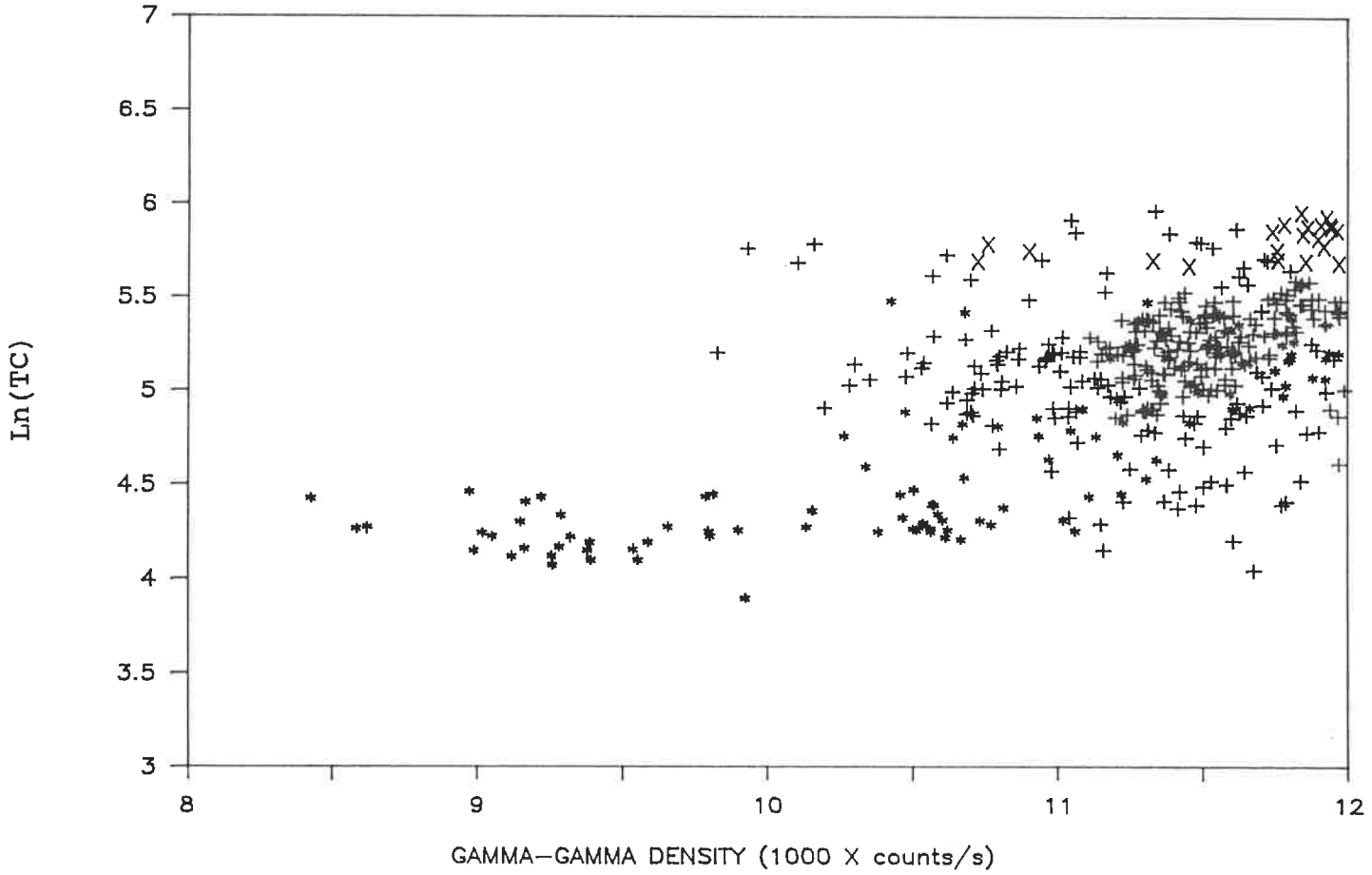


FIGURE E.8 Scatterplot diagram for hole 404a. Natural logarithmic values of total count (Ln(TC)) against gamma-gamma density values. (Symbols: (*): Canso Group, (+): Windsor shale and, (x): rhyolite).

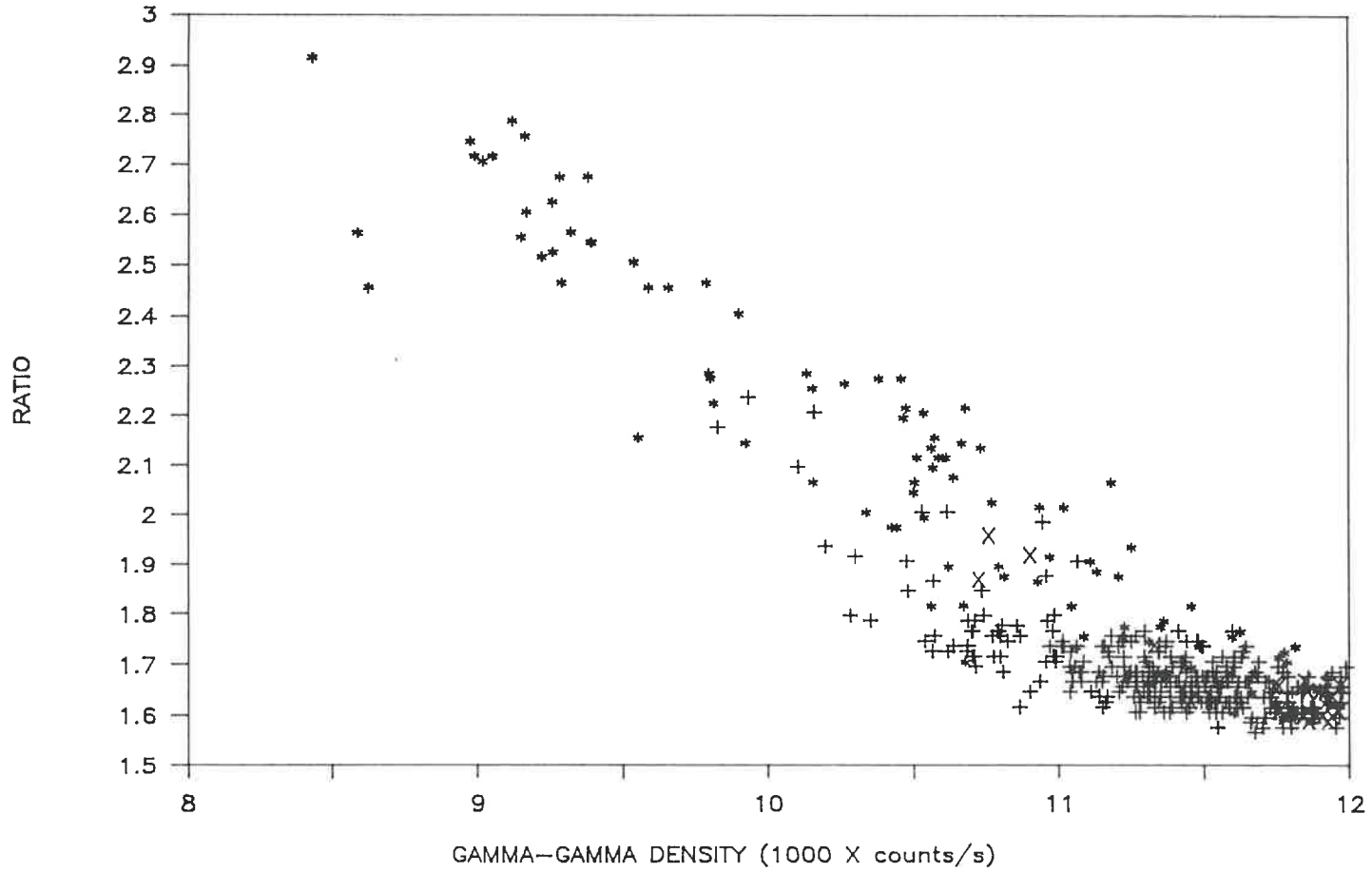


FIGURE E.9 Scatterplot diagram for hole 404a. Spectral ratio values against gamma-gamma density values (Symbols: (*): Canso Group, (+): Windsor shale and, (x): rhyolite).

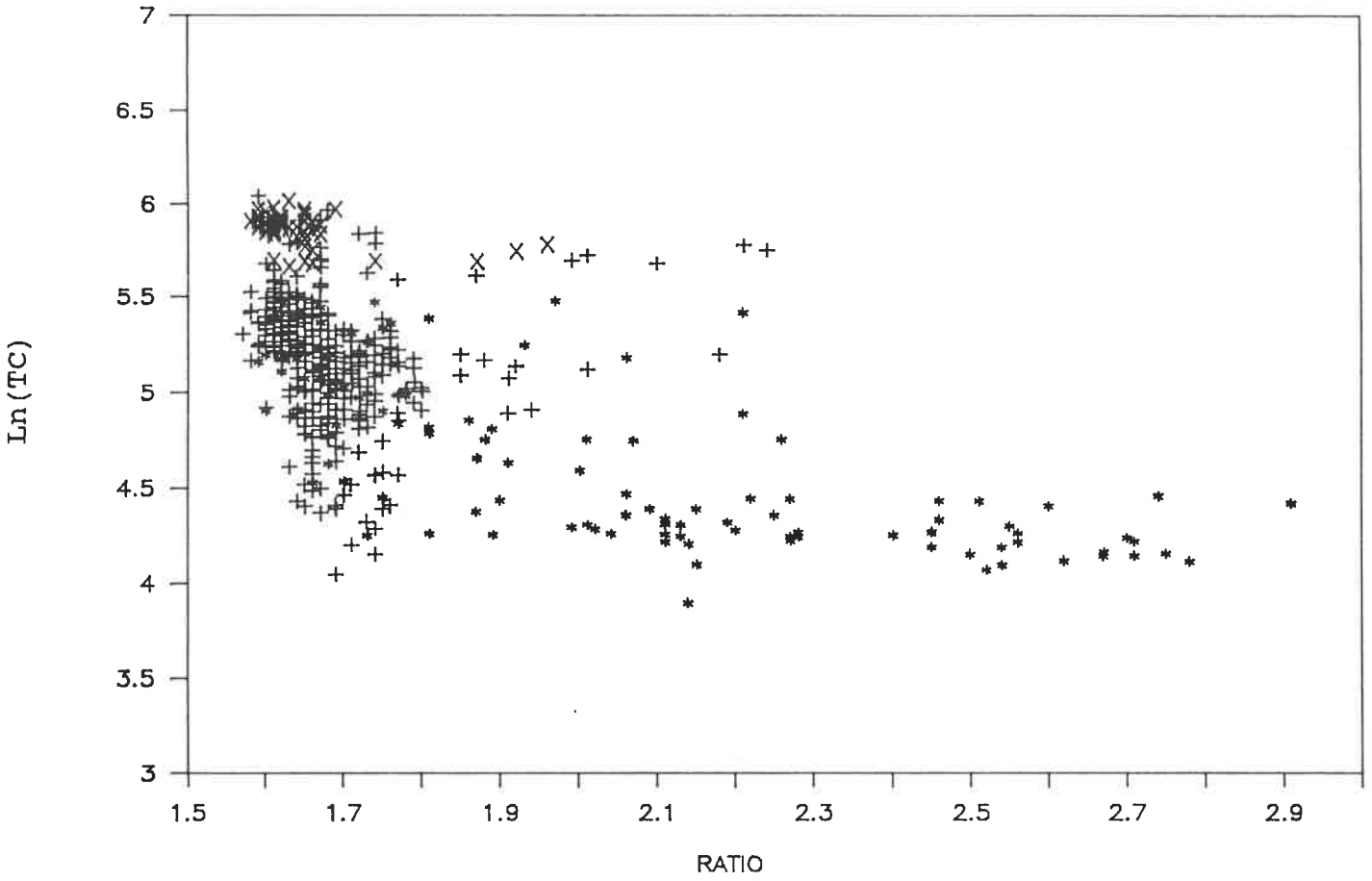


FIGURE E.10 Scatterplot diagram for hole 404a. Natural logarithmic values of total count (Ln(TC)) against spectral ratio values.
(Symbols: (*): Canso Group, (+): Windsor shale and, (x): rhyolite).

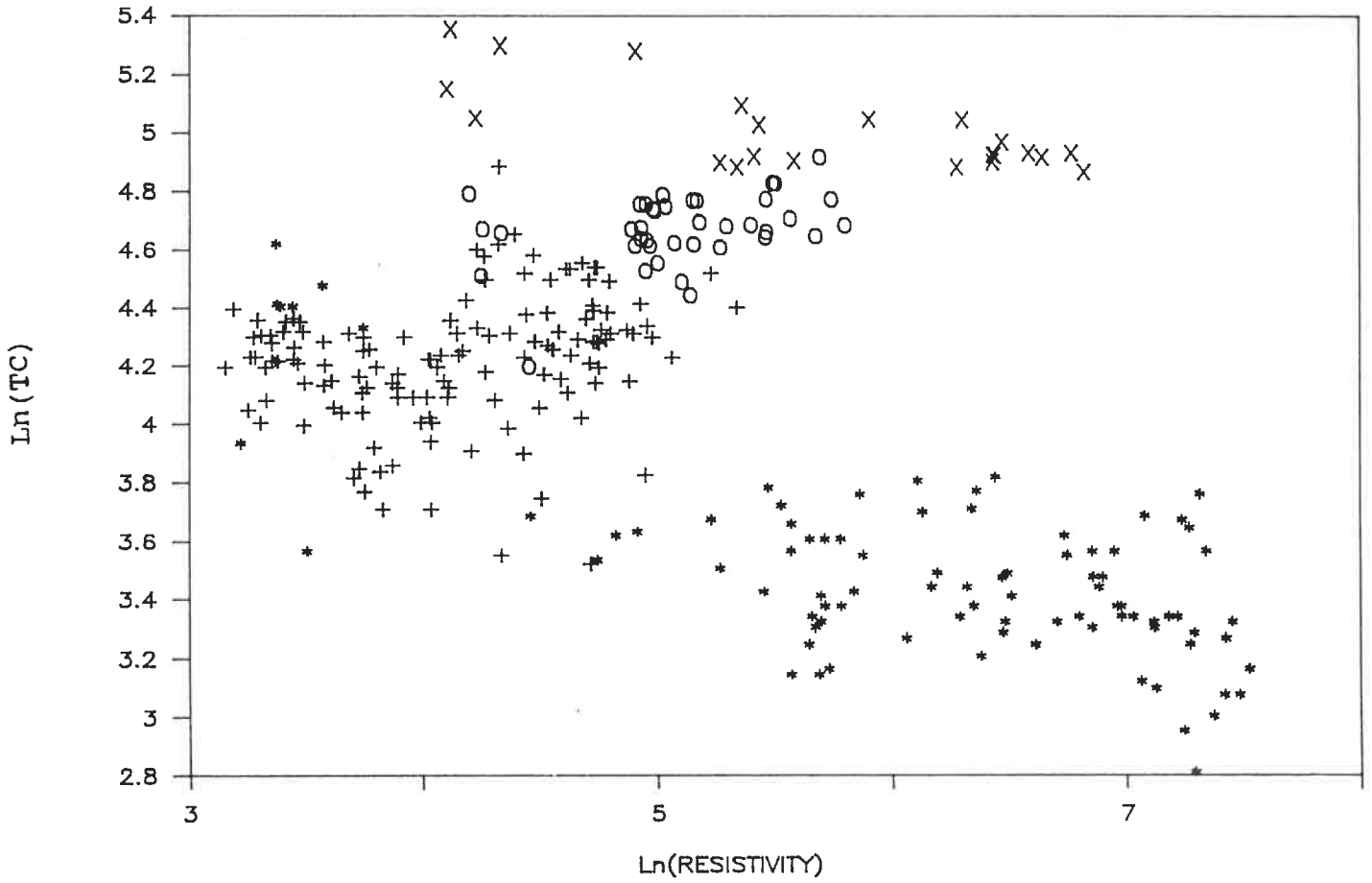


FIGURE E.11 Scatterplot diagram for hole 410a. Natural logarithmic values of total count (Ln(TC)) against the natural logarithmic values of resistivity (Symbols: (*): Canso Group, (+): Windsor shale, (o): rhyolite in the Windsor shale and, (x): rhyolite).

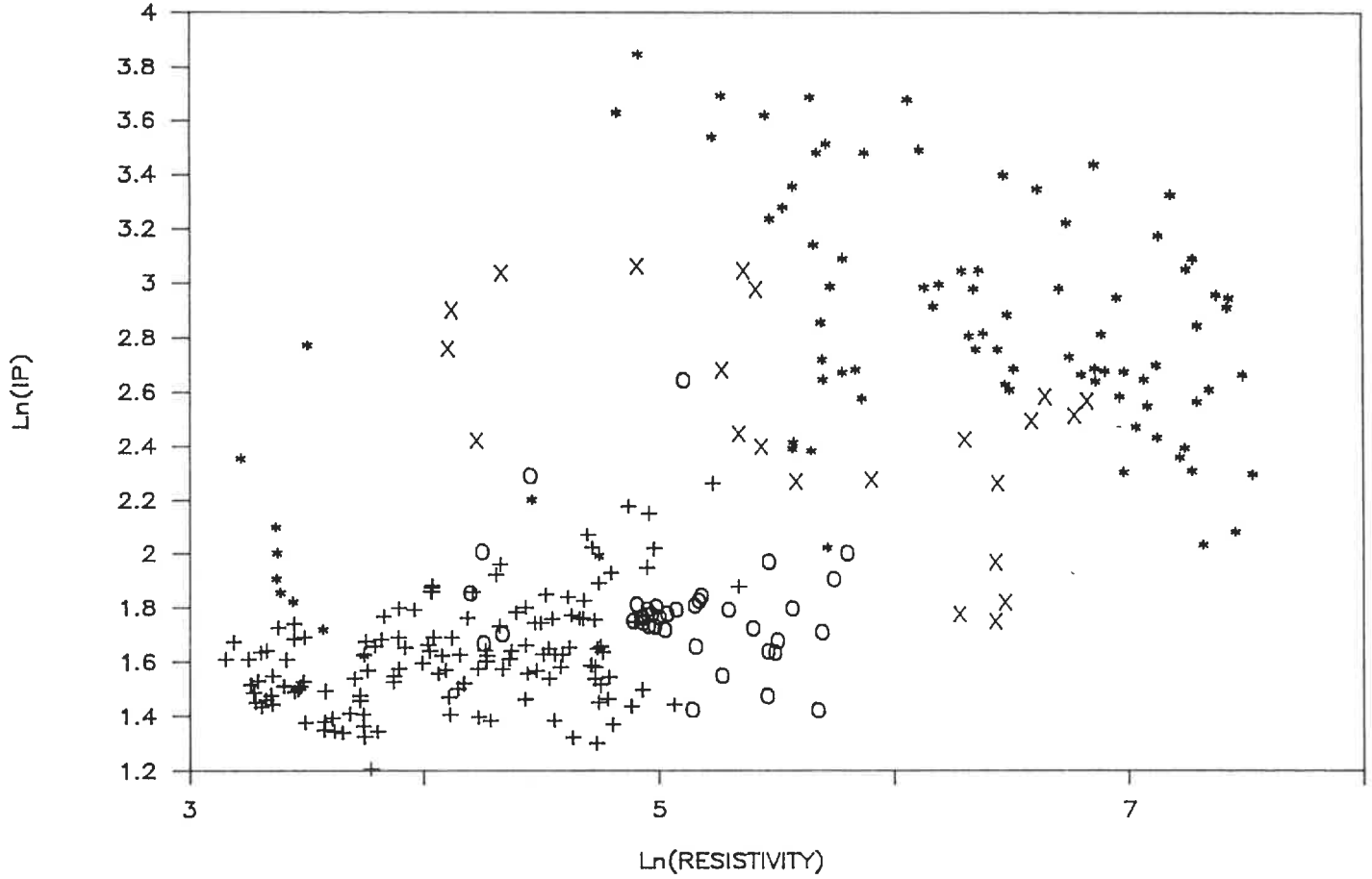


FIGURE E.12 Scatterplot diagram for hole 410a. Natural logarithmic values of induced polarization (Ln(IP)) against the natural logarithmic values of resistivity (Symbols: (*): Canso Group, (+): Windsor shale, (o): rhyolite in the Windsor shale and, (x): rhyolite).

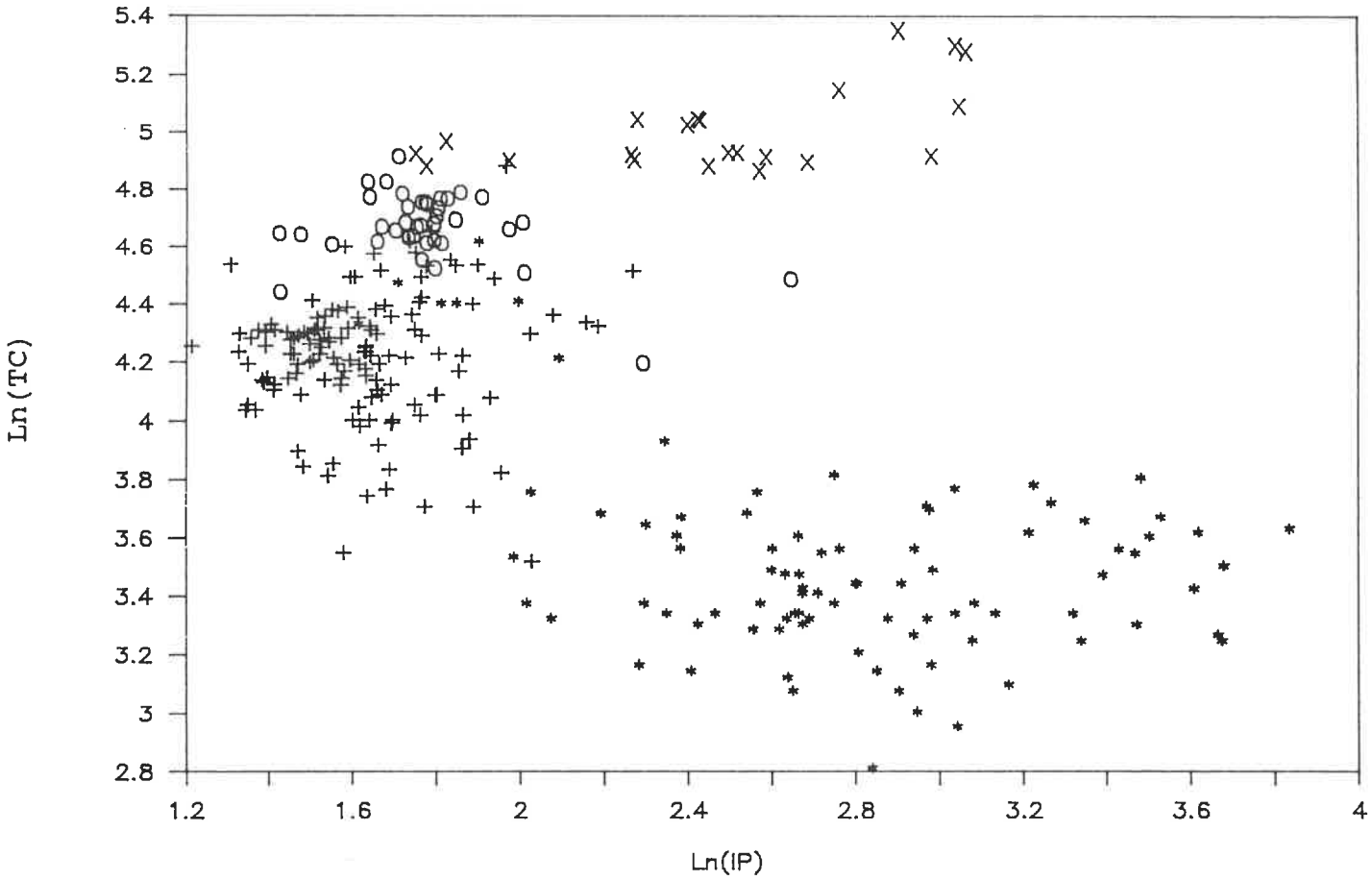


FIGURE E.13 Scatterplot diagram for hole 410a. Natural logarithmic values of total count (Ln(TC)) against the natural logarithmic values of induced polarization (Ln(IP)). Symbols: (*): Canso Gr., (+):Windsor shale, (o):rhyolite in the Windsor shale and, (x): rhyolite.

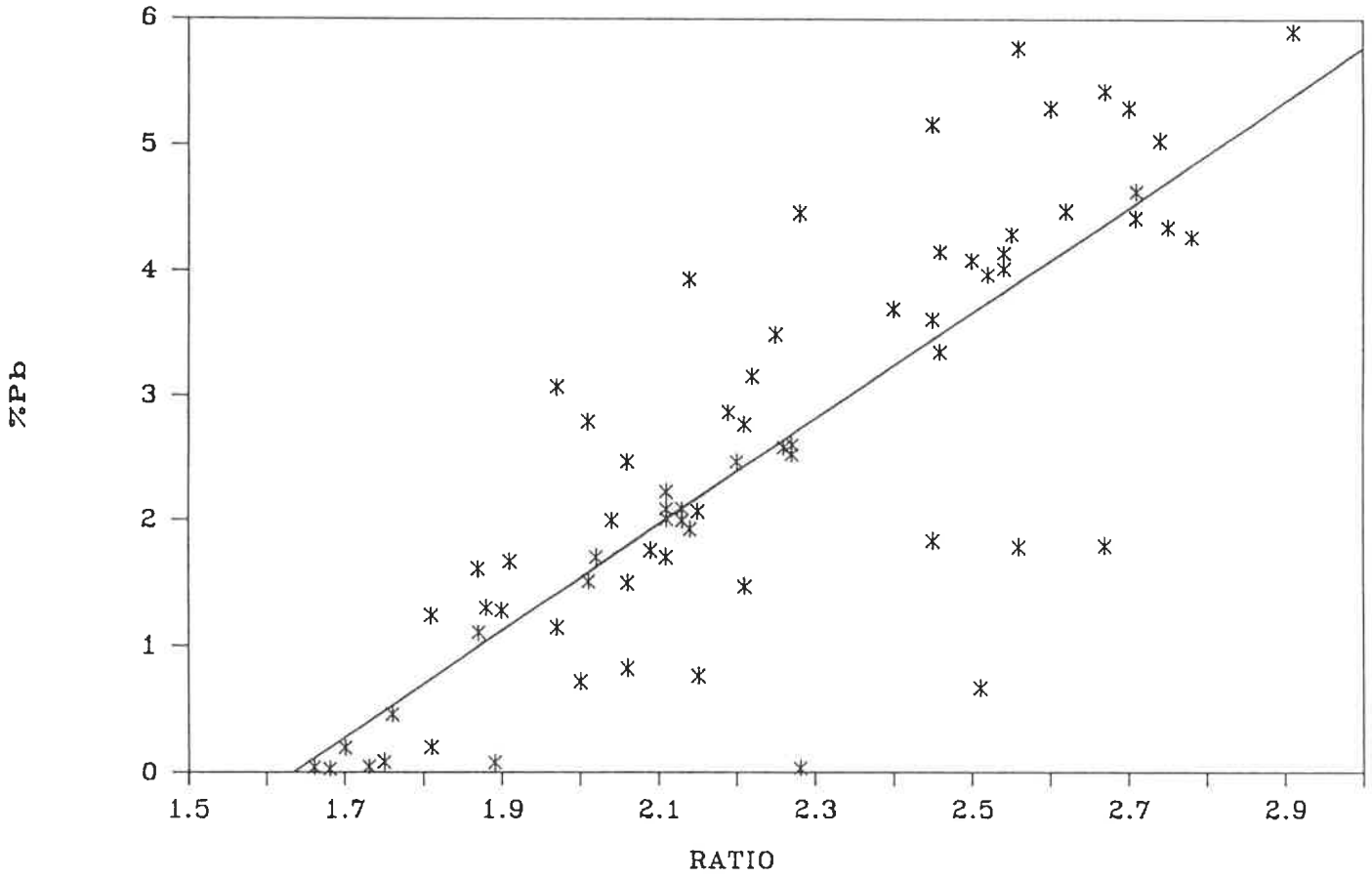


FIGURE E.14 Scatterplot diagram for hole 404a. Concentration lead in percent against the spectral ratio parameter.

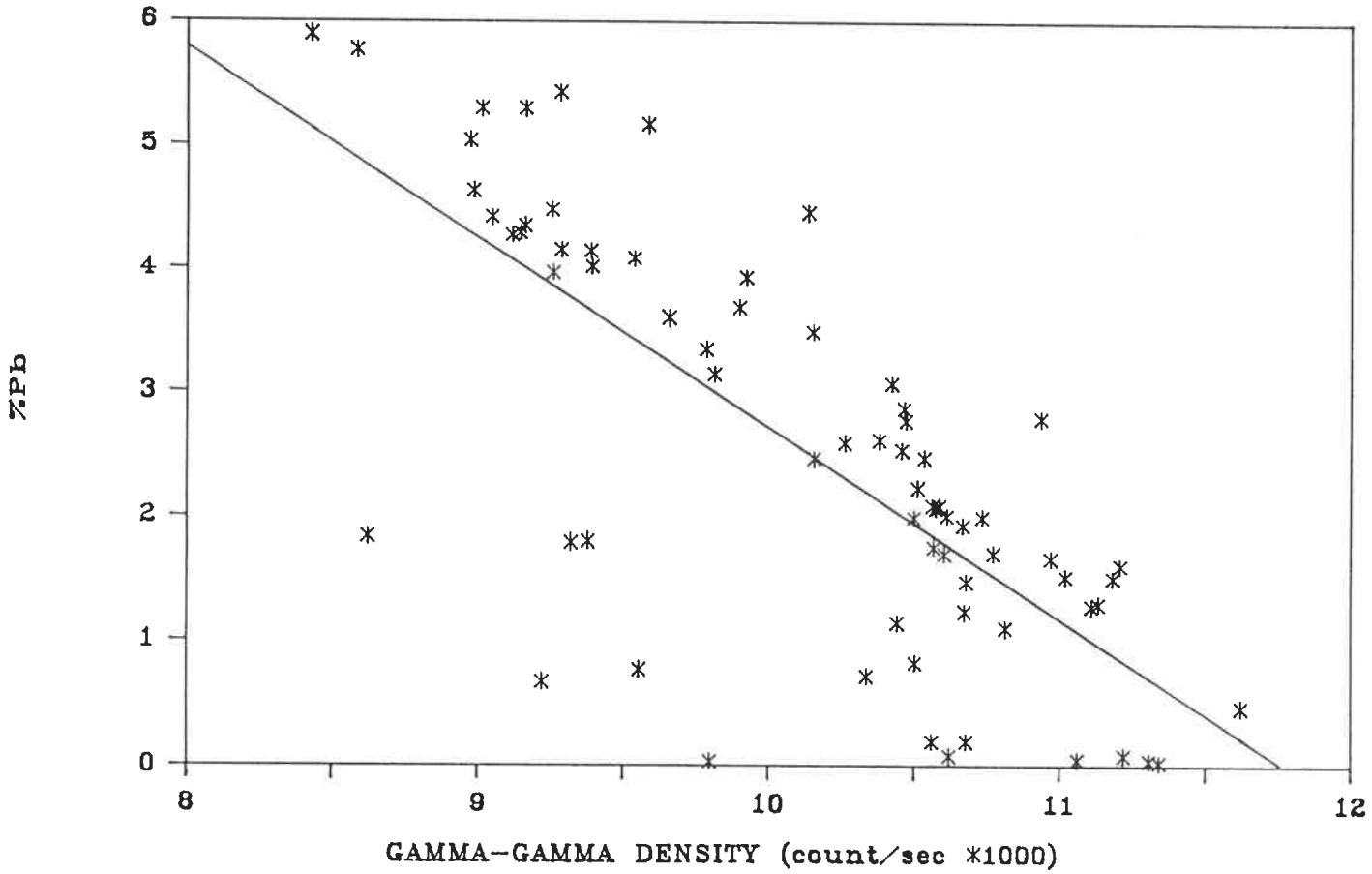


FIGURE E.15 Scatterplot diagram for hole 404a. Concentration lead in percent against the gamma-gamma density parameter (counts/sec).

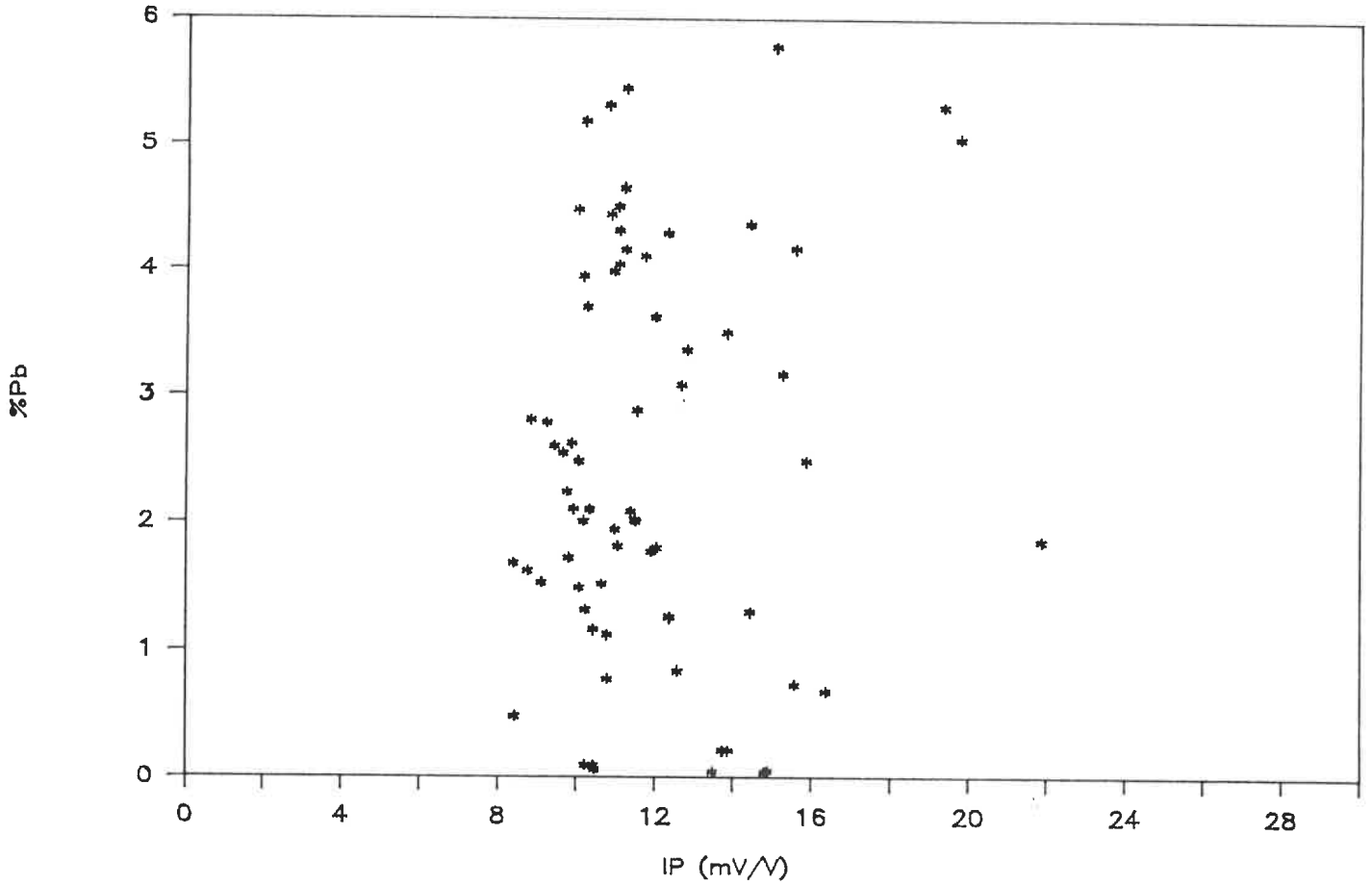


FIGURE E.16 Scatterplot diagram for hole 404a. Concentration lead in percent against the induced polarization parameter (IP) in mvolts/volts.

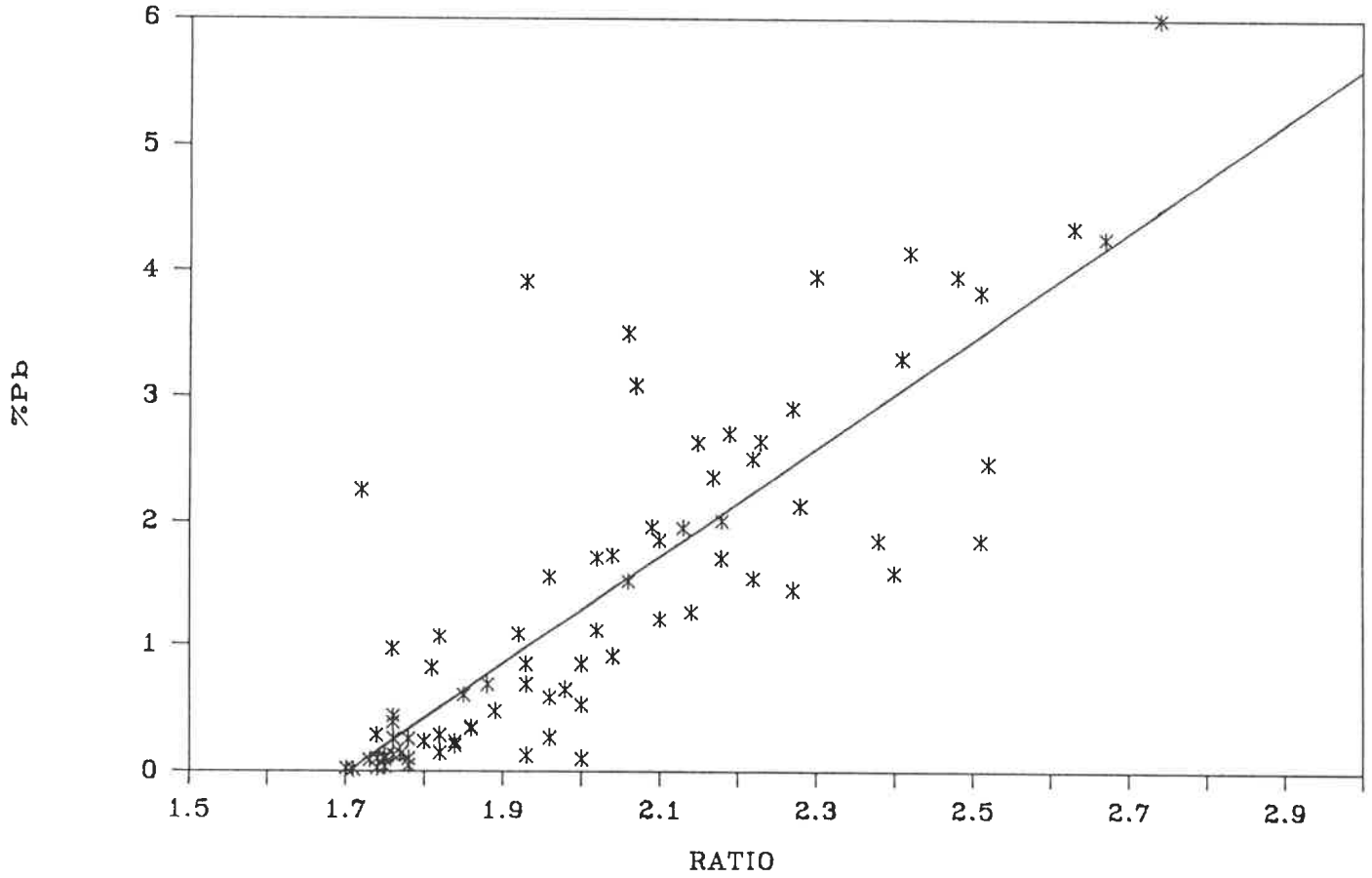


FIGURE E.17 Scatterplot diagram for hole 410a. Concentration lead in percent against the spectral ratio parameter.

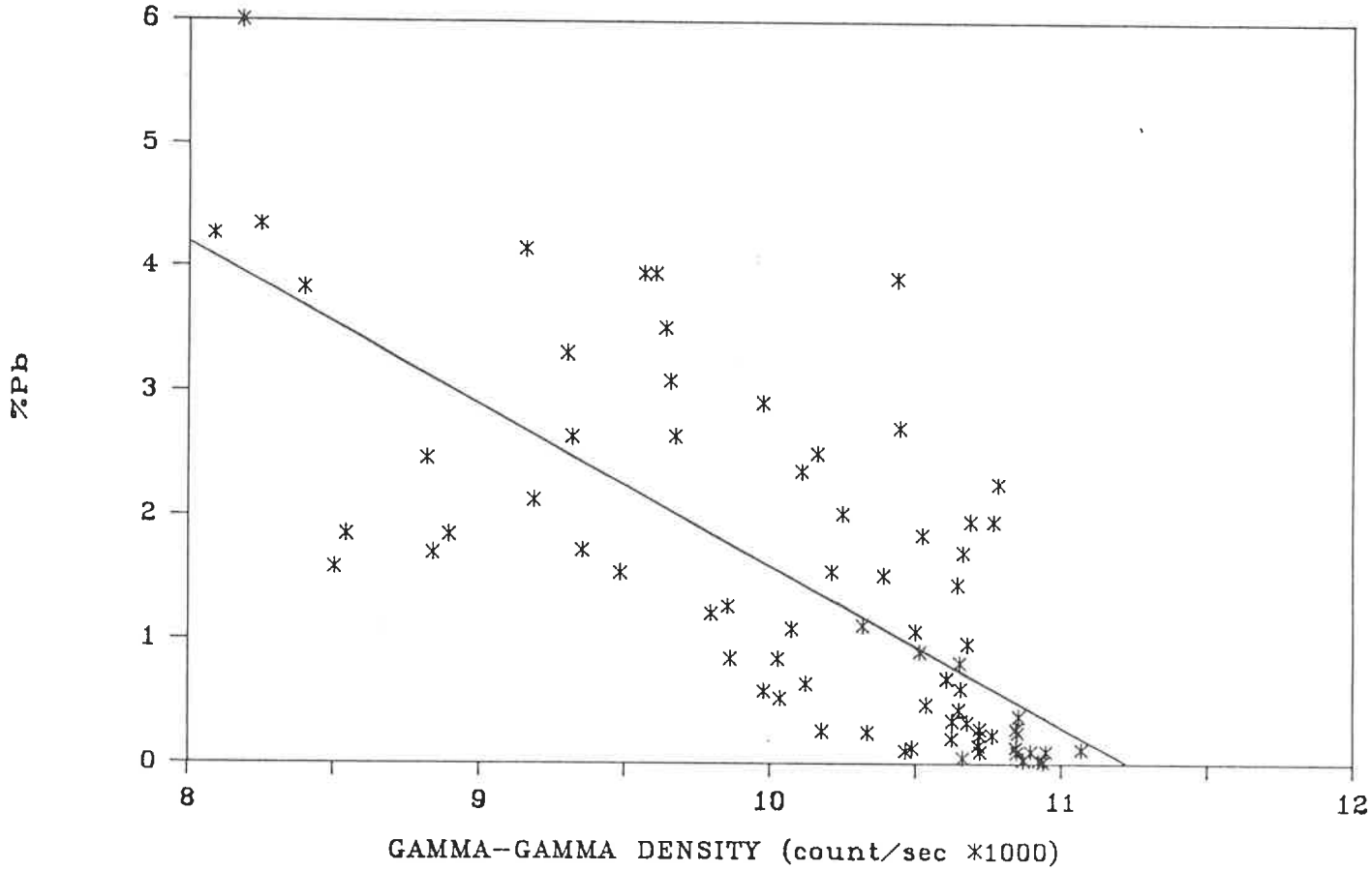


FIGURE E.18 Scatterplot diagram for hole 410a. Concentration lead in percent against the gamma-gamma density parameter (counts/sec).

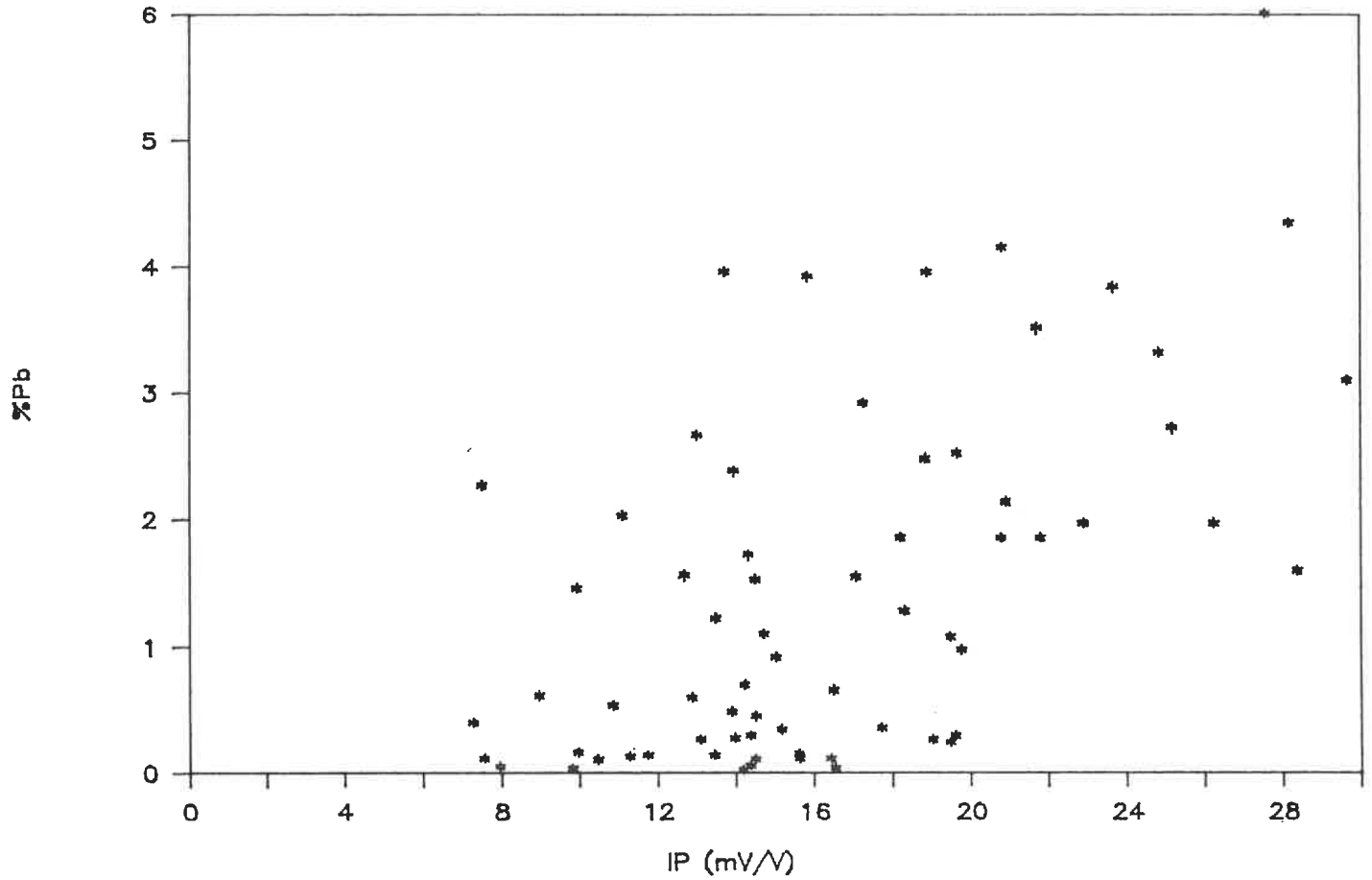


FIGURE E.19 Scatterplot diagram for hole 410a. Concentration lead in percent against the induced polarization parameter (IP) in mvolts/volts.

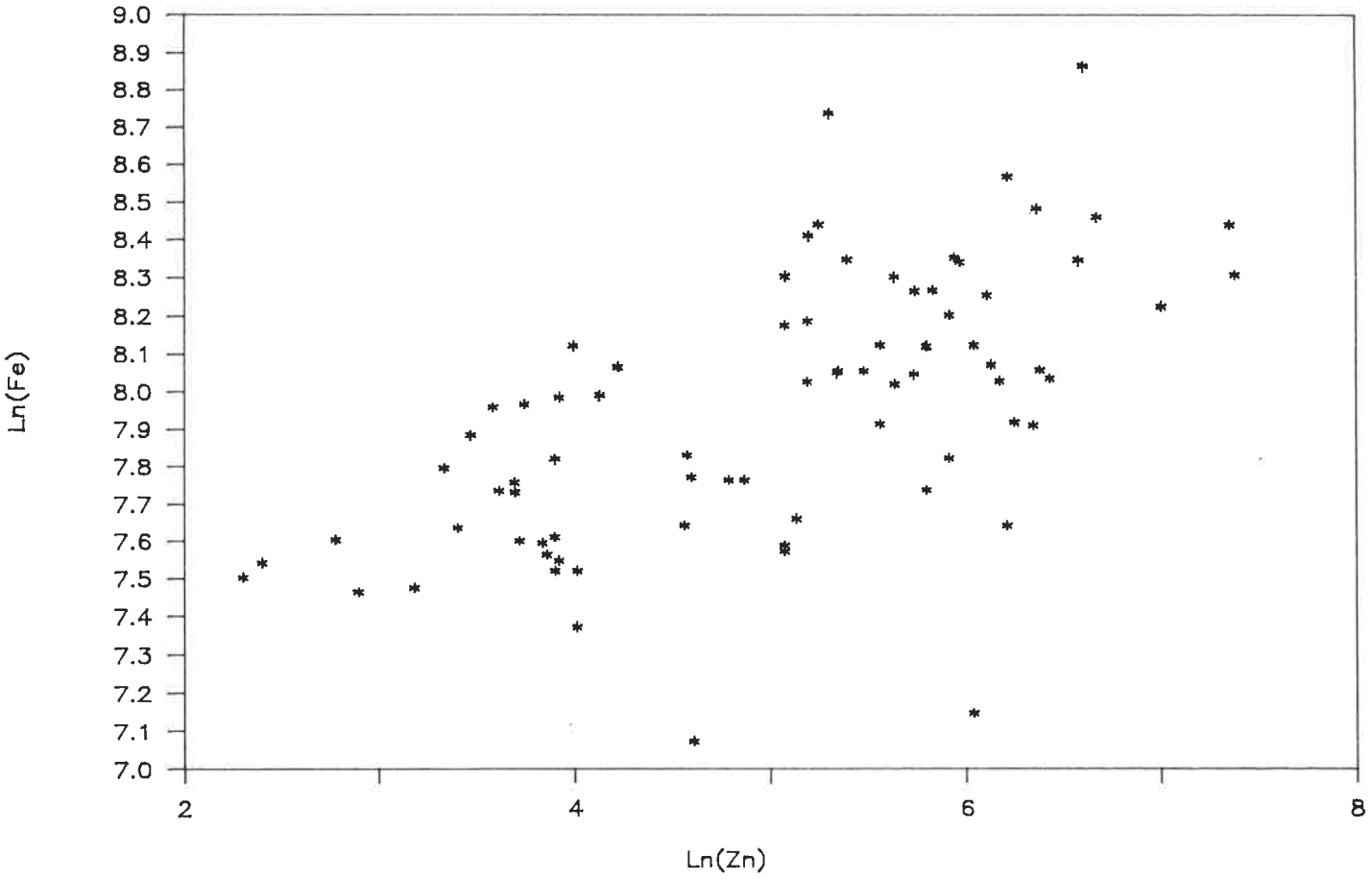


FIGURE E.20 Scatterplot diagram for hole 410a. Total iron concentration against zinc concentration (both in logarithmic values: the values have been multiplied by 10000 (from % to ppm) before applying the natural logarithm).

APPENDIX F - DATA (on diskette)

APPENDIX F - 1) GEOLOGIC CORE LOGS

The geologic core logs are summarized on diskette (360 kbytes, 5.25", 2S/2D), in file GEOLOGY. It can be seen with MS-DOS.

Geological legend

ob	:	Overburden
sst	:	Sandstone
xb sst	:	Cross-bedded sandstone
bl sh (bl shale,bl s)	:	Black shale
lst (Lst)	:	Limestone
lst pbc (lstp)	:	Limestone pebble conglomerate
co	:	with coal
puggy shale (Pug sh)	:	"Puggy" shale
Wea zone	:	Weathered zone
W sh (W shale)	:	Windsor shale
W sh/gyp	:	Windsor shale with gypsum
W bl sh	:	Windsor black shale
W blsh/g	:	Windsor black shale with gypsum
lst (Lst)	:	Limestone
lst bx	:	Limestone breccia
mst (mud)	:	Mudstone
mst/gyp	:	Mudstone with gypsum
Rhy bx	:	Rhyolite breccia
Trans bx	:	Rhyolite breccia (Transition zone)
rhyolite	:	Rhyolite

APPENDIX F - 2) GEOCHEMICAL ASSAYS

The geochemical assays are summarized on diskette (360 kbytes, 5.25", 2S/2D), in file CHIMIE. It can be seen with MS-DOS.

APPENDIX F - 3) MULTIPLE REGRESSION, PCA AND DISCRIMINANT ANALYSIS DATA

Data for multiple regression, PCA and discriminant analyses were saved on diskette (360 kbytes, 5.25", 2S/2D) in files as follows.

Regression and PCA analyses: Hole 404a : TABLEF.1
Hole 410a : TABLEF.2

Discriminant analysis: Hole 404a : TABLEF.3
Hole 410a : TABLEF.4

It can be seen with MS-DOS.

ÉCOLE POLYTECHNIQUE DE MONTRÉAL
3 9334 00290910 7